Development of Efficient and Accurate Approximations to Single Reference Correlation Methods using Pair Natural Orbitals

Dissertation

zur

Erlangung des Doktorgrades (Dr. rer. nat.)

der

Mathematisch-Naturwissenschaftlichen Fakultät

der

Rheinischen Friedrich-Wilhelms-Universität Bonn

vorgelegt von

Andreas Hansen

aus

Schlema (jetzt Bad Schlema)

Bonn 2012

Angefertigt mit Genehmigung der Mathematisch-Naturwissenschaftlichen Fakultät der
Rheinischen Friedrich-Wilhelms-Universität Bonn

1. Gutachter: Prof. Dr. Frank Neese

2. Gutachter: Prof. Dr. Thomas Bredow

Tag der Promotion: 13.08.2012

Erscheinungsjahr: 2012

Summary

Computational chemistry greatly enhances the scientific analysis of experiments and can predict quantities that are experimentally not accessible. However, there is still no approximate method available that is both efficient and accurate enough to serve as general basis for large-scale applications in computational chemistry, at least in the range of 20 to 100 atoms, which covers many challenging problems of present day chemical research. In this PhD dissertation, an accurate and efficient approximation to single reference correlation methods was developed which constitutes a new family of local correlation methods denoted 'local pair natural orbital' (LPNO) methods. To this end, the pair natural orbital (PNO) approach first introduced in the 1970s is revived and modified. The LPNO methods achieve efficiency through localization of the internal space and truncation of the electron pair list together with a tremendous compression of the external space using a truncated pair natural orbitals expansion. Of course, neither idea is unprecedented, but their combination and extension to coupled cluster approaches as well as their efficient implementation was carried out for the first time.

Using the LPNO approach, production level implementations for various coupled pair methods (LPNO-(N)CEPA/0,1,2,3; LPNO-(N)CPF/1,2,3), quadratic configuration interaction and coupled cluster with single and double excitations (LPNO-QCISD, LPNO-CCSD) including perturbative connected triple excitations as well (LPNO-QCISD(T), LPNO-CCSD(T)) were developed in the framework of the ORCA quantum chemistry program package. Furthermore, an LPNO version of variational CEPA (LPNO-VCEPA) and parametrized coupled cluster with single and double excitations (LPNO-pCCSD) was implemented and evaluated. The LPNO methods are available in two different versions: a spin-restricted form, suitable for efficient and accurate calculations of closed-shell molecules, and a spin-unrestricted open-shell version, which by default utilizes quasi-restricted orbitals, but is also general enough to be run with spin-unrestricted HF or KS reference determinants of broken-symmetry type. Two different algorithms are available for the closed-shell version denoted as LPNO_1 and LPNO_2. The latter entirely avoids the construction of the $\mathbf{J}^{ij}$ and $\mathbf{K}^{ij}$ integrals in the MO basis, which give rise to storage problems for large systems with more than 2000 basis functions. However, the LPNO_2 algorithm is also less accurate than the LPNO_1 variant.

Only three cut-off parameters enter the procedure, which control the number of PNOs per electron pair, the size of the significant electron pair list, and the number of contributing auxiliary basis functions per PNO. The rather conservatively chosen default values for the thresholds do not need to be changed or reinvestigated in detail prior to any application study and the LPNO methods can be used in the same way as their untruncated counterparts. The laborious integral transformation associated with the large number of PNOs becomes feasible through the extensive use of local density fitting (RI) techniques. The LPNO approach offers a number of attractive features: a) the smooth and controllable truncation errors; b) the excellent behavior with respect to basis set extension; c) the very compact form of the LPNO

wavefunction; d) the absence of any real-space cut-offs or fragmentation schemes.

Extended test calculations including thermochemistry, kinetics, weak molecular interactions and potential energy surfaces have consistently shown that the closed-shell LPNO variants together with our choice of the defaults for the cut-off parameters recover around 99.7 – 99.9 % of the basis set correlation energy. This is about one order of magnitude more accurate than the old PNO-CEPA implementations, which were extensively used in the 1970s. The less accurate algorithm ($LPNO_2$) still recovers 98.7 – 99.3 % of the target correlation energy in the given basis set and has modest disk space requirements. Comprehensive numerical tests on absolute and relative energies as well as timings consistently show that the outstanding performance of the LPNO methods carries over to the open-shell case with minor modifications. The open-shell version is slightly less accurate but still more than 99.5% of the canonical correlation energy is recovered on average. The LPNO-CCSD method is the most promising in terms of accuracy and robustness if open-shell molecules are involved in the respective computational study. For closed-shell systems LPNO-CEPA/1 is the method of choice, at least in terms of relative energy calculations. Furthermore, the LPNO based parameterized CCSD methods (LPNO-pCCSD) represent an attractive alternative for accurate predictions of reaction energies and barrier heights. Finally, hyperfine couplings calculated with the variational LPNO-VCEPA/1 method, for which a well defined expectation value type density exists, indicate the great potential of the LPNO approach for the efficient calculation of molecular properties.

Although the effective scaling of the computation time with respect to the system size N is still $\sim\mathcal{O}(N^3)$, the LPNO methods are efficient enough for studies on molecules with up to 100 atoms and 2000 basis functions in reasonable wall-clock times, *e.g.* not more than a few days for a single point energy calculation depending on the number of correlated electrons. They are up to three orders of magnitude faster than their canonical counterparts. For larger molecules, the total wall-clock time required to complete the correlation part of the calculations is only two to five times larger compared to the preceding SCF procedure. Parallelization and the use of the RIJCOSX approximation (for LPNO-CCSD) further enhance the range of applicability. However, the ultimate goal of finding an efficient and accurate approximation to the 'gold-standard' of computational chemistry provided by the CCSD(T) method, which consistently yields results with chemical accuracy, has not been fully achieved yet.

Although the current implementation leaves room for improvements and further developments are necessary to fully explore the potential of the LPNO approach, the present LPNO methods are already highly suitable and useful for large-scale computational chemistry applications. Thus, due to the high efficiency and accuracy combined with the robustness of the LPNO methods and and their simple 'black-box' use, they have a good chance at becoming a standard tool capable of tackling many interesting problems in contemporary chemical research.

Zusammenfassung

Computerchemische Methoden sind sehr hilfreich bei der Analyse von chemischen Experimenten und können experimentell unzugängliche Größen vohersagen. Es gibt jedoch noch keine quantenchemische Methode, die sowohl effizient als auch akkurat genug ist, um als allgemeine Grundlage für computerchemische Anwendungen zu dienen, zumindest für molekulare Syteme im Bereich 20 – 100 Atomen, welcher viele herausfordernde Problem der aktueller chemischen Forschung abdeckt. Im Rahmen dieser Dissertation wurde eine akkurate und effiziente Näherung für Einfachreferenzmethoden entwickelt, die sogenannten 'local pair natural orbital' (LPNO) Methoden, welche eine neue Klasse an lokalen Korrelationsmethoden repräsentieren. Dafür wurde der PNO Ansatz, welcher schon in den 1970ern intensiv benutzt wurde, aufgegriffen und modifiziert. Die LPNO Methoden erreichen ihre Effizienz durch Lokalisierung des besetzten Orbitalraumes und Verkürzung der Elektronenpaarliste zusammen mit einer enormen Kompression des vituellen Orbtialraumes durch eine abgebrochenen PNO Entwicklung. Natürlich ist keine dieser Ideen neu, aber deren Kombination und Erweiterung auf den Coupled-Cluster Ansatz sowie deren effiziente Implementierung wurde zum ersten Mal durchgeführt.

Unter Benutzung des LPNO Ansatzes wurden Produktionsimplementierungen für verschiedene Coupled-Pair Methoden (LPNO-(N)CEPA/0,1,2,3; LPNO-(N)CPF/1,2,3), quadratische Konfigurationswechselwirkung und Coupled-Cluster mit Einfach- und Zweifachanregungen (LPNO-QCISD, LPNO-CCSD) sowie die störungstheoretische Einbezeihung von verbundenen Dreifachanregungen (LPNO-QCISD(T), LPNO-CCSD(T)) im Rahmen des ORCA Quantenchemie Programmpakets entwickelt. Weiterhin wurden LPNO Varianten der variationellen CEPA (VCEPA) und parameterisierten CCSD (pCCSD) Methoden entwickelt und getestet. Die LPNO Methoden sind in zwei verschiedenen Version implementiert, eine spinbeschränkte Form, die für die effiziente und akkurate Berechnung von geschlossenschaligen Molekuelen geeignet ist und eine Form für offenschalige Moleküle, welche standardmäßig quasibeschränkte Orbitale (QROs) benutzt. Letztere ist jedoch so implemententiert, dass auch Rechnungen mit spinunbeschränkten Hartree-Fock (HF) oder Kohn-Sham (KS) Referenzdeterminaten mit gebrochener Symmetry möglich sind. Für die geschlossenschalige Version wurden zwei verschiedene Algorithmen entwickelt (LPNO_1 und LPNO_2). Während der erste Algorithmus kleinere Fehler liefert, wird im zweiten Algorithmus die Konstruktion der $\mathbf{J}^{ij}$ und $\mathbf{K}^{ij}$ Integrale in der MO Basis, welche zu Speicherengpässen für Systeme mit mehr als 2000 Basisfunktion führen, vollständig vermieden.

Die LPNO Methoden benutzen nur drei Abschneideparameter, welche die Anzahl an PNOs pro Elektronenpaar, die Größe der signifikanten Elektronenpaarliste und die Anzahl an Hilfsbasisfunktionen pro PNO festlegen. Die ziemlich konservativ gewählten Standardwerte für die Abschneideparameter müssen nicht vom Nutzer vor der Anwendung des Programms neu untersucht oder verändert werden. Daher können die LPNO Methoden analog zu ihren ungenäherten Entsprechungen benutzt werden. Die aufwändigen Integraltransformationen werden

handhabbar durch extensive Benutzung von lokalen RI Techniken. Der LPNO Ansatz bietet eine Reihe von Vorteilen: a) glatte und gut kontrollierbare Abschneidefehler; b) exzellentes Verhalten bezüglich Basissatzvergrößerung; c) sehr kompakte Form der LPNO Wellenfunktion; d) keine Realraumbeschneidungen oder Fragmentierungsschemata.

Umfassende Testrechungen (Thermochemie, Kinetik, nicht-kovalente Wechselwirkungen und Potentialkurven) haben übereinstimmend gezeigt, dass mit den geschlossenschaligen LPNO Varianten und den Standardwerten für die Abschneideparameter ~99.7 – 99.9 % der Zielkorrelationsenergie erhalten wird. Der etwas ungenauere Alogrithmus ($LPNO_2$) liefert noch immer ~98.7 – 99.3 % der Zielkorrelationsenergie und hat dabei nur einen moderaten Festplattenspeicherbedarf. Ausfürliche numerische Tests für absolute und relative Energien sowie Laufzeitanalysen haben gezeigt, dass die hervorragenden Ergebnisse der geschlossenschaligen LPNO Methoden mit kleinen Abstrichen auch für den offenschaligen Fall erzielt werden können. Die LPNO-CCSD Methode ist in Bezug auf Genauigkeit und Robustheit die Methode der Wahl, wenn offenschalige Molekuele an der entsprechenden Computerchemiestudie beteiligt sind, während im geschlossenschaligen Fall die LPNO-CEPA/1 Methode zu bevorzugen ist, zumindest zur Berechnung von Relativenergien. Eine vielversprechende Alternative für die Berechnung von Reaktionsenergien und Barrierenhöhen stellen die parameterisierten LPNO-pCCSD Methoden dar. Weiterhin deuten die Berechnungen von Hyperfeinkopplungskonstanten mit Hilfe der variationallen LPNO-VCEPA/1 Methode das große Potential des LPNO Ansatzes für die effiziente Berechnung von molekularen Eigenschaften an.

Obwohl das effektive Skalierungsverhalten der Rechenzeit in Abhängigkeit von der Systemgröße N immer noch von $\sim\mathcal{O}(N^3)$ Komplexität ist, sind die LPNO Methoden effizient genug für Studien an Molekuelen mit bis zu 100 Atomen und 2000 Basisfunktionen in vernüftigen Rechenzeiten, d.h. wenige Tage für eine Energieberechnung (abhängig von der Anzahl an korrelierten Elektronen). Sie sind bis zu drei Größenordnungen schneller im Vergleich zu ihren ungenäherten Entsprechungen. Für größere Moleküle dauert die Berechnung des Korrelationsteils nur zwei- bis fünfmal so lang wie die vorangegangene iterative Berechnung der Referenzwellenfunktion. Parallelisierung und die Benutzung der RIJCOSX Näherung (für LPNO-CCSD) erweitern zusätzlich den Anwendungsbereich. Das ultimative Ziel einer effizienten und akkuraten Näherung für die CCSD(T) Methode, dem 'Goldstandard' der Computerchemie, konnte jedoch noch nicht vollständig erreicht werden.

Obwohl noch Verbesserungen der derzeitigen Implementierung und weitere Entwicklungen nötig sind, um das gesamte Potential des LPNO Ansatzes auszuschöpfen, sind die beschriebenen LPNO Methoden schon sehr gut geeignet für Computerchemieanwendungen im großen Maßstab. Aufgrund ihrer hohen Effizienz, Genauigkeit und einfachen 'Black-Box' Benutzbarkeit haben die LPNO Methoden eine gute Chance, ein Standardinstrument für die Untersuchung vieler interessanter Probleme der gegenwärtigen chemischen Forschung zu werden.

List of Publications

Publications directly related to this thesis

- R. Izsák, **A. Hansen**, and F. Neese. The resolution of identity and chain of spheres approximations for the LPNO-CCSD singles Fock term. *Mol. Phys.*, accepted for publication.

  In this work, the RIJCOSX approximation, developed earlier for accelerating the SCF procedure, is applied to one of the limiting factors of LPNO-CCSD calculations: the evaluation of the singles Fock term.
  Parts of the numerical results presented in this paper are also included in this thesis, which was written in pseudo-cumulative form. I carried out parts of the numerical investigations.

- L. M. J. Huntington, **A. Hansen**, F. Neese, and M. Nooijen. Accurate thermochemistry from a parameterized coupled cluster singles and doubles model and a local pair natural orbital based implementation for applications to larger systems. *J. Chem. Phys.* **136**, 064101 (2012).

  In this paper, the parameterized coupled cluster (pCCSD) methods were investigated in order to find suitable parameters for applications in reaction thermochemistry and thermochemical kinetics. Furthermore, it was shown that the combination of pCCSD methods with the LPNO approach represents an attractive 'model chemistry' for large-scale thermochemical applications for sizeable molecular systems.
  The LPNO part of this paper is included in this pseudo-cumulative thesis. I carried out parts of the implementation of the pCCSD and LPNO-pCCSD methods into the ORCA program package as well as parts of the numerical investigations.

- **A. Hansen**, D. G. Liakos, and F. Neese. Efficient and accurate local single reference correlation methods for high-spin open-shell molecules using pair natural orbitals. *J. Chem. Phys.* **135**, 214102 (2011).

  In this work, the local pair natural orbital (LPNO) concept was extended to the high-spin open-shell (spin-unrestricted) single reference coupled pair, quadratic configuration interaction and coupled cluster methods with up to doubly excited determinants. Comprehensive numerical tests on absolute and relative energies as well as timings consistently showed that the outstanding performance of the LPNO methods carries over to the open-shell case with minor modifications.
  This paper represent an essential part of this thesis, which was composed in pseudo-

cumulative form. I carried out the implementation of the open-shell LPNO methods into the ORCA program package and their numerical investigation.

- F. Neese, **A. Hansen**, and D. G. Liakos. Efficient and accurate approximations to the local coupled cluster singles doubles method using a truncated pair natural orbital basis. *J. Chem. Phys.* **131**, 064103 (2009).

  In this work, a production level implementation of the closed-shell local quadratic configuration interaction and coupled cluster methods with single and double excitations based on the concept of pair natural orbitals (LPNO-QCISD and LPNO-CCSD) was reported, evaluated, and discussed.
  This paper is an essential part of this pseudo-cumulative thesis. I carried out the numerical investigations.

- F. Neese, F. Wennmohs, and **A. Hansen**. Efficient and accurate local approximations to coupled-electron pair approaches: An attempt to revive the pair natural orbital method. *J. Chem. Phys.* **130**, 114108 (2009).

  In this work, an efficient production level implementation of the closed shell CEPA and CPF methods was reported that can be applied to medium sized molecules in the range of 50 – 100 atoms and up to about 2000 basis functions. The internal space is spanned by localized internal orbitals while the external space is greatly compressed through the use of pair natural orbitals (PNOs).
  This paper represents an essential part of this thesis, which was written in pseudo-cumulative form. I carried out most of the numerical investigations.

Publications by the author not or only partly related to this thesis

- S. Ye, C. Riplinger, **A. Hansen**, C. Krebs, J. M. Bollinger Jr., and F. Neese. Electronic structure analysis of the oxygen activation mechanism by the Fe^{II}- and α-ketoglutarate-dependent dioxygenases. *Chem. Eur. J.* **18**, 6555 (2012).

  In this work, the mechanism of Fe^{II}- and α-ketoglutarate-dependent dioxygenases were studied computationally with DFT and high-level *ab initio* methods employing an active site cluster model.
  I carried out the implementation of the spin-unrestricted coupled cluster methods into the ORCA program package, which were employed in this study.

- D. G. Liakos, **A. Hansen**, and F. Neese. Weak molecular interactions studied with parallel implementations of the local pair natural orbital coupled pair and coupled cluster methods. *J. Chem. Theory Comput.* **7**, 76 (2011).

  In this paper, a parallel implementation of the LPNO-CEPA and LPNO-CCSD methods was described. A detailed analysis together with the corresponding pseudo-code was presented for the most important steps in terms of computational effort.
  Although this work is closely related to the subject of this thesis, the corresponding results are not discussed in the latter. I was involved in parts of the test calculations.

- F. Neese, **A. Hansen**, F. Wennmohs, and S. Grimme. Accurate theoretical chemistry with coupled pair models. *Acc. Chem. Res.* **42**, 641 (2009).

  In this work, the performance of coupled pair methods in chemical applications was examined. It was shown that the accuracy of the CEPA methods clearly surpasses that of DFT and MP2 theory.
  I carried out the entire computational study and the spin-unrestricted implementation of the coupled pair methods into the ORCA program package.

- F. Neese, F. Wennmohs, **A. Hansen**, and U. Becker. Efficient, approximate and parallel Hartree-Fock and hybrid DFT calculations. A 'chain-of-spheres' algorithm for the Hartree-Fock exchange. *Chem. Phys.* **356**, 98 (2009).

  In this work, the possibility was investigated to speed up Hartree-Fock and hybrid density functional calculations by forming the Coulomb and exchange parts of the Fock matrix by different approximations, the split-RI-J and 'chain-of-spheres exchange' (COSX) algorithms respectively.
  I was involved in parts of the numerical investigations.

- K. Morawetz, M. Schreiber, B. Schmidt, **A. Ficker**[a], and P. Lipavsky, Correlated two-particle scattering on finite cavities, *Phys. Rev. B* **72**, 014301 (2005).

  In this work, the correlated two-particle problem was solved analytically in the presence of a finite cavity. The methodology was evaluated in terms of exactly solvable models for both the cavity as well as the two-particle correlation where the two-particle potential was chosen in separable form.
  I derived unrestricted two-particle scattering expressions for different parameterizations of the form factors of separable interactions.

[a] Surname "Ficker" changed to "Hansen" in October 2005.

Acknowledgement

Over the past four years, many people have contributed to make the work on my PhD thesis a successful and enjoyable time.

First and foremost, I would like to express my deep gratitude to Prof. F. Neese, not only for his excellent supervision of my dissertation and the great support with his vast scientific knowledge and clever ideas, but also for teaching me good scientific practice and how to successfully manage a large research group. He gave me the opportunity to work on exciting projects and to attend many conferences and workshops. Furthermore, my special thanks go to Dr. F. Wennmohs, who helped me a lot to get used to the ORCA program package and supported me with his comprehensive knowledge on computer software and hardware and the nice and inspiring discussions while drinking his excellent coffee together. I also want to thank Prof. T. Bredow who was so kind to serve as second reviewer of this dissertation as well as Prof. S. Höger and Prof. B. Metsch who are the additional examiners for the doctoral viva.

I would like to Prof. S. Grimme for supporting me with his expertise in computational thermochemistry and providing test cases and the TMER program for analyzing the corresponding data. Furthermore, I am grateful to Prof. E. F. Valeev for imparting his huge knowledge on explicitly correlated methods and programming to me. I had a pleasant and inspiring time at the VirginiaTech University in Blacksburg, Virginia. I also wish to thank L. M. J. Huntington and Prof. M. Nooijen for the enjoyable and fruitful cooperation concerning the pCCSD methods and many inspiring discussions.

I want to thank all members of our research group for keeping such a good atmosphere and all the helpful discussions which proved most valuable. Especially, I am grateful to Dr. E. Klein for the careful proof-reading of the thesis and Dr. C. Riplinger for providing the LaTeX template and his expertise. Furthermore, I would like to thank Dr. R. Izsák, Dr. D. G. Liakos and U. Becker for the fruitful and pleasant cooperation concerning the RIJCOSX implementation and the parallelization of the code respectively.

Many other people in the Max-Planck-Institute in Mülheim a. d. Ruhr and the Institute for Physical and Theoretical Chemistry in Bonn contributed to a nice atmosphere over the last years. Especially, I wish to thank C. Kronz for managing our research group in such a professional and pleasant way and J. Mekelburger and R. Trinoga for their excellent maintenance of the computer facilities.

Not least, I am grateful to my friends and family who greatly supported me during this time and always provided a source of fun and inspiration. Finally, I want to thank the German-Israeli-Foundation (GIF), the University Bonn and the Max-Planck-Gesellschaft (MPG) for financial support.

Contents

List of Tables

List of Figures

Nomenclature

$\widehat{T}_2$	double excitation operator in CC theory
N	system size (number of atoms and basis functions respectively)
O	number of occupied orbitals
V	number of virtual orbitals
(T)	perturbative correction for connected triple excitations
AOs	atomic orbitals
B3LYP	Becke; three parameter; Lee-Yang-Parr
BLAS	basic linear algebra subprograms
BO	Born-Oppenheimer
BP86	Becke-Perdew 1986
BSSE	basis set superposition error
CBS	complete basis set
CC	coupled cluster
CC2	second-order approximate CCSD
CCSD	truncated coupled cluster with single and double excitations
CCSD(T)	coupled cluster singles doubles with perturbatively incorporated connected triple excitations
CCSD(T)$_{\overline{\mathrm{R12}}}$	CCSD(T) with a perturbative treatment of explicit correlation (Crawford, Valeev)
CCSD(T)-F12	CCSD(T) with approximate inclusion of explicit correlation (Adler, Knizia and Werner)
CCSD-T$_{1b}$	CCSD with approximate inclusion of connected triple excitations in an iterative form
CEPA	coupled electron pair approximation
CI	configuration interaction
CIM	cluster in molecule
CISD	configuration interaction with single and double excitations
CPF	coupled pair functional
CPU	central processing unit
CSFs	configuration state functions
DF	density fitting
DFT	density functional theory
DOMO	doubly occupied molecular orbitals
EEO	external exchange operator

EOM-CCSD	equation of motion CCSD
EPV	exclusion principle violating
full-CI	full configuration interaction (all possible excitations)
GGA	generalized gradient approximation
GTOs	gaussian-type orbitals
HEAT	high accuracy extrapolated *ab initio* thermochemistry
HF	Hartree-Fock
I/O	input/output
IEPA	independent electron pair approximation
KS	Kohn-Sham
LMOs	localized molecular orbitals
LPNO	local pair natural orbital
LPNO-VCEPA	local pair natural orbitals variant of variational CEPA
MOs	molecular orbitals
MP2	Møller-Plesset perturbation theory truncated at second order
MPI	message passing interface
MR-$(SC)^2$-CI	multireference size-consistent self-consistent configuration interaction method
NO	natural orbitals
OSV	orbital-specific virtual
OVS	optimized virtual space
PAOs	projected atomic orbitals
PC	personal computer
pCCSD	parameterized CCSD (general)
pCCSD(α, β)	parameterized CCSD (bivariate variant)
PESs	potential energy surfaces
PNO	pair natural orbital
pXCISD	prototype extensive CISD
QCI	quadratic configuration interaction
QCISD	quadratic configuration interaction with single and double excitations
QM/MM	quantum mechanics/molecular mechanics
QROs	quasi-restricted orbitals
RHF	restricted Hartree-Fock
RI	resolution of the identity
RIJCOSX	RI approximation for the Coulomb part and chain of spheres exchange approximation
ROHF	restricted open-shell Hartree-Fock
SAPT	symmetry adapted perturbation theory
SCEP	self-consistent electron pairs

SCF	self-consistent field
SCS-MP2	spin-component-scaled Møller-Plesset perturbation theory truncated at second order
SOMO	singly occupied molecular orbitals
TD-DFT	time-dependent density functional theory
TNOs	triple natural orbitals
UHF	unrestricted Hartree-Fock
VCPEA	variational CEPA
VMOs	virtual molecular orbitals
W_n	Weizmann thermochemistry protocols (n = 1 – 4)
ZPVE	zero point vibrational energy

1. Introduction

About two centuries ago mathematics did not play an important role in chemistry. The common opinion at that time was summarized in the following quote from the french philosopher of science, Auguste Comte, published in 1838:[1]

> *"Any attempt to use mathematical methods for the investigation of chemical questions must be considered as completely irrational and is strongly opposing the spirit of chemistry. If mathematics will ever occupy a prominent place in chemistry, an absurd idea that fortunately is completely unrealistic, this would lead to a rapid and irreversible decay of this scientific discipline."*

Fortunately, Comte has not been proven right since the development of quantum mechanics in the 1920s gave birth of quantum chemistry, which now plays an important role as investigative tool for various chemical problems. Quantum chemistry provides the physical and mathematical background necessary to describe chemical systems on a microscopic level. However, as it was already recognized by Paul A. M. Dirac in 1929,[2] it is the mathematical complexity that limits its practical application in chemistry:

> *"The fundamental laws necessary for the mathematical treatment of a large part of physics and the whole of chemistry are thus completely known, and the difficulty lies only in the fact that applications of these laws leads to equations that are too complex to be solved. ... hence it would be desirable to develop practical approximation schemes for the application of quantum mechanics."*

During the last decades many attempts have been made to construct suitable approximate methods and a large number of different approaches are now available.[3–5] The implementation of various quantum chemical methods into computer programs together with the tremendous increase of computer power has lead to the development of computational chemistry which has become an important tool for chemical research.[6] It greatly enhances the scientific analysis of experiments and can predict quantities that are experimentally not accessible. However, there is still no approximate method available that is both efficient and accurate enough to serve as general basis for large-scale applications in chemical research. In this work the pair natural orbital (PNO) approach, which was introduced in the 1970s

(see Refs. in Sec. 1.4) is revived and modified. The new family of approximate wavefunction based quantum chemical methods, denoted local pair natural orbital (LPNO) methods holds great promise to change this unfortunate situation to some extent.

1.1. Quantum chemistry and the electron correlation problem

Starting from Dirac's equations,[2] which give the most complete description of N-electron systems, many approximations have to be introduced until one arrives at methods applicable to practical computational chemistry. In many cases it is sufficient to treat relativistic effects only approximately or neglect them entirely and apply the Born-Oppenheimer (BO) approximation,[7] *i.e.* freeze the motion of the nuclei, which makes it possible to introduce the intuitive concept of chemical structures. The corresponding mathematical description is given by the stationary N-electron Schrödinger equation[8] (in atomic units; M: number of nuclei; N: number of electrons)

$$\widehat{H}_{BO}\Psi := \sum_{i=1}^{N}\left(-\tfrac{1}{2}\Delta_i - \sum_{j=1}^{M}\frac{Z_j}{|\mathbf{r}_i-\mathbf{R}_j|} + \tfrac{1}{2}\sum_{j\neq i}^{N}\frac{1}{|\mathbf{r}_i-\mathbf{r}_j|}\right)\Psi = E\Psi \quad . \tag{1.1}$$

The Born-Oppenheimer Hamiltonian $\widehat{H}_{BO}$ includes all the physics necessary to describe the N-electron system, *i.e.* the kinetic energy of the electrons, the electrostatic interactions between nuclei and electrons as well as electrons themselves (within the BO approximation, the nucleus-nucleus potential adds only as a constant). The N-electron wavefunction Ψ, which depends on N discrete spin variables and $3N$ spatial variables completely describes any non-relativistic N-electron system. Solving this equation yields an eigenvalue spectrum whose lowest eigenvalue corresponds to the ground state energy of the given system. Unfortunately, it is impossible to find an analytic solution to this equation for systems with more than one electron since the two-electron operator cannot be factorized. The Schrödinger equation fulfils a variational principle of Rayleigh-Ritz type,[9] which offers the possibility to obtain a numerically exact solution.[10] However, the high dimensionality makes it impossible to calculate systems with more than a few electrons.

Little is known about the general structure of the N-electron wavefunction, *e.g.* Born's probabilistic interpretation and the cusp conditions derived by Kato.[11] Since electrons are fermions, the N-electron wavefunction has to obey the Pauli principle,[12] *i.e.* it has to be antisymmetric with respect to interchange of electrons. This type of correlated electron movement is denoted Fermi correlation. In most electronic structure methods, the N-electron wavefunction is approximated by a finite set of one-electron wavefunctions (also called atomic orbitals (AOs)) which themselves are expanded in a set of basis functions (typically gaussian-type orbitals (GTOs)[13] are used). After a transformation to molecular orbitals (MOs) and proper orthonormalization, the one-electron wavefunctions are used to build the so called Slater determinant[14] which automatically fulfils the antisymmetry requirement. However,

the convergence of this expansion towards the exact energy is very slow since the Coulomb cusp, which arises due to the instantaneous electron-electron interaction (denoted Coulomb correlation), cannot be describe properly with smooth functions. Thus, large GTO-type basis sets are necessary or explicit correlation needs to be introduced into the approximate N-electron wavefunction in order to achieve highly accurate results.[15]

The starting point for most approximate wavefunction based quantum chemical methods is the mean field or Hartree-Fock (HF) approach,[16] in which each electron interacts only with the average electrostatic field of all other electrons. The orbitals are optimized according to the variational principle, and the resulting Slater determinant (HF determinant) contains the best possible one-electron functions within a given basis set. Typically, more than 99.5 % of the total energy is recovered with the HF method, but this is still far away from chemical accuracy. Furthermore, the HF wavefunction only accounts for Fermi correlation but not for Coulomb correlation since the instantaneous electron-electron interaction is missing in this model which, however, leads to a rather fast convergence to the complete basis set (CBS) limit. Due to this imbalanced treatment of electron correlation effects, the HF method can also give qualitatively wrong results, especially if Coulomb correlation plays a crucial role, for example in Werner-type transition metal complexes or dispersion interactions respectively.

Nonetheless, the HF wavefunction can be used as reference determinant for introducing configuration interaction (CI)[17] which corrects for the missing instantaneous electron-electron interaction. Figuratively said, the electrons avoid each other as much as possible and jump (with a certain probability measured by the excitation amplitudes) into the unoccupied (virtual) orbitals if they come to close to each other. These so called excitations can be described with excited Slater determinants, *i.e.* one or more occupied (internal) orbitals of the HF determinant are replaced by virtual (external) orbitals. Formally, this is most straightforwardly described in the the language of second quantization using the Fock space formalism and applying the appropriate normal ordered quasi-particle creation and annihilation operators to the reference determinant (the so called Fermi vacuum).[18] The full-CI method[17] takes all possible excitations into account. Applying the Rayleigh-Ritz variational principle to the full-CI wavefunction yields the exact non-relativistic energy within the BO approximation and a given finite basis set. Unfortunately, the high dimensionality and the exponential scaling of the computation time with respect to the system size limit the applicability of the full-CI method to very small molecules. However, it has great importance as benchmark for judging more approximate quantum chemical methods and serves as base for further approximations. Another way to introduce Coulomb correlation into the N-electron wavefunction is to use an exponential parameterization of the latter which is known as coupled cluster (CC) approach.[19] However, the CC expansion does not truncate and thus the variational principle cannot be applied directly, but other formalisms exist for solving the CC Schrödinger equation.[20] String-based algorithms make it possible to develop general order CC programs,[21] but their their usage is also restricted to very small molecules due to the tremendous computational effort.

Obviously, further approximations have to be introduced in order to arrive at something useful for 'real-life' computational chemistry. However, this necessitates a non-physical division of the Coulomb correlation into static and dynamic correlation effects (which themselves can be further subdivided).[18] The latter is well described with single reference correlation methods, while the appropriate treatment of static correlation effects requires more than one reference function (multireference correlation methods).[22] In this work, the simpler single reference case will be addressed. A generalization to the multireference case should be done afterwards. There are several requirements which approximate quantum chemical methods should fulfil:[23]

- The method should be variational, *i.e.* it should provide an upper bound to the exact energy of the investigated electronic state. This makes it easier to judge on the quality of the approximate energies and to extent the methodology to molecular properties calculations.
- The method should be well defined, specifically it should be invariant to unitary transformations of the spin orbitals. However, as it will be obvious from the results of this work, this is not the most strict criteria.
- The method should yield exact results (full-CI) for two-electron systems. This is important since most of the many-particle physics is already present in two-electron systems.
- The method should not contain adjustable parameters. Especially, it should be possible to systematically improve the method and converge in principle to the full-CI solution.
- The method should be computationally feasible (in reasonable times applicable to molecules with at least a few dozen atoms).
- The method should be generally applicable for ground and excited states of both closed- and open-shell type as well as molecular property calculations.
- The method should give an accurate approximation to the full-CI result, *i.e.* the deviation from the latter should be smaller than $\sim$1 kcal/mol.
- The method should be robust, *i.e.* applicable to any type of molecule and many chemical applications.
- The method should be size-consistent. This is the most crucial requirement for computational chemistry applications. A size-consistent methods yields for a non-interacting system A–B the sum of the monomer energies E_A and E_B if it is applied to the supermolecule A–B, *i.e.* $E_{AB} = E_A + E_B$. Size-consistency is a somewhat weaker formulation than the more fundamental requirement of size-extensivity. A method is size-extensive if in homogeneous systems the energy is a linear function of the system size. This implies that also the error increases linearly with the system size. In both definitions the fundamental question is that of separability of the wavefunction (multiplicatively separable) and energies (additively separable).

Up to now, no quantum chemical methods is known which satisfies all of these criteria simultaneously.

1.2. Present day computational chemistry

Although computational chemistry has become an important tool for chemical research, it is by far not guaranteed that accurate results can be obtained for most systems of interest. In principle, one aims at chemical accuracy, *i.e.* the systematic error of the method with respect to experimental reference values should not be larger than about 1 kcal/mol, which is already rather large on a chemical scale (*e.g.* it corresponds to about a factor of ten in reaction rates). Unfortunately, the methods that are able to produce such accurate results are of limited use since the steep increase of the computational costs with the size of the molecule in question restrict their applicability to about 20 atoms. It is also clear that very large systems with more than 1000 atoms cannot be treated with *ab-initio* quantum chemical methods. However, many interesting chemical problems deal with molecules in the range of 20 to 100 atoms (see Fig. 1.1).

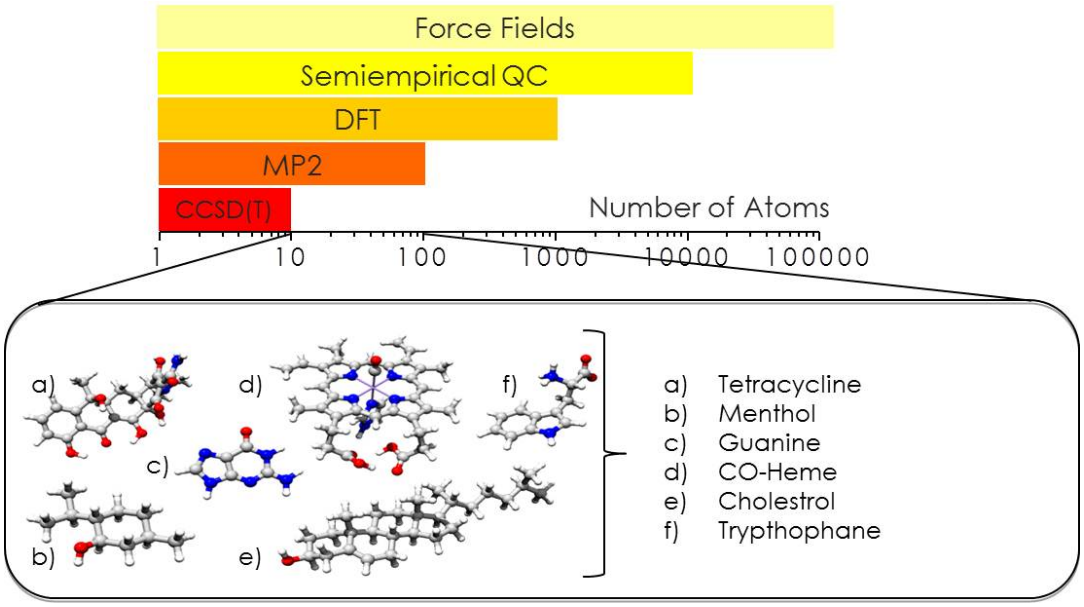

Figure 1.1.: Problematic balance between accuracy and computational costs (Fig. reproduced and modified from Ref. (24)).

Density functional theory (DFT) is the dominantly used computational tool in present day computational studies, particularly if open-shell molecules are involved.[25,26] It offers a very good price/performance ratio and also shows significant robustness.[27] In particular, DFT performs comparatively well in the difficult area of transition metal chemistry where wave-function based methods are sometimes challenging to apply.[25,28]

In the common forms of density functional theory, the energy is written as a functional of the electron density and the effective external potential is generated from a fictive non-interacting reference system (Kohn-Sham (KS) approach).[27] However, not all parts of the Hamiltonian can be written in this way and hence parameters have to be introduced which define a given functional. These usually large number of parameters have to be optimized

using benchmarking sets, and thus DFT methods cannot be improved systematically. The majority of DFT calculations is performed with only a few density functionals that have mainly been developed in the late 1980s (*e.g.* BP86)[29,30] or the hybrid functionals of the early 1990s (*e.g.* B3LYP).[31,32] Despite intense trials, functionals of the same (hybrid) general-gradient (GGA) type that perform uniformly better than these standard choices at comparable computational cost have not been found yet.

Despite the often good performance of DFT, it is still somewhat difficult to foresee areas where the present day functionals do not perform well. First, good performance for ground state energies and geometries may not extend to the calculation of response properties.[25,33–35] For example, time dependent DFT (TD-DFT) for excited states based on GGA or hybrid DFT has some significant problems.[25,36–38] Second, the combined effects of: a) not incorporating the van der Waals interaction; b) the self-interaction problem; and c) the too short-sighted DFT correlation sometimes leads to unexpectedly large errors and qualitative failures, even for molecules as 'simple' as hydrocarbons.[24,39–45] Although the empirical dispersion correction proposed by Grimme *et al.* usually reduces these errors significantly,[46–48] it is still almost unpredictable whether the DFT method will yield accurate results for the systems in question. Recently, new functionals were developed that partially improve on the accuracy of DFT methods for the calculation of *e*.g. barrier heights.[49,50] However, these functionals contain many empirical parameters which have to be optimized using test sets or include elements of correlated wavefunction theory respectively. Hence accurate results are usually only obtained for systems which are similar to the training sets used for the parameter optimization, or, if some wavefunction correlation contribution such as in the recently developed double-hybrid functionals is added at the expense of increased computation cost.[51–57] However, although being very efficient, DFT methods are not able to systematically deliver results of chemical accuracy, *i.e.* about 1 kcal/mol error compared to experimental reference values.[24,50,51,58] Moreover, every computational chemistry study with DFT methods also necessitates an investigation on the functional dependence of the results.

In principle, all of these shortcomings can be overcome by wavefunction based methods. The HF method itself is, of course, too inaccurate to be acceptable as 'modern model chemistry', but a straightforward improvement can be realized by applying perturbation theory. The most common partitioning of the (normal ordered) BO Hamiltonian was proposed by Møller and Plesset.[59] At second order Møller-Plesset perturbation theory (MP2), the correlation energy, defined as the difference between the full-CI energy and the HF energy, appears first. Typically about 70 – 90 % of the exact correlation energy is recovered with the MP2 method. MP2 represents the simplest single reference correlation method and is often a significant improvement over HF. In selected areas, such as weak intermolecular interactions, it performs also better than DFT, but it lacks robustness and is not very successful in application to open-shell systems.[24] However, using efficient approximations, such as the local approximation[60–62] or the 'resolution-of-the-identity' (RI) approximation,[63–69] MP2

energies can usually be calculated faster than the HF reference determinant itself. Hence, its computation time is competitive with (hybrid) DFT. Furthermore, the spin-component scaled MP2 (SCS-MP2) method proposed by Grimme is an improvement over standard MP2.[70,71] Although SCS-MP2 clearly improves the results, the drawbacks of perturbative methods, such as instabilities and convergence problems, remain. Thus, it is still not accurate and robust enough to serve as general basis for large-scale applications in computational chemistry. Concerning higher orders in the perturbative expansion, MP3 is not of great use since it is about as expensive as the coupled pair methods and coupled cluster methods truncated to single and double excitations (*vide infra*), which are generally more robust and accurate. MP4 can yield very accurate results but has a steep $\mathcal{O}(N^7)$ scaling with respect to the system size, and hence it is not of great practical use. Moreover, the general problems of perturbative approaches carry over to higher orders and it is not guaranteed that the perturbative expansion converges at all.[23] Thus, it is of high interest to develop more accurate and robust wavefunction based methods, which can treat larger molecules, particularly of open-shell type, efficiently.

It is evident from MP2 theory that the accuracy of the correlation energy is controlled by the double excitation amplitudes. Therefore, it is reasonable to also truncate the CI expansion at this excitation level. Clearly, an error is introduced in this way since the doubles amplitudes are coupled to quadruple amplitudes which are again coupled to hextuple amplitudes *etc.* Still, the most important part of dynamic correlation is already included at the double excitation level. In the resulting truncated CI singles doubles (CISD) method, the amplitudes are optimized variationally, which corresponds to an infinite order perturbative treatment of the double excitation amplitudes. In principle, this should lead to much better results than those obtained with MP2, where the doubles amplitudes are only determined up to first order. However, the CISD method suffers from a huge drawback. In contrast to Møller-Plesset perturbation theory which is always size-consistent since it fulfils the linked cluster theorem at each order of the perturbative expansion,[72] the truncated CI methods are not size-consistent, which results in a non-physical scaling of the error with the system size. Although many attempts have been made to partially repair this problem (*e.g.* the Davidson correction[73]), the CISD method is still not of great use for computational chemistry. As it will be discussed below, the best way to circumvent the lack of size-consistency is to approximately include higher excitations of disconnected type.

Over the past 50 years, coupled cluster (CC) theory has been developed to be a cornerstone of modern *ab initio* quantum chemistry.[19,74–78] The powerful hierarchy of CC approaches dominates contemporary quantum chemistry if highly accurate results are requested. CC theory based on a single reference determinant represents a systematic and well defined approach for the treatment of dynamical correlation effects. Although being distinctly more intricate than MP2, it combines the desirable feature of being size-extensive and size-consistent, unitary invariant, robust and numerically accurate. A number of highly accurate thermochemistry schemes have been devised on the basis of CC theory, including the W_n[79] or the HEAT

(high accuracy extrapolated *ab initio* thermochemistry)[80] protocols, which can yield results of sub-kJ accuracy. Impressive recent developments even allow the inclusion of connected excitations with arbitrary excitation level.[21,81] However, the tremendous computational cost of such methods limits their applicability to very small molecules which are of limited interest in contemporary computational chemistry.

Using a projective algorithm to solve the CC Schrödinger equation, it is possible to truncate the CC expansion at a certain excitation level. By considering only single and double excitations, which defines the CCSD method,[82] one still obtains the exact result for two-electron systems within a given basis set. Due to the exponential parameterization of the wavefunction, which corresponds to half of an orbital rotation in the single amplitudes case,[83] a certain amount of orbital relaxation is introduced, which greatly enhances the stability in cases where some static correlation comes into play. Furthermore, higher excitations of disconnected type are included automatically. The truncated CC methods are unitary invariant, size-consistent and also size-extensive (if a linked expansion is used). By itself CCSD is not a highly accurate method, but represents a feasible and robust electronic structure approach that is an excellent starting point for the calculation of the remaining correlation energy, molecular properties or excited states,[76,77,84] at least for systems whose mean-field wavefunction is qualitatively well described by a single (HF) determinant. In order to arrive at accurate predictions, however, it is necessary to proceed beyond the level of single and double excitations (CCSD) and include connected triple-excitations at least perturbatively (CCSD(T)). It is commonly referred to as the 'gold standard' of modern computational chemistry since results with chemical accuracy can be obtained for most molecular systems, at least close to their equilibrium geometry and if extensively polarized triple- or quadruple-ζ basis sets are used.[85] It was first proposed by Pople and co-workers in the framework of the quadratic configuration interaction (QCI) method[86] and afterwards employed in the CCSD method.[87] The CCSD(T) method is widely used for studying ground state properties of small molecules and provides benchmark results for more approximate quantum chemical methods. Various alternative formulations for the approximate inclusion of connected triple excitation have been proposed but the one denoted as '(T)' is the most successful in practical applications, although it rather benefits from slight cancellation of errors.[88]

The only obstacle that prevents an even more widespread use of CC methods in computational chemistry are the problems associated with their high intrinsic computational cost that, as pointed out in a similar way by Janowski *et al.*,[89] can only partially be overcome by going to large scale parallel computing facilities. First, these large scale facilities are not available in every research group and, second, the increase in computational effort due to larger system sizes is much faster than the growth of the available computational power. The CCSD method has iterative $\mathcal{O}(O^2V^4)$ asymptotic scaling of the computational cost, where 'O' denotes the number of occupied orbitals in the reference determinant and 'V' correspond to the number of unoccupied (virtual) orbitals that is mainly controlled by the size of the basis set, which in total gives rise to a $\mathcal{O}(N^6)$ complexity (N is a measure of the

system size). Typically, the virtual space is about one order of magnitude larger than the occupied space, at least if large and flexible basis sets are used which are mandatory in order to reach the intrinsic accuracy of the methods. Thus, the size of the virtual space is the actual limitation. Furthermore, the disk space requirements scale as $\mathcal{O}(N^4)$ which becomes rapidly unmanageable, particularly for two-electron integrals involving three or four virtual orbitals. In the CCSD(T) method, a perturbative correction for connected triple excitations is added to the converged CCSD energy which gives rise to a non-iterative $\mathcal{O}(O^3V^4)$ step. In fact, for much of computational chemistry CCSD(T) would be the method of choice if it was not associated with tremendous computational effort due to steep polynomial scaling. While calculations with more than 1000 basis functions are possible using large and massive parallel computation facilities[89] (at least if not too many electrons are correlated), routine applications of the CCSD(T) method become rather cumbersome if more than 500 basis functions are involved. The basis set error can be significantly reduced by extrapolation schemes[90,91] but the preferred extrapolation level involving calculations with triple- and quadruple-ζ correlation consistent basis sets[92,93] is already intractable for many molecular systems of chemical interest. Another possibility is provided by explicitly correlated single reference correlation methods which significantly improve the convergence to the basis set limit.[3,15] Particularly, explicitly correlated methods which include connected triples excitations perturbatively, such as the CCSD(T)$_{\overline{\mathrm{R12}}}$ approach of Valeev and Crawford[94] or the CCSD(T)-F12 methods of Adler, Knizia and Werner[95,96] are promising approaches. However, it is still impossible to treat systems with more than 20-30 atoms without introducing further approximations that significantly reduce both the asymptotic scaling and the computational effort.

Other single reference correlation methods with the same asymptotic scaling behavior are the coupled pair methods and the quadratic configuration interaction approach truncated to single and double excitations (QCISD).[86] The latter is no longer in common use since it is less complete and stable than CCSD, although the results are usually very similar. The first variant of coupled pair type approaches originates from Kelly[97,98] and was first used in a different context. In the 1970s, the coupled pair methods became popular in quantum chemistry and were extensively used at that time.[99–112] Despite the impressively accurate results of the coupled electron pair approximation (CEPA) and the coupled-pair functional (CPF) methods, they later fell into disuse in favour of DFT and CC methods. Recently, new interest has grown in these methods since they offer a number of features that makes them attractive for large-scale use in computational chemistry. The coupled pair approaches are conceptually simple and a variational formulation is straightforward.[106,113] Thus, they lend themselves well to efficient approximations, and the extension to the open-shell[109,110,113] and multireference cases is much easier and unambiguously defined. The latter has been most convincingly demonstrated by Taylor[114] as well as Fink and Staemmler.[115] Other important contributions originate from Fulde and Stoll[116] as well as Malrieu and co-workers in their development of the size-consistent self-consistent configuration interaction method (MR-(SC)^2-CI).[117,118] Furthermore, Nooijen and LeRoy[119] have developed an orbital invariant

CEPA-type approach. The asymptotic scaling of the coupled pair methods still goes with the sixth order of the system size, but compared to CCSD, the computation times are only about half as much. In contrast to CISD they are size-consistent (at least if localized orbitals are employed), but unitary invariance is usually not warranted. The major advantage of the coupled pair approaches are their accurate results. They clearly surpass DFT and MP2 in accuracy and are often more accurate than CCSD and QCISD,[120] sometimes even close to the accuracy of CCSD(T).[24,121,122] This is well documented for potential curves of small molecules[101,123–125] and has also been demonstrated for the thermochemistry of larger polyatomic molecules.[24] However, the coupled pair approaches cannot be extended to include higher connected excitations of arbitrary order. Although this may be seen as less problematic and there are attempts to include renormalized connected triples excitation as well,[119] the CEPA approach is still less complete than the more intricate CC approaches. This becomes obvious for calculations of open-shell systems with larger singles amplitudes, for which the couples pair methods quickly become unstable, and convergence problems can arise.

In a recent work, Huntington and Nooijen have developed the parameterized CCSD method (pCCSD(α, β))[126] and several $\beta = 0$ variants were shown to be closely related (rigourously orbital invariant analogues) of the CEPA methods (*i.e.* the CEPA/1, CEPA/2 methods developed by Meyer[99] and the CEPA/3 approach, which is the original CEPA method proposed by Kelly[97,98]). In fact, the inspiration for the pCCSD approaches stemmed from an investigation of these orbital invariant CEPA-type approaches in the previous work of Nooijen.[119] These so called pXCISD (prototype eXtensive CISD) methods were very much inspired by the original CEPA methods. The pCCSD approach is closer in spirit to CCSD, as its name implies, and explores freedom in the quadratic $\widehat{T}_2$ terms, without a particular emphasis on EPV (exclusion principle violating) type contributions. The pCCSD(α, β) methods are constructed by scaling certain terms in the CCSD doubles residual equations by parameters α and β (see Sec. 2.4) in such a way as to systematically improve accuracy without sacrificing any of its desirable properties (*e.g.* exactness for two-electron systems, size-extensivity and size-consistency, orbital invariance). It was shown that the pCCSD($-1, 1$) approach is a significant improvement over CCSD (which corresponds to pCCSD($1, 1$)) for the calculation of geometries and harmonic frequencies (often approaching the accuracy of CCSD(T)) and for potential energy curves for single bond dissociation in small molecules. The higher robustness of the pCCSD methods compared to the CEPA methods especially pays off for open-shell systems, which have a more complicated electronic structure. However, the introduction of adjustable parameters, which affect the theory itself, might also lead to unpredictably large errors, similar to those observed for DFT methods.

Nonetheless, the ground state of most main group compounds and organic molecules is described at least qualitatively correct by a closed-shell Slater determinant of the restricted Hartree-Fock (RHF) type (Fig. 1.2, part a)), for which the CEPA methods perform very well. On the other hand, many interesting chemical questions and computational studies

involve open-shell states, which naturally occur for radicals and radical pairs. They play a major role as transient reaction intermediates, but also in metal radical assemblies and in their stable form as spin labels.[127] Furthermore, open-shell states are often present in exited states, transition metal complexes[26] and oligonuclear transition metal cluster like the oxygen-evolving complex of photosystem II.[128]

The accurate quantum chemical description of open-shell molecules is more difficult than for closed-shell molecules. Nonetheless, the majority of open-shell states is conceptually well described by a single Slater determinant of high-spin type, where all unpaired electrons are coupled with parallel spins, as illustrated in Fig. 1.2, part b). Thus, single reference correlation methods are reasonable choices for the high-spin open-shell case. The question of choosing an appropriate reference determinant will be discussed in Sec. 2.1.

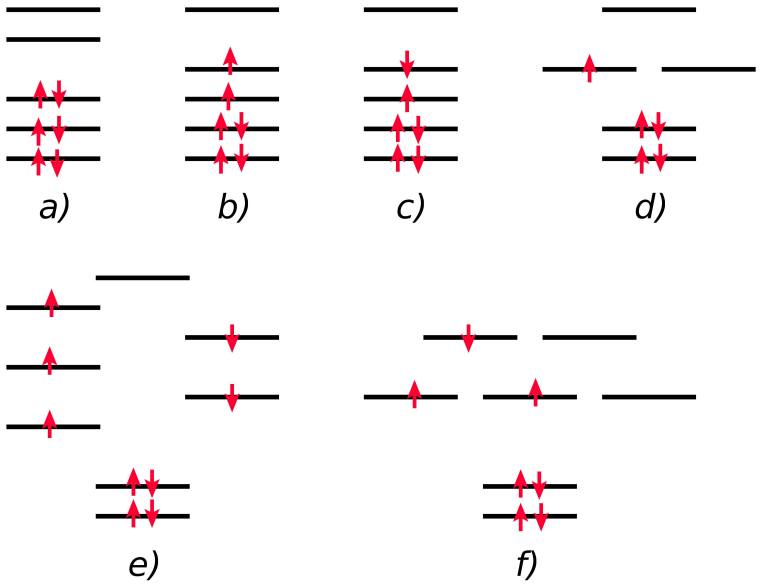

Figure 1.2.: Illustration of different electronic states: a) closed-shell, b) high-spin open-shell, c) open-shell singlet, d) degenerate state, e) antiferromagnetic coupling f) d-d multiplets.

However, a given orbital configuration can give rise to more than one electronic state. These so called multiplets are difficult to describe correctly with a single reference determinant. They can lead to degenerate states, which often occur for the d-d excitation manifold of transition metal complexes (Fig. 1.2, part f)), open-shell singlet states as found in biradicals and metal-radical interactions (Fig. 1.2, part c)) or, more generally, bonding situations involving antiferromagnetic coupling like *e.g.* exchange couplings in transition metal clusters[128] (Fig. 1.2, part e)). Although a restricted open-shell Hartree-Fock (ROHF) determinant[129] or a broken-symmetry approach[130,131] can be used to describe these more complicated open-shell states qualitatively correctly, a proper multideterminant reference wavefunction is required for an accurate and unambiguous quantum chemical treatment, but this is out of the scope of this work. Returning to the high-spin open-shell case treated here, MP2 is not particularly successful. Much better results are obtained with CEPA methods, but these are

usually not very robust and are prone to convergence problems if larger singles or doubles amplitudes occur, which are indicative of multireference character of the N-electron wavefunction to some extent. In this respect, the CCSD method is more reliable due to the orbital relaxation introduced via the exponential parametrization of the single excitations. The errors, compared to experimental reference values, however, are usually significantly larger and connected triple excitations have to be incorporated at least perturbatively in order to reliably obtain results with chemical accuracy.[24] Furthermore, it should be noted that the extension of the CC methods to the open-shell treatment is much more involved compared to the CEPA methods.[132,133]

The central hypothesis of the present work is that any method that promises to be of major utility for chemical applications must also not be much more expensive than hybrid DFT or MP2. Furthermore, extension to the open-shell case should be possible. Moreover, in order to find large acceptance by the computational chemistry community, such methods should be of 'black-box' character and significantly and systematically more accurate and robust than either hybrid DFT or MP2. The development and implementation of such a method is the aim of this work. Thus, it should be emphasized that the new approach does not try to compete with very high-accuracy quantum chemical approaches, but rather with DFT and MP2.[24] Ultimately, the aim is of course a method that can provide results with chemical accuracy and be applicable to larger molecules (up to ~150 atoms) while having reasonable computation times (not more than a few days for a single point energy calculation). Hence, the scope of this work is to find suitable approximations to the coupled pair and CC methods that retain their accuracy but reduce the asymptotic scaling of the computation time with respect to the systems size and the pre-factor as well. However, their desirable properties should be maintained as much as possible without introducing non-physical artifacts. Furthermore, these approximations should be generally applicable and robust.

1.3. Local correlation methods

Many attempts in this direction have been suggested in the literature, but only very few match all of the criteria discussed above. In order to reduce the high-order polynomial scaling of the single reference correlation methods, which clearly limits their applicability, it is beneficial to introduce approximations that take advantage of the local nature of dynamic correlation effects and reduce the information about the correlating space to the most important parts, either by taking advantage of the sparsity or compression of the internal and external space respectively. Both can be achieved using tensor decomposition and factorization,[134–137] which are closely related to (higher order) singular value decomposition techniques.[138] Furthermore, density fitting (DF) synonymic with the RI approximation[63–69] can be used to reduce the scaling of integral transformations, for example.

Since the total correlation energy is given by the sum of the individual pair correlation

energies, which decay rapidly if the two electrons are spatially distant, it is possible to truncate the number of electron pairs at a certain level. This is commonly referred to as 'strong pair approximation' and was first proposed by Pulay.[139] Such a truncation of the internal space is of course most effective if the orbitals have been localized in advance, since this provides the necessary sparsity.

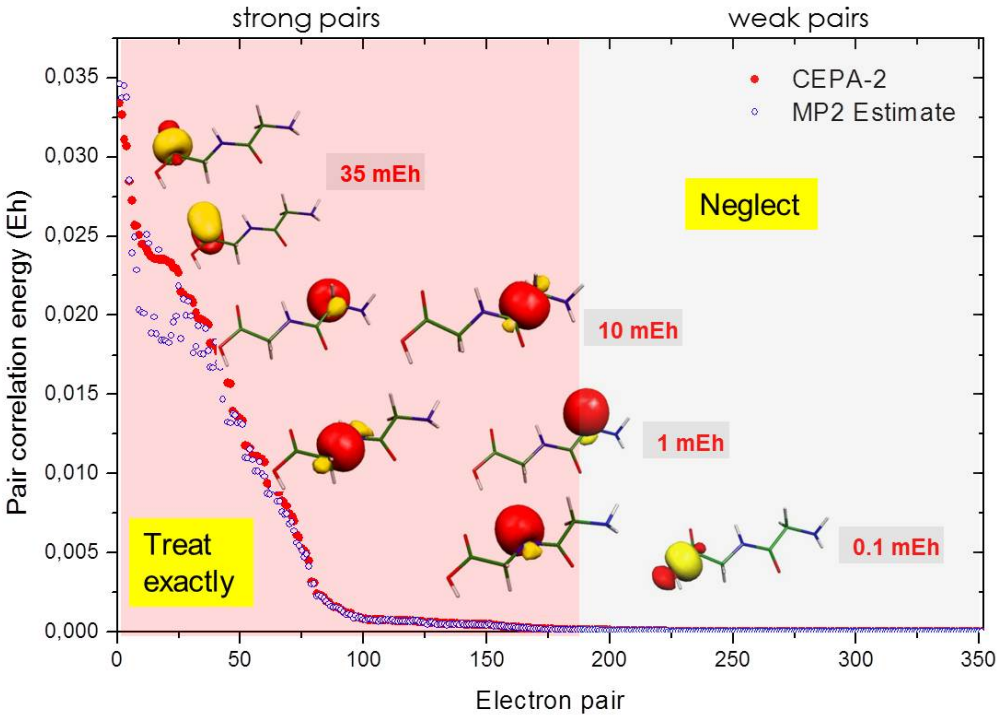

Figure 1.3.: The strong pair approximation for the glycine dimer (localized internal orbitals as well as MP2 and CEPA/2 pair correlation energies are plotted).

It is obvious from Fig. 1.3 that many electron pairs contribute only to a very small fraction of the total correlation energy (the so called 'weak pairs') and hence they may be rejected from the correlation treatment. Furthermore, the MP2 pair correlation energies for weak pairs are almost identical to that calculated by the more accurate (but also more expensive) CEPA/2 method. Thus, the former may be used as an estimate for the weak pair correlation energy. However, the external space is typically one order of magnitude larger than the internal space and it thus introduces the computational bottleneck in the calculations (contractions between two-electron integrals and excitation amplitudes involving many external labels). It is also possible to localize the external space, for example by using projected atomic orbitals (PAOs) introduced by Pulay and Saebo.[140] They have pioneered the local correlation approaches that make use of local correlation domains,[140,141] which gave birth to a large body of research on local correlation methods in recent decades. In this approach, localized internal orbitals and PAOs are used to span the occupied and virtual spaces respectively. Each localized orbital is assigned to a domain of projected PAOs that is located in the same region of space as

the parent internal orbital. Furthermore, unions of local domains are formed for the different excitations, and the corresponding excitations are only allowed into these local domains. Pulay and Saebo have also provided recipes to construct these domains and implemented various correlation methods within this scheme.[141–143]

Significant efforts have been made in the past two decades towards the development of low-order scaling correlation methods based on a variety of different ideas, but only a few of them will be mentioned here, *e.g.* the incremental scheme proposed by Stoll[144] and recently discussed by Friedrich and Dolg.[145] The method of Flocke and Bartlett based on Weinhold's natural bond orbitals,[146,147] the fragment correlation approach of Fedorov and co-workers[148] and the cluster in molecule (CIM) methods developed by Li and Piecuch[149,150] fall into a similar category (a recent review about fragmentation methods was published by Gordon and co-workers[151]). These schemes are potentially linear scaling since the full correlation treatment on the entire system in question is avoided, but it remains to be seen to which computational efficiency they can be developed. For the CIM approach applied to standard and renormalized CC methods,[149,150] this has been already achieved and first applications yielded promising results.[152]

Early local CC methods were developed by Laidig and co-workers.[153,154] Friesner and co-workers have developed local pseudo-spectral MP2 methods and demonstrated its efficiency.[155] Head-Gordon and co-workers have explored a number of creative local correlation approaches,[156,157] but apparently, the applicability and efficiency of these methods for large molecules has not yet been demonstrated.

As already mentioned, the dominant computational effort occurs in contractions between integrals and excitation amplitudes over virtual orbitals and thus, it is most important to compress the size of the external space. Efforts in this direction were reported by Helgaker, Klopper and co-workers, who used frozen approximate natural orbitals[158] and Urban *et al.*,[159] who employed an 'optimized virtual space' (OVS) first proposed by Adamowicz and Bartlett.[160] Recently, the latter has been reformulated by Yang and co-workers[134,135] in the framework of local MP2 and local CCSD. In this approach, orbital-specific virtual (OSV) subspaces are used to span the correlation space. Furthermore, Rolik and Kállay have combined the OSV approach with the CIM scheme for higher order CC methods.[161,162] Moreover, Hohenstein *et al.*[163] showed that the use of truncated virtual spaces via approximate natural orbitals is also of great advantage in the context of symmetry adapted perturbation theory (SAPT).

The probably most widespread variant of local correlation methods for which high computational efficiency and applications involving large molecules[164] were demonstrated is the work of Werner, Schütz and co-workers[165] within the domain concept originally proposed by Pulay and co-workers.[139–142] They have developed the domain concept to its full potential and produced highly efficient production level implementations.[60,165–167] Linear scaling spin-adapted closed-shell implementations for various local ground state correlation meth-

ods (MP2,[168] CCSD,[167] CCSD(T),[169] iterative CCSD-T_{1b}[170]) as well as local excited state correlation methods (EOM-CCSD[171] and CC2[172]) were developed during the last decade. Furthermore, this local correlation approach was successfully combined with explicit correlation.[173,174] However, open-shell implementations were only recently reported.[175] Although the general concepts of local correlation methods can be used for open-shell variants in an analogous way, the CC treatment of open-shell systems is significantly more complex.[132,133] With proper programming and extensive use of various thresholds, these methods can be made to scale linearly with respect to all computational resources (disk space, main memory and CPU). Furthermore the RI approximation (Werner and co-workers prefer to call this methodology density fitting) is used to further speed-up the calculations.[168] In order to maintain an accurate approximation to the parent methods, a number of cut-off parameters must be introduced that control the domain sizes. Furthermore, a hierarchical treatment of electron pairs based on real-space cut-offs is pursued in which pairs are assigned as 'strong' (treated as accurately as possible), 'close' (treated perturbatively), 'weak' (treated perturbatively), 'distant' (treated perturbatively), and 'very distant' (neglected).[176] With the standard definition of the correlation domains introduced by Boughton and Pulay,[177] the PAO based local correlation approaches recover ~98 – 99 % of the canonical correlation energy.[60,166,167] The definition of the domains appears to require insight and experimentation to avoid artifacts or discontinuities in potential energy surfaces.[178] Using 'extended domains', these problems are much less acute[165] (~99.6 % (for local CCSD) and ~99.1 % (for local MP2) of the respective target correlation energy are recovered on average), but the computations also become much more time consuming, at least at the CC level of theory.

1.4. The local pair natural orbitals (LPNO) approach

In the PAO-based local correlation approach, it is necessary to decide before the calculation which domains should be correlated. Such real-space cut-offs, although they allow to benefit from sparsity in the correlation space to maximum extent, are always dangerous to apply since it is the responsibility of the user to choose the appropriate domains. Therefore, besides using the sparsity of the internal space spanned by localized orbitals, compression of the entire virtual correlations space without applying real-space cut-offs should be preferred. This can be accomplished in an optimal way by using truncated pair specific subspaces spanned by approximate pair natural orbitals (PNOs). The combination of latter with the strong pair approximation (see Fig. 1.3) for the occupied space defines the new local correlation approach, denoted the 'local pair natural orbital' (LPNO) method.

PNOs were introduced first by Kraus and Edmiston[179,180] (denoted 'pseudo natural orbitals' at that time). Their use in chemistry was pioneered by Kutzelnigg and Ahlrichs in the framework of the independent pair approximation (IEPA)[181,182] and by Meyer within the more accurate CEPA approach.[99–101,107] They represent a highly compact, pair specific

set of orbitals that was extensively and successfully used in the 1970s.[101–103,108,109] Meyer showed that the non-orthogonality between PNOs of different pairs only leads to small complications in the solution of the CEPA equations.[107] However, the computer hardware available at that time did not allow calculations on large molecules, and thus local correlation approaches did not play an important role at that time.

The the additional trick of spanning the external orbital space by approximate pair natural orbitals allowed the pioneers of the CEPA methods to perform calculations with, at the time, extended basis sets and to obtain accurate results that were greatly ahead of their time. It is acknowledged that the old PNO-CEPA methods recover 98 – 99 % of the corresponding CEPA correlation energy, similar to what is achieved with the PAO-based local correlation methods using standard domains. The old PNO methods were later abandoned in favor of matrix-driven direct CI approaches such as the 'self-consistent electron pairs' (SCEP) method proposed by Meyer.[183,184] Most of the modern implementations of truncated CI and CC methods are based on this concept.[185,186]

In order to understand why the PNOs are particularly suited for the compression of the external correlation space, it is instructive to reiterate the theory of natural orbitals (NO) first. Applying a suitable unitary transformation that diagonalizes the first order spin-free reduced density matrix[187] yields a set of so called natural orbitals (NOs) which were first introduced by Löwdin in 1955.[188,189] They are arranged by decreasing occupation numbers which are in the range of zero to two and sum up to the total number of electrons. Usually, the complete set of NOs can be divided into orbitals with an occupation number close to two (strongly occupied NOs) and remaining orbitals with small occupation numbers (weakly occupied NOs). A Slater determinant constructed from the strongly occupied NOs usually closely resembles the Hartree-Fock determinant. Hence, their occupation numbers reflect the importance of the corresponding orbitals in the N-electron wavefunction. NOs can be used to illustrate electron correlation effects and to gain insights about the electron correlation problem since the correlation brought in by a given NO is also closely related to its occupation number.[190]

The selection of an optimal set of orbitals for the CI expansion is a crucial point for correlation methods based on a multideterminantal expansion of the N-electron wavefunction, *i.e.* the corresponding CI expansion should need the fewest number of configurations to converge to a given accuracy. Already Löwdin[188,189] presented mathematical arguments showing that a CI expansion based on NOs ('natural expansion') leads to particularly fast convergence of the latter. Löwdin and Shull[191] then presented a rigorous proof that for two-electron systems a natural expansion is the most rapid. Later, Davidson[190] showed for N-electron systems that NOs lead to the fastest convergence of the first order reduced density matrix. Shavitt *et al.*[192] analysed the energy convergence of natural expansions and found remarkable advantages compared to CI expansions based on canonical MOs.

Recently, Ruedenberg *et al.*[193] proposed another set of orbitals called 'split-localized orbitals', which can indeed yield stronger convergence of the CI expansion than natural orbitals, both

in the wavefunction as well as in the energy, at least within the chemical accuracy range of about 1 kcal/mol. A split-localized orbital set consists of two subsets, strongly and weakly occupied localized MOs. They are obtained by separate localization of the strongly and weakly occupied NOs. However, besides a few exceptions, a good localization destroys symmetry adaption. Hence split-localized orbitals are, in contrast to NOs, usually not symmetry adapted. Its their special localized nature that leads to a very compact CI expansion and extremely rapid convergence of the energy, at least for accuracies smaller than 0.1 $\mathrm{mE_h}$. However, exact NOs can only be obtained from the exact first order reduced density matrix which implies the knowledge of the exact N-electron wavefunction. Fortunately, it could be shown that the convergence of approximate NOs towards the exact ones is rather fast.[194,195] NOs with very small occupation numbers can be omitted from the one-electron space with negligible consequence on the accuracy of the CI expansion. Initially, the energetic convergence is very rapid but becomes extremely slow towards the end. This is not surprising since it is very difficult to recover the last few thousandths of the exact correlation energy with correlation methods based on antisymmetrized orbital products composed from smooth one-electron functions.

Approximate pair natural orbitals (PNOs) can be constructed from the so called virtual pair density.[194,195] To this end, one assumes a two-electron problem equivalent to an electron pair. For a single Slater determinant wavefunction, the spin-free reduced one-particle density matrix equals two times the unity matrix, and thus the virtual correlation space cannot be represented at all. However, it is of course possible to yield a better and more sophisticated spin-free reduced one-particle density matrix within a perturbative, configuration interaction or coupled cluster scheme. It then exhibits diagonal elements different from two and non-vanishing off-diagonal elements. The spin-free one-electron reduced density matrix of a two-electron system is denoted pair density. For each pair (i, j) of internal orbitals, it is now possible to define such a pair density. The set of unoccupied orbitals are the same as for the many-electron system. Using this orbital subset, one can again apply perturbation theory to yield a better wavefunction with a non-diagonal reduced one-particle density matrix. That of pair (i, j) is called the 'virtual pair density', which can be diagonalized to obtain the approximate PNOs. The eigenvalues correspond to the occupation number of the given PNO. All PNOs with a smaller occupation number than a certain threshold value can be neglected.[195] In this way, the external correlating space is greatly compressed. Figurative speaking, this procedure picks out the most important part of the virtual subspace which is necessary to describe the electron correlation of pair (i, j) physically correct. This is closely related to the mathematical concept of (higher order) singular value decomposition.[136,138]

The PNOs have a number of attractive features. As shown in Fig 1.4, they are located in the same region of space as the associated internal pair, but as delocalized as the physics demands it. Moreover, there is only a small number of significant PNOs per electron pair and a vanishing number of PNOs (0 – 5) that span the virtual correlation space of a weak pair.

In contrast to PNOs, canonical virtual molecular orbitals (VMOs) are maximally delocalized (see Fig. 1.5), and hence truncation schemes based on canonical VMOs are not particularly successful. On the other hand, PAOs are maximal localized which can lead to an inappropriate description of the external correlation space. Thus, a truncated PNO expansion seem to be the best choice for reducing the complexity of the external correlation space.

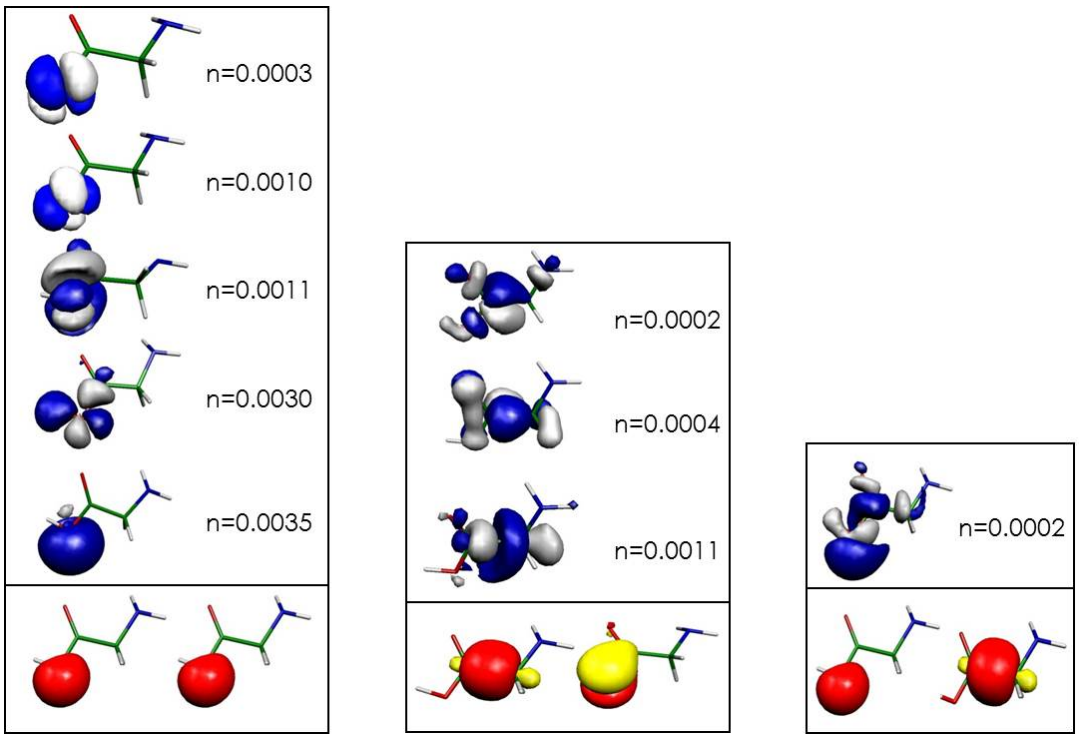

Figure 1.4.: Illustration of the PNOs (in the upper part of each sub-figure; n: occupation number of the respective PNO) associated to three electron pairs of the glycine molecule (left: strong pair; middle: medium pair; right: weak pair).

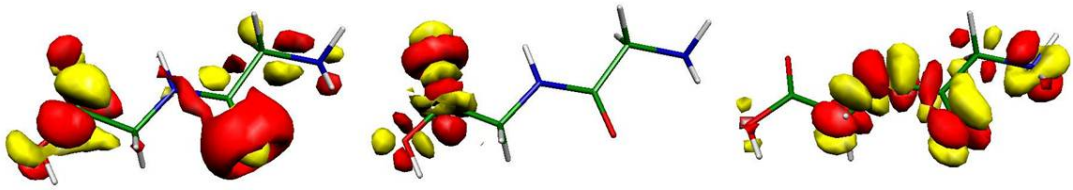

Figure 1.5.: Illustration of three canonical virtual orbitals of the glycine dimer.

In this work, the early PNO methods were revived and combined with the strong pair approximation for the internal space which gave birth to the LPNO methods. Compared to the early PNO-CI and PNO-CEPA programs, the LPNO approach proposed in this work reveals some important differences (a more detailed comparison of the LPNO methods with the old PNO-CEPA methods can be found in Sec. 4.2). The most significant of these are,

- that the RI approximation[66] is used to generate all integrals over MOs and PNOs,
- that doubles amplitudes are not transformed to the AO basis to construct the external exchange operator (EEO, Eq. (2.11)) but transformed integrals over PNOs are stored on disk,
- that single excitations are not truncated,
- that no diagonal approximation to the CI expansion is made.

Using the LPNO approach, serial and parallel production level implementations of various closed-shell and open-shell coupled pair methods as well as QCISD and CCSD were developed and extensively tested.[196–199] The use of approximate PNOs in the CC framework is reported for the first time. Moreover, it was investigated whether the adaptation of the perturbative triples correction to accommodate pair natural orbitals appears to be possible in an efficient and accurate way since this would significantly extent the scope of the LPNO approach for chemical applications. Schütz and Werner have impressively shown that this can be realized with high efficiency in the PAO based framework.[165,169] Furthermore, an LPNO implementation of the pCCSD methods is reported. Since we have kept the local scheme as simple as possible, the LPNO methods are 'black-box' and do not require lengthy experimentation with thresholds or cut-offs prior to an computational chemistry application. Comprehensive test calculations and timings show that the approximate PNOs combine in a very natural and efficient way with local correlation approaches to yield methods that are efficient, accurate and robust.

2. Theory and Implementation

2.1. The reference wavefunction

Reliable results with single reference methods can only be obtained if the reference wavefunction provides a qualitatively correct description of the systems electronic structure. Thus, the choice of the reference determinant plays a crucial role. Usually, a single Slater determinant obtained from a preceding Hartree-Fock calculation is utilized in this context. This works well for closed-shell molecules. However, for open-shell molecules and in particular for transition metal complexes it is much more difficult to find a good reference wavefunction (for a recent discussion see Ref. (83)). Using the single determinant HF approach, high-spin open-shell states can either be described with a spin-polarized, spin-unrestricted wave function (UHF) using different spatial orbitals for α and β spin electrons or, alternatively, with a spin-adapted restricted open-shell determinant (ROHF). In the latter case, the doubly occupied (DOMO) subspace is described with restricted orbitals analogously to the closed-shell case and the singly occupied (SOMO) subspace is treated separately. The UHF wave function is not an eigenfunction of the $\hat{S}^2$ operator, which can lead to convergence problems and spoils the accuracy of the respective post-HF method, especially if spin-dependent properties are calculated. By contrast, the ROHF wave function does not suffer from spin-contamination. Owing to the smaller number of variational parameters, the ROHF energy is higher than the UHF energy. Additionally, the ROHF equations are often more difficult to converge.[200] A compromise between both approaches is offered by the construction of quasi-restricted orbitals (QROs).[201] The QRO determinant is identical with the determinant formed from the leading natural orbitals of the UHF wavefunction. This determinant is a spin eigenfunction that is very close to the ROHF determinant.[202] According to their occupation numbers unrestricted natural orbitals obtained from UHF orbitals are classified as DOMOs, SOMOs or virtual MOs (VMOs). The DOMOs diagonalize the spin-down Fock operator, the VMOs the spin-up Fock operator and the open-shell orbitals their average.

A crucial point of the LPNO approach is to take advantage of the locality of pair correlation energies, *i*.e. to exploit the sparsity of the occupied space. Thus, it is necessary to localize the internal orbitals, which can be done in many ways.[175] Based on numerical investigations (see Sec. 3.2.6), the Foster-Boys localization algorithm[203] is slightly preferred since it is efficient and uses a physically motivated localization criterion. In the extension of the LPNO approach to the open shell case, only the DOMO subspace will be localized since the SOMO subspace is usually too small to obtain well localized orbitals. However, even with a restricted

open-shell reference determinant, the coupled cluster equations are still solved in a spin-unrestricted manner since there is no straightforward and unambiguous way of defining a restricted open-shell coupled cluster method.[204] Although general spin adaptation of open-shell coupled-cluster theory is possible,[132] the resulting equations are even more complex and expensive to solve than in the spin-unrestricted formalism. The present open-shell LPNO implementation is general enough to deal with either spin-restricted or unrestricted reference determinants of both HF or non-HF type (*e.g.* determinants obtained from unrestricted Kohn-Sham (UKS) DFT calculations). The ability to use other than HF orbitals is very important since the UHF reference tends to be an extremely poor starting point for many transition metal complexes.[83]

2.2. Truncated configuration interaction and the coupled electron pair approximation

2.2.1. Closed-shell spin-restricted CISD and CEPA equations

Since the LPNO approach was first implemented in the framework of closed-shell coupled pair methods, we will start we a discussion of the corresponding theoretical background and implementation details of the latter. The same diagrammatic and projective techniques to derive the working equations as well as the iterative procedure for solving the resulting equations as for for the CCSD method (see Sec. 2.3) can be applied in the framework of the coupled pair methods. The respective diagrammatic representations of the singles and doubles residuals as well as their algebraic translations correspond to subsets of Fig. 2.2 and Fig. 2.1 (only the diagrams without amplitude products). It should be noted that the CI amplitudes are commonly denoted $\mathbf{C}$ (in contrary to the exponentially parameterized CC amplitudes, which are usually denoted $\mathbf{t}$). Following Saebo, Meyer and Pulay,[186] the generator state formalism leads to the following linearly parameterized closed-shell CISD wavefunction (as usual, (i,j,k,l) refer to occupied orbitals in the HF reference determinant, and (a,b,c,d) to virtual orbitals):

$$\Psi = \Psi_{HF} + \sum_{ia} C_a^i \Psi_i^a + \sum_{i \leqslant j} \sum_{ab} C_{ab}^{ij} \Psi_{ij}^{ab} \quad . \tag{2.1}$$

The singles and doubles configuration state functions (CSFs) are

$$\Psi_i^a = \widehat{E}_i^a \Psi_{HF} = \Phi_i^a + \Phi_{\bar{i}}^{\bar{a}} \quad , \tag{2.2}$$

$$\Psi_{ij}^{ab} = \widehat{E}_j^b \widehat{E}_i^a \Psi_{HF} = \Phi_{ij}^{ab} + \Phi_{\bar{i}\bar{j}}^{\bar{a}\bar{b}} + \Phi_{\bar{i}j}^{\bar{a}b} + \Phi_{i\bar{j}}^{a\bar{b}} \qquad (i \neq j) \quad , \tag{2.3}$$

$$\Psi_{ii}^{ab} = \Phi_{i\bar{i}}^{a\bar{b}} \qquad (i = j) \quad , \tag{2.4}$$

where $\widehat{E}_q^p = \hat{a}_{p\alpha}^\dagger \hat{a}_{q\alpha} + \hat{a}_{p\beta}^\dagger \hat{a}_{q\beta}$ is the usual spin-free orbital replacement operator and $\Phi_{ij..}^{ab..}$ is the Slater determinant in which the occupied spin-orbitals $(i, j, \dots)$ are replaced by the spin-orbitals $(a, b, \dots)$. The overbar denotes spin-down orbitals. The corresponding contravariant CSFs are given by

$$\tilde{\Psi}_{ij}^{ab} = \frac{1}{6}\left[\Phi_{ij}^{ab} + \Phi_{\bar{i}\bar{j}}^{\bar{a}\bar{b}} + 2\Phi_{ij}^{\bar{a}\bar{b}} + 2\Phi_{i\bar{j}}^{a\bar{b}} - \Phi_{i\bar{j}}^{a\bar{b}} - \Phi_{\bar{i}j}^{\bar{a}b}\right] \quad , \tag{2.5}$$

$$\tilde{\Psi}_{ii}^{ab} = \Phi_{ii}^{ab} \quad , \tag{2.6}$$

$$\tilde{\Psi}_{i}^{a} = \tfrac{1}{2}\left[\Phi_{i}^{a} + \Phi_{\bar{i}}^{\bar{a}}\right] \quad . \tag{2.7}$$

The doubles residual

$$\sigma = \left\langle \tilde{\Psi}_{ij}^{ab} | H - E_0 - \Delta^{ij} | \Psi \right\rangle \quad (\text{with} \quad E_0 = \langle \Psi_{HF} | H | \Psi_{HF} \rangle) \tag{2.8}$$

for the closed-shell CEPA methods is given by ($i \leqslant j$, all a, b)[186]

$$\begin{aligned}
\sigma_{ab}^{ij} = \quad & K_{ab}^{ij} + \mathbf{K}(\mathbf{C}^{ij})_{ab} + \left(\mathbf{F}^{V\dagger}\mathbf{C}^{ij} + \mathbf{C}^{ij}\mathbf{F}^{V}\right)_{ab} - \sum_k \left(F_{jk}C_{ab}^{ik} + F_{ik}C_{ab}^{kj}\right) + \sum_{kl} K_{kl}^{ij} C_{ab}^{kl} \\
& + \sum_k \left((2\mathbf{C}^{ik} - \mathbf{C}^{ik\dagger})(\mathbf{K}^{kj} - \tfrac{1}{2}\mathbf{J}^{kj}) + (\mathbf{K}^{ik} - \tfrac{1}{2}\mathbf{J}^{ik})(2\mathbf{C}^{kj} - \mathbf{C}^{kj\dagger})\right)_{ab} \\
& - \sum_k \left(\tfrac{1}{2}\mathbf{C}^{ik\dagger}\mathbf{J}^{jk\dagger} + \tfrac{1}{2}\mathbf{J}^{ik}\mathbf{C}^{kj\dagger} + \mathbf{J}^{jk}\mathbf{C}^{ik} + \mathbf{C}^{kj}\mathbf{J}^{ik\dagger}\right)_{ab} \\
& - \sum_k \left(K_{ka}^{ji} C_b^k + K_{kb}^{ij} C_a^k\right) + \left(\mathbf{K}^{ia}\mathbf{C}^{j} + \mathbf{K}^{ja}\mathbf{C}^{i}\right)_b \\
& - \Delta^{ij} C_{ab}^{ij} \quad ,
\end{aligned} \tag{2.9}$$

and the corresponding singles residual reads[121,186]

$$\begin{aligned}
\sigma_a^i = \quad & F_a^i + \left(\mathbf{F}^V\mathbf{C}^i\right)_a - \sum_j F_{ij}C_a^j - \sum_{jkb}(2K_{jb}^{ik} - J_{jb}^{ik})C_{ba}^{kj} \\
& + \sum_j \left((2\mathbf{K}^{ij} - \mathbf{J}^{ij})\mathbf{C}^j + \mathbf{F}^j(2\mathbf{C}^{ij\dagger} - \mathbf{C}^{ij}) + \left\langle (2\mathbf{K}^{ia} - \mathbf{K}^{ia\dagger})\mathbf{C}^{ij\dagger} \right\rangle\right)_a \\
& - \Delta^i C_a^i \quad ,
\end{aligned} \tag{2.10}$$

where the following definitions were applied:

$$\mathbf{K}(\mathbf{C}^{ij})_{ab} = \sum_{cd}(ac|bd)C_{cd}^{ij} \quad , \tag{2.11}$$

$$K_{rs}^{pq} = (pr|qs) \quad , \tag{2.12}$$

$$J_{rs}^{pq} = (pq|rs) \quad , \tag{2.13}$$

$$\langle \mathbf{AB} \rangle = \sum_{pq} A_{pq}B_{qp} \quad . \tag{2.14}$$

The two-electron integrals are written in (11|22) notation and $\mathbf{F}$ is the closed-shell Fock operator with $\mathbf{F}^V$ being its virtual sub-block. The validity of Brillouin's theorem[205] is not assumed. The amplitudes C_a^i, C_{ab}^{ij} are collected in vectors $\mathbf{C}^i$ and matrices $\mathbf{C}^{ij}$ wherever appropriate. The so called shifts Δ^i and Δ^{ij} are dependent on the respective coupled pair variant and their individual definitions can be found in Ref. (121). For the CISD method, they correspond to E_{corr}, the total correlation energy, that is given by

$$E_{corr} = \sum_{i \leqslant j} K_{ab}^{ij} \tilde{C}_{ab}^{ij} \quad , \tag{2.15}$$

with

$$\tilde{C}_{ab}^{ij} = \tfrac{1}{1+\delta_{ij}}(4C_{ab}^{ij} - 2C_{ba}^{ij}) \quad . \tag{2.16}$$

For the various CEPA methods, the shifts are a function of the individual pair-correlation energies:

$$\varepsilon_{ij} = \sum_{ab} K_{ab}^{ij} \tilde{C}_{ab}^{ij} \quad . \tag{2.17}$$

These equations were implemented in an efficient, matrix driven form into the 'orca_mdci' module of the ORCA quantum chemistry program package.[206] Moreover, stationarity of the CI-coefficients is straightforwardly restored by passing on to the coupled pair (CPF) formalism or variational CEPA methods that yield results closely related to the standard CEPA methods.[104,113,207] The LPNO approach was also applied to this type of coupled pair methods, but a detailed discussion of the latter can be found elsewhere.[121] Furthermore, the extension of the coupled pair approach to the spin-unrestricted open-shell case[113] is straightforward and will not be repeated here.

Typically, the construction of the external exchange operators (EEOs) defined in Eq. (2.11), account for about 80% of the computation time which is due to the steep $\mathcal{O}(O^2V^4)$ scaling. This contribution can either be calculated in the MO basis or in the AO basis as discussed on various occasions by Meyer,[107] Saebo *et al.*,[186] and Werner.[208]

2.2.2. Pair Natural Orbitals

In the present work, we seek for an efficient approximation to these equations. Obviously, the most important issue is the treatment of the external orbital space. With high-quality basis sets the external space is much larger than the internal space and practically all of the computation time is spent in contractions involving the external labels. In addition, the storage requirements rise steeply with the number of external orbitals. Thus, it is highly desirable to compress the information contained in the external orbital space to the largest possible extent. This was impressively achieved by the pioneers of the CEPA methods by passing on to a pair-natural orbital (PNO) formalism. In this approach, each electron pair is treated by the most rapidly converging expansion of external orbitals, that, by definition is provided by the natural orbitals that are specific for this pair. A rigorous calculation of

these orbitals would require the CISD equations to be solved for each pair separately in the absence of the other pairs (e.g. the independent electron pair approximation, IEPA[182]). Since this involves the repeated construction of the EEO, it would be as expensive as the original CISD calculation. Ahlrichs and Driessler have discussed an iterative method that converges to the exact PNOs of a pair.[195] In practice, it turns out that approximate PNOs perform almost equally well. Clearly, the simplest way to construct the PNOs is to start from the MP2 amplitudes for a given pair

$$C_{ab}^{ij} = -\frac{K_{ab}^{ij}}{\varepsilon_a + \varepsilon_b - \varepsilon_i - \varepsilon_j} \quad , \tag{2.18}$$

where the ε's represent the orbital energies. If one uses localized internal orbitals (as it is done throughout in the LPNO framework), the internal orbital energies are replaced by the diagonal elements of the closed-shell Fock operator in the local MO basis. From these amplitudes, the virtual pair density can be calculated which is given by

$$\mathbf{D}^{ij} = \frac{1+\delta_{ij}}{N_{ij}} \left(\tilde{\mathbf{C}}^{ij\dagger} \mathbf{C}^{ij} + \tilde{\mathbf{C}}^{ij} \mathbf{C}^{ij\dagger} \right) \quad , \tag{2.19}$$

with the norm

$$N_{ij} = 1 + \left\langle \tilde{\mathbf{C}}^{ij\dagger} \mathbf{C}^{ij} \right\rangle \quad . \tag{2.20}$$

Diagonalization of $\mathbf{D}^{ij}$ yields the so called MP2-PNOs expanded in terms of virtual MOs (from now on, the overbar is used to denote PNOs rather than spin-down orbitals):

$$\mathbf{D}^{ij} \mathbf{d}^{ij} = n^{ij} \mathbf{d}^{ij} \tag{2.21}$$

The n^{ij} are the PNO occupation numbers. Using the PNO expansion coefficients $\mathbf{d}^{ij}$, any virtual MO can be projected onto the respective pair-specific PNO subspace:

$$\left| \bar{a}^{ij} \right\rangle = \sum_a d_{a\bar{a}}^{ij} \left| a \right\rangle \quad . \tag{2.22}$$

However, the back-projection onto the full VMO space is, at least in principle, only possible if the PNO expansion would not be truncated. Otherwise, such a projection must be considered as an approximation:

$$|a\rangle = \sum_{\bar{a}^{ij}} d_{\bar{a}a}^{ij} \left| \bar{a}^{ij} \right\rangle \quad . \tag{2.23}$$

Obviously, the PNOs inside each pair are orthonormal but the PNOs of different pairs are not. The overlap between the PNOs of different pairs is given by

$$\left\langle \bar{a}^{ij} | \bar{b}^{kl} \right\rangle = (\mathbf{d}^{ij\dagger} \mathbf{d}^{kl})_{\bar{a}\bar{b}} \equiv S_{\bar{a},\bar{b}}^{ij,kl} \quad . \tag{2.24}$$

In the early implementations of coupled pair methods, it was customary to differentiate

between singlet and triplet pairs.[209] As discussed by Saebo, Meyer and Pulay,[186] in the generator state formalism this is neither necessary nor desirable and hence, it is preferable to work with a single set of PNOs for each (i,j) pair.

2.2.3. Improved PNOs

In his pioneering work, Meyer suggested an elegant method to obtain improved PNOs.[99,100] To this end, he started from the CID equations of a diagonal pair, neglected terms with four distinct indices in the EEO and replaced the charge distributions $|a(\mathbf{r}_1)|^2$ by $|i(\mathbf{r}_1)|^2$ with the argument that the PNOs must be located in the same region of space as the parent orbital i in order to give sizeable contributions. A straightforward analysis then shows that the eigenfunctions of the operator

$$\mathbf{G}^{ii} = \mathbf{F} + \mathbf{K}^{ii} - \mathbf{J}^{ii} \tag{2.25}$$

yield a CID matrix for the diagonal pair that is nearly diagonal which should be the best choice for first order perturbation theory.[99] Denoting the eigenvalues of this operator with g_a and g_b, the pair coefficients in the new basis become

$$\bar{C}^{ii}_{ab} \approx -\frac{\bar{K}^{ii}_{ab}}{g_a + g_b - 2\varepsilon_i} \quad , \tag{2.26}$$

where the overlined Exchange operator now refers to the eigenfunctions of $\mathbf{G}^{ii}$. For off-diagonal pairs, the situation is less straightforward. Symmetric ('+') and antisymmetric ('-') combinations of the CSFs defined in Eq. (2.5) were taken to obtaine the following pair operators:

$$\mathbf{G}^{ij+} = \mathbf{F} + \tfrac{1}{2}\mathbf{K}^{ii} + \tfrac{1}{2}\mathbf{K}^{jj} - \tfrac{1}{2}\mathbf{J}^{ii} - \tfrac{1}{2}\mathbf{J}^{jj} \tag{2.27}$$

$$\mathbf{G}^{ij-} = \mathbf{F} + \tfrac{3}{2}\mathbf{K}^{ii} + \tfrac{3}{2}\mathbf{K}^{jj} - \tfrac{1}{2}\mathbf{J}^{ii} - \tfrac{1}{2}\mathbf{J}^{jj} \quad . \tag{2.28}$$

The average of these two operators was chosen as the off-diagonal pair operator. Hence, the eigenfunctions of

$$\mathbf{G}^{ij} = \mathbf{F} + \mathbf{K}^{ii} + \mathbf{K}^{jj} - \tfrac{1}{2}\mathbf{J}^{ii} - \tfrac{1}{2}\mathbf{J}^{jj} \tag{2.29}$$

were used to construct the PNO expansions for the off-diagonal pairs.

2.2.4. PNO form of the residual

In terms of PNOs, the spin-restricted closed-shell CISD wavefunction becomes:

$$\Psi = \Psi_{HF} + \sum_{ia} C^i_a \Psi^a_i + \sum_{i \leqslant j} \sum_{\bar{a}^{ij}\bar{b}^{ij}} \bar{C}^{ij}_{\bar{a}^{ij}\bar{b}^{ij}} \Psi^{\bar{a}^{ij}\bar{b}^{ij}}_{ij} \quad . \tag{2.30}$$

Two important choices were made that deviate clearly from the treatments pursued in the old PNO-CEPA methods: a) no expansion of the single excitations in terms of PNOs and b) no diagonal form of the PNO expansion. The PNO form of the residuals is straightforwardly obtained by repeatedly inserting Eq. (2.22) into Eqs. (2.9) and (2.10), which results in

$$
\begin{aligned}
\bar{R}^{ij}_{\bar{a}\bar{b}} = \quad & \Big(\bar{\mathbf{K}}^{ij}\Big)_{\bar{a}\bar{b}} + \Big(\mathbf{d}^{ij\dagger}\mathbf{F}^{v\dagger}\mathbf{d}^{ij}\bar{\mathbf{C}}^{ij} + \bar{\mathbf{C}}^{ij}\mathbf{d}^{ij\dagger}\mathbf{F}^{v}\mathbf{d}^{ij}\Big)_{\bar{a}\bar{b}} + \bar{\mathbf{K}}\Big(\bar{\mathbf{C}}^{ij}\Big)_{\bar{a}\bar{b}} \\
& - \sum_k \left(F_{jk}\Big(\mathbf{S}^{ij,ik}\bar{\mathbf{C}}^{ik}\mathbf{S}^{ij,ik\dagger}\Big)_{\bar{a}\bar{b}} + F_{ik}\Big(\mathbf{S}^{ij,kj}\bar{\mathbf{C}}^{kj}\mathbf{S}^{ij,kj\dagger}\Big)_{\bar{a}\bar{b}} \right) \\
& + \sum_{k,l} (ik|jl) \left(\mathbf{S}^{ij,kl}\bar{\mathbf{C}}^{kl}\mathbf{S}^{ij,kl\dagger} \right)_{\bar{a}\bar{b}} \\
& + \sum_k \Bigg(\mathbf{S}^{ij,ik}(2\bar{\mathbf{C}}^{ik} - \bar{\mathbf{C}}^{ik\dagger})\mathbf{d}^{ki\dagger}(\mathbf{K}^{kj} - \tfrac{1}{2}\mathbf{J}^{kj})\mathbf{d}^{ij} \\
& \qquad + \mathbf{d}^{ij\dagger}(\mathbf{K}^{ik} - \tfrac{1}{2}\mathbf{J}^{ik})\mathbf{d}^{ik}(2\bar{\mathbf{C}}^{kj} - \bar{\mathbf{C}}^{kj\dagger})\mathbf{S}^{ij,kj\dagger} \Bigg)_{\bar{a}\bar{b}} \\
& - \sum_k \Bigg(\tfrac{1}{2}\mathbf{S}^{ij,ik}\bar{\mathbf{C}}^{ik\dagger}\mathbf{d}^{ki\dagger}\mathbf{J}^{jk\dagger}\mathbf{d}^{ij} + \tfrac{1}{2}\mathbf{d}^{ij\dagger}\mathbf{J}^{ik}\mathbf{d}^{kj}\bar{\mathbf{C}}^{kj\dagger}\mathbf{S}^{kj,ij} \\
& \qquad + \mathbf{d}^{ij\dagger}\mathbf{J}^{jk}\mathbf{d}^{ki}\bar{\mathbf{C}}^{ik}\mathbf{S}^{ik,ij} + \mathbf{S}^{ij,kj}\bar{\mathbf{C}}^{kj}\mathbf{d}^{kj\dagger}\mathbf{J}^{ik\dagger}\mathbf{d}^{ij} \Bigg)_{\bar{a}\bar{b}} \\
& - \sum_k \left(\Big(\sum_a (jk|ia) d^{ij}_{a\bar{a}}\Big)\bar{C}^k_{\bar{b}} + \Big(\sum_b (ik|jb) d^{ij}_{b\bar{b}}\Big)\bar{C}^k_{\bar{a}} \right) \\
& + \sum_{\bar{c}} \left((i\bar{a}|\bar{c}\bar{b})\bar{C}^j_{\bar{c}} + (j\bar{b}|\bar{a}\bar{c})\bar{C}^i_{\bar{c}} \right) - \Delta^{ij}\bar{C}^{ij}_{\bar{a}\bar{b}} \\
\overset{!}{=} \quad & 0 \quad , \qquad (2.31)
\end{aligned}
$$

$$
\begin{aligned}
R^i_a = \quad & F_{ia} + \sum_b F_{ba}C^i_b - \sum_j F_{ij}C^j_a + \sum_j \Big((2\,\mathbf{K}^{ij} - \mathbf{J}^{ij})\mathbf{C}^j \Big)_a \\
& + \sum_{j,b} \Big(\mathbf{d}^{ji}\Big(2\,\bar{\mathbf{C}}^{ji} - \bar{\mathbf{C}}^{ji\dagger}\Big)\mathbf{d}^{ji\dagger} \Big)_{ab} F_{jb} \\
& + \sum_{j,\bar{a}} d^{ij}_{a\bar{a}} \left(\sum_{\bar{b},\bar{c}} \left(\Big(2\,(i\bar{b}|\bar{a}\bar{c}) - (i\bar{c}|\bar{a}\bar{b})\Big)\bar{C}^{ij}_{\bar{b}\bar{c}} + \Big(2\,(j\bar{b}|\bar{a}\bar{c}) - (j\bar{c}|\bar{a}\bar{b})\Big)\bar{C}^{ij}_{\bar{c}\bar{b}} \right) \right) \\
& - \sum_{j,k,b} \Big(2\,(ik|jb) - (ij|kb)\Big) \Big(\mathbf{d}^{kj}\bar{\mathbf{C}}^{kj}\mathbf{d}^{kj\dagger} \Big)_{ab} - \Delta^i C^i_a \\
\overset{!}{=} \quad & 0 \quad , \qquad (2.32)
\end{aligned}
$$

where the EEO is given by

$$\mathbf{K}(\bar{\mathbf{C}}^{ij})_{ab} = \sum_{\bar{c}\bar{d}} (\bar{a}\bar{c}|\bar{b}\bar{d})\bar{C}^{ij}_{\bar{c}\bar{d}} \quad . \tag{2.33}$$

Furthermore, necessary PNO singles amplitudes are projected to the PNO pair basis in question (*e.g.* $\bar{C}^i_{\bar{a}} = \sum_a d^{ij}_{a\bar{a}} C^i_a$) or PNO doubles amplitudes from the respective PNO basis to the full VMO basis ($\mathbf{C}^{ij} = \mathbf{d}^{ij}\bar{\mathbf{C}}^{ij}\mathbf{d}^{ij+}$). This is of course a rather crude approximation since that part of the external space which will be neglected due to the truncation of the PNO expansion cannot be restored via back-projection onto the full VMO basis. However, the extensive test calculations documented in Chapter 3 clearly demonstrate that this approximation is not crucial in terms of accuracy. The efficient implementation of Eqs. (2.31) – (2.32) is discussed in the following Sections.

2.2.5. Approximations

In the form the Eqs. (2.31) – (2.33) are given above nothing has yet been achieved in terms of computational efficiency. In contrary, the full evaluation of Eqs. (2.31) – (2.33) would be much more expensive than the original CISD or CEPA equations while giving identical results. Thus, in order to arrive at a computationally efficient method, we make the following approximations:

1.) Truncation of the PNO expansion of each pair. Thus, only those PNOs for each pair are kept for which the occupation number $n_{ij} > \mathrm{T}_{\mathrm{CutPNO}}$, where $\mathrm{T}_{\mathrm{CutPNO}}$ is a user defined threshold with a default value of 3.33×10^{-7} (*vide infra*). This is the most important truncation parameter in the present treatment.

2.) Take advantage of locality in a conservative way by not including pairs with a pair correlation energy $|\varepsilon_{ij}| < \mathrm{T}_{\mathrm{CutPairs}}$ (strong pair approximation). The user defined threshold $\mathrm{T}_{\mathrm{CutPairs}}$ has a default value of 10^{-4} $\mathrm{E_h}$ (*vide infra*).

These two approximations define the LPNO-CEPA method. Without applying the strong pair approximation, it is simply referred to as PNO-CEPA, but it should be noted that the present approach differs in important details from the early PNO-CEPA methods developed in the 1970s. The alternative approximation, where only the internal pair truncation is pursued, refers to SL-CEPA, where 'SL' stands for 'semi-local'. This approximation is semi-local in the sense that only the internal space is truncated while the entire external space is kept. A single additional approximation is made (see Sec. 2.2.7) in order to further enhance the computational efficiency which then defines the actual computational method. Thus, the entire treatment is devoid of any real-space cut-offs that are characteristic of other local correlation approaches. The merits of the LPNO approach relative to other local correlation methods will be addressed in Sec. 4.3.

2.2.6. Perturbative Correction

Obviously, these two approximations introduce a truncation error into the correlation energy. The largest part of this error can be compensated for by second-order perturbation theory in a straightforward manner. Since initially the full operators $C_{\bar{a}\bar{b}}^{ij}$ and $\bar{K}_{\bar{a}\bar{b}}^{ij}$ are constructed, they can be used to calculate an estimate for the PNO error made by truncating the expansion of pair (i,j),

$$\Delta\varepsilon_{ij} = \varepsilon_{ij}^{PT2;trunc} - \varepsilon_{ij}^{PT2;full} \quad , \tag{2.34}$$

where $\varepsilon_{ij}^{PT2;trunc}$ refers to the truncated pair correlation energy with the perturbative amplitudes and $\varepsilon_{ij}^{PT2;full}$ refers to the full perturbative pair correlation energy without PNO truncation or strong pair approximation. For neglected pairs and those pairs that have no surviving PNO in their expansion space, the full (semi-local) perturbative pair correlation energy is used as a correction for the correlation energy. These corrections are of moderate size (see Sec. 3.2.1) but further enhance the accuracy of the LPNO methods.

2.2.7. Implementation details for the LPNO based coupled pair methods

The program (implemented in the 'orca_mdci' module of the ORCA program package[206]) starts by re-calculating the Fock operator in order to enable also the use of non-HF reference determinants. The internal orbitals are then localized. The default localization method is the Foster-Boys procedure[203] that was found to be more robust than the Pipek-Mezey method,[210] but the latter is also available. However, as it will be demonstrated in Sec. 3.2.6, the results of the calculations do not significantly depend on the actual localization method in use.

For the integral transformations, the RI approximation is employed.[66] First, the three sets of three-index integrals $(ij|K)$, $(ia|K)$ and $(ab|K)$ are generated, where K is an orthogonalized auxiliary basis function in the Coulomb metric. From these integrals, the four-index integral classes $(ik|jl)$, $(ik|ja)$, $(ij|ab) \equiv (\mathbf{J}^{ij})_{ab}$ and $(ia|jb) \equiv (\mathbf{K}^{ij})_{ab}$ are produced and stored. This is the worst scaling step of the entire procedure and ways to avoid at least part of the computational effort are readily envisioned and will be studied in future work. Using the Exchange operators $\mathbf{K}^{ij}$, the MP2 doubles amplitudes and the MP2 pair correlation energies are calculated, which serve as initial guess to the doubles amplitudes and the correlation energy respectively. Furthermore, negligible pairs are sorted out according to the threshold $\mathrm{T}_{\mathrm{CutPairs}}$. For the remaining linear scaling number of pairs, the virtual pair density is calculated followed by the generation of the PNOs according to the prescription given in Eqs. (2.21). This step scales as $\mathcal{O}(N^4)$ with respect to the system size N. The PNOs with occupation numbers below the threshold $\mathrm{T}_{\mathrm{CutPNO}}$ are rejected from the procedure and the perturbative estimate for the corresponding truncation error is calculated on the fly. The retained PNOs of a given pair are transformed into a quasi-canonical form that diagonalizes the Fock operator in the subspace spanned by the respective PNOs. This is advantageous

for the amplitude update procedure and also saves some computation time for the intra-pair contributions to the residuals that involve the virtual part of the Fock operator (see first line of Eq. (2.31)).

It should be noted that there are many more PNOs than virtual orbitals entering the calculations. Thus, the computational effort for the integral transformation producing the electron-electron repulsion integrals over PNOs becomes significant and must be carefully optimized to avoid a new computational bottleneck. To this end, a local RI integral transformation scheme was implemented that generates all required PNO integrals efficiently. It starts with an outer loop over auxiliary functions and the calculation of the matrices $(K|\mu\nu)$, where μ, ν are basis functions. These matrices are first transformed to the canonical VMO basis. Afterwards, a loop over surviving pairs generates the integrals $(K|a^{ij}b^{ij})$, $(K|ia^{ij})$ and $(K|ja^{ij})$ (for each pair). These intermediate quantities are stored in high-speed memory. Once all of these integrals are available, another loop over pairs is performed generating the three- and four-external integrals over PNOs $(ia^{ij}|b^{ij}c^{ij})$, $(ja^{ij}|b^{ij}c^{ij})$, and $(a^{ij}c^{ij}|b^{ij}d^{ij})$, which are stored on disk. In order to save computation time, one additional approximation was introduced that has very little impact on the accuracy of the results (*vide infra*). The auxiliary functions are restricted to the set of atoms where the parent internal orbitals are localized. Since the PNOs are localized in the same region of space, this set is also appropriate for fitting the PNOs themselves. The selection of the respective atoms is performed on the basis of the third threshold, $\mathrm{T}_{\mathrm{CutMKN}}$. Any atom with a Mulliken population larger than the user defined value for $\mathrm{T}_{\mathrm{CutMKN}}$ in the occupied internal orbitals (i, j) is included in the fitting list. The default value was set to $\mathrm{T}_{\mathrm{CutMKN}} = 0.001$ (see Sec. 3.2.1). It should be noted that a very similar procedure was developed by Schütz in the context of the PAO based local correlation methods.[211,212] It may be argued that this cut-off violates the statement that the LPNO approach does not contain any real-space cut-offs. However, $\mathrm{T}_{\mathrm{CutMKN}}$ is wavefunction based and does not have units of length. The Mulliken populations do, however, depend on the overlap integrals and therefore on the geometry of the respective molecule. Since the same holds for the pair correlation energies, we prefer to not regard $\mathrm{T}_{\mathrm{CutMKN}}$ as a real-space cut-off. It should be also noted that the PAO based approach makes use of Mulliken population based domain construction schemes.[177,211] However, there is a substantial difference between the two approaches. In the LPNO procedure the Mulliken cut-off does not control the correlation space for each electron pair but only the accuracy of the fit to the PNOs of a given pair. As will be shown in Sec. 3.2.1, the LPNO results are insensitive to the choice of $\mathrm{T}_{\mathrm{CutMKN}}$, while in the PAO based procedures the domain sizes have a large impact on the accuracy of the calculations.[176]

The number of three- and four-external integrals over PNOs is linear scaling and hence, no storage bottlenecks arise. From these stored integrals, it is trivial to generate the corresponding contributions to the residuals directly in the truncated pair-specific PNO basis with high-efficiency. Thus, the actual computer time for these steps now becomes negligible. This is a major deviation from the procedures used in the old PNO-CEPA implementations

from the 1970s. At the time, the amplitudes were transformed to the AO basis and then contracted with the four-index integrals over AOs to generate all EEOs in the AO basis, that were subsequently projected back to the MO or PNO bases respectively. This was a logical and pioneering choice at that time, which allowed for impressive calculations on very limited hardware. On the other hand, this was probably also the reason for the discard of the old PNO methods in favor of the SCEP methods introduced by Meyer. From today's perspective, however, it is the tremendous compression of the external space that renders the PNO approach attractive in the framework of local correlation methods. Moreover, if the early PNO prescriptions would be used for the LPNO approach, basically all computational advantages of the procedure is lost and storage bottlenecks arise for the AO basis amplitudes if larger molecules are considered.

The next step in the procedure consists of the pre-calculation of the two-external pair-pair interaction operators (line 4 – 8 of Eq. 2.31). Storing these quantities on disk is advantageous in order to avoid the repeated projection of the Coulomb and Exchange operators into the PNO bases of the various pairs. This procedure ('Algorithm 0') significantly reduces the computation time required for the calculation of two-external pair-pair interactions. The remaining parts of the residuals are essentially self-evident and need little further comment. In 'Algorithm 0', the PNO overlap matrices (Eq. (2.24)) are calculated on the fly whenever they are needed. However, this also implicates that the calculation of the contribution involving the four-internal Exchange integrals $(ik|jl)$ becomes the most expensive part in the doubles residual since the contraction with the respective doubles amplitudes necessitates the projection of the amplitudes of pair (k,l) into the PNO basis of pair (i,j) in each iteration. In order to speed up this part to some extent, we check for the value of $|(ik|jl)|$ and neglect the four-internal pair-pair interaction once it falls below a very conservatively chosen threshold of 10^{-14} $\mathrm{E_h}$. The computationally most expensive term in the calculation of the singles residual turns out to be the singles-doubles interaction that involves the one-external integrals $(ik|ja)$ (fourth line of Eq. (2.32)). Since the single excitations are not truncated in the present LPNO approach, the scaling of this contribution is still as steep as $\mathcal{O}(O^3V^2)$. Thus, although its prefactor is rather small, the calculation of this term will dominate the computation time needed for the LPNO coupled pair iterations, at least if larger systems are treated. Routes to circumvent this bottleneck will be discussed in Sec. 4.4.

2.3. Coupled cluster theory

In this section, the single-reference CCSD equations will be discussed in a spin-orbital basis using the language of second quantization.[78] The single determinant reference wavefunction (usually of HF type) is denoted by $|\Phi_0\rangle$. Again, the spin-orbitals which are occupied in $|\Phi_0\rangle$ (internal orbitals) are labelled as (i,j,k,l), while the unoccupied (virtual or external) spin-orbitals are labelled as (a,b,c,d). The CCSD wavefunction is exponentially parameterized

as

$$|\Psi\rangle = e^{\widehat{T}_1+\widehat{T}_2}\,|\Phi_0\rangle \quad , \tag{2.35}$$

in which $\widehat{T}_1 = \sum_{i,a} t_a^i\ \widehat{a}^\dagger\ \widehat{i}$ and $\widehat{T}_2 = \frac{1}{4}\sum_{i,j,a,b} t_{ab}^{ij}\ \widehat{a}^\dagger\ \widehat{b}^\dagger\ \widehat{j}\ \widehat{i}$ are single and double excitation operators respectively. The CCSD energy can be expressed in terms of the singles t_a^i and doubles t_{ab}^{ij} excitation amplitudes and is obtained by taking the Fermi vacuum expectation value of the similarity transformed normal ordered BO Hamiltonian $\widehat{\overline{H}}_{BO}$,

$$\begin{aligned} E &= \langle\Phi_0|\,\widehat{\overline{H}}_{BO}\,|\Phi_0\rangle = \langle\Phi_0|\,e^{-\widehat{T}_1-\widehat{T}_2}\widehat{H}_{BO}e^{\widehat{T}_1+\widehat{T}_2}\,|\Phi_0\rangle \\ &= E_0 + E_{corr} \\ &= E_0 + \sum_{i,a} F_{ia}t_a^i + \frac{1}{2}\sum_{i,j,a,b}\langle ij|\,|ab\rangle\, t_a^i t_b^j + \frac{1}{4}\sum_{i,j,a,b}\langle ij|\,|ab\rangle\, t_{ab}^{ij} \quad , \end{aligned} \tag{2.36}$$

in which E_0 and E_{corr} are the reference energy and the correlation energy respectively, the F_{ia} denote elements of the outer-diagonal sub-block of the Fock matrix and $\langle ij|\,|ab\rangle$ are antisymmetric two-electron integrals. This expression is generally valid for any truncation level of the cluster operator, since only one- and two-body operators enter the Hamiltonian. Therefore, only three closed and connected diagrams can contribute to correlation energy in single-reference CC theory. At the level of single and double excitations, the amplitudes t_a^i and t_{ab}^{ij} can be determined by iterative solutions of a set of non-linear equations $R_a^i = 0$ and $R_{ab}^{ij} = 0$. The corresponding singles R_a^i and doubles R_{ab}^{ij} residuals are obtained by projecting the similarity transformed Schrödinger equation $\widehat{\overline{H}}_{BO}\,|\Phi_0\rangle = E\,|\Phi_0\rangle$ onto the single respectively double excitation manifolds,

$$\begin{aligned} R_a^i &= \langle\Phi_i^a|\,\widehat{\overline{H}}_{BO}\,|\Phi_0\rangle \\ &= \langle\Phi_i^a|\left[\widehat{H}_{BO}\left(1+\widehat{T}_1+\widehat{T}_2+\frac{1}{2}\widehat{T}_1^2+\widehat{T}_1\widehat{T}_2+\frac{1}{6}T_1^3\right)\right]_C|\Phi_0\rangle \quad , \end{aligned} \tag{2.37}$$

$$\begin{aligned} R_{ab}^{ij} &= \left\langle\Phi_{ij}^{ab}\right|\widehat{\overline{H}}_{BO}\,|\Phi_0\rangle \\ &= \left\langle\Phi_{ij}^{ab}\right|\left[\widehat{H}_{BO}\left(1+\widehat{T}_1+\widehat{T}_2+\frac{1}{2}\widehat{T}_1^2+\widehat{T}_1\widehat{T}_2+\frac{1}{6}\widehat{T}_1^3\right.\right. \\ &\quad \left.\left.+\frac{1}{2}\widehat{T}_2^2+\frac{1}{2}\widehat{T}_1^2\widehat{T}_2+\frac{1}{24}\widehat{T}_1^4\right)\right]_C|\Phi_0\rangle \quad . \end{aligned} \tag{2.38}$$

The subscript C indicates the restriction to connected diagrams. Furthermore, the similarity transformation ensures that only linked diagrams enter the expansion and the projection leads to a fast truncation. The respective matrix elements can be evaluated by using antisymmetrized Goldstone diagrams,[78] for example. The resulting (non-redundant) diagrams and their algebraic translations are shown in Fig. 2.1 and 2.2. Implementing these equations in spin-orbital form without defining suitable intermediates and further factorization would result in an algorithm of $\mathcal{O}(N^8)$ complexity with many redundancies. Thus, further manipulations are necessary in order to arrive at a form suitable for an efficient production level implementation.

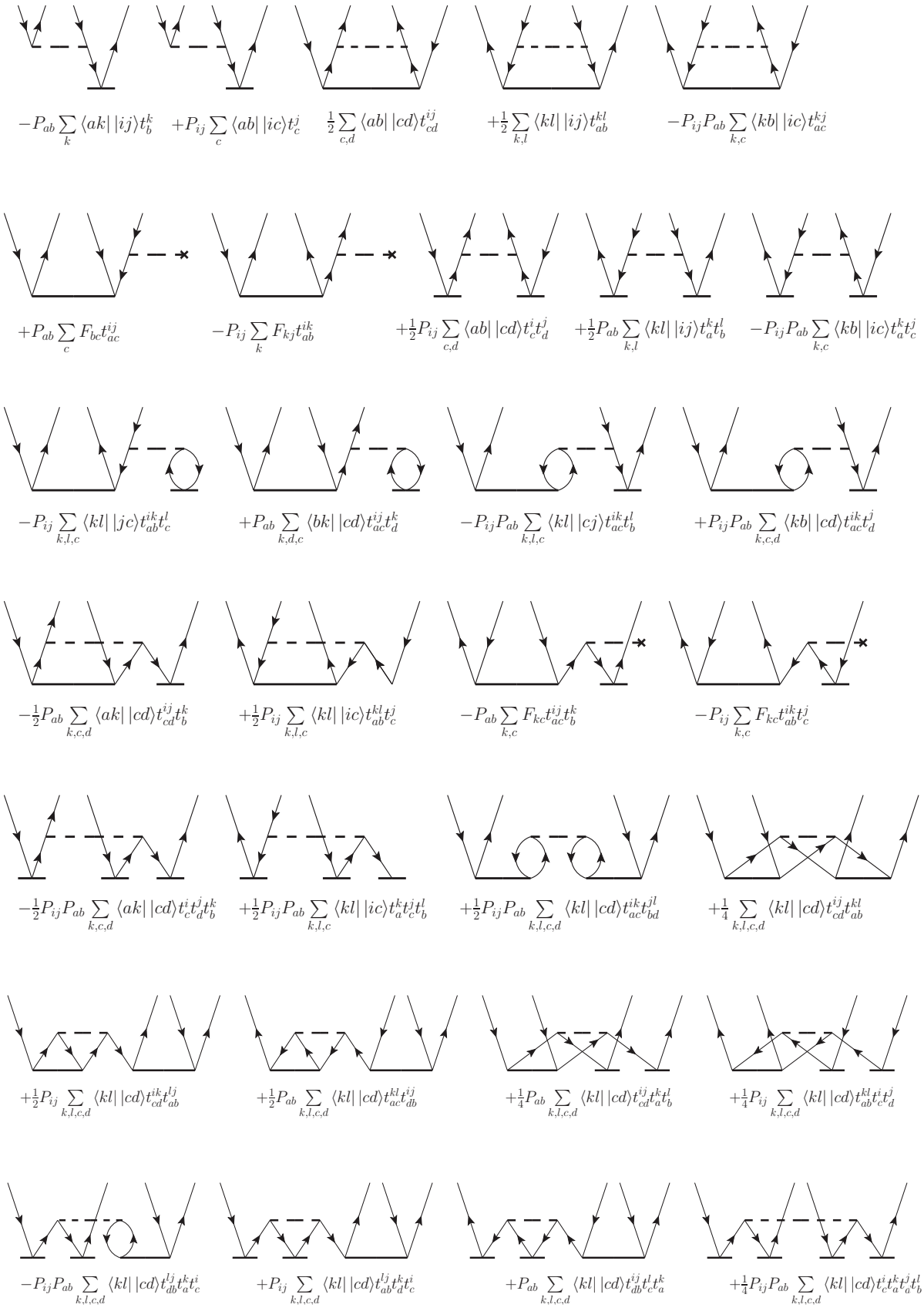

Figure 2.1.: Diagrammatic representation of the CCSD doubles residual and the corresponding algebraic translation.

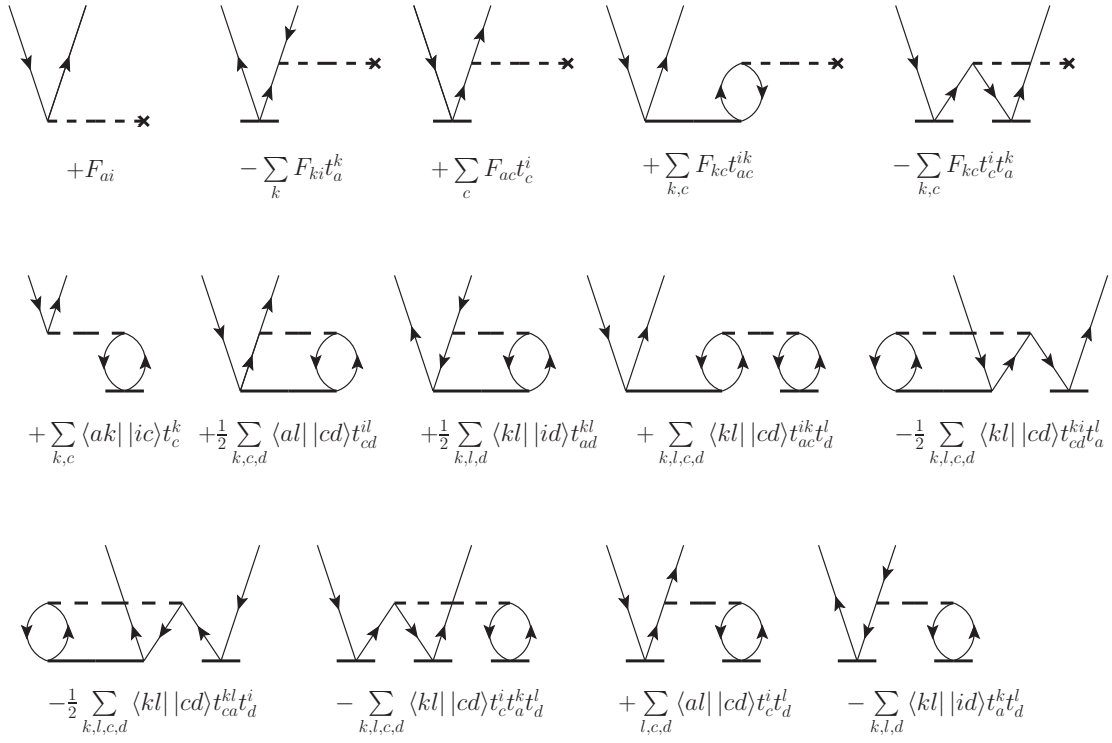

Figure 2.2.: Diagrammatic representation of the CCSD singles residual and the corresponding algebraic translation.

2.3.1. Spin-restricted closed-shell QCISD and CCSD equations

The closed-shell CCSD equations are solved in the generator state formalism[185,186] essentially as a dressed CISD problem leading to the following working equations for the residuals (the terms in curly brackets are omitted in the QCISD method, for which only terms up to quadratic order are included in the CC expansion while the terms in squared brackets only appear for QCISD):

$$\begin{aligned}
R_{ab}^{ij} = \quad & K_{ab}^{ij} + \mathbf{K}(\boldsymbol{\tau}^{ij})_{ab} + (\tilde{\tilde{\mathbf{F}}}^{\dagger}\mathbf{t}^{ij} + \mathbf{t}^{ij}\tilde{\tilde{\mathbf{F}}})_{ab} - \sum_k \left(\tilde{\tilde{F}}_{jk}\mathbf{t}^{ki\dagger} + \tilde{\tilde{F}}_{ik}\mathbf{t}^{kj}\right)_{ab} + \sum_{kl}(\widetilde{ik|jl})\tau_{ab}^{kl} \\
& + \sum_k \left((2\mathbf{t}^{ki\dagger} - \mathbf{t}^{ki})(\tilde{\mathbf{K}}^{jk\dagger} - \tfrac{1}{2}\tilde{\mathbf{J}}^{jk}) - \tfrac{1}{2}\mathbf{t}^{ki}\tilde{\mathbf{J}}^{jk} - \tilde{\mathbf{J}}^{jk\dagger}\mathbf{t}^{ki\dagger}\right)_{ab} \\
& + \sum_k \left((\tilde{\mathbf{K}}^{ik} - \tfrac{1}{2}\tilde{\mathbf{J}}^{ik\dagger})(2\mathbf{t}^{kj} - \mathbf{t}^{kj\dagger}) - \tfrac{1}{2}\tilde{\mathbf{J}}^{ik\dagger}\mathbf{t}^{kj\dagger} - \mathbf{t}^{kj}\tilde{\mathbf{J}}^{ik}\right)_{ab} \\
& - \sum_k \left((jk|ia)t_b^k + (ik|jb)t_a^k\right) + \sum_c \left((ia|cb)t_c^j + (jb|ac)t_c^i\right) \\
& - \left\{\sum_k \left((\mathbf{K}^{ik}\mathbf{t}^j)_a t_b^k + (\mathbf{K}^{jk}\mathbf{t}^i)_b t_a^k + (\mathbf{J}^{ik}\mathbf{t}^j)_b t_a^k + (\mathbf{J}^{jk}\mathbf{t}^i)_a t_b^k\right)\right\} \\
\stackrel{!}{=} \quad & 0 \quad , \qquad (2.39)
\end{aligned}$$

$$
\begin{aligned}
R_a^i = \quad & F_{ia} + \sum_b \tilde{F}_{ba} t_b^i - \sum_j \tilde{F}_{ij} t_a^j + \{\mathbf{G}(\mathbf{t}_1)_{ia}\} + \left[\sum_j \Big((2\,\mathbf{K}^{ij} - \mathbf{J}^{ij}) \mathbf{C}^j \Big)_a \right] \\
& + \sum_{jb} (2\mathbf{t}^{ji} - \mathbf{t}^{ji\dagger})_{ba} \tilde{F}_{bj} - \sum_{kjb} \left(2(ik|jb) - (ij|kb) \right) \tau_{ab}^{kj} \\
& + \sum_{jbc} \Big((2(ib|ac) - (ic|ab)) \tau_{bc}^{ij} + (2(jb|ac) - (jc|ab)) \tau_{cb}^{ij} \Big) \\
& + \left\{ \sum_{jb} (\tilde{F}_{jb} - 2F_{jb}) t_b^i t_a^j \right\} \\
\stackrel{!}{=} \quad & 0 \quad .
\end{aligned}
\tag{2.40}
$$

In this way, they were implemented in the ORCA quantum chemistry program package[206] in an efficient, matrix driven form. Note that all labels now refer to spatial rather than spin-orbitals and the unique amplitudes obey the index restrictions $i \leqslant j$ and all a, b (for $i = j$, only $a \leqslant b$ would be required, but it is more convenient to keep a symmetric coefficient matrix t_{ab}^{ij} in this case.[186] The 'dressed' quantities (denoted by a tilde) are defined as follows:[185,213]

$$\tau_{ab}^{ij} = t_{ab}^{ij} \left\{ + t_a^i t_b^j \right\} \quad , \tag{2.41}$$

$$\tilde{F}_{ij} = F_{ij} + \sum_k \Big\langle (2\mathbf{K}^{jk} - \mathbf{K}^{jk\dagger}) \boldsymbol{\tau}^{ik} \Big\rangle \quad , \tag{2.42}$$

$$\tilde{F}_{ab} = F_{ab} - \sum_{kl} \Big(\boldsymbol{\tau}^{kl} (2\,\mathbf{K}^{lk} - \mathbf{K}^{lk\dagger}) \Big)_{ab} \quad , \tag{2.43}$$

$$\tilde{F}_{ai} = F_{ai} + \sum_k \Big((2\,\mathbf{K}^{ik} - \mathbf{K}^{ik\dagger}) \mathbf{t}^k \Big)_a \quad , \tag{2.44}$$

$$\tilde{\tilde{F}}_{ij} = \tilde{F}_{ij} + \left\{ \mathbf{G}(\mathbf{t}_1)_{ij} + \sum_a F_{ia} t_a^j \right\} \quad , \tag{2.45}$$

$$\tilde{\tilde{F}}_{ab} = \tilde{F}_{ab} + \left\{ \mathbf{G}(\mathbf{t}_1)_{ab} - \sum_i F_{ib} t_a^i \right\} \quad , \tag{2.46}$$

$$\mathbf{G}(\mathbf{t}_1)_{pq} = \sum_{jb} t_b^j \Big(2\,(pq|jb) - (pj|qb) \Big) \quad , \tag{2.47}$$

$$\mathbf{K}(\boldsymbol{\tau}^{ij})_{ab} = \sum_{cd} \Big((ac|bd) \left\{ - \sum_k (kd|ac) t_b^k + (kc|bd) t_a^k \right\} \Big) \tau_{cd}^{ij} \quad , \tag{2.48}$$

$$\widetilde{(ik|jl)} = (ik|jl) + \Big\langle \mathbf{K}^{kl} \boldsymbol{\tau}^{ij\dagger} \Big\rangle + \left\{ \sum_a \Big((ki|la) t_a^j + (lj|ka) t_a^i \Big) \right\} \quad , \tag{2.49}$$

$$\tilde{K}_{ab}^{ij} = K_{ab}^{ij} + \sum_k \left(\mathbf{t}^{ik} (\mathbf{K}^{kj} - \tfrac{1}{2}\mathbf{K}^{kj\dagger}) - \tfrac{1}{2}\boldsymbol{\tau}^{ki}\mathbf{K}^{kj} \right)_{ab} + \left\{ \sum_c (jc|ab) t_c^i - \sum_k (ik|jb) t_a^k \right\} \quad , \tag{2.50}$$

$$\tilde{J}_{ab}^{ij} = J_{ab}^{ij} - \tfrac{1}{2} \sum_k (\mathbf{K}^{kj} \boldsymbol{\tau}^{ki\dagger})_{ab} + \left\{ \sum_c (jb|ac) t_c^i - \sum_k (ij|ka) t_b^k \right\} \quad , \tag{2.51}$$

where angled brackets are used as shorthand notation for the matrix trace operation. $K_{ab}^{ij} = (ia|jb)$ and $J_{ab}^{ij} = (ij|ab)$ denote the two-external Exchange and Coulomb operators and the two-electron repulsion integrals in round brackets are written in $(11|22)$ notation.

The computational effort involved in evaluating Eqs. (2.39) – (2.51) grows with the sixth power of the molecular size. The most expensive terms are the construction of the EEO (Eq. (2.48)) and the semi-joint pair-pair interactions (second and third line of Eq. (2.39). These terms were implemented with maximum use of large-scale matrix multiplications thus making use of the extremely efficient BLAS (basis linear algebra subprograms) level 3 routines.[184,208] The construction of the EEO in the MO or AO basis respectively was implemented based on the idea of Pulay *et al.*,[186] *i.e.* forming symmetric and antisymmetric combinations of amplitudes and integrals as explained in detail by Scuseria *et al.*[185] This is similar to the formerly prevalent practice to differentiate between singlet and triplet spin-coupled external pairs.[107,183] The storage of all transformed integrals grows with the fourth power of the basis set size, and it quickly becomes impossible to store the numerous transformed integrals with three- and four-external labels. It is feasible to develop CCSD programs that avoid the explicit generation of these integrals, as shown first by Meyer[183] and later discussed by Werner *et al.*[122] For example, Janowski *et al.*[89] described an efficient parallel algorithm that only involves storage of integrals with up to two-external labels while all other terms are done in an AO integral direct fashion. The ORCA program also offers such an option for closed-shell CEPA, QCISD and CCSD calculations. However, even disregarding the very large CPU requirements of this algorithm, the storage of the amplitudes, Coulomb and Exchange operators becomes unfeasible once a limit of about 500 – 1000 basis functions for molecules with C_1 symmetry is reached (depending on the number of correlated electrons).

2.3.2. The LPNO approach for closed-shell QCISD and CCSD

In developing an efficient and yet accurate approximation to the canonical QCISD and CCSD equations we have applied the LPNO approach to more intricate CC theory for the first time. In extending the LPNO-CEPA method to the QCISD and CCSD cases, some problems had to be overcome. Two different algorithms for solving the spin-restricted closed-shell LPNO-QCISD and LPNO-CCSD equations were developed that will be described below and are being referred to as LPNO_1-QCISD/CCSD and LPNO_2-QCISD/CCSD respectively. The latter variant ('Algorithm 2') will be described first.

The LPNO-CEPA method achieves a part of its efficiency by projecting the MO basis semi-joint pair-pair operators onto the PNO pair basis in question before entering the iterations

(see Sec. 2.2.7). At first sight, it appears that this is no longer possible in the QCISD and CCSD methods since the effective Coulomb and Exchange operators are 'dressed' by amplitudes that change in every iteration (see Eqs. (2.50) – (2.51)). The repeated pre-computation of these terms is, of course, possible but would take away much of the gained efficiency. However, it turned out that this technical problem becomes manageable in the following way: during the PNO integral transformation, the PNO basis Coulomb and Exchange operators ($\bar{J}^{ij}_{\bar{a}\bar{b}}$ and $\bar{K}^{ij}_{\bar{a}\bar{b}}$) are generated for each surviving pair using the RI approximation. These operators are then inserted wherever they appear in the equations and projected on the fly to the PNO basis of the 'target pair' in question. For example, the term $R^{ij}_{ab} \leftarrow \left(\mathbf{t}^{kj}\tilde{\mathbf{J}}^{ik}\right)_{ab}$ reads in the PNO basis:

$$\bar{R}^{ij}_{\bar{a}\bar{b}} \leftarrow \left(\mathbf{S}^{ij,kj}\bar{\mathbf{t}}^{kj}\mathbf{S}^{kj,ik}\bar{\tilde{\mathbf{J}}}^{ik}\mathbf{S}^{ik,ij}\right)_{\bar{a}\bar{b}} \quad , \tag{2.52}$$

where $\bar{\tilde{\mathbf{J}}}^{ik}$ is defined in the PNO basis of pair (i,k). The pair-pair overlaps can be efficiently generated by a simple matrix multiplication (see Eq.(2.24)). In contrast to the LPNO-CEPA implementation (referred to as 'Algorithm 0'; see Sec. 2.2.7), the PNO overlap matrices, due to their frequent use, have been pre-computed and stored on disk in a compressed form. The storage requirements are not negligible for larger molecules (several GB of disk space), but the number of significant elements in the overlap matrices is only increasing linearly with system size and hence, no real storage bottleneck arises. Moreover, the computation time required for this step is negligible compared to the total wall-clock time and as it will be shown in Sec. 3.4.2, it is computationally more efficient to store these overlap matrices, particularly for the calculation of the four-internal pair-pair interaction term.

Not having to store the entire set of canonical $\mathbf{J}^{ij}$ and $\mathbf{K}^{ij}$ operators leads to significant savings of disk space compared to 'Algorithm 0' (LPNO-CEPA) and hence, larger calculations with more than 2000 basis functions (depending on the number of correlated electrons) become feasible. In fact, the only MO basis integrals that are stored in 'Algorithm 2' are those with up to one-external label. All other transformed integrals are directly produced over PNOs and lead to linear scaling storage requirements. The operators $\mathbf{K}^{ij}$ that are initially needed for the calculation of the PNOs are made on the fly via the RI-approximation and immediately discarded after use. However, as a consequence of not having the MO basis $\mathbf{J}^{ij}$ operators available, the LPNO$_2$-QCISD and LPNO$_2$-CCSD methods cannot make use of the Meyer-style PNOs (see Sec. 2.2.3) that are used by default in the LPNO-CEPA method. Instead approximate MP2-PNOs are constructed as described in Sec. 2.2.2.

The singles Fock matrix $\mathbf{G}(\mathbf{t}_1)$ (Eq. (A.9)) is calculated in an AO direct fashion. It accounts for the singles-singles interaction involving the two-external integrals and the singles correction to the dressed Fock operator (Eqs. (2.45) and (2.46)). If large and accurate basis sets are used, the evaluation of this term becomes expensive (actual timings can be found in Sec. 3.4.2). Recently, the RIJCOSX approximation[214,215] was introduced as an efficient way

to form approximate Fock type matrices. The use of this approximation in the context of the LPNO based CCSD method will be discussed in Sec. 2.3.5 and the efficiency gains due to this additional approximation are documented in Sec. 3.4.3.

Analogously to Eq. (2.52), it is straightforward to convert all terms that appear in the singles and doubles residuals as well as the 'dressed' operators to the PNO basis in question noting that for each pair (i,j) the following classes of PNO integrals are available: (a) the four-external integrals $(\bar{a}\bar{c}|\bar{b}\bar{d})$ (stored on disk); (b) the three-external integrals $(i\bar{a}|\bar{b}\bar{c})$ and $(j\bar{a}|\bar{b}\bar{c})$ (stored on disk); (c) the two-external integrals $(ij|\bar{a}\bar{b})$ and $(i\bar{a}|j\bar{b})$ (kept in memory). No storage bottlenecks arise from these integrals since their number increases only linearly with the molecular size. However, for the LPNO based CCSD methods, the term

$$\bar{R}^{ij}_{\bar{a}\bar{b}} \leftarrow \sum_{\bar{c}\bar{d}} \left((\bar{a}\bar{c}|\bar{b}\bar{d}) - \sum_k \left((k\bar{d}|\bar{a}\bar{c})\bar{t}^k_{\bar{b}} + (k\bar{c}|\bar{b}\bar{d})\bar{t}^k_{\bar{a}} \right) \right) \bar{\tau}^{ij}_{\bar{c}\bar{d}} \tag{2.53}$$

is problematic due to the unrestricted sum over k that involves integrals which have not been generated during the PNO integral transformation since this would lead to significantly increased computational effort. Based on extensive numerical investigations, it can be concluded that it is possible to neglect the non-linear singles contribution to the 'dressed' EEO (*i.e.* the sum over k) since the additional error due to this approximation is very small (see Sec. 3.3.1). Throughout the development, it was ensured that the LPNO results exactly match the canonical ones (evaluated with the RI approximation for all two-electron integrals) if the thresholds T_{CutPNO} and T_{CutMKN} were set to zero and no electron pairs were neglected. Except from discarding the non-linear 'dressing' of the EEO (Eq. (2.53)), this equivalence was exactly obtained.

During the numerical investigation of the LPNO$_2$-QCISD and LPNO$_2$-CCSD methods it became evident that the recovered fraction of the canonical correlation energy is somewhat smaller than what was observed for LPNO-CEPA (see Sec. 3.3.1). This was finally traced back to the less accurate way of treating the two-external pair-pair interactions. Rather than transforming the full $\mathbf{J}^{ij}$ and $\mathbf{K}^{ij}$ operators into the truncated PNO basis of the target pair, they are transformed from the PNO basis of one pair into that of another pair, which introduces a significant error. In order to retain the accuracy of the LPNO-CEPA implementation ('Algorithm 0'), 'Algorithm 1' was developed, which differs in the following aspects from 'Algorithm 2':

a) During the initial RI integral transformation, all MO basis $\mathbf{J}^{ij}$ and $\mathbf{K}^{ij}$ operators are constructed and stored on disk just as it is done in the LPNO-CEPA implementation;
b) The two-external pair-pair interactions are pre-computed as in the LPNO-CEPA method;
c) The approximation to the linear terms in the semi-joint pair-pair interaction terms made for LPNO-CEPA is kept but the non-linear terms are approximated as in 'Algorithm 2'.

Thus, the semi-joint pair-pair interactions are computed as follows in 'Approximation 1':

$$
\begin{aligned}
\bar{R}^{ij}_{\bar{a}\bar{b}} = \quad & + \sum_k \Bigg(\mathbf{S}^{ij,ki} (2\bar{\mathbf{t}}^{ki\dagger} - \bar{\mathbf{t}}^{ki}) \mathbf{S}^{ki,jk} (\Delta\bar{\tilde{\mathbf{K}}}^{jk\dagger} - \tfrac{1}{2}\Delta\bar{\tilde{\mathbf{J}}}^{jk}) \mathbf{S}^{jk,ij} \\
& \quad - \tfrac{1}{2}\mathbf{S}^{ij,ki}\bar{\mathbf{t}}^{ki}\mathbf{S}^{ki,jk}\Delta\bar{\tilde{\mathbf{J}}}^{jk}\mathbf{S}^{jk,ij} - \mathbf{S}^{ij,jk}\Delta\bar{\tilde{\mathbf{J}}}^{jk\dagger}\mathbf{S}^{jk,ki}\bar{\mathbf{t}}^{ki\dagger}\mathbf{S}^{ki,ij} \Bigg)_{\bar{a}\bar{b}} \\
& + \sum_k \Bigg(\mathbf{S}^{ij,ik} (\Delta\bar{\tilde{\mathbf{K}}}^{ik} - \tfrac{1}{2}\Delta\bar{\tilde{\mathbf{J}}}^{ik\dagger}) \mathbf{S}^{ik,kj} (2\bar{\mathbf{t}}^{kj} - \bar{\mathbf{t}}^{kj\dagger}) \mathbf{S}^{kj,ij} \\
& \quad - \tfrac{1}{2}\mathbf{S}^{ij,ik}\Delta\bar{\tilde{\mathbf{J}}}^{ik\dagger}\mathbf{S}^{ik,kj}\bar{\mathbf{t}}^{kj\dagger}\mathbf{S}^{kj,ij} - \mathbf{S}^{ij,kj}\bar{\mathbf{t}}^{kj}\mathbf{S}^{kj,ik}\Delta\bar{\tilde{\mathbf{J}}}^{ik}\mathbf{S}^{ik,ij} \Bigg)_{\bar{a}\bar{b}} \\
& + \sum_k \Bigg(\mathbf{S}^{ij,ik} (2\bar{\mathbf{t}}^{ik} - \bar{\mathbf{t}}^{ik\dagger}) \mathbf{d}^{ki\dagger} (\mathbf{K}^{kj} - \tfrac{1}{2}\mathbf{J}^{kj}) \mathbf{d}^{ij} \\
& \quad + \mathbf{d}^{ij\dagger} (\mathbf{K}^{ik} - \tfrac{1}{2}\mathbf{J}^{ik}) \mathbf{d}^{ik} (2\bar{\mathbf{t}}^{kj} - \bar{\mathbf{t}}^{kj\dagger}) \mathbf{S}^{ij,kj\dagger} \Bigg)_{\bar{a}\bar{b}} \\
& - \sum_k \Bigg(\tfrac{1}{2}\mathbf{S}^{ij,ik}\bar{\mathbf{t}}^{ik\dagger}\mathbf{d}^{ki\dagger}\mathbf{J}^{jk\dagger}\mathbf{d}^{ij} + \tfrac{1}{2}\mathbf{d}^{ij\dagger}\mathbf{J}^{ik}\mathbf{d}^{kj}\bar{\mathbf{t}}^{kj\dagger}\mathbf{S}^{kj,ij} \\
& \quad + \mathbf{d}^{ij\dagger}\mathbf{J}^{jk}\mathbf{d}^{ki}\bar{\mathbf{t}}^{ik}\mathbf{S}^{ik,ij} + \mathbf{S}^{ij,kj}\bar{\mathbf{t}}^{kj}\mathbf{d}^{kj\dagger}\mathbf{J}^{ik\dagger}\mathbf{d}^{ij} \Bigg)_{\bar{a}\bar{b}} \quad , \qquad (2.54)
\end{aligned}
$$

where $\Delta\bar{\tilde{J}}^{ij}_{\bar{a}\bar{b}} = \bar{\tilde{J}}^{ij}_{\bar{a}\bar{b}} - \bar{J}^{ij}_{\bar{a}\bar{b}}$, $\Delta\bar{\tilde{K}}^{ij}_{\bar{a}\bar{b}} = \bar{\tilde{K}}^{ij}_{\bar{a}\bar{b}} - \bar{K}^{ij}_{\bar{a}\bar{b}}$ and the $d^{ij}_{a\bar{a}}$ are the expansion coefficients of PNOs in terms of canonical VMOs defined in Eq. (2.21). The complete working equations for the closed-shell LPNO$_1$-CCSD method can be found in Appendix A. Note that the $\mathbf{J}^{ij}$ and $\mathbf{K}^{ij}$ operators, which appear in the two final summations, are formed in the canonical VMO basis. Although this way of computing the two-external pair-pair interactions seems wasteful, the numerical investigations (see Chapter 3) clearly show that the 'Algorithm 1' reduces the error of the LPNO based CCSD method by almost one order of magnitude while not being much more expensive. For large calculations, however, the generation and storage of the MO basis $\mathbf{J}^{ij}$ and $\mathbf{K}^{ij}$ operators becomes cumbersome and sets a limit to about 1500 – 2500 basis functions (depending on the number of correlated electrons) on present day computing facilities.

2.3.3. Spin-unrestricted open-shell QCISD and CCSD equations

The unrestricted QCISD and CCSD equations are presented below as they are implemented into the ORCA quantum chemistry program package.[206] They are formulated essentially as a dressed CI problem and hence differ somewhat from other implementations.[175,216] The QCISD equations represent a subset of the CCSD equations with fewer dressed terms. Hence, all contributions that are only contained in CCSD are identified by curly brackets while the QCISD specific terms are denoted with squared brackets. As in the closed-shell case described

in the previous Section, dressed quantities have been denoted with a tilde and angled brackets indicate the trace operation. All two-electron integrals are written in $(11|22)$ notation. As it is common practice, the integrals with two-external labels are collected in Exchange ($K^{i_\alpha j_\alpha}_{a_\alpha b_\alpha} = (i_\alpha a_\alpha | j_\alpha b_\alpha)$) and Coulomb ($J^{i_\alpha j_\alpha}_{a_\alpha b_\alpha} = (i_\alpha j_\alpha | a_\alpha b_\alpha)$) operators respectively. For genuine spin-unrestricted integrals it should be noted that for the Coulomb operators two different crossed spin cases appear, $J^{i_\alpha j_\alpha}_{a_\beta b_\beta} = (i_\alpha j_\alpha | a_\beta b_\beta)$ and $J^{i_\beta j_\beta}_{a_\alpha b_\alpha} = (i_\beta j_\beta | a_\alpha b_\alpha)$ denoted as $\alpha\beta$ and $\beta\alpha$ respectively. For the two-external Exchange operators only the $\alpha\beta$-case has to be considered due to permutational symmetry. The correlation energy is calculated according to

$$\begin{aligned} E_{corr} = &\sum_{i_\alpha, a_\alpha} F_{i_\alpha a_\alpha} t^{i_\alpha}_{a_\alpha} + \sum_{i_\beta, a_\beta} F_{i_\beta a_\beta} t^{i_\beta}_{a_\beta} + \tfrac{1}{2} \sum_{i_\alpha < j_\alpha, a_\alpha, b_\alpha} \left(K^{i_\alpha j_\alpha}_{a_\alpha b_\alpha} - K^{i_\alpha j_\alpha}_{b_\alpha a_\alpha} \right) \tau^{i_\alpha j_\alpha}_{a_\alpha b_\alpha} \\ &+ \tfrac{1}{2} \sum_{i_\beta < j_\beta, a_\beta, b_\beta} \left(K^{i_\beta j_\beta}_{a_\beta b_\beta} - K^{i_\beta j_\beta}_{b_\beta a_\beta} \right) \tau^{i_\beta j_\beta}_{a_\beta b_\beta} + \sum_{i_\alpha, j_\beta, a_\alpha, b_\beta} K^{i_\alpha j_\beta}_{a_\alpha b_\beta} \tau^{i_\alpha j_\beta}_{a_\alpha b_\beta} \quad . \end{aligned} \tag{2.55}$$

The α-spin singles residual is given by (analogously for β-spin):

$$\begin{aligned} R^{i_\alpha}_{a_\alpha} = \quad & F_{a_\alpha i_\alpha} + \sum_{b_\alpha} \tilde{F}_{a_\alpha b_\alpha} t^{i_\alpha}_{b_\alpha} - \sum_{j_\alpha} t^{j_\alpha}_{a_\alpha} \tilde{F}_{j_\alpha i_\alpha} + \left\{ \mathbf{G}_\alpha(\mathbf{t}^1)_{i_\alpha a_\alpha} \right\} \\ & \left[+ \sum_{j_\alpha} \left(\left(\mathbf{K}^{i_\alpha j_\alpha} - \mathbf{J}^{i_\alpha j_\alpha} \right) \mathbf{t}^{j_\alpha} \right)_{a_\alpha} + \sum_{j_\beta} \left(\mathbf{K}^{i_\alpha j_\beta} \mathbf{t}^{j_\beta} \right)_{a_\alpha} \right] \\ & + \sum_{j_\alpha, b_\alpha} \left(\tilde{F}_{j_\alpha b_\alpha} t^{i_\alpha j_\alpha}_{a_\alpha b_\alpha} + \left\{ t^{j_\alpha}_{a_\alpha} \left(\tilde{F}_{j_\alpha b_\alpha} - 2\, F_{j_\alpha b_\alpha} \right) t^{i_\alpha}_{b_\alpha} \right\} \right) + \sum_{j_\beta, b_\beta} \tilde{F}_{j_\beta b_\beta} t^{i_\alpha j_\beta}_{a_\alpha b_\beta} \\ & - \sum_{j_\alpha, k_\alpha, b_\alpha} \tau^{j_\alpha k_\alpha}_{a_\alpha b_\alpha} (i_\alpha j_\alpha | k_\alpha b_\alpha) - \sum_{j_\alpha, k_\beta, b_\beta} \tau^{j_\alpha k_\beta}_{a_\alpha b_\beta} (i_\alpha j_\alpha | k_\beta b_\beta) \\ & + \sum_{j_\alpha, b_\alpha, c_\alpha} (j_\alpha b_\alpha | a_\alpha c_\alpha) \tau^{i_\alpha j_\alpha}_{c_\alpha b_\alpha} + \sum_{j_\beta, b_\beta, c_\alpha} (j_\beta b_\beta | a_\alpha c_\alpha)\, \tau^{i_\alpha j_\beta}_{c_\alpha b_\beta} \quad . \end{aligned} \tag{2.56}$$

The doubles $\alpha\alpha$ and $\alpha\beta$ residuals read ($\beta\beta$-case analogously):

$$\begin{aligned} R^{i_\alpha j_\alpha}_{a_\alpha b_\alpha} = \quad & \left(\mathbf{K}^{i_\alpha j_\alpha} - \mathbf{K}^{i_\alpha j_\alpha \dagger} \right)_{a_\alpha b_\alpha} + \left(\mathbf{t}^{i_\alpha j_\alpha} \tilde{\tilde{\mathbf{F}}}^{v\dagger}_{\alpha\alpha} - \tilde{\tilde{\mathbf{F}}}^{v}_{\alpha\alpha} \mathbf{t}^{i_\alpha j_\alpha \dagger} \right)_{a_\alpha b_\alpha} + \tilde{\mathbf{K}} \left(\boldsymbol{\tau}^{i_\alpha j_\alpha} \right)_{a_\alpha b_\alpha} \\ & + \sum_{k_\alpha} \left(\left(\tilde{\tilde{F}}_{k_\alpha i_\alpha} \mathbf{t}^{j_\alpha k_\alpha} - \tilde{\tilde{F}}_{k_\alpha j_\alpha} \mathbf{t}^{i_\alpha k_\alpha} \right)_{a_\alpha b_\alpha} + \sum_{l_\alpha} \left(\widetilde{(i_\alpha k_\alpha | j_\alpha l_\alpha)} \boldsymbol{\tau}^{k_\alpha l_\alpha} \right)_{a_\alpha b_\alpha} \right) \\ & + \sum_{k_\alpha} \left(-\mathbf{t}^{i_\alpha k_\alpha} \left(\mathbf{J}^{j_\alpha k_\alpha}_{\alpha\alpha} - \tilde{\mathbf{K}}^{j_\alpha k_\alpha} \right)^\dagger + \left(\mathbf{J}^{j_\alpha k_\alpha}_{\alpha\alpha} - \tilde{\mathbf{K}}^{j_\alpha k_\alpha} \right) \mathbf{t}^{i_\alpha k_\alpha \dagger} \right. \\ & \left. + \mathbf{t}^{j_\alpha k_\alpha} \left(\mathbf{J}^{i_\alpha k_\alpha}_{\alpha\alpha} - \tilde{\mathbf{K}}^{i_\alpha k_\alpha} \right)^\dagger - \left(\mathbf{J}^{i_\alpha k_\alpha}_{\alpha\alpha} - \tilde{\mathbf{K}}^{i_\alpha k_\alpha} \right) \mathbf{t}^{j_\alpha k_\alpha \dagger} \right. \end{aligned}$$

$$
\begin{aligned}
&\Big\{-t^{k_\alpha}_{a_\alpha}\Big(\Big(\mathbf{K}^{j_\alpha k_\alpha}\mathbf{t}^{i_\alpha}\Big)_{b_\alpha}-\Big(\mathbf{J}^{j_\alpha k_\alpha}_{\alpha\alpha}\mathbf{t}^{i_\alpha}\Big)_{b_\alpha}-\Big(\mathbf{K}^{i_\alpha k_\alpha}\mathbf{t}^{j_\alpha}\Big)_{b_\alpha}+\Big(\mathbf{J}^{i_\alpha k_\alpha}_{\alpha\alpha}\mathbf{t}^{j_\alpha}\Big)_{b_\alpha}\Big)\\
&\quad+\Big(\Big(\mathbf{K}^{j_\alpha k_\alpha}\mathbf{t}^{i_\alpha}\Big)_{a_\alpha}-\Big(\mathbf{J}^{j_\alpha k_\alpha}_{\alpha\alpha}\mathbf{t}^{i_\alpha}\Big)_{a_\alpha}-\Big(\mathbf{K}^{i_\alpha k_\alpha}\mathbf{t}^{j_\alpha}\Big)_{a_\alpha}+\Big(\mathbf{J}^{i_\alpha k_\alpha}_{\alpha\alpha}\mathbf{t}^{j_\alpha}\Big)_{a_\alpha}\Big)\,t^{k_\alpha}_{b_\alpha}\Big\}\Big)_{a_\alpha b_\alpha}\\
&+\sum_{k_\beta}\Big(+\mathbf{t}^{i_\alpha k_\beta}\tilde{\mathbf{K}}^{j_\alpha k_\beta\dagger}-\tilde{\mathbf{K}}^{j_\alpha k_\beta}\mathbf{t}^{i_\alpha k_\beta\dagger}-\mathbf{t}^{j_\alpha k_\beta}\tilde{\mathbf{K}}^{i_\alpha k_\beta\dagger}+\tilde{\mathbf{K}}^{i_\alpha k_\beta}\mathbf{t}^{j_\alpha k_\beta\dagger}\Big)_{a_\alpha b_\alpha}\\
&+\sum_{k_\alpha}\Big(\Big((i_\alpha k_\alpha|j_\alpha a_\alpha)-(j_\alpha k_\alpha|i_\alpha a_\alpha)\Big)t^{k_\alpha}_{b_\alpha}-t^{k_\alpha}_{a_\alpha}\Big((i_\alpha k_\alpha|j_\alpha b_\alpha)-(j_\alpha k_\alpha|i_\alpha b_\alpha)\Big)\Big)\\
&+\sum_{c_\alpha}\Big(\Big((i_\alpha a_\alpha|c_\alpha b_\alpha)-(i_\alpha b_\alpha|a_\alpha c_\alpha)\Big)t^{j_\alpha}_{c_\alpha}-\Big((j_\alpha a_\alpha|c_\alpha b_\alpha)-(j_\alpha b_\alpha|a_\alpha c_\alpha)\Big)t^{i_\alpha}_{c_\alpha}\Big)\quad,
\end{aligned}
\tag{2.57}
$$

$$
\begin{aligned}
R^{i_\alpha j_\beta}_{a_\alpha b_\beta}=\quad&\Big(\mathbf{K}^{i_\alpha j_\beta}\Big)_{a_\alpha b_\beta}+\Big(\mathbf{t}^{i_\alpha j_\beta}\tilde{\bar{\mathbf{F}}}^{v\dagger}_{\beta\beta}+\tilde{\bar{\mathbf{F}}}^{v}_{\alpha\alpha}\mathbf{t}^{i_\alpha j_\beta}\Big)_{a_\alpha b_\beta}+\tilde{\mathbf{K}}\Big(\boldsymbol{\tau}^{i_\alpha j_\beta}\Big)_{a_\alpha b_\beta}\\
&+\sum_{k_\alpha}\Bigg(-\Big(\tilde{\bar{F}}_{k_\alpha i_\alpha}\mathbf{t}^{k_\alpha j_\beta}\Big)_{a_\alpha b_\beta}+\sum_{l_\beta}\Big((i_\alpha\widetilde{k_\alpha|j_\beta}l_\beta)\boldsymbol{\tau}^{k_\alpha l_\beta}\Big)_{a_\alpha b_\beta}\Bigg)-\sum_{k_\beta}\Big(\tilde{\bar{F}}_{k_\beta j_\beta}\mathbf{t}^{i_\alpha k_\beta}\Big)_{a_\alpha b_\beta}\\
&+\sum_{k_\alpha}\Bigg(-\Big(\mathbf{J}^{i_\alpha k_\alpha}_{\alpha\alpha}-\tilde{\mathbf{K}}^{i_\alpha k_\alpha}\Big)\mathbf{t}^{k_\alpha j_\beta}\Big\{-t^{k_\alpha}_{a_\alpha}\Big(\Big(\mathbf{K}^{k_\alpha j_\beta\dagger}\mathbf{t}^{i_\alpha}\Big)_{b_\beta}+\Big(\mathbf{J}^{k_\alpha i_\alpha\dagger}_{\alpha\beta}\mathbf{t}^{j_\beta}\Big)_{b_\beta}\Big)\Big\}\\
&\qquad-\mathbf{t}^{k_\alpha j_\beta}\tilde{\mathbf{J}}^{k_\alpha i_\alpha}_{\alpha\beta}+\mathbf{t}^{i_\alpha k_\alpha}\tilde{\mathbf{K}}^{j_\beta k_\alpha\dagger}\Bigg)_{a_\alpha b_\beta}\\
&+\sum_{k_\beta}\Bigg(-\mathbf{t}^{i_\alpha k_\beta}\Big(\mathbf{J}^{j_\beta k_\beta}_{\beta\beta}-\tilde{\mathbf{K}}^{j_\beta k_\beta}\Big)^\dagger\Big\{-\Big(\Big(\mathbf{K}^{i_\alpha k_\beta}\mathbf{t}^{j_\beta}\Big)_{a_\alpha}+\Big(\mathbf{J}^{j_\beta k_\beta}_{\beta\alpha}\mathbf{t}^{i_\alpha}\Big)_{a_\alpha}\Big)\,t^{k_\beta}_{b_\beta}\Big\}\\
&\qquad-\tilde{\mathbf{J}}^{j_\beta k_\beta}_{\beta\alpha}\mathbf{t}^{i_\alpha k_\beta}+\tilde{\mathbf{K}}^{i_\alpha k_\beta}\mathbf{t}^{k_\beta j_\beta}\Bigg)_{a_\alpha b_\beta}\\
&-\sum_{k_\alpha}t^{k_\alpha}_{a_\alpha}(i_\alpha k_\alpha|j_\beta b_\beta)-\sum_{k_\beta}(j_\beta k_\beta|i_\alpha a_\alpha)t^{k_\beta}_{b_\beta}+\sum_{c_\alpha}(j_\beta b_\beta|a_\alpha c_\alpha)t^{i_\alpha}_{c_\alpha}+\sum_{c_\beta}(i_\alpha a_\alpha|c_\beta b_\beta)t^{j_\beta}_{c_\beta}\quad.
\end{aligned}
\tag{2.58}
$$

The 'dressed' amplitudes are given by ($\beta\beta$-case analogously)

$$
\tau^{i_\alpha j_\alpha}_{a_\alpha b_\alpha}=t^{i_\alpha j_\alpha}_{a_\alpha b_\alpha}\Big\{+\tfrac{1}{2}t^{i_\alpha}_{a_\alpha}t^{j_\alpha}_{b_\alpha}-\tfrac{1}{2}t^{j_\alpha}_{a_\alpha}t^{i_\alpha}_{b_\alpha}-\tfrac{1}{2}t^{i_\alpha}_{b_\alpha}t^{j_\alpha}_{a_\alpha}+\tfrac{1}{2}t^{j_\alpha}_{b_\alpha}t^{i_\alpha}_{a_\alpha}\Big\}\quad, \tag{2.59}
$$

$$
\tau^{i_\alpha j_\beta}_{a_\alpha b_\beta}=t^{i_\alpha j_\beta}_{a_\alpha b_\beta}\Big\{+\tfrac{1}{2}t^{i_\alpha}_{a_\alpha}t^{j_\beta}_{b_\beta}+\tfrac{1}{2}t^{j_\beta}_{b_\beta}t^{i_\alpha}_{a_\alpha}\Big\}\quad. \tag{2.60}
$$

The 'dressing' of the internal-internal, external-external and internal-external block of the

Fock matrix reads ($\beta\beta$-case analogously except the terms given explicitly)

$$\tilde{F}_{k_\alpha i_\alpha} = F_{k_\alpha i_\alpha} + \tfrac{1}{2}\sum_{l_\alpha}\left\langle\left(\mathbf{K}^{k_\alpha l_\alpha} - \mathbf{K}^{k_\alpha l_\alpha\dagger}\right)\boldsymbol{\tau}^{i_\alpha l_\alpha\dagger}\right\rangle + \sum_{l_\beta}\left\langle\mathbf{K}^{k_\alpha l_\beta}\boldsymbol{\tau}^{i_\alpha l_\beta\dagger}\right\rangle \quad , \tag{2.61}$$

$$\tilde{F}_{k_\beta i_\beta} = \cdots + \sum_{l_\alpha}\left\langle\mathbf{K}^{l_\alpha k_\beta}\boldsymbol{\tau}^{l_\alpha i_\beta\dagger}\right\rangle \quad , \tag{2.62}$$

$$\tilde{\tilde{F}}_{k_\alpha i_\alpha} = \tilde{F}_{k_\alpha i_\alpha}\left\{+\mathbf{G}_\alpha(\mathbf{t}^1)_{i_\alpha k_\alpha} + \sum_{a_\alpha} t^{i_\alpha}_{a_\alpha} F_{k_\alpha a_\alpha}\right\} \quad , \tag{2.63}$$

$$\begin{aligned}\tilde{F}_{a_\alpha c_\alpha} = \quad & F_{a_\alpha c_\alpha} - \tfrac{1}{2}\sum_{k_\alpha,l_\alpha}\left(\boldsymbol{\tau}^{k_\alpha l_\alpha}\left(\mathbf{K}^{k_\alpha l_\alpha} - \mathbf{K}^{k_\alpha l_\alpha\dagger}\right)^\dagger\right)_{a_\alpha c_\alpha} \\ & - \sum_{k_\beta,l_\alpha}\left(\boldsymbol{\tau}^{l_\alpha k_\beta}\mathbf{K}^{l_\alpha k_\beta\dagger}\right)_{a_\alpha c_\alpha} \quad ,\end{aligned} \tag{2.64}$$

$$\tilde{F}_{a_\beta c_\beta} = \cdots - \sum_{k_\alpha,l_\beta}\left(\boldsymbol{\tau}^{k_\alpha l_\beta\dagger}\mathbf{K}^{k_\alpha l_\beta}\right)_{a_\beta c_\beta} \quad , \tag{2.65}$$

$$\tilde{\tilde{F}}_{a_\alpha c_\alpha} = \tilde{F}_{a_\alpha c_\alpha}\left\{+\mathbf{G}_\alpha(\mathbf{t}^1)_{c_\alpha a_\alpha} - \sum_{i_\alpha} t^{i_\alpha}_{a_\alpha} F_{i_\alpha c_\alpha}\right\} \quad , \tag{2.66}$$

$$\tilde{F}_{k_\alpha c_\alpha} = F_{k_\alpha c_\alpha} + \sum_{l_\alpha}\left(\left(\mathbf{K}^{k_\alpha l_\alpha} - \mathbf{K}^{k_\alpha l_\alpha\dagger}\right)\mathbf{t}^{l_\alpha}\right)_{c_\alpha} + \sum_{l_\beta}\left(\mathbf{K}^{k_\alpha l_\beta}\mathbf{t}^{l_\beta}\right)_{c_\alpha} \quad , \tag{2.67}$$

$$\tilde{F}_{k_\beta c_\beta} = \cdots + \sum_{l_\alpha}\left(\mathbf{K}^{l_\alpha k_\beta\dagger}\mathbf{t}^{l_\alpha}\right)_{c_\beta} \quad . \tag{2.68}$$

The singles Fock matrix is given by ($\beta\beta$-case analogously except for part which is stated explicitly)

$$\mathbf{G}_\alpha(\mathbf{t}^1)_{p_\alpha q_\alpha} = \sum_{j_\alpha,b_\alpha}\left((p_\alpha q_\alpha|j_\alpha b_\alpha) - (p_\alpha j_\alpha|q_\alpha b_\alpha)\right)t^{j_\alpha}_{b_\alpha} + \sum_{j_\beta,b_\beta}(p_\alpha q_\alpha|j_\beta b_\beta)\,t^{j_\beta}_{b_\beta} \quad , \tag{2.69}$$

$$\mathbf{G}_\beta(\mathbf{t}^1)_{p_\beta q_\beta} = \cdots + \sum_{j_\alpha,b_\alpha}(p_\beta q_\beta|j_\alpha b_\alpha)\,t^{j_\alpha}_{b_\alpha} \quad . \tag{2.70}$$

The 'dressing' of the four-internal integrals reads ($\beta\beta$-case analogously)

$$\begin{aligned}\widetilde{(i_\alpha k_\alpha|j_\alpha l_\alpha)} = \quad & (i_\alpha k_\alpha|j_\alpha l_\alpha) \\ & + \tfrac{1}{2}\left\langle\mathbf{K}^{k_\alpha l_\alpha}\boldsymbol{\tau}^{i_\alpha j_\alpha\dagger}\right\rangle\left\{+\sum_{a_\alpha}\left((l_\alpha j_\alpha|k_\alpha a_\alpha)t^{i_\alpha}_{a_\alpha} + (k_\alpha i_\alpha|l_\alpha a_\alpha)t^{j_\alpha}_{a_\alpha}\right)\right\} \quad ,\end{aligned} \tag{2.71}$$

$$(i_\alpha \widetilde{k_\alpha | j_\beta} l_\beta) = (i_\alpha k_\alpha | j_\beta l_\beta) + \left\langle \mathbf{K}^{k_\alpha l_\beta} \boldsymbol{\tau}^{i_\alpha j_\beta \dagger} \right\rangle \left\{ + \sum_{a_\alpha} (l_\beta j_\beta | k_\alpha a_\alpha) t_{a_\alpha}^{i_\alpha} + \sum_{a_\beta} (k_\alpha i_\alpha | l_\beta a_\beta) t_{a_\beta}^{j_\beta} \right\} \quad , \quad (2.72)$$

and the 'dressed' external Exchange operator (EEO) in the MO basis is given by ($\beta\beta$-case analogously)

$$\mathbf{K}(\boldsymbol{\tau}^{i_\alpha j_\alpha})_{a_\alpha b_\alpha} = \sum_{c_\alpha, d_\alpha} \Bigg((a_\alpha c_\alpha | b_\alpha d_\alpha) \left\{ - \sum_{k_\alpha} \Big((k_\alpha d_\alpha | a_\alpha c_\alpha) t_{b_\alpha}^{k_\alpha} + t_{a_\alpha}^{k_\alpha} (k_\alpha c_\alpha | b_\alpha d_\alpha) \Big) \right\} \Bigg) \tau_{c_\alpha d_\alpha}^{i_\alpha j_\alpha} \quad , \quad (2.73)$$

$$\mathbf{K}(\boldsymbol{\tau}^{i_\alpha j_\beta})_{a_\alpha b_\beta} = \sum_{c_\alpha, d_\beta} \Bigg((a_\alpha c_\alpha | b_\beta d_\beta) \left\{ - \sum_{k_\beta} (k_\beta d_\beta | a_\alpha c_\alpha) t_{b_\beta}^{k_\beta} - \sum_{k_\alpha} t_{a_\alpha}^{k_\alpha} (k_\alpha c_\alpha | b_\beta d_\beta) \right\} \Bigg) \tau_{c_\alpha d_\beta}^{i_\alpha j_\beta} \quad . \quad (2.74)$$

The most cumbersome terms are the 'dressed' two-external Exchange and Coulomb operators:

$$\begin{aligned} \tilde{K}_{a_\alpha c_\alpha}^{i_\alpha k_\alpha} = \; & K_{a_\alpha c_\alpha}^{i_\alpha k_\alpha} + \sum_{l_\alpha} \Bigg(\Big(\tfrac{1}{2} \mathbf{t}^{i_\alpha l_\alpha} \left(\mathbf{K}^{k_\alpha l_\alpha} - \mathbf{K}^{k_\alpha l_\alpha \dagger} \right)^\dagger \Big)_{a_\alpha c_\alpha} \Big\{ - t_{a_\alpha}^{l_\alpha} \left(\mathbf{K}^{k_\alpha l_\alpha} \mathbf{t}^{i_\alpha} - \mathbf{K}^{k_\alpha l_\alpha \dagger} \mathbf{t}^{i_\alpha} \right)_{c_\alpha} \\ & + t_{a_\alpha}^{l_\alpha} \Big((i_\alpha k_\alpha | l_\alpha c_\alpha) - (i_\alpha l_\alpha | k_\alpha c_\alpha) \Big) \Big\} \Bigg) + \tfrac{1}{2} \sum_{l_\beta} \left(\mathbf{t}^{i_\alpha l_\beta} \mathbf{K}^{k_\alpha l_\beta \dagger} \right)_{a_\alpha c_\alpha} \\ & \Big\{ + \sum_{d_\alpha} \Big((k_\alpha c_\alpha | a_\alpha d_\alpha) - (k_\alpha d_\alpha | a_\alpha c_\alpha) \Big) t_{d_\alpha}^{i_\alpha} \Big\} \quad , \end{aligned} \quad (2.75)$$

$$\begin{aligned} \tilde{K}_{b_\beta c_\beta}^{j_\beta k_\beta} = \; & K_{b_\beta c_\beta}^{j_\beta k_\beta} + \sum_{l_\beta} \Bigg(\Big(\tfrac{1}{2} \mathbf{t}^{j_\beta l_\beta} \left(\mathbf{K}^{k_\beta l_\beta} - \mathbf{K}^{k_\beta l_\beta \dagger} \right)^\dagger \Big)_{b_\beta c_\beta} \Big\{ - t_{b_\beta}^{l_\beta} \left(\mathbf{K}^{k_\beta l_\beta} \mathbf{t}^{j_\beta} - \mathbf{K}^{k_\beta l_\beta \dagger} \mathbf{t}^{j_\beta} \right)_{c_\beta} \\ & + t_{b_\beta}^{l_\beta} \Big((j_\beta k_\beta | l_\beta c_\beta) - (j_\beta l_\beta | k_\beta c_\beta) \Big) \Big\} \Bigg) + \tfrac{1}{2} \sum_{l_\alpha} \left(\mathbf{t}^{l_\alpha j_\beta \dagger} \mathbf{K}^{l_\alpha k_\beta} \right)_{b_\beta c_\beta} \\ & \Big\{ + \sum_{d_\beta} \Big((k_\beta c_\beta | b_\beta d_\beta) - (k_\beta d_\beta | b_\beta c_\beta) \Big) t_{d_\beta}^{j_\beta} \Big\} \quad , \end{aligned} \quad (2.76)$$

$$\tilde{K}^{i_\alpha k_\beta}_{a_\alpha c_\beta} = K^{i_\alpha k_\beta}_{a_\alpha c_\beta} + \sum_{l_\alpha} \left(\tfrac{1}{2} \left(\mathbf{t}^{i_\alpha l_\alpha} \mathbf{K}^{l_\alpha k_\beta} \right)_{a_\alpha c_\beta} \left\{ -t^{l_\alpha}_{a_\alpha} \left(\mathbf{K}^{l_\alpha k_\beta \dagger} \mathbf{t}^{i_\alpha} \right)_{c_\beta} - t^{l_\alpha}_{a_\alpha} (i_\alpha l_\alpha | k_\beta c_\beta) \right\} \right) + \tfrac{1}{2} \sum_{l_\beta} \left(\mathbf{t}^{i_\alpha l_\beta} \left(\mathbf{K}^{k_\beta l_\beta} - \mathbf{K}^{k_\beta l_\beta \dagger} \right)^\dagger \right)_{a_\alpha c_\beta} \left\{ + \sum_{d_\alpha} (k_\beta c_\beta | a_\alpha d_\alpha) t^{i_\alpha}_{d_\alpha} \right\} \quad , \tag{2.77}$$

$$\tilde{K}^{j_\beta k_\alpha}_{b_\beta c_\alpha} = \left(\mathbf{K}^{k_\alpha j_\beta \dagger} \right)_{b_\beta c_\alpha} + \sum_{l_\beta} \left(\tfrac{1}{2} \left(\mathbf{t}^{j_\beta l_\beta} \mathbf{K}^{k_\alpha l_\beta \dagger} \right)_{b_\beta c_\alpha} \left\{ -t^{l_\beta}_{b_\beta} \left(\mathbf{K}^{k_\alpha l_\beta} \mathbf{t}^{j_\beta} \right)_{c_\alpha} - t^{l_\beta}_{b_\beta} (j_\beta l_\beta | k_\alpha c_\alpha) \right\} \right) + \tfrac{1}{2} \sum_{k_\alpha} \left(\mathbf{t}^{l_\alpha j_\beta \dagger} \left(\mathbf{K}^{k_\alpha l_\alpha} - \mathbf{K}^{k_\alpha l_\alpha \dagger} \right)^\dagger \right)_{b_\beta c_\alpha} \left\{ + \sum_{d_\beta} (k_\alpha c_\alpha | b_\beta d_\beta) t^{j_\beta}_{d_\beta} \right\} \quad , \tag{2.78}$$

$$\tilde{J}^{k_\alpha i_\alpha}_{c_\beta b_\beta} = J^{k_\alpha i_\alpha}_{c_\beta b_\beta} + \sum_{l_\beta} \left(-\tfrac{1}{2} \left(\mathbf{K}^{k_\alpha l_\beta \dagger} \mathbf{t}^{i_\alpha l_\beta} \right)_{c_\beta b_\beta} \left\{ - \left(\mathbf{K}^{k_\alpha l_\beta \dagger} \mathbf{t}^{i_\alpha} \right)_{c_\beta} t^{l_\beta}_{b_\beta} - (i_\alpha k_\alpha | l_\beta c_\beta) t^{l_\beta}_{b_\beta} \right\} \right) \left\{ + \sum_{d_\alpha} t^{i_\alpha}_{d_\alpha} (k_\alpha d_\alpha | b_\beta c_\beta) \right\} \quad , \tag{2.79}$$

$$\tilde{J}^{j_\beta k_\beta}_{a_\alpha c_\alpha} = J^{j_\beta k_\beta}_{a_\alpha c_\alpha} + \sum_{l_\alpha} \left(-\tfrac{1}{2} \left(\mathbf{t}^{l_\alpha j_\beta} \mathbf{K}^{l_\alpha k_\beta \dagger} \right)_{a_\alpha c_\alpha} \left\{ -t^{l_\alpha}_{a_\alpha} \left(\mathbf{K}^{l_\alpha k_\beta} \mathbf{t}^{j_\beta} \right)_{c_\alpha} - t^{l_\alpha}_{a_\alpha} (j_\beta k_\beta | l_\alpha c_\alpha) \right\} \right) \left\{ + \sum_{d_\beta} t^{j_\beta}_{d_\beta} (k_\beta d_\beta | a_\alpha c_\alpha) \right\} \quad . \tag{2.80}$$

While for CCSD the singles-singles contribution involving the two-external integrals is already included via the singles Fock matrix, the latter has to be calculated explicitly in the singles residuals for QCISD (indicated by squared brackets in Eq. (2.56)). If the EEO is constructed using an AO-direct algorithm, these terms and parts of the interaction between the external-external and internal-internal 'dressed' Fock operators with singles amplitudes (first line of Eq. (2.56)) are already done together with the EEO. The residual equations for unrestricted CEPA methods are very similar to those presented above for QCISD. The difference is that no 'dressed' quantities are necessary, but an additional term, the energy shift, appears. The explicit form for different CEPA variants in spin-unrestricted form can be found elsewhere.[113]

2.3.4. The LPNO approach for the spin-unrestricted case

As already discussed in detail for the closed-shell case, the most straightforward approach to construct approximate PNOs is to take the MP2 amplitudes ($\beta\beta$-case analogously)

$$t^{i_\alpha j_\alpha}_{a_\alpha b_\alpha} = -\frac{K^{i_\alpha j_\alpha}_{a_\alpha b_\alpha} - K^{i_\alpha j_\alpha}_{b_\alpha a_\alpha}}{\varepsilon_{a_\alpha} + \varepsilon_{b_\alpha} - \varepsilon_{i_\alpha} - \varepsilon_{j_\alpha}} \quad , \tag{2.81}$$

$$t_{a_\alpha b_\beta}^{i_\alpha j_\beta} = -\frac{K_{a_\alpha b_\beta}^{i_\alpha j_\beta}}{\varepsilon_{a_\alpha} + \varepsilon_{b_\beta} - \varepsilon_{i_\alpha} - \varepsilon_{j_\beta}} \quad , \tag{2.82}$$

and use them to calculate the virtual pair densities ($\beta\beta$-case analogously)

$$\mathbf{D}^{i_\alpha j_\alpha} = \frac{4\,\mathbf{t}^{i_\alpha j_\alpha \dagger}\mathbf{t}^{i_\alpha j_\alpha}}{1 + 2\,tr\left(\mathbf{t}^{i_\alpha j_\alpha \dagger}\mathbf{t}^{i_\alpha j_\alpha}\right)} \quad , \tag{2.83}$$

$$\mathbf{D}^{i_\alpha j_\beta(\alpha)} = \frac{2\,\mathbf{t}^{i_\alpha j_\beta}\mathbf{t}^{i_\alpha j_\beta \dagger}}{1 + tr\left(\mathbf{t}^{i_\alpha j_\beta}\mathbf{t}^{i_\alpha j_\beta \dagger}\right)} \quad , \tag{2.84}$$

$$\mathbf{D}^{i_\alpha j_\beta(\beta)} = \frac{2\,\mathbf{t}^{i_\alpha j_\beta \dagger}\mathbf{t}^{i_\alpha j_\beta}}{1 + tr\left(\mathbf{t}^{i_\alpha j_\beta \dagger}\mathbf{t}^{i_\alpha j_\beta}\right)} \quad . \tag{2.85}$$

The PNOs are obtained as eigenfunctions of the virtual pair density, e.g. for the $\alpha\alpha$-case:

$$\mathbf{D}^{i_\alpha j_\alpha}\mathbf{d}^{i_\alpha j_\alpha} = n^{i_\alpha j_\alpha}\mathbf{d}^{i_\alpha j_\alpha} \quad . \tag{2.86}$$

PNOs with an occupation number below the threshold $\mathrm{T}_{\mathrm{CutPNO}}$ are neglected. Note that for the $\alpha\beta$-pairs two sets of PNOs are needed (denoted with the superscripts (α) and (β) respectively) since there are α-spin and β-spin virtual orbitals associated with the respective electron pair. Expansion of the virtual orbitals in the truncated PNO pair basis and *vice versa* is achieved analogously to the closed-shell case (Eqs. (2.22) and (2.23)).

However, in the open-shell case, a complication due to the unrestricted sum over the intermediate label k in the non-linear part of the two-external pair-pair contribution to the doubles residual (Eqs. (2.57) and (2.58)) and the dressing of the two-external pair-pair operators (Eqs. (2.75) – (2.80)) arises. For these terms, one would need $\alpha\alpha$- or $\beta\beta$-spin PNOs respectively with e.g. $i = k$ which, however, cannot be mapped onto physical $\alpha\alpha$- or $\beta\beta$-pairs. For interactions of this type which belong to the DOMO subspace, the PNOs of the corresponding $\alpha\beta$-pair (i_α, i_β) are used instead. This does not lead to additional an error since the closed-shell α- and β-spin spatial orbitals are exactly the same if localized QROs are used to build up the α- and β-spin orbital subspaces. However, this substitution is not possible for the (i_α, i_α) combinations within the open-shell orbitals since the corresponding β-spin orbitals do not exist. Thus, a small set of alternative approximate PNOs obtained from two-external Exchange integrals for the 'diagonal' pair-pair interactions within the SOMO subspace is employed instead, which is constructed through:

$$\mathbf{K}^{i_\alpha i_\alpha}\mathbf{d}^{i_\alpha i_\alpha} = n^{i_\alpha i_\alpha}\mathbf{d}^{i_\alpha i_\alpha} \quad . \tag{2.87}$$

This choice was motivated by an early work of Ahlrichs *et al.*[182] and Jungen et al.[217] who showed that the $\mathbf{K}^{ii}$ integrals are local and can be used for the direct calculation of approximate pair natural orbitals for the intra-pair case within the independent electron pair approximation (IEPA). In a preliminary study (unpublished data) it was found that by using

approximate PNOs obtained as eigenfunctions of the symmetrized two-external Exchange operators, about twice as many correlating orbitals are needed to obtain the same accuracy as for MP2-PNOs. Hence, at most twice as many $\mathbf{K}^{ii}$-PNOs than the average number of MP2-PNOs per pair are kept. The comprehensive test calculations presented in Chapter 3 consistently show that the small set of $\mathbf{K}^{ii}$-PNOs does not have a significant effect on the accuracy of the open-shell LPNO-QCISD or LPNO-CCSD methods.

As already discussed in the context of the closed-shell LPNO methods, a small complication arises from the fact that PNOs belonging to different pairs are non-orthogonal. The PNOs associated with the $\alpha\alpha$-pairs do not interact with $\beta\beta$-pairs, but both interact with $\alpha\beta$-pairs. Moreover, the two sets of PNOs for $\alpha\beta$-pairs give rise to two different overlaps matrices. Additionally, the overlap between the $\mathbf{K}^{ii}$-PNOs of the SOMO subspace with $\alpha\alpha$- and $\alpha\beta$-pairs has to be taken into account. Thus, in total 10 different overlap matrices have to be calculated and stored on disk. For example, the overlap between MP2-PNOs for $\alpha\alpha$-pairs reads:

$$S^{i_\alpha j_\alpha, k_\alpha l_\alpha}_{\bar{a}_\alpha, \bar{b}_\alpha} = \left\langle \bar{a}^{i_\alpha j_\alpha} \middle| \bar{b}^{k_\alpha l_\alpha} \right\rangle = (\mathbf{d}^{i_\alpha j_\alpha \dagger} \mathbf{d}^{k_\alpha l_\alpha})_{\bar{a}_\alpha \bar{b}_\alpha} \quad . \tag{2.88}$$

The double excitation amplitudes in the truncated PNO pair basis ($\alpha\alpha$ and $\beta\beta$ spin cases analogously) become

$$\bar{\mathbf{t}}^{i_\alpha j_\beta} = \mathbf{d}^{i_\alpha j_\beta(\alpha)\dagger} \mathbf{t}^{i_\beta j_\beta} \mathbf{d}^{i_\alpha j_\beta(\beta)} \quad , \tag{2.89}$$

thus leading to a very compact representation of the first order interacting space with a linear scaling number of doubles amplitudes. The doubles residuals can be calculated with high efficiency. For instance, the construction of the EEO representing the computational bottleneck in conventional single reference correlation methods can now be calculated in negligible computation times and with linear scaling behavior since the four-external integrals are calculated entirely in the truncated PNO of the respective electron pair. If different pairs are involved in a contraction, it is necessary to insert the appropriate overlap matrices. For example, the four-internal pair-pair contribution to the '$\alpha\alpha$' doubles residual becomes

$$\bar{R}^{i_\alpha j_\alpha}_{\bar{a}_\alpha \bar{b}_\alpha} \leftarrow + \sum_{k_\alpha, l_\alpha} \left(\widetilde{(i_\alpha k_\alpha | j_\alpha l_\alpha)} \mathbf{S}^{i_\alpha j_\alpha, k_\alpha l_\alpha} \bar{\boldsymbol{\tau}}^{k_\alpha l_\alpha} \mathbf{S}^{i_\alpha j_\alpha, k_\alpha l_\alpha \dagger} \right)_{\bar{a}_\alpha \bar{b}_\alpha} \quad . \tag{2.90}$$

As in the closed-shell case, this contribution to the doubles residual is skipped if the absolute value of the 'dressed' four-internal integral in questions falls below 10^{-14} $\mathrm{E_h}$ with negligible consequences on the accuracy of the LPNO methods (see Chapter 3). The single excitations are not truncated and thus, the singles residual are calculated in the full VMO basis. However, singles amplitudes that occur in the doubles residuals must be projected to the respective PNO pair basis (β-spin singles amplitudes analogously)

$$\bar{t}^{i_\alpha}_{\bar{a}_\alpha} = \sum_{a_\alpha} d^{i_\alpha j_\alpha}_{a_\alpha \bar{a}_\alpha} t^{i_\alpha}_{a_\alpha} \tag{2.91}$$

to perform the necessary contractions. Likewise, doubles amplitudes in the singles residuals

are back-projected on the fly onto the full VMO basis in order to avoid storage bottlenecks. This formally rather crude approximation will be numerically justified in Sec. 3.2.8.
Analogously to the closed-shell case, a large part of the LPNO error can be compensated for by adding an estimate (based on second order perturbation theory) for the weak pair correlation energy and PNO truncation error to the total correlation energy. It can be easily calculated during the initial guess since the MP2 amplitudes and two-external Exchange integrals are available in the full PNO pair basis, *e.g.* for $\alpha\alpha$-pairs:

$$\Delta\varepsilon_{i_\alpha j_\alpha} = \varepsilon_{i_\alpha j_\alpha}^{\text{MP2;trunc}} - \varepsilon_{i_\alpha j_\alpha}^{\text{MP2;full}} \quad . \tag{2.92}$$

In the open-shell case, the treatment of the two-external pair-pair interactions is more intricate. The PNO form of the corresponding terms (only the loops over the intermediate label k_α are shown) contributing to '$\alpha\beta$' LPNO-CCSD residual is given by

$$\begin{aligned}
\bar{R}_{\bar{a}_\alpha\bar{b}_\beta}^{i_\alpha j_\beta} = \quad & \cdots \\
& + \sum_{k_\alpha} \Bigg(+ \left(\mathbf{d}^{i_\alpha j_\beta(\alpha)\dagger} \mathbf{K}^{i_\alpha k_\alpha} \mathbf{d}^{k_\alpha j_\beta(\alpha)} - \mathbf{d}^{i_\alpha j_\beta(\alpha)\dagger} \mathbf{J}_{\alpha\alpha}^{i_\alpha k_\alpha} \mathbf{d}^{k_\alpha j_\beta(\alpha)} \right) \bar{\mathbf{t}}^{k_\alpha j_\beta} \mathbf{S}^{k_\alpha j_\beta(\beta), i_\alpha j_\beta(\beta)} \\
& \quad - \mathbf{S}^{i_\alpha j_\beta(\alpha), k_\alpha j_\beta(\alpha)} \bar{\mathbf{t}}^{k_\alpha j_\beta} \left(\mathbf{d}^{i_\alpha j_\beta(\beta)\dagger} \mathbf{J}_{\alpha\beta}^{i_\alpha k_\alpha} \mathbf{d}^{k_\alpha j_\beta(\beta)} \right)^\dagger \\
& \quad + \mathbf{S}^{i_\alpha k_\alpha, i_\alpha j_\beta(\alpha)\dagger} \bar{\mathbf{t}}^{i_\alpha k_\alpha\dagger} \mathbf{d}^{i_\alpha k_\alpha\dagger} \mathbf{K}^{k_\alpha j_\beta} \mathbf{d}^{i_\alpha j_\beta(\beta)} \Bigg)_{\bar{a}_\alpha\bar{b}_\beta} \\
& + \sum_{k_\alpha} \Bigg(+ \mathbf{S}^{i_\alpha k_\alpha, i_\alpha j_\beta(\alpha)\dagger} \bar{\tilde{\mathbf{K}}}^{i_\alpha k_\alpha} \mathbf{S}^{i_\alpha k_\alpha, k_\alpha j_\beta(\alpha)} \bar{\mathbf{t}}^{k_\alpha j_\beta} \mathbf{S}^{k_\alpha j_\beta(\beta), i_\alpha j_\beta(\beta)} \\
& \quad - \mathbf{S}^{i_\alpha j_\beta(\alpha), k_\alpha j_\beta(\alpha)} \bar{\mathbf{t}}^{k_\alpha j_\beta} \mathbf{d}^{k_\alpha j_\beta(\beta)\dagger} \tilde{\mathbf{J}}_{\alpha\beta}^{k_\alpha i_\alpha} \mathbf{d}^{i_\alpha j_\beta(\beta)} \\
& \quad + \mathbf{S}^{i_\alpha k_\alpha, i_\alpha j_\beta(\alpha)\dagger} \bar{\mathbf{t}}^{i_\alpha k_\alpha} \mathbf{S}^{i_\alpha k_\alpha, k_\alpha j_\beta(\alpha)} \bar{\tilde{\mathbf{K}}}^{j_\beta k_\alpha\dagger} \mathbf{S}^{k_\alpha j_\beta(\beta), i_\alpha j_\beta(\beta)} \Bigg)_{\bar{a}_\alpha\bar{b}_\beta} \\
& + \sum_{k_\alpha} \left(-\bar{t}_{\bar{a}_\alpha}^{k_\alpha} \left(\left(\mathbf{S}^{i_\alpha j_\beta(\beta), k_\alpha j_\beta(\beta)} (\bar{\mathbf{K}}^{k_\alpha j_\beta\dagger} \bar{\mathbf{t}}^{i_\alpha}) \right)_{\bar{b}_\beta} + \left(\mathbf{d}^{i_\alpha j_\beta(\beta)\dagger} (\mathbf{J}_{\alpha\beta}^{k_\alpha i_\alpha\dagger} \mathbf{t}^{j_\beta}) \right)_{\bar{b}_\beta} \right) \right)_{\bar{a}_\alpha\bar{b}_\beta} .
\end{aligned} \tag{2.93}$$

In the LPNO variants of the spin-unrestricted open-shell CEPA and CPF methods, only the linear terms given in the first sum of Eq. (2.93) contribute to the doubles residual. They are calculated analogously to the closed-shell LPNO-CEPA implementation (Sec. 2.2.7). The projection of the MO basis Coulomb and Exchange operators onto the PNO pair basis in question is performed in a preceding step and in the iterations, only their contraction with the respective PNO doubles amplitudes has to be carried out. For LPNO-QCISD and LPNO-CCSD, these terms are done in the same way as in 'Algorithm 1' of the closed-shell LPNO-CCSD implementation (see Sec. 2.3.2). The non-linear terms given in the second

and third sum of Eq. (2.93) only appear for LPNO-QCISD and CCSD. The corresponding contractions are carried out with the 'dressed' Coulomb and Exchange integrals which are given by (the explicit expression for further 'dressed' two-external integrals can be found in Appendix B):

$$\begin{aligned}\bar{\tilde{K}}^{i_\alpha k_\alpha}_{\bar{a}_\alpha \bar{c}_\alpha} = & \sum_{l_\alpha} \Bigg(\Big(\tfrac{1}{2} \mathbf{S}^{i_\alpha k_\alpha, i_\alpha l_\alpha} \bar{\mathbf{t}}^{i_\alpha l_\alpha} \mathbf{S}^{i_\alpha l_\alpha, k_\alpha l_\alpha} \left(\bar{\mathbf{K}}^{k_\alpha l_\alpha} - \bar{\mathbf{K}}^{k_\alpha l_\alpha \dagger} \right)^\dagger \mathbf{S}^{k_\alpha l_\alpha, i_\alpha k_\alpha} \Big)_{\bar{a}_\alpha \bar{c}_\alpha} \\ & - \bar{t}^{l_\alpha}_{\bar{a}_\alpha} \left(\mathbf{S}^{k_\alpha l_\alpha, i_\alpha k_\alpha \dagger} \left(\bar{\mathbf{K}}^{k_\alpha l_\alpha} \bar{\mathbf{t}}^{i_\alpha} - \bar{\mathbf{K}}^{k_\alpha l_\alpha \dagger} \bar{\mathbf{t}}^{i_\alpha} \right) \right)_{\bar{c}_\alpha} \\ & + \bar{t}^{l_\alpha}_{\bar{a}_\alpha} \left(\sum_{c_\alpha} \left((i_\alpha k_\alpha | l_\alpha c_\alpha) - (i_\alpha l_\alpha | k_\alpha c_\alpha) \right) d^{i_\alpha k_\alpha}_{c_\alpha \bar{c}_\alpha} \right) \Bigg) \\ & + \tfrac{1}{2} \sum_{l_\beta} \left(\mathbf{S}^{i_\alpha k_\alpha, i_\alpha l_\beta(\alpha)} \bar{\mathbf{t}}^{i_\alpha l_\beta} \mathbf{S}^{i_\alpha l_\beta(\beta), k_\alpha l_\beta(\beta)} \bar{\mathbf{K}}^{k_\alpha l_\beta \dagger} \mathbf{S}^{k_\alpha l_\beta(\alpha), i_\alpha k_\alpha} \right)_{\bar{a}_\alpha \bar{c}_\alpha} \\ & + \sum_{\bar{d}_\alpha} \left((k_\alpha \bar{c}_\alpha | \bar{a}_\alpha \bar{d}_\alpha) - (k_\alpha \bar{d}_\alpha | \bar{a}_\alpha \bar{c}_\alpha) \right) \bar{t}^{i_\alpha}_{\bar{d}_\alpha} \quad , \end{aligned} \tag{2.94}$$

$$\begin{aligned}\tilde{J}^{k_\alpha i_\alpha}_{c_\beta b_\beta} = & \sum_{l_\beta} \Bigg(-\tfrac{1}{2} \left(\mathbf{d}^{k_\alpha l_\beta(\beta)} \bar{\mathbf{K}}^{k_\alpha l_\beta \dagger} \mathbf{S}^{k_\alpha l_\beta(\alpha), i_\alpha l_\beta(\alpha)} \bar{\mathbf{t}}^{i_\alpha l_\beta} \mathbf{d}^{i_\alpha l_\beta(\beta) \dagger} \right)_{c_\beta b_\beta} \\ & - \left((\mathbf{d}^{k_\alpha l_\beta(\alpha)} \bar{\mathbf{K}}^{k_\alpha l_\beta \dagger} \mathbf{d}^{k_\alpha l_\beta(\beta) \dagger}) \mathbf{t}^{i_\alpha} \right)_{c_\beta} t^{l_\beta}_{b_\beta} - (i_\alpha k_\alpha | l_\beta c_\beta)\, t^{l_\beta}_{b_\beta} \Bigg) \\ & + \sum_{d_\alpha} t^{i_\alpha}_{d_\alpha} \, (k_\alpha d_\alpha | b_\beta c_\beta) \quad . \end{aligned} \tag{2.95}$$

Contractions involving singles amplitudes do only appear in the LPNO-CCSD form of these 'dressed' quantities. In the 'dressing' of the '$\alpha\alpha$' Exchange operator (Eq. (2.94)), the $\mathbf{K}^{ii}$-PNOs are needed. Furthermore, the three-external contribution (last term of Eq. (2.94), highlighted in blue) has to be neglected for LPNO-CCSD since no PNO integrals are available for $i_\alpha = k_\alpha$. For all contractions involving two-external Exchange integrals, the PNO integrals are used. More problematic are the 'dressed' Coulomb integrals since '$\beta\beta$' PNOs would be needed for $\alpha\alpha$-pairs and *vice versa*. Thus, in contrast to the 'dressed' Exchange operators, the 'dressed' Coulomb integrals have to be back-projected onto the MO basis and the subsequent projection onto the PNO pair basis in question is done on the fly during the residual calculation (see Eq. (2.93)). This implies that the contractions with singles amplitudes, which contribute to the 'dressed' Coulomb operators in the LPNO-CCSD case (Eq. (2.95), the terms highlighted in blue), need to be calculated in MO basis as well. Thus, a relatively expensive fifth order scaling step would be necessary and hence, the corresponding terms are neglected and the LPNO-QCISD form of this 'dressed' operator is used instead. However, these terms are small and the accuracy of the present open-shell LPNO-CCSD method does not suffer significantly from this approximation since the truncation errors are

about one order of magnitude larger (see Sec. 3.2.2). The dressed '$\beta\beta$' Exchange operator and '$\beta\alpha$' Coulomb operator are calculated analogously. For the dressed '$\alpha\beta$' and '$\beta\alpha$' Exchange operators, no terms have to be discarded.

Another complication in the present open-shell LPNO-CCSD variant arises for the non-linear singles contribution to the two-external pair-pair interaction (third sum of Eq. (2.93)) since the appropriate two-external PNO integrals are not available for the undressed '$\alpha\beta$' and '$\beta\alpha$' Coulomb operators. Hence, the corresponding contractions have to be performed in the full VMO basis, which introduces another fifth order scaling step. Furthermore, for the analogous contractions in the '$\alpha\alpha$' and '$\beta\beta$' doubles residuals with $i = k$ or $j = k$, no PNO transformation matrices are available since only $\mathbf{K}^{ii}$-PNOs for the open-shell orbitals are available in the present implementation. Thus, these contributions have to be calculated in the MO basis as well. Attempts to discard these terms were not successful and led to unacceptable large errors as well as convergence problems. Unfortunately, as it will be evident from detailed timings presented in Sec. 3.4.2, this fifth order scaling step gives adds significantly to the total computation time needed for the calculation of the doubles residuals.

The last approximation associated with the present open-shell LPNO-CCSD formalism arises from neglecting the 'dressing' of the EEO (Eq. (2.73) and (2.74)), but this term was also discarded in the closed-shell LPNO-CCSD implementation (see Sec. 2.3.2). This approximation can be optionally avoided since the generation of these integrals is definitely required for the calculation of perturbative triple excitations (see Sec. 2.5.2). Hence, the complete list of three-external PNO integrals is also optionally available in the open-shell and closed-shell LPNO-CCSD iterations respectively (referred to as 'Algorithm 3').

All remaining steps are executed analogously to the closed-shell case but by keeping track of the different spin-cases that arise in the spin-unrestricted formalism. The complete working equation for the open-shell LPNO-CCSD method can be found in Appendix B. Note that the actual ORCA input keyword for choosing the different algorithms ('$PNOSigmaOpt$'; to be putted in the 'mdci' block of the input file) is slightly different defined than the number of the respective algorithm:

a) '$PNOSigmaOpt\,0$': (closed-shell) LPNO based coupled pair methods;
b) '$PNOSigmaOpt\,1$': closed-shell LPNO$_2$-QCISD/CCSD;
c) '$PNOSigmaOpt\,2$': closed-shell LPNO$_1$-QCISD/CCSD (or equivalently the name LPNO-QCISD/CCSD is used); open-shell LPNO-QCISD/CCSD and also open-shell coupled-pair methods;
d) '$PNOSigmaOpt\,3$': closed-shell and open-shell LPNO$_3$-CCSD.

This somewhat confusing notation goes back to the different development stages during the implementation and evaluation of the LPNO based single-reference correlation methods. The LPNO-VCEPA methods were only implemented in the open-shell formalism. By default, the open-shell implementation employs QROs to construct the reference determinant. However, it is also possible to use a genuine spin-unrestricted reference determinant or a ref-

erence determinant of broken-symmetry type,[130,131] but this requires that the corresponding ORCA input keyword ('$UseSeparateAlphaBeta$') is set to 'true' in the 'mdci' block of the respective input file.

2.3.5. The RIJCOSX approximation for the singles Fock term

As it is evident from the detailed timings presented in Sec. 3.4.2, three time consuming steps remain for an LPNO-CCSD calculation: $1)$ the SCF procedure to obtain the reference function, $2)$ the PNO integral transformation (mainly depending on the available memory), and $3)$ the calculation of the residuals, which is dominated by the formation of the singles Fock matrix (Eq. (A.9)), at least in the closed-shell case and if large basis sets are used.
As already mentioned in Sec. 2.3.2, due to the similarity of this term to the SCF Fock matrix, the efficient calculation of the singles Fock matrix may be performed through approximations developed for the latter. In particular, it will be shown how the RIJCOSX approximation[214,215] may be used to this end. The closed-shell singles Fock term may be written as

$$G(\mathbf{t}_1)_{pq} = \sum_{jb} t_b^j (2(pq|jb) - (pj|qb)) = \sum_{\mu\nu} c_\mu^p c_\nu^q G(\mathbf{t}_1)_{\mu\nu} \quad , \tag{2.96}$$

where j being an occupied, b a virtual orbital, while p and q may belong to either of these orbital subsets. The t_b^j are the singles excitation amplitudes, and c_μ^p denote MO coefficients. The singles Fock matrix can be obtained via transformation from its counterpart ($G(\mathbf{t}_1)_{\mu\nu}$) in the AO basis

$$G(\mathbf{t}_1)_{\mu\nu} = \sum_{jb} t_b^j (2(\mu\nu|jb) - (\mu j|\nu b)) = \sum_{\kappa\tau} P(\mathbf{t}_1)_{\kappa\tau} (2(\mu\nu|\kappa\tau) - (\mu\kappa|\nu\tau)) \quad , \tag{2.97}$$

where

$$P(\mathbf{t}_1)_{\kappa\tau} = \sum_{jb} t_b^j c_\kappa^j c_\tau^b \tag{2.98}$$

is the analogue of the SCF density matrix for the singles Fock case, and μ, ν, κ, τ are AO basis functions. For the singles Coulomb ($J(\mathbf{t}_1)_{\mu\nu}$) case, the density may be symmetrized ($\tilde{P}(\mathbf{t}_1)_{\kappa\tau} = P(\mathbf{t}_1)_{\kappa\tau} + P(\mathbf{t}_1)_{\tau\kappa}$), and

$$J(\mathbf{t}_1)_{\mu\nu} = \sum_{\kappa\tau} \tilde{P}(\mathbf{t}_1)_{\kappa\tau} (\mu\nu|\kappa\tau) \approx \sum_{AB} \sum_{\kappa\tau} \tilde{P}(\mathbf{t}_1)_{\kappa\tau} (\mu\nu|r_{12}^{-1}|A) V_{AB}^{-1} (B|r_{12}^{-1}|\kappa\tau), \tag{2.99}$$

where

$$V_{AB} = (A|r_{12}^{-1}|B), \tag{2.100}$$

and A, B are elements of the auxiliary basis used for the density fitting. Note that the factor of 2 in (2.97) is taken care of by symmetrization. Since we are using a symmetric density, the same efficient routine to evaluate the singles Coulomb term can be used as in the SCF

case.[218] The exchange part ($K(\mathbf{t}_1)_{\mu\nu}$) can be written as

$$K(\mathbf{t}_1)_{\mu\nu} = \sum_{\kappa\tau} P(\mathbf{t}_1)_{\kappa\tau}(\mu\kappa|\nu\tau) \approx \sum_g Q_{\mu g} \sum_\tau A_{\nu\tau}(\mathbf{r}_g) \sum_\kappa P(\mathbf{t}_1)_{\kappa\tau} X_{\kappa g} \quad , \tag{2.101}$$

where

$$A_{\nu\tau}(\mathbf{r}_g) = \int \frac{\nu(\mathbf{r})\tau(\mathbf{r})}{|\mathbf{r}-\mathbf{r}_g|} d\mathbf{r} \quad , \tag{2.102}$$

and

$$X_{\kappa g} = w_g^{1/2} \kappa(\mathbf{r}_g) \quad . \tag{2.103}$$

These are the equations of the chain of spheres exchange (COSX) approximation,[214] and $\kappa(\mathbf{r}_g)$ denotes the value of κ evaluated at grid point g. In the overlap fitted case,[215] the matrix elements $Q_{\mu g}$ are obtained from the equation

$$\mathbf{S} = \mathbf{Q}\mathbf{X}^T \quad , \tag{2.104}$$

where $\mathbf{S}$ is the analytic overlap matrix. The COSX routine is able to deal with asymmetric densities as well and thus, it can be used here similar to the SCF case. The RIJCOSX approximation can be analogously applied to the the singles Fock term in spin-unrestricted form and is also implemented for the open-shell LPNO-CCSD method. As it will be shown in Sec. 3.4.3, this approximation leads to a significant speed-up of the computation time needed for the LPNO-CCSD iterations while the additional error is negligible.

2.4. Parameterized CCSD (pCCSD)

For fixed occupied i, j and virtual a, b spin-orbital labels, the explicit algebraic expressions for the quadratic $\widehat{T}_2$ terms in the CCSD doubles residual (see Fig. 2.1) can be written as

$$\left\langle \Phi_{ij}^{ab} \right| \left(\frac{1}{2} \widehat{H}_{BO} \widehat{T}_2^2 \right)_C |\Phi_0\rangle = \underbrace{-\frac{1}{2} \sum_{k,l,c,d} \left(\langle kl||cd\rangle \, t_{ab}^{il} t_{cd}^{kj} + \langle kl||cd\rangle \, t_{ab}^{kj} t_{cd}^{il} \right)}_{A} + \underbrace{\frac{1}{4} \sum_{k,l,c,d} \langle kl||cd\rangle \, t_{ab}^{kl} t_{cd}^{ij}}_{B}$$
$$\underbrace{-\frac{1}{2} \sum_{k,l,c,d} \left(\langle kl||cd\rangle \, t_{ad}^{ij} t_{cb}^{kl} + \langle kl||cd\rangle \, t_{cb}^{ij} t_{ad}^{kl} \right)}_{C} + \underbrace{\sum_{k,l,c,d} \langle kl||cd\rangle \, t_{cb}^{kj} t_{ad}^{il}}_{D} \quad , \tag{2.105}$$

where $\langle kl||cd\rangle$ are antisymmetrized two-electron integrals.
These four contributions to the $\left\langle \Phi_{ij}^{ab} \right| \left(\frac{1}{2} \widehat{H}_{BO} \widehat{T}_2^2 \right)_C |\Phi_0\rangle$ terms of the doubles residual given in Eq. (2.39) and Eqs. (2.57) – (2.58) respectively are denoted by A, B, C and D as in Eq. (2.105). For two-electron systems, $(k, l) \in (i, j)$ and from Eq. (2.105), it can easily be deduced that

$$\frac{1}{2}A + B = 0 \quad , \quad C + D = 0 \quad , \tag{2.106}$$

and one can introduce the following bivariate (α, β) parameterization of the $\frac{1}{2}\widehat{T}_2^2$ terms in Eq. (2.105):

$$\left\langle \Phi_{ij}^{ab} \right| \left(\frac{1}{2}\widehat{H}\widehat{T}_2^2 \right)_C |\Phi_0\rangle \rightarrow \frac{1}{2}A + \alpha\left(\frac{1}{2}A + B\right) + \beta\left(C + D\right) \quad . \tag{2.107}$$

The theory remains exact for two-electron systems (*i.e.* for two-electron systems Eq. (2.105) reduces to $\frac{1}{2}A$ just as in CCSD, according to Eq. (2.106)). This defines the pCCSD(α, β) methodology outlined in the work of Huntington and Nooijen,[126] where it was noted that for any values (α, β) of the parameters, the corresponding pCCSD(α, β) method retains the desirable properties of the CCSD approach itself: i) exact for two-electron systems by construction, ii) size-extensive and size-consistent and iii) invariant to rotations of the occupied or virtual orbitals. For systems with more than two electrons, the doubles residual equations and hence, the excitation amplitudes and the correlation energy become functions of the parameters α and β.

A similar freedom can be explored in the singles residual equations given in Eq. (2.40) and (2.56) respectively. If one considers the three diagrams of Fig. 2.2 which appear in the $\widehat{T}_1\widehat{T}_2$ contribution to the CCSD singles residual R_i^a, the following equation results (for fixed occupied i, j and virtual a, b labels)

$$\begin{aligned} \langle \Phi_i^a | \left(\widehat{H}_{BO}\widehat{T}_1\widehat{T}_2 \right)_C |\Phi_0\rangle = & \underbrace{-\frac{1}{2}\sum_{k,l,c,d} \langle kl| \, |cd\rangle \, t_{ad}^{kl} t_c^i}_{E} + \underbrace{\sum_{k,l,c,d} \langle kl| \, |cd\rangle \, t_{da}^{li} t_c^k}_{F} \\ & + \underbrace{\left(-\frac{1}{2}\sum_{k,l,c,d} \langle kl| \, |cd\rangle \, t_{cd}^{il} t_a^k \right)}_{G} \quad . \end{aligned} \tag{2.108}$$

For two-electron systems (*i.e.* k, l equal to i or j), it can be again shown that the terms labelled by E and F exactly cancel,

$$E + F = 0 \quad , \tag{2.109}$$

and in a simlilar fashion as for pCCSD(α, β), one can multiply these contributions by an arbitrary factor γ,

$$\langle \Phi_i^a | \left(\widehat{H}\widehat{T}_1\widehat{T}_2 \right)_C |\Phi_0\rangle \rightarrow \gamma\left(E + F\right) + G \quad . \tag{2.110}$$

This parameterization of the singles residual equations, coupled with the bivariate (α, β) parameterization of Eq. (2.107), defines the hierarchy of pCCSD(α, β, γ) methods[219] and $\forall\ \alpha, \beta, \gamma$ the corresponding pCCSD(α, β, γ) approach is rigourously exact for two-electron systems and size-extensive/size-consistent.

The LPNO formalism as described in detail for LPNO-CCSD above (see Sec. 2.3.2 and Sec. 2.3.4 respectively) can be applied analogously to the pCCSD approach. The canonical pCCSD(α, β, γ) and the LPNO-pCCSD(α, β, γ) methods were implemented into the ORCA quantum chemistry program package[206] in both spin-restricted (closed-shell) and spin-unrestricted (open-shell) form. To this end, the 'dressings' of the Fock matrix (Eqs. (2.42) – (2.44)), two-external integrals (Eqs. (2.50) and (2.51)) and four-internal integrals (Eqs. (2.49)) were modified to include the respective parameters correctly. Despite for the latter, this can be achieved straightforwardly. In order to ensure the correct parameterization of the quadratic $\widehat{T}_2$ terms which enter the 'dressing' of the four-internal integrals, an additional function is needed to subtract a contribution which was parameterized unintentionally due to recasting the CCSD residual into 'dressed' CI form. However, the computational overhead due to this additional function is not significant.

2.5. Perturbative treatment of connected triple excitations

2.5.1. Closed-shell formulation of the canonical (T) correction

In the spin-restricted (closed-shell) formalism, the canonical (T) correction might be computed from the equation derived by Lee *et al.*:[85]

$$\Delta E^{(T)} = \sum_{i\leqslant j\leqslant k} \sum_{a\leqslant b\leqslant c} P_{ijk}\Big((Y^{ijk}_{abc} - 2\,Z^{ijk}_{abc})(W^{ijk}_{abc} + W^{ijk}_{bca} + W^{ijk}_{cab}) + (Z^{ijk}_{abc} - 2\,Y^{ijk}_{abc})(W^{ijk}_{cab} + W^{ijk}_{bac} + W^{ijk}_{cba}) + 3\,X^{ijk}_{abc}\Big)/(\varepsilon_i + \varepsilon_j + \varepsilon_k - \varepsilon_a - \varepsilon_b - \varepsilon_c) \quad . \tag{2.111}$$

As usual, the indices (i, j, k, l) refer to occupied orbitals of the reference determinant, (a, b, c, d) to unoccupied orbitals and (p, q, r, s) to orbitals from either subspace. The t^i_a and t^{ij}_{ab} are the converged singles and doubles QCISD or CCSD amplitudes respectively. The other quantities are defined as follows:

$$Y^{ijk}_{abc} = V^{ijk}_{abc} + V^{ijk}_{bca} + V^{ijk}_{cab} \quad , \tag{2.112}$$

$$Z^{ijk}_{abc} = V^{ijk}_{acb} + V^{ijk}_{bac} + V^{ijk}_{cba} \quad , \tag{2.113}$$

$$X^{ijk}_{abc} = W^{ijk}_{abc}V^{ijk}_{abc} + W^{ijk}_{acb}V^{ijk}_{acb} + W^{ijk}_{bac}V^{ijk}_{bac} + W^{ijk}_{bca}V^{ijk}_{bca} + W^{ijk}_{cab}V^{ijk}_{cab} + W^{ijk}_{cba}V^{ijk}_{cba} \quad , \tag{2.114}$$

$$V^{ijk}_{abc} = \left(W^{ijk}_{abc} + f_S(t^i_a K^{jk}_{bc} + t^j_b K^{ik}_{ac} + t^k_c K^{ij}_{ab})\right)/P_{abc} \quad , \tag{2.115}$$

$$P_{abc} = 1 + \delta_{ab} + \delta_{bc} \quad , \tag{2.116}$$

$$P_{ijk} = 2 - \delta_{ij} - \delta_{jk} \quad , \tag{2.117}$$

and $f_S = 2$ for QCISD(T) or $f_S = 1$ for CCSD(T).[85] The Fock operator F_{pq} is assumed to be diagonal with eigenvalues ε_p. The key intermediate is given as:

$$W_{abc}^{ijk} = \quad \hat{P}_{ijk}^{abc} \left\{ \sum_d t_{cd}^{kj} (ia|bd) - \sum_l t_{ab}^{il} (kc|jl) \right\} \quad , \tag{2.118}$$

with $\hat{P}_{ijk}^{abc}$ being the following permutation operator:

$$\hat{P}_{ijk}^{abc} = \begin{pmatrix} abc \\ ijk \end{pmatrix} + \begin{pmatrix} acb \\ ikj \end{pmatrix} + \begin{pmatrix} cab \\ kij \end{pmatrix} + \begin{pmatrix} cba \\ kji \end{pmatrix} + \begin{pmatrix} bca \\ jki \end{pmatrix} + \begin{pmatrix} bac \\ jik \end{pmatrix} \quad . \tag{2.119}$$

The integrals $(pq|rs)$ are again written in $(11|22)$ notation and $K_{ab}^{ij} = (ia|jb)$ denotes the usual two-external Exchange operator. Eq. (2.111) was efficiently implemented into the ORCA quantum chemistry program package.[206] Furthermore, a spin-unrestricted implementation of the canonical (T) correction is also available. However, due to the steep $\mathcal{O}(O^3V^4)$ scaling of the canonical (T) correction, the applicability of the QCISD(T) and CCSD(T) methods is restricted to molecules with up to ~25 atoms (depending on the number of correlated electrons). Hence, it would be very attractive if the LPNO approach can be extended to include connected triples excitations in an efficient and accurate way.

2.5.2. The LPNO approach for the (T) correction

The success of the LPNO single and double excitation models is based on identifying the relevant subspace of the virtual correlation space for each electron pair (i, j). To this end, the LPNO approach uses approximate pair natural orbitals. Obviously, the calculation of the connected triple excitation correction involves the three electron pairs (i, j), (i, k) and (j, k). In a local correlation scheme, the pair (i, j) is only kept if the pair correlation energy of the respective localized internal orbital pair is sufficiently large, which only occurs if the orbitals (i) and (j) are spatially close to each other, but real space criteria for the pair selection scheme are never used within the LPNO framework. The same holds for (i, k) and (j, k). Hence, the orbital triple (i, j, k) only contributes to the triples energy if all three orbitals are close in space and thus, only a linearly scaling number of index combinations (i, j, k) has to be treated. This alone would reduce the scaling from $\mathcal{O}(N^7)$ to $\mathcal{O}(N^5)$.

In order to compute the perturbative triples correction in the framework of the LPNO approach, it is necessary to identify the subspace of the virtual space that is relevant for the internal orbital combination (i, j, k). In the domain based approaches this is achieved by

generating the union of the domains associated with the orbitals (i), (j) and (k).[169] The central idea of the present LPNO approach for the (T) correction is to construct 'triple natural orbitals' (TNOs), which span the significant subspace of the three pairs (i,j), (i,k) and (j,k) in question. Following the logics of the PNO construction scheme (see Sec. 2.2.2), the first step consists of generating a virtual 'pair' density of the three orbital pairs,

$$D_{ab}^{ijk} = D_{ab}^{ij} + D_{ab}^{ik} + D_{ab}^{jk} \quad , \tag{2.120}$$

where the pair densities D_{ab}^{ij} are calculated (using the generator state formalism,[186] *i.e.* contravariant amplitudes) according to the scheme presented in Eq. (2.19) and (2.20). However, the amplitudes are computed in the PNO basis for each pair. Thus, the pair densities are back-projected onto the VMO basis before constructing the TNOs:

$$\mathbf{D}^{ij} = \mathbf{d}^{ij}\bar{\mathbf{D}}^{ij}\mathbf{d}^{ij\dagger} \quad . \tag{2.121}$$

The eigenfunctions of $\mathbf{D}^{ijk}$ are the desired TNOs with the corresponding occupation numbers n^{ijk} and eigenvectors $\mathbf{d}^{ijk}$. As for the PNO expansion, a cut-off value ($\mathrm{T}_{\mathrm{CutTNO}}$) for the respective TNO occupation numbers is introduced. The TNOs essentially span the joint virtual correlation subspace of the three pairs in question. However, a slight complication arises from the fact that the perturbative triples formalism requires the orbitals to diagonalize the Fock operator. In order to arrive at canonical TNOs, the Fock operator is diagonalized in the space of the surviving TNOs. Since there is only a linear number of (i,j,k) triples, the algorithm to construct the TNOs is of $\mathcal{O}(N^4)$ complexity and generates a linear scaling number of significant TNOs.

Obviously, all integrals and amplitudes that occur in the triples equation (Eq. 2.111) have to be projected onto the TNO basis in question. This is readily achieved by first computing the triples/pair overlaps

$$\mathbf{S}^{ij,ijkl} = \mathbf{d}^{ij\dagger}\mathbf{d}^{ijk} \quad , \tag{2.122}$$

and afterwards, forming the respective TNO amplitudes:

$$\breve{\mathbf{t}}^{ij} = \mathbf{S}^{ij,ijk\dagger}\mathbf{t}^{ij}\mathbf{S}^{ij,ijk} \quad . \tag{2.123}$$

While these projections appear to be cumbersome, it should be noted that the matrices involved are very compact and the contraction lengths are asymptotically independent of the system size such that the scaling of these projection steps is overall linear.

In the same way, the one-, two- and three-external integrals are projected from the respective PNO bases of the three pairs involved to their common TNO basis. Obviously, this involves the integrals $(k\bar{b}|\bar{a}\bar{c})$ $(\forall k)$ for a given pair (i,j). The construction of these integrals was avoided in the LPNO based CCSD implementations where for each pair only the integrals with k equal to i or j were kept. For LPNO-CEPA and LPNO-QCISD, only the latter

are required while the higher order disconnected 'dressing' of the EEO necessitates the full set of three-external PNO integrals for LPNO-CCSD (Eq. (2.53)). Thus, these terms were neglected in the LPNO-CCSD implementation. However, since this set of PNO integrals must be available for the calculation of the (T) correction within the LPNO framework and it might be also important for accurate response property calculations, these additional approximation in the LPNO-CCSD residual was omitted (referred to as 'Algorithm 3'; LPNO$_3$-CCSD). This will always be the default setting if triple excitations are to be computed within the LPNO framework.

The integrals $(k\bar{b}|\bar{a}\bar{c})$ are obviously local. Since all PNOs $\bar{a}$ associated to the pair (i,j) are located in the same region of space, the differential overlap of k with $\bar{b}$ restricts k to be in the vicinity of the pair (i,j) in order to significantly contribute to the respective integrals. These decay properties will eventually be used in linear scaling versions of the LPNO approaches, but in the present implementation, all integrals $(k\bar{b}|\bar{a}\bar{c})$ were kept with overall quadratic scaling in memory and disk storage requirements. Note that the involved two-external Exchange integrals are constructed via the PNO integral transformation, *i.e.* they are defined in the respective truncated PNO pair basis. The same integrals were used for the calculation of the two-external pair-pair interactions in 'Algorithm 2' of the LPNO based QCISD and CCSD methods (see Sec. 2.3.2).

In evaluating Eq. (2.111) within the TNO approach, the final issue to be addressed concerns the off-diagonal contributions from the internal Fock matrix elements F_{ij}. In order to avoid a potentially expensive iterative procedure, these terms were neglected and hence, only the diagonal elements of the Fock matrix in the localized MO basis are considered. Thus, what is really approximated is a 'semi-canonical' triples correction with canonical virtual and localized internal orbitals. This is similar to the approximation made in in PAO based perturbative triples correction developed by Schütz *et al.*.[169]

Finally, it should be noted that the extension of the TNO approach to the spin-unrestricted (open-shell) case cannot be achieved without introducing further approximation since not all projection matrices for the spin-cases '$\alpha\alpha\beta$' and '$\beta\beta\alpha$' are available based on the TNO construction scheme described above (Eq. (2.120)). However, preliminary investigations showed that these additional approximations significantly reduce the accuracy of the triples correction and hence, the present spin-unrestricted LPNO-CCSD(T) implementation is not of great practical use. However, a better treatment of the (T) correction within the LPNO framework is already envisioned and subject of current investigations in our research group. The present implementations of the TNO approach were carried out in a development version of the ORCA quantum chemistry program package.[206]

2.6. Summary of the implementation

Production level implementations of the CCSD and QCISD method as well as various coupled pair methods in both spin-restricted (closed-shell) and spin-unrestricted (open-shell) form were developed within the LPNO framework. Furthermore, first attempts were made to incorporate the perturbative correction for connected triple excitations as well. The scheme presented in Fig. 2.3 summarizes the general program flow of LPNO based calculations carried out with the ORCA program package.[206] Except for the calculation of the reference wavefunction and the localization of the internal orbitals, all steps are performed within the 'orca_mdci' module. The working equations were recast in matrix form whenever possible in order to make maximum use of the extremely efficient BLAS level 3 routines (*i.e.* matrix operations). The part of Fig. 2.3 highlighted in blue refers to the non-PNO part of the program. As in the canonical case, the DIIS algorithm[220] is used to solve the linear equations system to obtain the update of the amplitudes which is needed for the iterative optimization of the latter. Note that the DIIS solver is not used in the first iteration since better convergence and of the iterative procedure is observed in this way. All other steps of LPNO based calculations were already discussed in detail above.

The production level code was also parallelized using the MPI (message passing interface) libraries which have the advantage that the code is portable to both distributed and shared memory machines. A detailed discussion of the parallel LPNO implementations can be found elsewhere.[199] Given that the target platforms are standard PC cluster architectures, for which in general load-balancing is not a crucial factor, a static distribution model was chosen. This choice offers also the possibility to distribute data over local hard drives. The basic strategy was to divide pair loops over processes in a round-robin fashion. In this way, no communication among the different processes is needed during the pair loops and only the gathering of the local data leads to a small overhead in the parallel computation time.

After convergence has been reached, density matrices can be calculated based on the converged amplitudes. The calculated densities are of unrelaxed type. Moreover, they are linearized in the QCISD and CCSD case. Thus, in the present implementations, the only LPNO density which may be of greater practical use for the calculation of molecular properties like *e.g.* hyperfine coupling constants is that of the variational LPNO-VCEPA methods since a well defined expectation value type density exists for the latter. Further developments concerning the efficient and accurate molecular properties calculations within the framework of the LPNO approach are in progress in our research group.

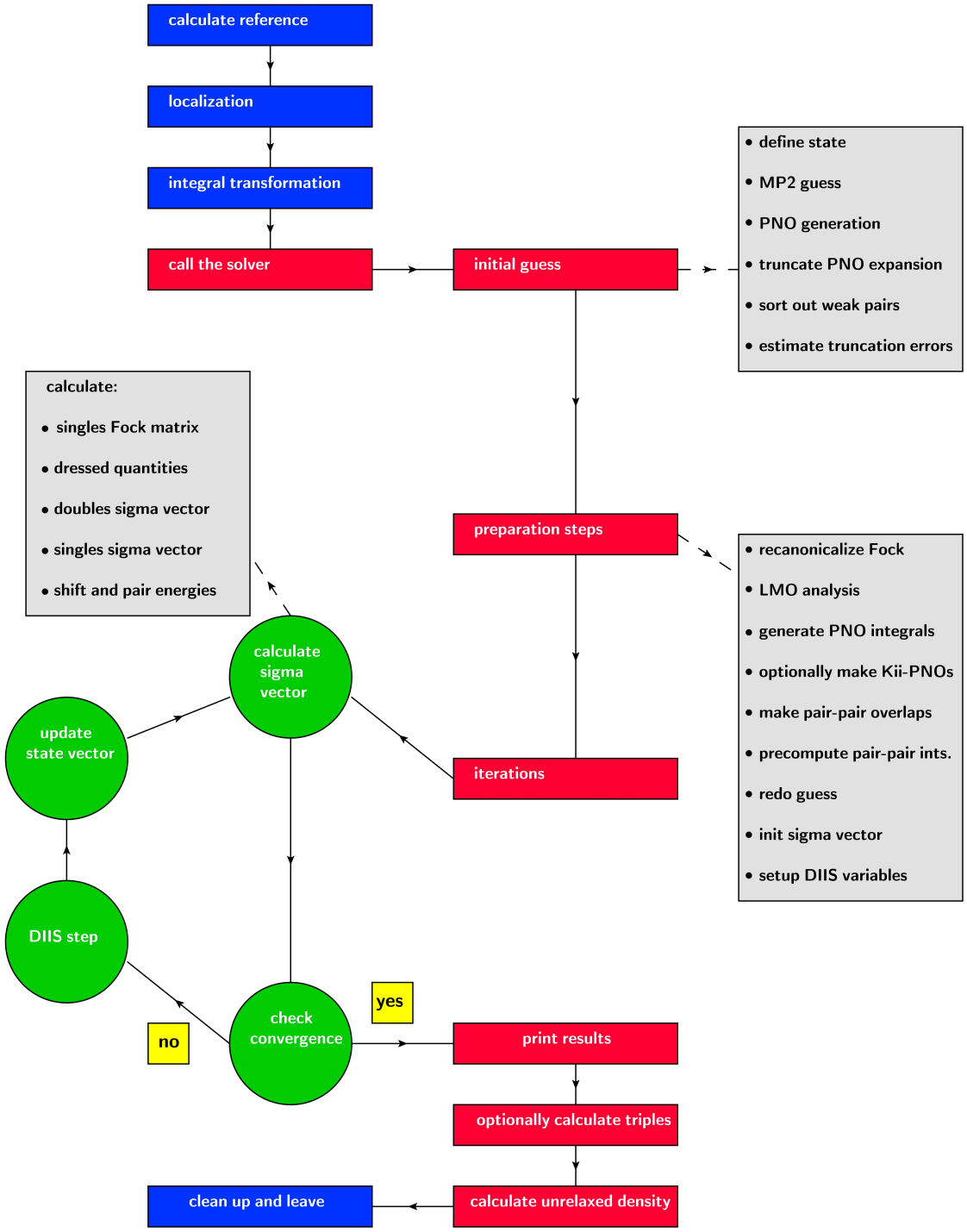

Figure 2.3.: Program flow for LPNO based calculations with the ORCA program package.

3. Numerical Investigation

3.1. Computational setup

All calculations were carried out with a development version of the ORCA program package.[206] As indicated below, the split-valence (SV), triple-ζ valence (TZV) and quadruple-ζ valence (QZV) basis sets[221] of Ahlrichs *et al.* were used together with the appropriate polarization functions (P) from the TURBOMOLE basis set library[222] and auxiliary bases developed by Weigend *et al.*[69] in the context of RI-MP2 calculations. Furthermore, the correlation consistent basis sets of Dunning[93] were used together with the corresponding auxiliary bases for the RI approximation.[223] The hyperfine coupling constants were calculated with Barone's triple-ζ EPR-III basis set[224] except for Si, Cl and S, for which the IGLO-III basis set of Kutzelnigg *et al.*[225] was employed. The def2-TZVPP/JK auxiliary basis set was used in this case.[226] Unless otherwise noted, optimized B3LYP[32]/TZVP geometries were used throughout. Localization of the orbitals was always carried out with the Foster-Boys algorithm.[203] Unless explicitly noted below, the SCF iterations were converged to 10^{-8} for the DIIS error (ORCA keyword 'VeryTightSCF') and the residual to 10^{-6} for its maximum element which corresponds to an accuracy of about 10^{-7} E_h in the correlation energy. The frozen core approximation has been used throughout, *i.e.* only the valence electrons of the molecular system in question enter the correlation treatment. Fig. 3.1 shows the structures of four molecules which are extensively employed as test systems for the numerical investigations presented below.

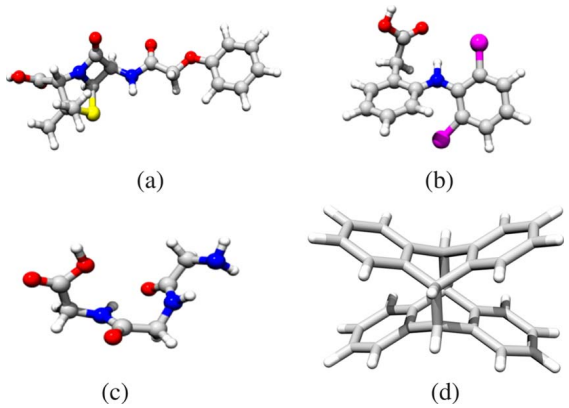

Figure 3.1.: Structures of some of the molecules studied in this work: (a) Penicillin; (b) Diclophenac; (c) $(Gly)_3$; (d) anthracene dimer (Fig. reproduced and modified from Ref. (196)).

3.2. Behavior with respect to the approximations

3.2.1. Convergence with respect to the thresholds

At first, the behavior of the closed-shell LPNO-CEPA type procedures with respect to the threshold T_{CutPNO} was studied on the $(Gly)_3$ molecule in a SV(P) basis set and using the CEPA/1 variant. The reference value is the untruncated CEPA/1 correlation energy of -2.048964 E_h. As can be seen in Fig. 3.2, the correlation energy converges monotonically towards the target value upon tightening of the threshold.

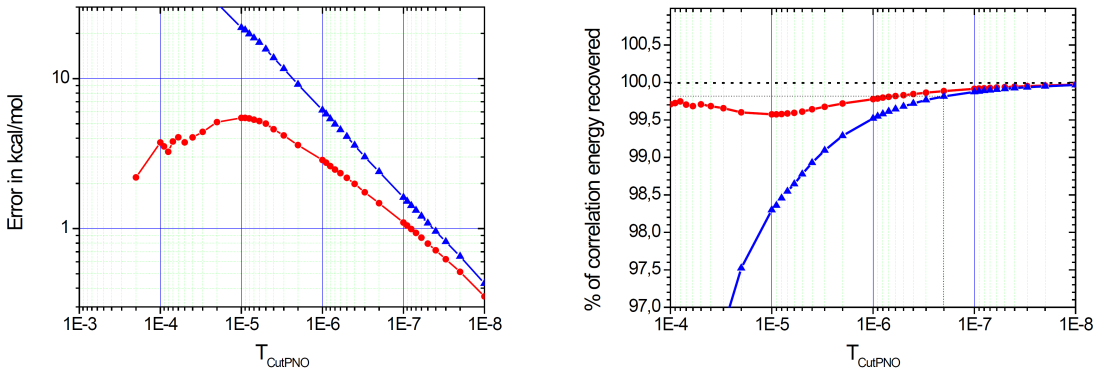

Figure 3.2.: The convergence of the closed-shell LNO-CEPA/1 method with respect to variations of the T_{CutPNO} parameter (left: absolute error in kcal/mol on a double logarithmic scale; right: relative error in %). Calculations were carried out on the $(Gly)_3$ molecule (optimized BPW91/DZVP geometry) with the SV(P) basis set (round circles: results with perturbative correction for the PNO error; triangles: results without perturbative correction for the PNO error). No local cut-offs were applied (Fig. reproduced and modified from Ref. (196)).

At a value of $T_{CutPNO} = 10^{-6}$, 99.4 % of the correlation energy is recovered. Below this value the calculations quickly become more expensive as there are many PNOs per pair with small occupation numbers. The error of the PNO expansion is significantly reduced by the perturbative correction (Eq. (2.34)). Hence, the correlation energy is never more than 0.4 % off the target value. However, the apparently excellent behavior of the correlation energy at $T_{CutPNO} = 10^{-4}$ is probably fortuitous and the convergence is only monotonic for threshold values below 10^{-5}. The chosen default value is $T_{CutPNO} = 3.33 \times 10^{-7}$ which leads to errors of ~0.1 – 0.2 % in the correlation energy or, in absolute terms, results that are within ~1 kcal/mol of the CEPA/1 reference value.

It is interesting to study how the PNOs distribute over the electron pairs as a function of the PNO cut-off parameter. Again, we have employed the $(Gly)_3$ molecule for the numerical investigation. The distribution of PNOs was studied as a function of T_{CutPNO} using the TZV(2d,2p) basis set. The local cut-off $T_{CutPairs}$ was set to zero and the Mulliken cut-off T_{CutMKN} to 10^{-3}. It is evident from Fig. 3.3 that for low thresholds the PNO distribution function has a strong peak towards small number of PNOs. For T_{CutPNO} values in the range 10^{-4} – 10^{-5}, there are still many pairs without any significant number of PNOs and

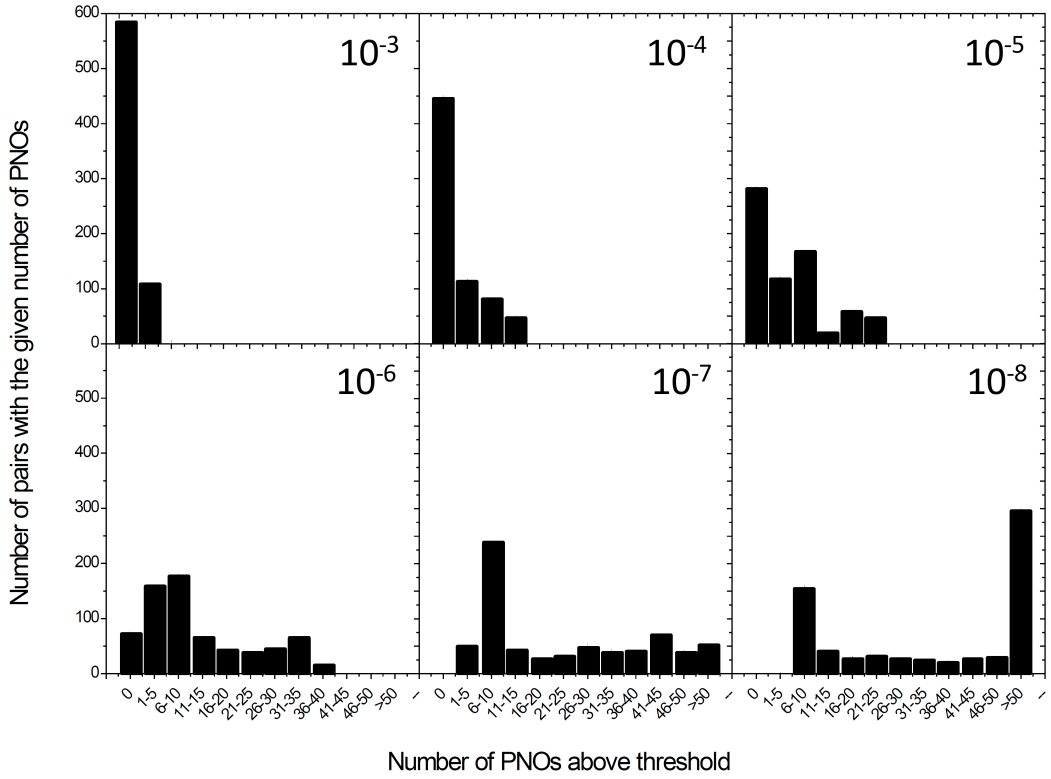

Figure 3.3.: The PNO distribution as a function of the threshold T_{CutPNO} (given in the upper right of each panel). All calculations were done on the $(Gly)_3$ molecule using the TZV(2d,2p) basis set (Fig. reproduced and modified from Ref. (196)).

most pairs are correlated with very few PNOs. This situation changes drastically for tighter thresholds. In the range 10^{-6} – 10^{-7} the distribution becomes quite broad and featureless while for 10^{-8} their function has a double maximum type appearance with many strongly correlated pairs (more than 50 PNOs) and a significant number of weakly correlated pairs (6 – 10 PNOs). Unfortunately, the numerical results obtained so far indicate that threshold values between 10^{-6} and 10^{-7} are necessary in order to achieve high accuracy (less than 1 kcal/mol error in the correlation energies). Obviously, large efficiency gains would be possible if one could accept more aggressive values for T_{CutPNO}. However, the first aim is reliability, and hence conservatively chosen values for all truncation parameters should be preferred. If better estimates for the PNO error than the simple MP2 estimate pursued in the present implementation become available, further computationally gains may be possible.

The behavior of the procedure with respect to the localization threshold T_{CutPairs} was studied as well. The reference value was obtained from a LPNO-CEPA calculation with $T_{\mathrm{CutPNO}} = 10^{-6}$. The additional errors due to the local approximation are very small and quickly fall below 0.1 kcal/mol if the same MP2 perturbative estimate for the truncated pairs as for the PNO error is made (see Fig. 3.4). In this respect, the neglected pairs behave identical to pairs with no surviving PNO. The default value is $T_{\mathrm{CutPairs}} = 10^{-4}$ E_{h}, which is again a rather conservative choice.

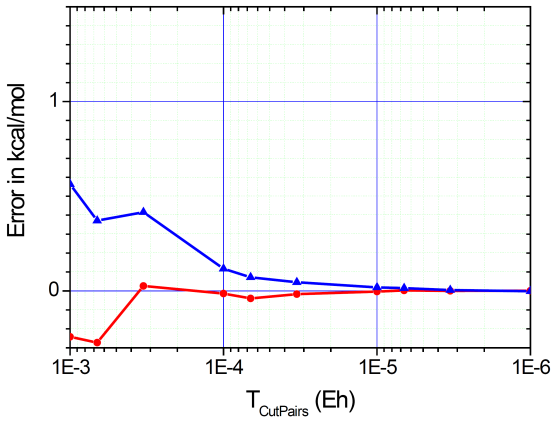

Figure 3.4.: The convergence of the closed-shell LPNO-CEPA/1 method with respect to variations of the $T_{CutPairs}$ parameter. Calculations were carried out on the $(Gly)_3$ molecule with the SV(P) basis set (round circles: results with perturbative correction for the PNO and local errors; triangles: results without perturbative correction of the PNO and local errors; Fig. reproduced and modified from Ref. (196)).

The glycine trimer was also used to study the dependence of the results on the remaining threshold, T_{CutMKN}. The reference calculation was performed with $T_{CutMKN} = 0$, $T_{CutPairs} = 0$ and $T_{CutPNO} = 10^{-6}$. It is obvious from Fig. 3.5 that the errors due to T_{CutMKN} are very small and are well below 0.1 kcal/mol for $T_{CutMKN} = 10^{-3}$, which is the chosen default value.

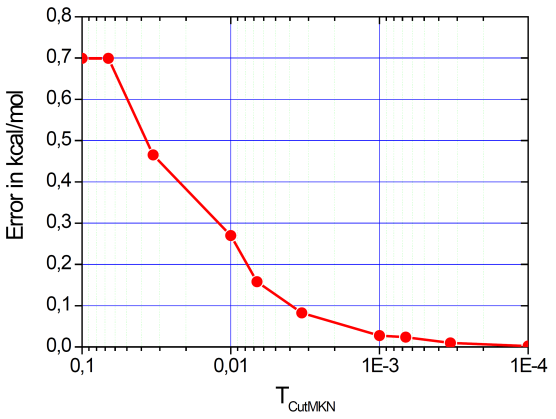

Figure 3.5.: The convergence of the closed-shell LPNO-CEPA/1 method with respect to variations of the T_{CutMKN} parameter. Calculations were carried out on the $(Gly)_3$ molecule with the SV(P) basis set (Fig. reproduced and modified from Ref. (196)).

In this section, we have defined highly conservative thresholds that should work under almost any circumstance. In many cases, slightly less tight cut-offs would also be appropriate, and hence some of the calculations below have been done with $T_{CutPNO} = 10^{-6}$ and $T_{CutMKN} = 10^{-2}$.

Secondly, the closed-shell LPNO variants of the QCISD and CCSD methods have been examined. The behavior of the LPNO approximation with respect to the local truncation

thresholds T_{CutPairs} and T_{CutMKN} is not documented again as it is very similar to that of the LPNO-CEPA/1 method discussed above. However, the behavior with respect to the PNO truncation threshold needs to be reinvestigated since the behavior of the $\mathrm{LPNO}_{1/2}$-QCISD and $\mathrm{LPNO}_{1/2}$-CCSD methods differ slightly in this respect from LPNO-CEPA/1. The errors obtained for the cyclohexane molecule in the cc-pVTZ basis (341 basis functions) relative to the canonical QCISD and CCSD calculations are shown in Fig. 3.6. The RI error has been investigated for this example and with the chosen combination of orbital and fitting basis, it only amounts to 0.16 $\mathrm{mE_h}$ compared to the total correlation energy of -1.10745 $\mathrm{E_h}$.

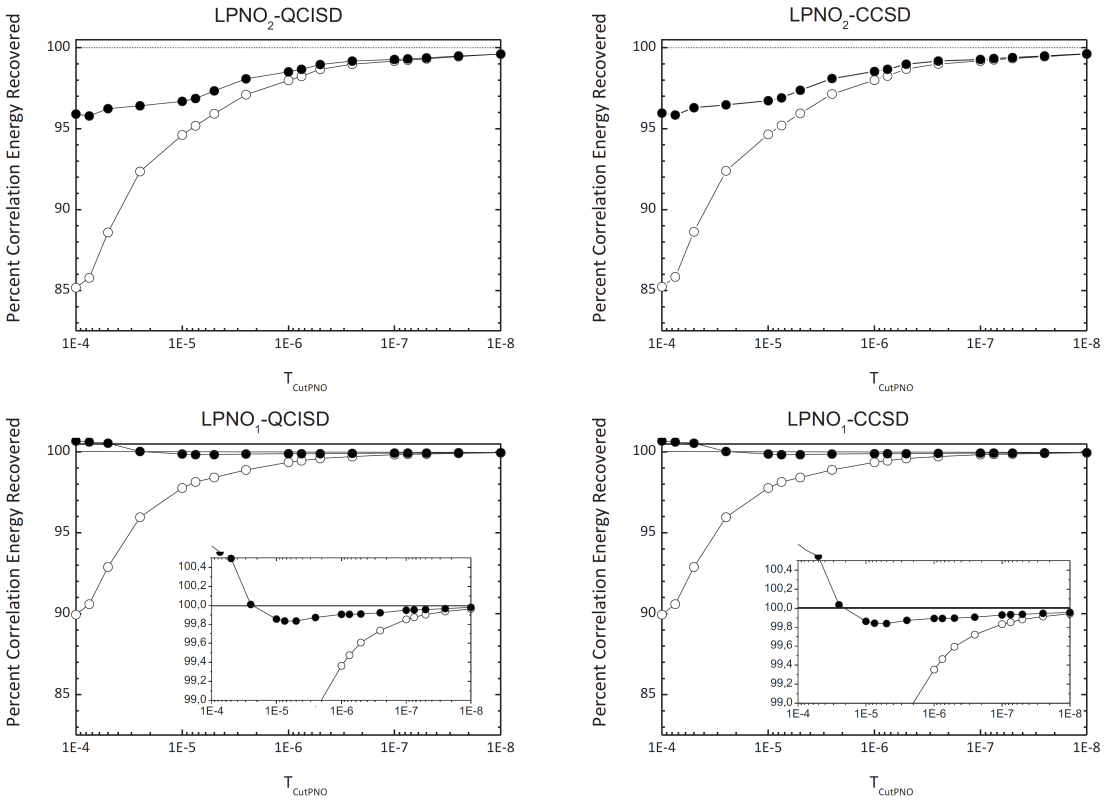

Figure 3.6.: Behavior of the closed-shell $\mathrm{LPNO}_{1/2}$-QCISD and $\mathrm{LPNO}_{1/2}$-CCSD methods as a function of the PNO truncation threshold T_{CutPNO}. Calculations were carried out for cyclohexane with the cc-pVTZ basis set (def2-QZVPP/C auxiliary basis). T_{CutPairs} was set to 10^{-9} (no pair is rejected based on the local cut-off) and the Mulliken cut-off T_{CutMKN} was left at its default value of 10^{-3} (open circles: LPNO methods without perturbative correction for the PNO error; closed circles: with perturbative correction; Fig. reproduced and modified from Ref. (197)).

It is evident from Fig. 3.6 that all LPNO-QCISD and LPNO-CCSD methods smoothly converge to the reference correlation energy. Secondly, as observed before, the perturbative correction for the local and PNO errors greatly improves the results. It slightly overshoots for very aggressive values of T_{CutPNO}. The LPNO_2-QCISD and LPNO_2-CCSD methods behave essentially identically. The error at a T_{CutPairs} value of 10^{-7} amounts to roughly 1 % of the target correlation energy. Unfortunately, it appears to be difficult to recover much more than 99.0 – 99.5 % of the correlation energy with the LPNO_2 variants. However, the observed

errors are very smooth and they should cancel to some extent in relative energies. Based on Fig. 3.6, the behavior of the LPNO$_1$-QCISD and LPNO$_1$-CCSD methods with respect to convergence to the canonical limit is outstanding. At a threshold value of $T_{\mathrm{CutPNO}} = 10^{-5}$ already 99.8 % of the correlation energy is recovered and at $T_{\mathrm{CutPNO}} = 10^{-6}$ one reaches an accuracy of 99.9 %. Furthermore, the error as a function of T_{CutPNO} is seen to be a smooth and essentially flat curve. This behavior is even better compared to what was observed for the LPNO-CEPA/1 method where a threshold of $T_{\mathrm{CutPNO}} = 10^{-7}$ was required to recover 99.9 % of the target correlation energy. This may be traced back to the fact that the CEPA methods slightly overshoot the singles and doubles correlation energy which crudely simulates a connected triples effect.[107,209] This overshooting is not present in the perturbative correction and hence the corrected correlation energy tends to slightly undershoot the final CEPA value. The same is not true for QCISD and CCSD, which are both consistent with Møller-Plesset perturbation theory.[87,227] Hence, the second-order perturbative estimate for the small remainder of the correlation energy brings the result very close to the canonical QCISD or CCSD correlation energy. The almost identical behavior of the LPNO$_{1/2}$-QCISD and LPNO$_{1/2}$-CCSD methods relative to their canonical counterparts also indicates that the additional approximation (Eq. (2.53)) that was made for the LPNO variants of the CCSD method does not significantly affect the accuracy of the method, but this issue will be further addressed below.

Finally, the behavior of the truncation thresholds associated with the LPNO methods was reinvestigated for the open-shell variants, since it differs to some extent from the behavior of the corresponding closed-shell variants. The trityl radical shown in Fig. 3.7 (optimized geometry taken from Denekamp *et al.*[228]) serves as test system. The SVP basis set was used together with the SV/C auxiliary basis set. The system possesses a doublet ground state, but the UHF wave function is largely spin-contaminated with a $\hat{S}^2$ value of about 2.5. Thus, using QROs is essential for obtaining meaningful results.

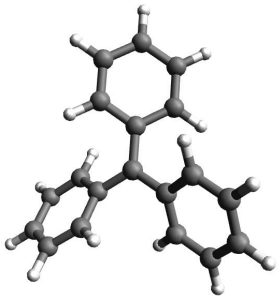

Figure 3.7.: Structure of the trityl radical which serves as test system for the open-shell LPNO methods (Fig. reproduced and modified from Ref. (198)).

First, the convergence of the PNO truncation threshold T_{CutPNO}, which plays the central role for the efficiency of the LPNO methods, was reinvestigated. For this purpose a series of LPNO calculations with various T_{CutPNO} values was carried out and compared to the standard CEPA/1, QCISD and CCSD reference values obtained with QROs and localized

internal orbitals (the latter choice matters only for the CEPA/1 calculations of course). All other thresholds were set to zero. The reference correlation energies are -2.505577 E_h (CEPA/1), -2.470242 E_h (QCISD), and -2.467421 E_h (CCSD).

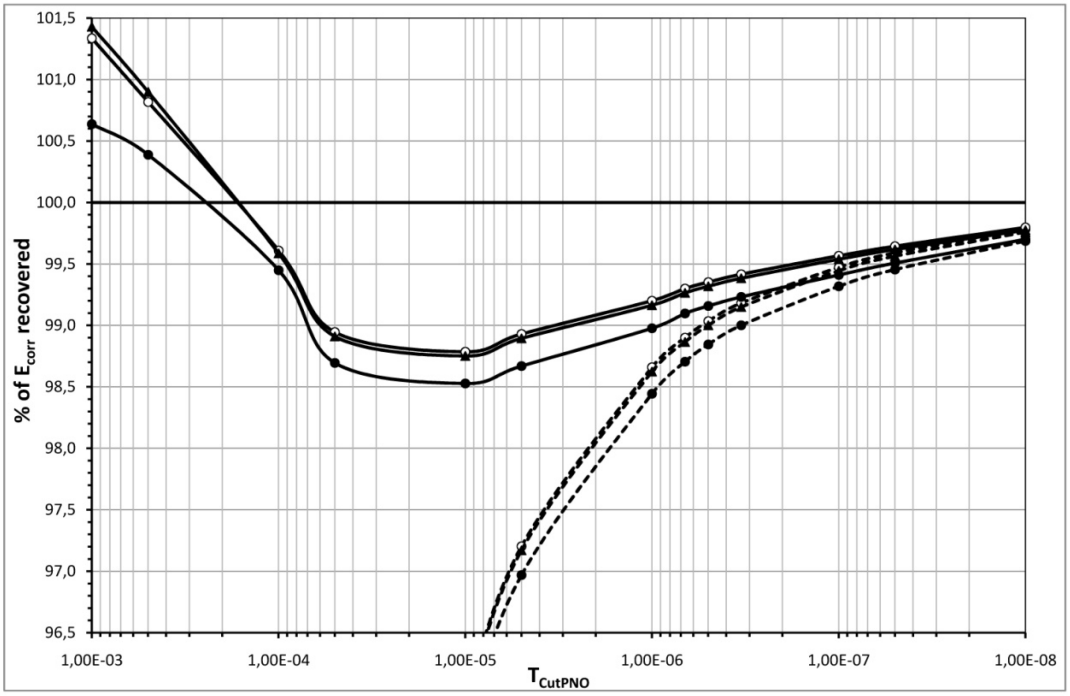

Figure 3.8.: Convergence of the open-shell LPNO methods with respect to T_{CutPNO}. The trityl radical serves as test system and the thresholds T_{CutPairs} and T_{CutMKN} were set to zero. The SVP basis set together with the SV/C fitting basis was used (solid line: with MP2 correction; dashed line: only strong pairs; filled circles: LPNO-CEPA/1; triangles: LPNO-QCISD; open circles: LPNO-CCSD; Fig. reproduced and modified from Ref. (198)).

As shown in Fig. 3.8, the correlation energy converges smoothly to the reference value as the PNO truncation threshold is tightened, similar to what was observed for the closed-shell variants. However, reliable results are only obtained with $T_{\mathrm{CutPNO}} = 10^{-6}$ or even tighter threshold values. For the closed-shell variants the default value of T_{CutPNO} was fixed to 3.33×10^{-7} which leads to more than 99.6 % of the target correlation energy. However, only 99.0 % of the reference correlation energy is recovered with open-shell LPNO-CEPA/1 and 99.2 % with open-shell LPNO-QCISD and LPNO-CCSD using the same value for the PNO truncation. The perturbative correction (Eq. (2.92)) improves the results to 99.2 % and 99.4 % of the correlation energy respectively. Compared to the excellent performance of the closed-shell variants, these errors are slightly larger. It should be noted, however, that the average number of PNOs per pair is significantly smaller in the open-shell case (Fig. 3.9). For small basis sets, only 10 – 15 PNOs are associated to an electron pair on average if the PNO truncation threshold is set to 3.33×10^{-7}. This situation changes significantly if very tight threshold values are applied, for which the PNO distribution becomes broader and more than 99.5 % of the target correlation energy is recovered. However, this improvement

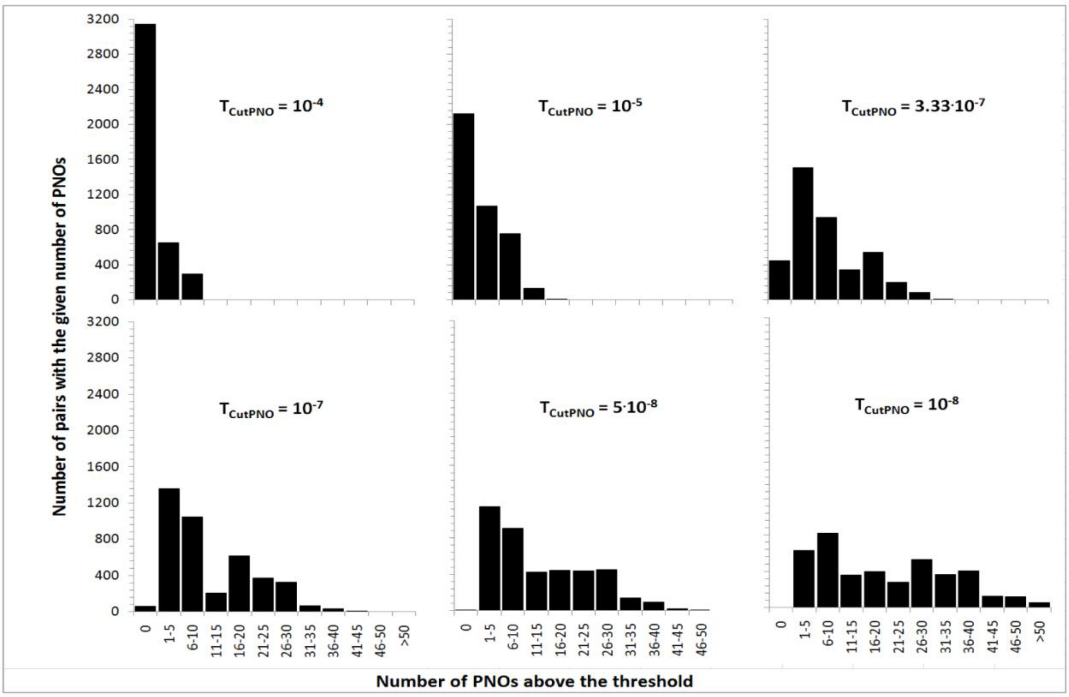

Figure 3.9.: PNO distribution as function of the PNO truncation threshold T_{CutPNO}. The test system is the trityl radical. The thresholds T_{CutPairs} and T_{CutMKN} were set to zero. All calculations were done with the open-shell LPNO-CCSD method using QROs and the SVP basis set (SV/C fitting basis; Fig. reproduced and modified from Ref. (198)).

comes at a high price in terms of significantly increased computational effort. Obviously, the truncation of the PNO expansion works less effectively if the virtual pair density is obtained from spin-unrestricted MP2 amplitudes whose elements decrease generally less smoothly. After extensive test calculations involving absolute and relative energies, we have decided to keep the same values for truncation parameters as in the closed-shell case. It will be shown in Sec. 3.3.2 that this choice leads to comparable accuracy in energy differences. The convergence with respect to the two other thresholds, T_{CutPairs} and T_{CutMKN} was also reinvestigated for the open-shell variants. To this end, the threshold for the local pair cut-off was varied while the threshold for the local fitting functions was set to zero and *vice versa*. The PNO cut-off was left at its default value of 3.33×10^{-7}. Since the behavior of LPNO-CEPA/1, LPNO-QCISD and LPNO-CCSD is very similar, only the LPNO-CCSD results are presented in Fig. 3.10 and 3.11. The corresponding LPNO-CCSD correlation energies (-2.452997 E_h with MP2 correction, -2.447227 E_h without) obtained with T_{CutPairs} and T_{CutMKN} equal to zero and the default value for T_{CutPNO} serve as reference values. For the closed-shell variants the absolute error due to the strong pair approximation is well below 0.1 kcal/mol if the default value of $T_{\mathrm{CutPairs}} = 10^{-4}$ E_h is applied. In the open-shell case, however, it is more difficult to converge to the target value since the pair correlation energies decrease less smoothly and the '$\alpha\alpha$' and '$\beta\beta$' pair correlation energies are typically one order of magnitude smaller than the '$\alpha\beta$' pair correlation energies.

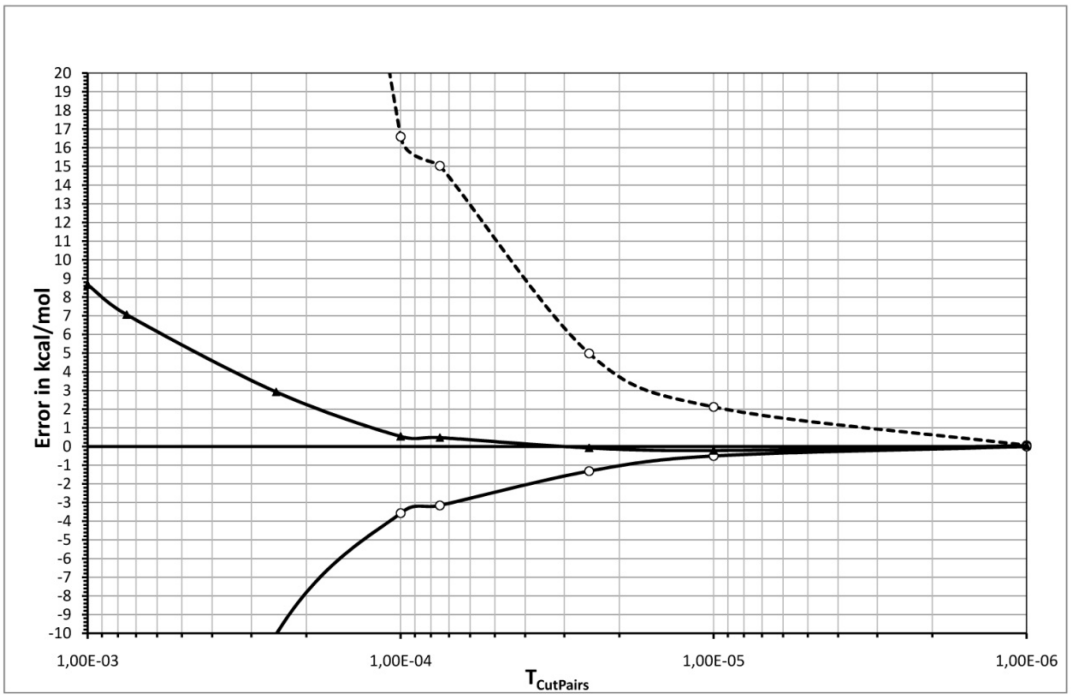

Figure 3.10.: Convergence of open-shell LPNO-CCSD with respect to variations in the threshold T_{CutPairs}. The test system is the trityl radical (SVP basis set, SV/C fitting basis). The threshold T_{CutMKN} was set to zero. The error is given relative to a LPNO-CCSD calculation with $T_{\mathrm{CutPNO}} = 3.33 \times 10^{-7}$ and $T_{\mathrm{CutPairs}} = T_{\mathrm{CutMKN}} = 0$ (solid line: with MP2 correction; dashed line: only strong pairs; circles: LPNO-CCSD with QROs; triangles: LPNO-CCSD with UHF orbitals; Fig. reproduced and modified from Ref. (198)).

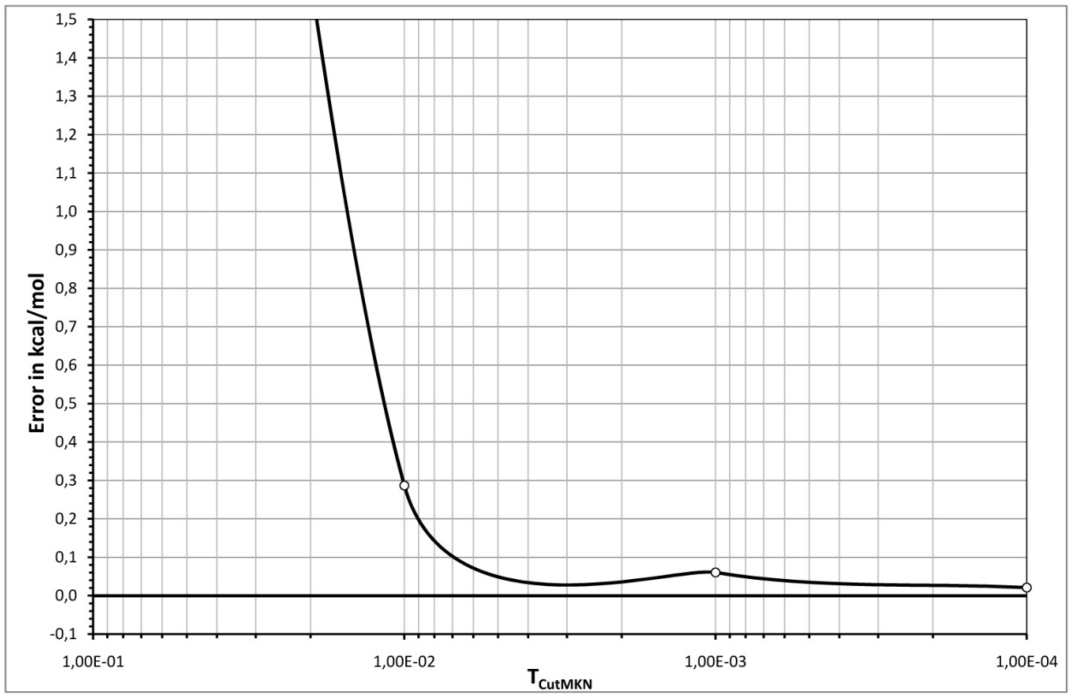

Figure 3.11.: Convergence of the open-shell LPNO-CCSD method with respect to variations in the threshold T_{CutMKN}. The trityl radical serves as the test system (SVP basis set; SV/C fitting basis). The threshold T_{CutPairs} was set to zero and QROs were used. The error is given relative to a LPNO-CCSD calculation with $T_{\mathrm{CutPNO}} = 3.33 \times 10^{-7}$ and $T_{\mathrm{CutPairs}} = T_{\mathrm{CutMKN}} = 0$ (Fig. reproduced and modified from Ref. (198)).

As shown in Fig. 3.10, the use of the MP2 correction for the weak pairs improves the results significantly. With the default value of $T_{\mathrm{CutPairs}} = 10^{-4}$ E_h the error is about 0.5 kcal/mol for UHF orbitals (in this case the reference values were also calculated with UHF orbitals). However, the correction overshoots if QROs are used as reference orbitals since the orbital energy differences are smaller compared to UHF orbitals. Thus, a truncation error of -3.5 kcal/mol still remains if the default value for the pair cut-off is applied. Nonetheless, the spin-contamination introduced by the UHF orbitals will eventually worsen the results much more than a larger error in the local approximation. Thus, the default is to use QROs as reference orbitals for the open-shell LPNO methods. Furthermore, the local and PNO truncation errors may cancel to some extend since they have opposite signs.
It can be seen from Fig. 3.11 that the convergence with respect to T_{CutMKN} is rapid. With the default value of $T_{\mathrm{CutMKN}} = 10^{-3}$ the error is well below 0.1 kcal/mol, analogously to what was observed for the closed-shell variants.

3.2.2. Errors of open-shell specific approximations

In order to investigate how the errors due to the further approximations associated with the open-shell LPNO-CCSD formalism affect the accuracy of the method, further test calculations were carried out on a closed-shell system since the approximations are not essential if only closed-shell orbitals enter the respective calculation, and hence an estimation of the additional errors is possible. The glycine molecule served as test system and the SVP basis set together with the large QZVPP/C fitting basis was used. The reference correlation energy of -0.834075 E_h was obtained with canonical spin-unrestricted CCSD using QROs. Without applying further approximations and setting all thresholds to zero, only the RI error remains which amounts to -0.003 kcal/mol in this case. The additional error due to the neglect of the three external dressing of the EEO (Eqs. (2.73) and (2.74)) of -0.083 kcal/mol is not crucial since it is more than one order of magnitude smaller than the total error of the open-shell LPNO-CCSD method. A significant error of -0.457 kcal/mol is introduced due to the approximations applied to the dressings of the two-external pair-pair operators (Eqs. (B.24) – (B.29)). However, this error has the opposite sign compared to the larger PNO truncation error and should cancel effectively. Applying all approximations simultaneously and using the default setup for the truncation thresholds, the error of the open-shell LPNO-CCSD method amounts to +1.826 kcal/mol which corresponds to 99.64 % of the reference correlation energy. By contrast, the closed-shell LPNO-CCSD variant recovers 99.87 % (+0.697 kcal/mol absolute error) of the reference correlation energy if MP2-PNOs and the default values for the thresholds are used. However, the larger errors were also observed for open-shell LPNO-CEPA/1 for which no additional approximation were made. They mainly result the different MP2 guess amplitudes used to construct the PNOs. However, despite the slightly larger errors in absolute energies, the errors in energy differences which are much more relevant for chemical applications have comparable accuracy (see Sec. 3.3.2).

3.2.3. Investigation of the LPNO-CCSD(T) method

In order to investigate the LPNO methods which perturbatively include connected triple excitations via 'triple natural orbitals' (TNOs), the heptahexaene molecule was studied in the SVP basis set (SV/C fitting basis set). This molecule is part of the reaction energy test set composed of medium-sized closed-shell molecules that have been used extensively in the numerical tests for relative energies (see Sec. 3.3.3). Only the LPNO-CCSD(T) results are documented here, but the same conclusions also hold for LPNO-QCISD(T). The canonical (and semi-canonical CCSD(T)) results serve as reference values. They amount to -0.049837 E_h (-0.045299 E_h) for the triples contribution (E_T) to the total correlation energy (E_{corr}) and -0.970163 E_h (-0.965627 E_h) for E_{corr} respectively. Fig. 3.12 shows the convergence of E_T with respect to the TNO truncation threshold T_{CutTNO}. The semi-canonical CCSD(T) triples energy is used as reference since this is the value which is actually approximated by the TNO approach. The calculations were performed with two different values for the PNO truncation threshold, $T_{CutPNO} = 3.33 \times 10^{-7}$ (filled circles) and $T_{CutPNO} = 0$ (open circles), but without applying local cut-offs ($T_{CutPairs} = 0$ E_h, $T_{CutMKN} = 0$).

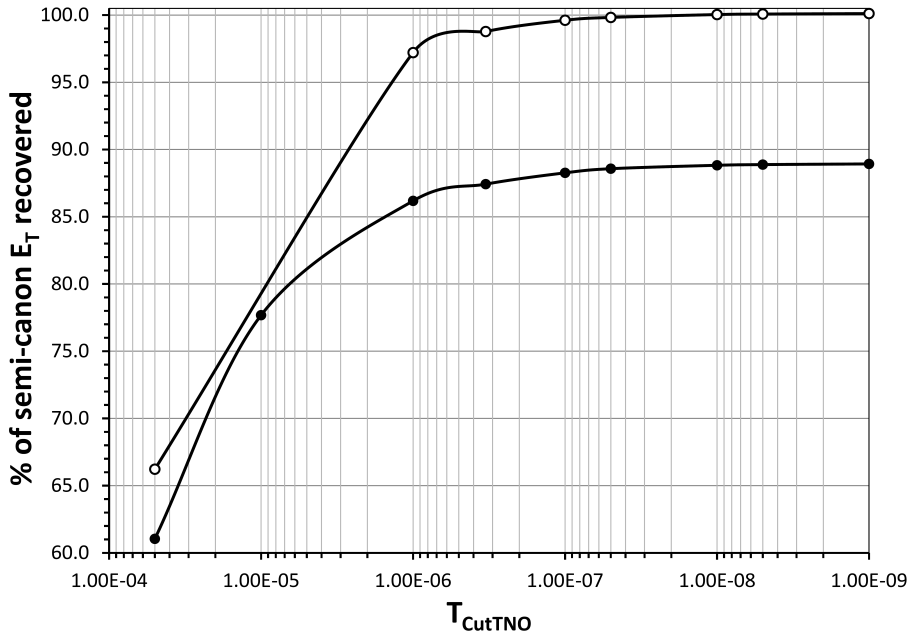

Figure 3.12.: The convergence of the triples contribution to the total LPNO-CCSD(T) correlation energy as a function of the T_{CutTNO} parameter. The relative error (%) with respect to the semi-canonical CCSD(T) result is plotted. The calculations were carried out on the heptahexaene molecule with the SVP basis set (SV/P fitting basis set) using two different values for the PNO truncation threshold ($T_{CutPNO} = 3.33 \times 10^{-7}$: filled circles; $T_{CutPNO} = 0$: open circles). The local cut-offs were set to zero.

The convergence to the $T_{CutTNO} = 0$ limit is rapid and for $T_{CutTNO} = 3.33 \times 10^{-7}$ already ~98.8 % of E_T are recovered. Hence, the latter threshold value will serve as preliminary default for the TNO truncation threshold. However, for the calculations with the default

value of the PNO truncation threshold, not more than ~89 % of the semi-canonical E_T could be reached. Obviously, the error due to T_{CutPNO} is much more crucial for the calculation of the triples contribution than for the singles and doubles contribution to the total correlation energy. At first, one might think that this error is caused by the PNO doubles amplitudes. However, calculations of hyperfine couplings with the LPNO-VCEPA/1 method (see Sec. 3.3.5) indicate that the PNO amplitudes themselves should be accurate enough with $T_{CutPNO} = 3.33 \times 10^{-7}$. On the other hand, it was observed that the errors of the $LPNO_2$ methods are clearly larger than for the $LPNO_1$ variants which can be traced back to the approximate treatment of the two-external pair-pair operators. This would also give a reasonable explanation for the large error observed for LPNO-CCSD(T) since the approximate two-external Exchange integrals are used in the present TNO approach as well. Another potential error source might be introduced by the singles amplitudes. Although the single excitation manifold has not been truncated, the projections from the truncated pair subspace to the full virtual MO space, needed in the singles-doubles coupling terms, introduce an error as well. This subject will be further discussed in Sec. 3.2.8, but it has not been attempted yet to investigate this issue in the context of the TNO approach. However, the error in the singles amplitudes is most likely much smaller than that coming from the approximate treatment of the two-external Exchange operators whose accuracy primarily depends on the PNO truncation threshold.

In order to check the convergence of the E_T upon tightening the PNO truncation threshold the latter was varied while the TNO truncation threshold was fixed at a value of $T_{CutTNO} = 3.33 \times 10^{-7}$. The corresponding relative errors with respect to the canonical CCSD(T) value are pictured in Fig. 3.13. Given that for heptahexaene only ~90.9 % of the canonical triples energy is recovered with semi-canonical CCSD(T), it is not surprising that only 80 – 90 % of it (depending on the value of T_{CutPNO}) can be obtained with the LPNO-CCSD(T). Even with a very small value (10^{-9}) of the PNO truncation threshold, the relative error is still ~2 % larger than what is observed for the LPNO-CCSD(T) calculation with $T_{CutPNO} = 0$ and $T_{CutTNO} = 3.33 \times 10^{-7}$.

Since connected triple excitations contribute only a small fraction (typically less than ~5 %) to the total LPNO-CCSD(T) correlation energy, the error for E_T is less pronounced for the latter. Fig. 3.14 shows the relative error in the total E_{corr} as a function the TNO truncation threshold. The results obtained with $T_{CutPNO} = 0$ (solid line) and $T_{CutPNO} = 3.33 \times 10^{-7}$ (dashed line) are both compared to the canonical (filled circles) and semi-canonical CCSD(T) (open circles) reference values. For the calculations carried out with $T_{CutPNO} = 0$ it is observed that for $T_{CutTNO} = 10^{-6}$, more than 99.9 % of the semi-canonical E_{corr} is recovered. For the preliminary default value of $T_{CutTNO} = 3.33 \times 10^{-7}$, the target value is almost perfectly reproduced. Going to even tighter threshold values one observes that the total semi-canonical correlation energy is slightly overshot, but this can be traced back to the singles and doubles contribution. However, focussing on the error with respect to the canonical reference value, it becomes obvious that both, the error due to the

semi-canonical formalism and the one arising from the PNO truncation threshold, lead to a loss of about 0.5 % of the total correlation energy. Unfortunately, this errors have the same sign and hence they add up to a relative error of ~1 % with respect to the canonical E_{corr} (for $T_{CutTNO} = 10^{-9}$) which corresponds to an absolute error of 6.23 kcal/mol. For the preliminary default value of $T_{CutTNO} = 3.33 \times 10^{-7}$ the deviation from the canonical reference value is still of the same size (1.1 % and 6.66 kcal/mol respectively) which once again emphasizes the insensitivity of the TNO approach with respect to the TNO truncation threshold.

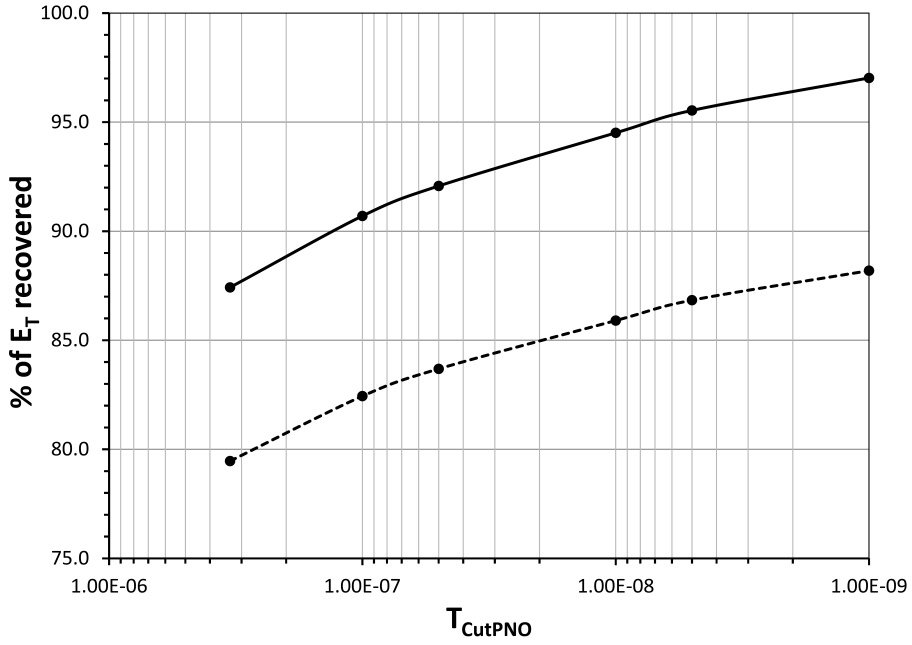

Figure 3.13.: The convergence of the triples contribution to the total LPNO-CCSD(T) correlation energy with respect to variations of the T_{CutPNO} parameter. The relative errors (%) with respect to the canonical (dashed line) and semi-canonical CCSD(T) values (solid line) are plotted. The calculations were carried out on the heptahexaene molecule with the SVP basis set (SV/P fitting basis set) and $T_{CutTNO} = 3.33 \times 10^{-7}$. The local cut-offs were set to zero.

However, the error might be too large for an accurate calculation of relative energies which are of much more concern for computational chemistry applications. This issue will be addressed in Sec. 3.3.3.

Although the convergence with respect to T_{CutTNO} is quite rapid and the introduced error due to the truncated TNO expansion is small (at least with reasonably tight threshold values), its smooth behavior suggests the use of extrapolation techniques to further reduce at least this part of the total error observed for the LPNO-CCSD(T) method. Applying a simple three point extrapolation for E_T calculated with $T_{CutTNO} = 10^{-6}$, 6.66×10−7, and 3.33×10−7, the error in the triples contribution decreases by ~1.5 % and 98.98 % of the canonical correlation energy is recovered based on this procedure. However, the relative error is only slightly reduced compared to a single calculation with the tightest threshold value (both

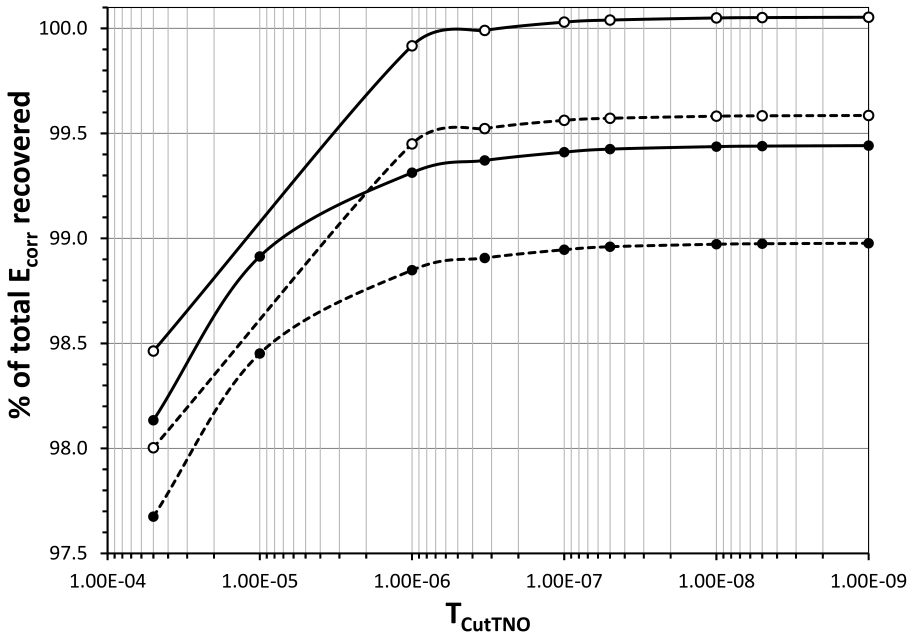

Figure 3.14.: The convergence of the total LPNO-CCSD(T) correlation energy with respect to variations of the T_{CutTNO} parameter. The relative error (%) with respect to the canonical (dashed line) and semi-canonical CCSD(T) (solid line) values are plotted. The calculations were carried out on the heptahexaene molecule with the SVP basis set (SV/P fitting basis set) using two different values for the PNO truncation threshold ($T_{\mathrm{CutPNO}} = 3.33 \times 10^{-7}$: filled circles; $T_{\mathrm{CutPNO}} = 0$: open circles). The local cut-offs were set to zero.

calculations were carried out with $T_{\mathrm{CutPNO}} = 3.33 \times 10^{-7}$). Hence, extrapolation to the $T_{\mathrm{CutTNO}} = 0$ limit does not significantly improve the accuracy of LPNO-CCSD(T). Although the convergence of the singles and doubles contribution to the correlation energy with respect to the PNO truncation threshold is also fast and smooth, an analogous extrapolation to the $T_{\mathrm{CutPNO}} = 0$ limit will not improve on the quality of the PNO amplitudes or two-external Exchange operators themselves. Furthermore, using the default value for the PNO truncation threshold already ensures that the canonical CCSD correlation energy of the heptahexaene molecule is reproduced with high accuracy by the LPNO_1-CCSD method (~0.1 % relative error with MP2 correction, ~0.3 % without). Hence, the inaccurate treatment of the two-external Exchange operators remains the largest source of error for the LPNO-CCSD(T) method since the error due to the semi-canonical approximation is typically much less pronounced for relative energies (at least with respect to experimental reference values, see Sec. 3.3.3). Thus, it would be very useful to find a reliable and computationally cheap estimation of this error similar to the MP2 correction for LPNO methods including single and double excitations only. Unfortunately, first attempts in this direction based on the semi-empirical estimate of E_{T} proposed by Grimme (unpublished work) were not successful. Despite these slightly discouraging observations, there is hope that the errors are less pronounced in the calculation of relative energies. This issue will be investigated in Sec. 3.3.3. Furthermore, it should be taken into account that the heptahexaene molecule represents

a rather challenging case for the LPNO-CCSD(T) method and distinctly smaller errors are expected for other molecules whose triples contribution to the total correlation and errors due to the semi-canonical formalism are significantly smaller.

3.2.4. Basis set dependence

Furthermore, it is interesting to examine the basis set dependence of the PNO expansion. We have investigated the average number of PNOs per pair as a function of basis set size using $T_{CutPNO} = 10^{-6}$, $T_{CutMKN} = 10^{-3}$ and the local pair cut-off set to zero. It is evident from Fig. 3.15 that the number of PNOs per electron pair is a very weak function of the basis set size (roughly proportional to the square root of the number of basis functions)[105,108] and only increases by a factor of two upon going from the small, unpolarized SV basis set to the very large QZVPP basis set.

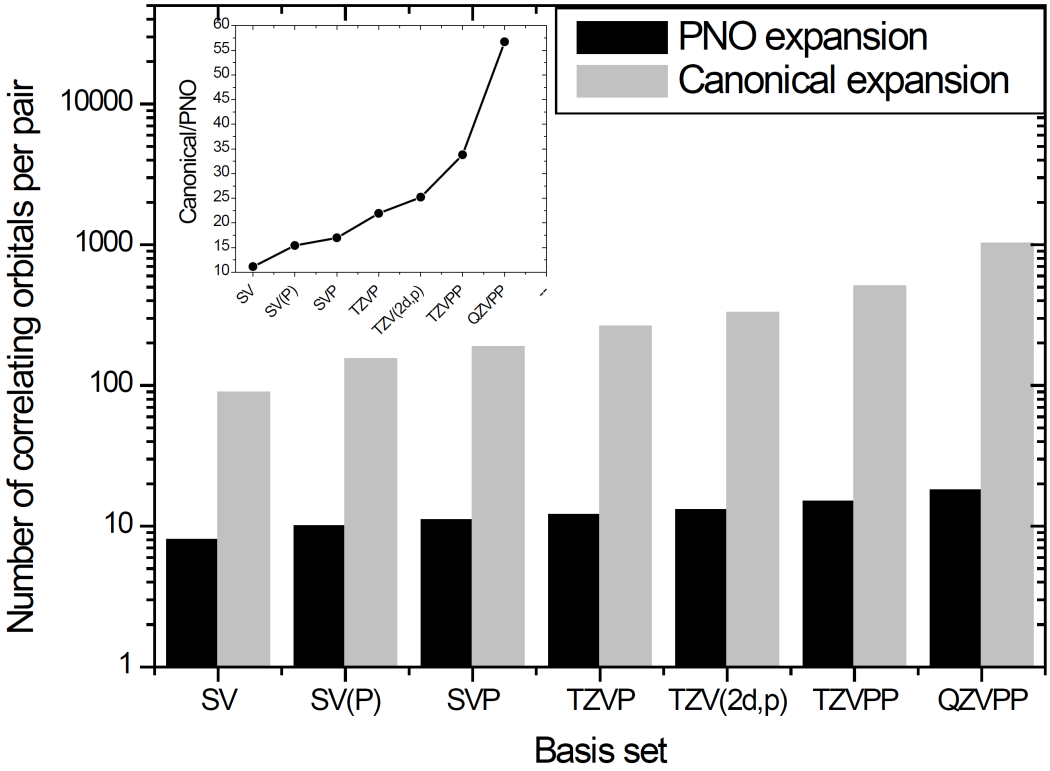

Figure 3.15.: The average number of correlating orbitals per electron pair as a function of the basis set size (logarithmic scale). All calculations were done on the $(Gly)_3$ molecule (thresholds: $T_{CutPNO} = 10^{-6}$, $T_{CutPairs} = 0\ E_h$, $T_{CutMKN} = 10^{-3}$). The inset shows the ratio of the canonical expansion to the PNO expansion (Fig. reproduced and modified from Ref. (196)).

At the same time, the number of canonical correlating orbitals increases by a factor of twelve. Thus, the ratio between canonical expansion and PNO expansion quickly becomes much more favorable for the PNO expansion and reaches a factor of 56 for the QZVPP basis set. If one assumes a computational effort proportional to the fourth power of the number of

correlating orbitals it might be concluded that the PNO expansion is about 10^7 times more efficient than the canonical expansion, even for a system as small as $(Gly)_3$. In practice, the savings are less than this impressive ratio due to all the overhead involved, especially for the calculation of various integrals over PNOs. Nevertheless, it is clear from Fig. 3.15 that very large and accurate correlation calculations become spectacularly efficient with the truncated PNO expansion.

3.2.5. Dependence on the PNO construction method

The reason for preferring Meyer-style PNOs over the straightforward MP2-PNOs can be seen from Fig. 3.16 which shows the error of the closed-shell LPNO-CEPA/1 method relative to the untruncated CEPA/1 result as a function of the PNO truncation threshold.

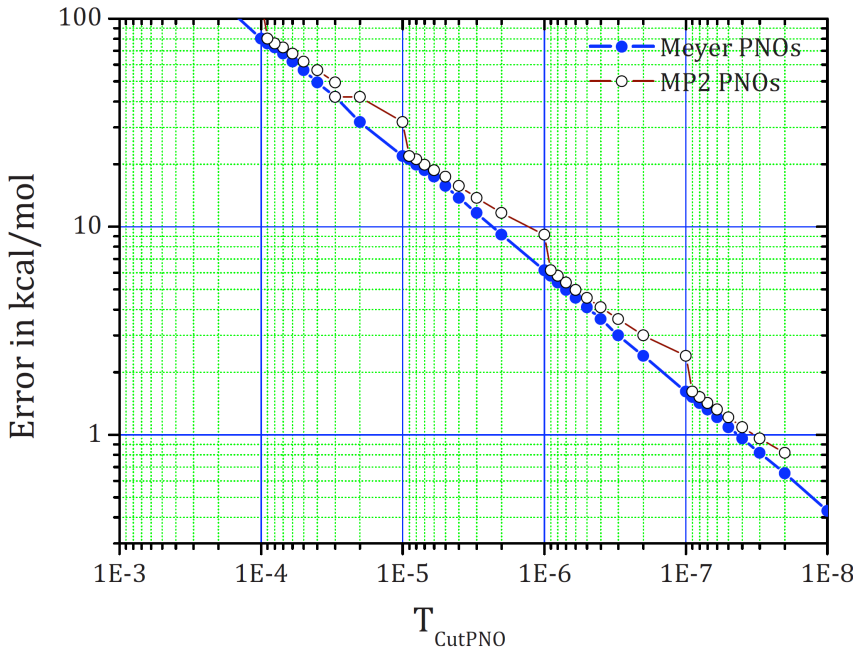

Figure 3.16.: Comparison of the behavior of the Meyer-style PNOs and the MP2-PNOs for $(Gly)_3$ using the LPNO-CEPA/1 method and the SVP basis set (SV/C auxiliary basis). The uncorrected absolute error is shown as a function of the PNO truncation threshold (closed circles: Meyer-style PNOs, open-circles: MP2-PNOs; Fig. reproduced and modified from Ref. (196)).

It is observed that the error of the Meyer-style PNO based calculations is always smaller than that obtained with MP2-PNOs. Furthermore, the behavior with respect to T_{CutPNO} is much smoother for the Meyer-style PNOs. In fact, the almost perfect linearity of the error (in the double logarithmic plot) may suggest extrapolation techniques in place of the perturbative error estimate, but this has not been fully explored yet.

3.2.6. Dependence on the localization method

A further dependence of the errors could result from the localization method. This subject was investigated on two test systems employing two different basis sets. The results in Table 3.1 demonstrate that the dependence of total energies (obtained with closed-shell LPNO-CEPA/1) on the localization methods is very weak.

Table 3.1.: Dependence of the closed-shell LPNO-CEPA/1 method on the localization method (Pipek-Mezey vs. Foster-Boys) for two test systems and two different basis sets. The LPNO error refers to the difference of the total energy obtained with LPNO-CEPA/1 and CEPA/1.

		LPNO error (kcal/mol)	
Method	Molecule	Foster-Boys	Pipek-Mezey
LPNO-CEPA/1	Benzene	0.51	0.53
(cc-pVDZ)	Octahedrane	1.46	1.49
LPNO-CEPA/1	Benzene	0.53	0.47
(aug-cc-pVDZ)	Octahedrane	1.63	1.79

Despite the fact that the Foster-Boys localization procedure[203] procedure produces banana-type bonds while the Pipek-Mezey[210] keeps the π/σ–separation for *e*.g. benzene, correlation energies only differ by a few hundredth of a kcal/mol . On the other hand, the Pipek-Mezey localization algorithm produces some very poorly localized orbitals with basis sets that contain diffuse functions, which may be problematic for local correlation methods that make use of real-space criteria for the truncation.[177] An example are the C–H bonds in benzene as shown in Fig. 3.17.

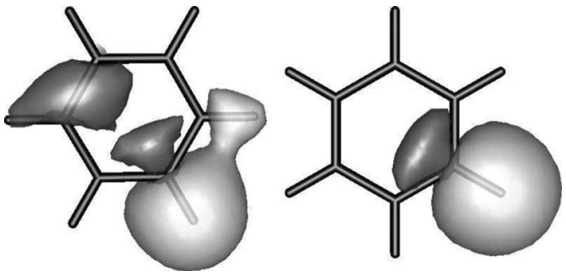

Figure 3.17.: Localized C-H bonding orbital from the benzene molecule as produced by different localization algorithms (left: Pipek-Mezey, right: Foster-Boys). The aug-cc-pVDZ basis set was used (Fig. reproduced and modified from Ref. (196)).

Obviously, the localized MOs (LMOs) generated with the Pipek-Mezey procedure show artificial delocalized tails while the Foster Boys procedure behaves as expected in this case. It is gratifying to observe that despite the unphysical behavior of the Pipek-Mezey LMOs, the obtained LPNO-CEPA/1 results are almost identical to those which are based on the Foster-Boys LMOs (see Table 3.1). Since the Foster-Boys localization criteria is more physically sound, it is used as default localization procedure for the LPNO methods.

3.2.7. Basis set superposition error for LPNO methods

The calculation of weak molecular interactions represents a challenging case for local correlation methods since they are of small magnitude but long range. Since these types of calculations are affected by the basis set superposition error (BSSE)[229] that may be different between the canonical and LPNO approaches, we have investigated this issue numerically for three weakly bonded systems using the closed-shell $LPNO_{1/2}$-QCISD and $LPNO_{1/2}$-CCSD methods. The results in Table 3.2 demonstrate that the LPNO methods have a similar BSSE as the canonical methods and the interaction energies are reproduced with high accuracy. Thus, the LPNO approach should be also suitable for the efficient and accurate calculation of weak molecular interactions which will be demonstrated in detail below (see Sec. 3.3.2).

Table 3.2.: Comparison of canonical and LPNO based BSSE corrected interaction energies of three weakly bonded systems using the closed-shell LPNO based QCISD and CCSD methods and the def2-QZVPP basis set (E_{int}^{BSSE}: BSSE corrected dimer interaction energy; ΔE_{int}: LPNO error without correction for the BSSE; ΔE_{int}^{BSSE}: LPNO error with correction for the BSSE; BSSE: basis set superposition error). All values are given in kcal/mol.

	QCISD		$LPNO_1$-QCISD			$LPNO_2$-QCISD		
(kcal/mol)	E_{int}^{BSSE}	BSSE	ΔE_{int}^{BSSE}	ΔE_{int}	BSSE	ΔE_{int}^{BSSE}	ΔE_{int}	BSSE
HCl···HCl	1.46	0.1	0.02	0.02	0.09	-0.1	-0.12	0.12
HF···H_2O	8.07	0.46	-0.11	-0.09	0.44	-0.29	-0.25	0.42
HF···HCN	6.88	0.28	-0.02	-0.01	0.28	-0.17	-0.15	0.25
	CCSD		LPNO1-CCSD			LPNO2-CCSD		
(kcal/mol)	E_{int}^{BSSE}	BSSE	ΔE_{int}^{BSSE}	ΔE_{int}	BSSE	ΔE_{int}^{BSSE}	ΔE_{int}	BSSE
HCl···HCl	1.47	0.1	0.03	0.03	0.09	-0.09	-0.11	0.12
HF···H_2O	8.07	0.45	-0.09	-0.08	0.44	-0.27	-0.23	0.41
HF···HCN	6.87	0.28	0.01	0.01	0.27	-0.15	-0.12	0.25

3.2.8. Further investigations

As already mentioned in the Introduction, size-consistency is a very crucial criterium that approximate quantum chemical methods should fulfil. Not all coupled pair methods are rigorously size-consistent[121] while for QCISD and CCSD this is always the case. CEPA/1 and CPF/1 should be preferred since they are 'numerically' size-consistent, at least if the orbitals are localized on the different subsystems. This is also true for the LPNO variants of the coupled pair methods, at least in a numerical sense. For benzene, the deviations from exact size-consistency (~1 μE_h) are three orders of magnitude smaller than the LPNO error itself and further decreases if the thresholds are tightened. The LPNO variants of the QCISD and CCSD methods also keep the important property of being (at least approximately) size-consistent despite further approximations were made in the treatment of the higher order disconnected terms, especially in the open-shell variants. Since a fully linked CC

expansion was used that is strictly size-extensive, it is possible to neglect contributions without destroying the size-consistency.

Another point is the unitary invariance with respect to rotation of internal orbitals. While the CPF, QCISD, and CCSD methods satisfy this criterium it is not the case for the CEPA methods. This invariance is not present in the LPNO methods due to the projection on the truncated PNO pair basis which is one of the basic steps in the LPNO approach and the key to large efficiency gains. However, the differences between total energies obtained with canonical and localized internal orbitals respectively is relatively small, *e.g.* for the water molecule it never exceeds 0.1 kcal/mol regardless of the LPNO method used. Moreover, localized internal orbitals lead to less diffuse PNOs and a better compression of the external space since their orbital energies indirectly effect the PNO construction. Furthermore, localized internal orbitals offer the possibility to apply the strong pair approximation which additionally enhances the efficiency gains. Hence, the loss of unitary variance is not considered as a crucial issue since the advantages of using truncated PNO pair subspaces to span the external correlation space in combination with localized internal orbitals do more than compensate for it.[230]

The last issue which is addressed in this section is the treatment of single excitations. Although the correlation subspace spanned by the single excitations is not truncated in the present LPNO approach, an additional error arises from the projection of the singles amplitudes to the truncated PNO pair basis (Eq. (2.91)). Furthermore, the projection of doubles amplitudes from the truncated pair-specific PNO basis to the virtual MO basis is only approximately possible since a part of the information was already lost due to the truncation. Thus, formally speaking, the single excitations are only treated in an approximate manner. However, the leading terms to the single residual and the singles-singles interactions do not suffer from these approximations. They only appear in the doubles-singles interaction (doubles residual) and the singles-doubles interaction (singles residual) that would be both of higher order in a perturbative treatment and the introduced errors are supposed to be small. They were estimate for a single test case, the fluoroethane molecule calculated the closed-shell LPNO-CCSD method and the def2-TZVP basis set. The singles PNO error amounts to $+22\ \mu E_h$ which is one order of magnitude smaller compared to the doubles PNO error (-373 μE_h). Moreover, it has the opposite sign and is effectively eliminated by the doubles LPNO error. Thus, the approximations that were made for the single excitations do not significantly affect the numerical accuracy of the LPNO methods. However, a better treatment of the single excitations is preferable and work in this direction is under way in our research group.

3.3. Errors of the LPNO methods using default settings

3.3.1. Errors in the correlation energies and basis set dependence

At first, the closed-shell LPNO-CEPA/1 method will be investigated. In order to test the robustness of our defaults we have calculated the correlation energies of some medium sized molecules. The results in Table 3.3 demonstrate that with our default values for the cut-offs the absolute error of the closed-shell LPNO-CEPA/1 method is ~1 kcal/mol. Obviously, most of this error arises from the truncation of the PNO expansion since semi-local CEPA/1 (SL-CEPA/1), for which only the local approximation is applied, shows an error that is roughly four times smaller. Typically about 99.9 % of the correlation energy is recovered, and in the worst case of this test set ($Ni(CO)_4$), it is still 99.8 %. The PNO error always has the same sign, the correlation energies are always slightly underestimated. Thus it is further reduced through error cancellation in case of a negative error arising from the strong pair approximation. Moreover, a large part of the absolute PNO error is expected to cancel in the calculation of energy differences.

Table 3.3.: Errors in correlation energies obtained with closed-shell semi-local (SL) CEPA/1 and LPNO-CEPA/1 using the default values for the thresholds and the TZV(2d,2p) basis set. The untruncated CEPA/1 correlation energies serve as reference values (MAD: mean absolute deviation; MD: mean deviation; MAX: maximum absolute deviation).

	E_{corr} (E_h)	Error (kcal/mol)		$\%E_{corr}$(CEPA/1)
	CEPA/1	SL-CEPA/1	LPNO-CEPA/1	LPNO-CEPA/1
Adamantane	-1.672683	-0.59	0.38	99.96
Asparagine	-1.463752	0.20	1.09	99.88
cis-bicyclo[4.4.0]decane	-1.704964	-0.28	0.65	99.94
Hexanoic acid	-1.455469	0.07	0.72	99.92
Indolizine	-1.401352	0.05	1.14	99.87
$Ni(CO)_4$	-1.887487	0.45	2.38	99.80
Bicyclo[4.3.0]nonane	-1.529633	-0.19	0.62	99.94
	MAD (kcal/mol)	0.26	0.99	
	MD (kcal/mol)	-0.04	0.99	
	MAX (kcal/mol)	0.59	2.38	

Secondly, we have investigated the performance of the closed-shell $LPNO_{1/2}$-QCISD and $LPNO_{1/2}$-CCSD methods. Table 3.4 reports an analysis of the average errors in the correlation energies of ten medium sized molecules with up to 17 atoms for the $LPNO_1$-QCISD method using the TZV(2df,2pd) basis set. It is evident that $LPNO_1$-QCISD recovers 99.85 – 99.97 % (99.93 % on average) of the canonical correlation energies which amounts to absolute errors of only a few tenths of a kcal/mol (0.5 kcal/mol on average). In order to separate the error due to the PNO truncation from the local errors and the perturbative estimate of the remainder, we have also collected the corresponding results computed without the MP2 correction and local approximations ($T_{CutPairs} = 0$ E_h, $T_{CutMKN} = 0$) in Table 3.4.

It is observed that the mean absolute error increases by more than a factor of three to 1.8 kcal/mol and the mean relative error increases from 0.07 % to 0.27 % of the correlation energy. Thus, the perturbative correction, while not being an essential component of the LPNO approach, does markedly improve the accuracy of the LPNO methods.

Table 3.4.: Error analysis for correlation energies obtained with closed-shell $LPNO_1$-QCISD and the TZVPP basis set (TZVPP/C fitting basis) for a series medium sized molecules using the default values for the thresholds. The reference values are given by the corresponding canonical QCISD results. The PNO truncation error refers to calculations without local approximations and the MP2 correction for the truncation errors (N_{BF}: number of basis functions; N_{Aux}: number of auxiliary basis functions; N_{PNO} (av): average number of significant PNOs for each electron pair; $\%E_{corr}$: percentage of the recovered correlation energy; Δ_{abs}: absolute deviation from the canonical reference values).

				$LPNO_1$-QCISD		PNO truncation error	
	N_{BF}	N_{Aux}	N_{PNO} (av)	$\%E_{corr}$	Δ_{abs} (kcal/mol)	$\%E_{corr}$	Δ_{abs} (kcal/mol)
Heptahexaene	273	424	44	99.85	1.00	99.71	1.99
2-hydroxypyridine	287	439	37	99.90	0.76	99.67	2.55
1-pyrazoline	239	350	37	99.94	0.38	99.73	1.60
Neopentane	323	440	32	99.97	0.20	99.75	1.52
Vinylcylopropane	267	380	39	99.94	0.33	99.76	1.30
Norbornadiene	329	484	37	99.94	0.46	99.68	2.38
Cyclooctatetraene	360	536	35	99.94	0.48	99.70	2.47
Dimethylperoxid	208	298	33	99.92	0.42	99.76	1.30
Oxetane	208	298	37	99.94	0.28	99.77	1.15
Vinyl acetate	270	402	33	99.92	0.60	99.72	1.99
			Mean value:	99.93	0.49	99.73	1.82

In order to put the comparison on a more solid basis the calculations on the test molecules shown in Table 3.4 were repeated with three different basis sets and closed-shell $LPNO_2$-QCISD as well as $LPNO_{1/2}$-CCSD (see Table 3.5). Turning first to $LPNO_1$-QCISD it is evident that neither the absolute nor the relative error depends markedly on the size of the basis set which is an advantage of the LPNO methods. However, it should be noted that the error due to the PNO approximation itself does increase slightly with basis set size but this error appears to be almost perfectly compensated by the perturbative correction. This necessarily implies that the errors of the LPNO methods become slightly larger if MP2 fails badly. One such case is heptahexaene where the LPNO error increases by ~0.15 % which still seems acceptable. For the $LPNO_1$-QCISD method, the dependence on the PNO construction method was reinvestigated. Consistent with the observations made for LPNO-CEPA/1, it was found that the Meyer-style PNOs perform marginally better than the more straightforward (semi-local) MP2-PNOs. This is evident from both the relative and the absolute errors. The $LPNO_1$-CCSD method behaves very similarly to the $LPNO_1$-QCISD method but shows a slightly larger absolute error (1 kcal/mol or 0.1 – 0.2 % of the correlation energy) that is most plausible attributed to the neglect of the higher order disconnected three-

external singles contribution (Eq. (2.53)). For $LPNO_1$-CCSD/SVP it was obtained that in the sequence $T_{CutPNO} = 3.33\times10^{-7}, 10^{-6}, 3.33\times10^{-6}, 10^{-5}$, the average correlation energy loss increases by 0.05 % in each step (data not shown in Table 3.5) which again indicates the very smooth and regular behavior of the LPNO error with respect to the truncation thresholds.

Table 3.5.: Mean values of absolute and relative errors and their dependence and dependence on the basis set and PNO construction method for closed-shell $LPNO_{1/2}$-QCISD as well as $LPNO_{1/2}$-CCSD.Three different basis sets of increasing size were employed together with the corresponding auxiliary basis sets and the default values for the truncation thresholds. The test set shown in Table 3.4 was used. The reference values are given by the corresponding canonical QCISD or CCSD results. The PNO truncation error refers to calculations without local approximations and MP2 correction for the truncation errors. ($\%E_{corr}$: percentage of the recovered correlation energy; Δ_{abs}: absolute deviation from the canonical reference values).

		LPNO default settings		PNO truncation error	
		$\%E_{corr}$	Δ_{abs} (kcal/mol)	$\%E_{corr}$	Δ_{abs} (kcal/mol)
$LPNO_2$-QCISD	SVP	99.16	4.59	99.05	5.21
	TZVP	99.10	5.18	98.96	6.03
	TZVPP	98.90	7.25	98.67	8.78
$LPNO_2$-CCSD	SVP	98.98	5.58	98.87	6.21
	TZVP	98.90	6.31	98.73	7.30
	TZVPP	98.72	8.41	98.49	9.96
$LPNO_1$-QCISD	SVP	99.90	0.53	99.83	0.97
	TZVP	99.91	0.54	99.79	1.21
	TZVPP	99.93	0.49	99.73	1.82
(MP2-PNOs)	SVP	99.88	0.69	99.75	1.44
	TZVP	99.88	0.69	99.75	1.44
	TZVPP	99.89	0.70	99.67	2.11
$LPNO_1$-CCSD	SVP	99.73	1.49	99.65	1.96
	TZVP	99.70	1.74	99.58	2.44
	TZVPP	99.74	1.73	99.53	3.09

Turning to the $LPNO_2$-QCISD and $LPNO_2$-CCSD methods, it is observed that the errors are significantly larger than in the $LPNO_1$ case and amount to roughly 1 % of the correlation energy or a few kcal/mol respectively. Only a fraction of this error is recovered by the perturbative correction. This is not surprising since the only difference between the $LPNO_1$ and $LPNO_2$ algorithms is the treatment of the pair-pair interactions that are not contained in the MP2-based estimation of the truncation errors. The real issue, however, is whether the LPNO error is smooth enough to essentially cancel in chemically relevant energy differences. This important subject will be investigated in Sec. 3.3.2.

Finally, we have investigated the accuracy of the open-shell LPNO methods in terms of absolute energies. To this end, a set of nine medium sized molecules with up to 25 atoms was

employed using the default settings for the thresholds. The test set contains simple organic radicals, such as the octyl radical, but also more difficult cases such as the quinone radical anion and the benzyl radical, a transition state taken from the GMTKN24 database of Goerigk and Grimme[58] and high-spin $[Mn(H_2O)_6]^{2+}$ with a sextet ground state. The calculations were carried out for three different basis sets of increasing size (SVP, TZVP, TZVPP). The open-shell LPNO-CCSD calculations with the largest basis set yield consistently more than 99.7 % of the reference correlation energy (canonical CCSD with QROs) and the absolute errors are in the range of 1-2 kcal/mol (see Table 3.6). Without applying the MP2 correction for the neglected pairs the errors are significantly larger.

Table 3.6.: Error analysis of open-shell LPNO-CCSD calculations for a series of medium sized high-spin open-shell molecules using QROs and default cut-off values together with the TZVPP basis set (TZVPP/C auxiliary basis). The geometries were either taken from the GMTKN24 data base[58] or can be found in the supplementary material of Ref. (198) (N_{BF}: number of basis functions; N_{Aux}: number of auxiliary functions; N_{PNO} (av): average number of significant PNOs for each electron pair; $\%E_{corr}$: percentage of the recovered correlation energy; Δ_{abs}: absolute deviation from the canonical reference values; TS: transition state; hs: high-spin).

				With MP2 correction		Only strong pairs	
Molecule	N_{BF}	N_{Aux}	N_{PNO} (av)	$\%E_{corr}$	Δ_{abs} (kcal/mol)	$\%E_{corr}$	Δ_{abs} (kcal/mol)
Quinone	304	728	27	99.75	2.23	98.68	11.81
Benzyl radical	315	742	31	99.70	2.17	98.89	7.95
Octyl radical	486	1118	26	99.87	1.16	98.93	9.88
$[Mn(H_2O)_6]^{2+}$ (hs)	394	973	24	99.90	1.09	98.66	14.14
$H_2NCHCONH_2$	225	530	26	99.81	1.18	99.03	5.97
$(CH_3)_3CCH_2$	309	710	26	99.90	0.57	98.76	7.20
$CH_3SO_2CH_2$	228	554	23	99.85	0.95	98.85	7.32
$NH_2 + C_2H_5$ (TS)	191	438	29	99.75	0.92	99.19	3.03

In contrast to the closed-shell LPNO variants the errors are slightly larger for the smaller basis sets, but the basis set dependence is still relatively weak (see Table 3.7). Among the three tested methods LPNO-CCSD performs best. For LPNO-QCISD and LPNO-CEPA/1 the observed errors are about 0.10 % and 0.15 % larger. LPNO-CCSD benefits from the slight overshooting of the correlation energy due to the further approximations made for the dressed two-external pair-pair operators (see Sec. 2.3.4 and Sec. 3.2.2), whereas the LPNO-CEPA/1 method is more sensitive to larger singles and doubles amplitudes indicating a slight multireference character of the respective molecule. The complete error analysis of the LPNO-CEPA/1 and LPNO-QCISD results obtained with the TZVPP basis set can be found in Appendix C. Using $\mathbf{K}^{ii}$-PNOs (Eq. (2.87)) for the diagonal SOMO space interactions does not affect the accuracy of LPNO-QCISD and LPNO-CCSD. In fact, the LPNO-CEPA/1 calculations for the sextet state of the manganese complex show slightly larger errors although $\mathbf{K}^{ii}$-PNOs are not used for this method. Importantly, the observed LPNO errors are always of the same sign and are of similar magnitude. Thus, they should largely cancel if relative energies are considered.

Table 3.7.: Mean value of percentage recovered correlation energy ($\%E_{corr}$) and mean absolute deviation (Δ_{abs}) of correlation energies obtained with open-shell LPNO methods using QROs and the default values for the thresholds. Three different basis sets (together with the corresponding auxiliary basis sets) were employed. The test set shown in Table 3.6 was used.

		With MP2 correction		Only strong pairs	
Method	Basis set	$\%E_{corr}$	Δ_{abs} (kcal/mol)	$\%E_{corr}$	Δ_{abs} (kcal/mol)
LPNO-CEPA/1	SVP	99.55	2.70	98.52	9.10
(QROs)	TZVP	99.56	2.77	98.53	9.62
	TZVPP	99.66	2.44	98.73	9.57
LPNO-QCISD	SVP	99.60	2.38	98.56	8.78
(QROs)	TZVP	99.61	2.42	98.58	9.27
	TZVPP	99.72	2.01	98.78	9.14
LPNO-CCSD	SVP	99.68	1.91	98.64	8.31
(QROs)	TZVP	99.73	1.71	98.69	8.56
	TZVPP	99.82	1.28	98.87	8.41

3.3.2. Errors in relative energies

For chemical applications the absolute errors in the calculated correlation energies are of much less concern than the errors in energy differences, for which the LPNO error may cancel to some extent. In order to investigate this point the reaction energies for a test set that consists of 21 reactions composed of 39 small closed-shell molecules out of the G2/97 test set of Curtiss *et al.*[231] were calculated with the closed-shell LPNO-CEPA/1 method. The mean value of the experimental reference values (back-corrected heats of formation in order to obtain pure electronic reaction energies) amounts to 98.50 kcal/mol (99.32 kcal/mol for the CCSD(T) reference values). This test set represents a subset of a larger test set contained in the GMTKN24 data base.[58] The electronic structure of some molecules involved in this test set (e.g. ozone) is complicated to describe correctly with single reference molecules, which is indicated by relatively large singles and doubles amplitudes. Furthermore, the connected triples contribution to the total correlation energy is significant for some test cases. As shown in Table 3.8 the performance of the closed-shell LPNO-CEPA/1 method is almost identical to that of the parent CEPA/1 method. Both methods reproduce the high-level CCSD(T) reaction energies to within 1.5 kcal/mol which corresponds to a mean relative error of less than 2 %. The mean absolute deviations from the CCSD(T) reference values are almost identical for CEPA/1 and LPNO-CEPA/1. Thus, the truncation errors of the LPNO approach indeed largely cancel in calculations of relative energies. However, although the large and flexible def2-QZVPP basis set was used, the mean absolute deviation from the experimental reference values is still about 2.5 kcal/mol for the LPNO-CEPA methods and chemical accuracy is only reached with the CCSD(T) method if the basis set limit is reached and relativistic and vibrational effects are properly taken into account. Nonetheless, the LPNO-CEPA/1 method is more accurate than MP2, QCISD, CCSD, and B3LYP for the same

test set,[24] indicating its potential for accurate computational chemistry applications. Since the experimental reference values only have an accuracy of ± 1 kcal/mol,[58] the comparison to the CCSD(T) results might be less ambiguous and leaves less room for fortunate error cancellation since it directly measures the quality of calculated electronic energies.[24]

The same reaction energy test set was employed to investigate the performance of the closed-shell LPNO$_{1/2}$-QCISD and LPNO$_{1/2}$-CCSD methods relative to their canonical variants. The corresponding analysis of the LPNO error is presented in Table 3.9. Not surprisingly, it is observed that the LPNO$_1$ approaches are slightly more accurate than their LPNO$_2$ counterparts. As evident from Table 3.9, the PNO truncation threshold needs to be tightened to $T_{\mathrm{CutPNO}} = 10^{-7}$ for the latter in order to reach the same accuracy as for the LPNO$_1$ variants which again indicates the sensitivity of the truncation error if the semi-joint pair-pair interactions are treated only approximately. However, the difference is not nearly as large as for the absolute correlation energies. In fact, the LPNO$_1$ variants show mean absolute errors of only 0.6-0.7 kcal/mol relative to the canonical methods and for the LPNO$_2$ approaches the observed errors are still below 1 kcal/mol which again suggests that the error cancellation is effective.

However, the molecules from the G2/97 test set are fairly small and hardly represent a critical test for local correlation approaches. An more conclusive comparison is documented in Table 3.10, where a set of reactions involving somewhat larger molecules was investigated. It consists of 23 closed-shell reactions, 16 of which were taken from the ISO34 test set of the GMNTK24 data base[58] (isomerization reactions of organic molecules) and seven electronically more complicated reactions were taken from other test sets contained in the same data base. This test set was previously found to be challenging for DFT methods, *e.g.* the widely used B3LYP method shows an average error of more than 7 kcal/mol.[24] As evident from Table 3.10, both CEPA/1 and LPNO-CEPA/1 reproduce the CCSD(T) results with high accuracy and mean absolute deviations of less than 1 kcal/mol. The only slightly disappointing case is reaction (5) where the error approaches about 4 kcal/mol. Nevertheless, the results again underline that CEPA/1 is a sufficiently accurate method for large-scale chemical applications and that the approximations contained in its LPNO variant do not significantly reduce the achievable accuracy.

The same test was also calculated with the closed-shell LPNO$_{1/2}$-QCISD and LPNO$_{1/2}$-CCSD methods. As it is obvious from Table 3.11, the LPNO methods are very successful in reproducing the canonical QCISD and CCSD reaction energies. The QCISD and CCSD results are very similar. The LPNO$_1$ methods reproduce the reference values to within 0.2 kcal/mol on average which again demonstrates their excellent performance. The less accurate LPNO$_2$ methods are also quite successful and show mean absolute errors of only about 1 kcal/mol. The maximum errors of about 3 – 3.5 kcal/mol are, however, significant. Nevertheless, this test set is much closer to what one is likely to meet in computational chemical applications and it demonstrates the great potential of the LPNO methods for the latter.

Table 3.8.: Statistical evaluation of the closed-shell LPNO-CEPA/1 method (default threshold values) for the calculation of reaction energies. The def2-QZVPP basis set together with the corresponding fitting basis set has been used (MAD: mean absolute deviation; MD: mean deviation; MAX: maximum absolute deviation). The experimental reference values (Exp.) were taken from the GMTKN24 data base.[58]

Reaction	Reference values		Error [kcal/mol]			
	Exp.	CCSD(T)	LPNO-CEPA/1		CEPA/1	
	E_{reac} (kcal/mol)		Δ_{exp}	$\Delta_{CCSD(T)}$	Δ_{exp}	$\Delta_{CCSD(T)}$
(1) $H_2 + F_2 \rightarrow 2\ HF$	-133.92	-135.12	-0.33	0.87	-0.66	0.54
(2) $OF_2 + H_2 \rightarrow F_2 + H_2O$	-68.5	-68.99	-0.65	-0.16	-0.33	0.16
(3) $O_3 + 3\ H_2 \rightarrow 3\ H_2O$	-222.09	-225.19	-4.09	-0.99	-4.14	-1.04
(4) $N_2 + 3\ H_2 \rightarrow 2\ NH_3$	-38.52	-39.13	-1.03	-0.42	-1.50	-0.89
(5) $N_2O + H_2 \rightarrow N_2 + H_2O$	-80.99	-81.46	-2.15	-1.68	-2.27	-1.80
(6) $C_2H_2 + H_2 \rightarrow C_2H_4$	-48.4	-49.41	-1.88	-0.87	-2.09	-1.08
(7) $CO + H_2O \rightarrow CO_2 + H_2$	-6.86	-6.11	2.09	1.34	2.04	1.29
(8) $CO_2 + H_2O \rightarrow HCOOH$	-2.09	-2.36	-1.08	-0.81	-1.18	-0.91
(9) $C_2H_2 + HF \rightarrow H_2C{-}CHF$	-25.37	-26.85	-2.38	-0.90	-2.62	-1.14
(10) $H_3C{-}CHO \rightarrow CO + CH_4$	-2.59	-3.12	-1.09	-0.56	-1.00	-0.47
(11) $C_2H_2 + C_2H_4 \rightarrow$ cyclobutene	-32.63	-32.51	0.72	0.60	0.27	0.15
(12) $C_2H_4 + 4\ F_2 \rightarrow C_2F_4 + 4\ HF$	-430.44	-437.17	-2.78	3.95	-4.93	1.80
(13) $SiO + 3\ H_2 \rightarrow SiH_4 + H_2O$	-33.39	-38.05	-6.70	-2.04	-5.97	-1.31
(14) $SiCl_4 + CF_4 \rightarrow SiF_4 + CCl_4$	-28.01	-23.11	6.99	2.09	6.58	1.68
(15) $BCl_3 + AlF_3 \rightarrow BF_3 + AlCl_3$	-27.02	-28.71	-3.66	-1.97	-3.23	-1.54
(16) $F_2 + Cl_2 \rightarrow 2\ ClF$	-26.29	-26.76	-0.12	0.35	-0.57	-0.10
(17) $CH_2O + H_2 \rightarrow CH_3OH$	-29.09	-29.33	-0.35	-0.11	-0.59	-0.35
(18) $P_2 + 3\ F_2 \rightarrow 2\ PF_3$	-495.05	-492.18	3.74	0.87	2.05	-0.82
(19) $Li_2 + F_2 \rightarrow 2\ LiF$	-212.24	-210.98	4.49	3.23	3.34	2.08
(20) $SO_2 + 3\ H_2 \rightarrow H_2S + 2\ H_2O$	-60.42	-64.57	-6.98	-2.83	-7.14	-2.99
(21) $CO + 3\ H_2 \rightarrow H_2O + CH_4$	-64.51	-64.55	-0.40	-0.36	-0.67	-0.63
		MAD (kcal/mol)	2.56	1.29	2.53	1.08
		MD (kcal/mol)	-0.84	-0.02	-1.17	-0.35
		MAX (kcal/mol)	6.99	3.95	7.14	2.99

Perhaps one of the most challenging applications for local correlation methods are weak intermolecular interactions which are well known to be dominated by long range correlation effects.[232] In order to test the applicability of the LPNO methods for that purpose, a subset of Hobza's S22 test set,[233] for which dispersion interactions are dominant, was investigated. Furthermore, a test set of H-bonded dimers proposed by Boese *et al.*[234] was evaluated using the closed-shell LPNO-CEPA/1 method. The charged H-bonded systems have been analyzed separately since their interaction energy is one order of magnitude larger compared to the neutral systems. No BSSE correction has been applied since it was ruled out as an additional error source of the LPNO approach relative to their parent methods (see Sec. 3.2.7). Previous results have indicated that CEPA/1 performs excellently for this test set.[24] Thus, we were curious to see whether this also carries over to the LPNO approach. The results collected in Table 3.12 and Table 3.13 indeed show that LPNO-CEPA/1 is as accurate as the parent CEPA/1 method for these delicate weak interactions. Both reproduce the CCSD(T)/aug-cc-

Table 3.9.: Analysis of the LPNO error for the small molecules reaction energy test set calculated with the closed-shell $LPNO_{1/2}$-QCISD and $LPNO_{1/2}$-CCSD methods using the def2-QZVPP basis set and matching auxiliary basis set (MAD: mean absolute deviation; MD: mean deviation; MAX: maximum absolute deviation). Unless stated explicitly, the default threshold values have been used.

Reaction	E_{reac} (kcal/mol)	Error (kcal/mol)		E_{reac} (kcal/mol)	Error (kcal/mol)		
	QCISD	$LPNO_2$-QCISD	$LPNO_1$-QCISD	CCSD	$LPNO_2$-CCSD	$LPNO_2$-CCSD ($T_{CutPNO} = 10^{-7}$)	$LPNO_1$-CCSD
(1) $H_2 + F_2 \rightarrow 2\ HF$	-138.00	-0.91	-0.19	-138.08	-0.97	-0.64	0.07
(2) $OF_2 + H_2 \rightarrow F_2 + H_2O$	-71.00	-1.36	-1.01	-71.73	-1.26	-0.80	0.54
(3) $O_3 + 3\ H_2 \rightarrow 3\ H_2O$	-237.30	-2.60	-2.29	-239.32	-2.58	-1.63	1.70
(4) $N_2 + 3\ H_2 \rightarrow 2\ NH_3$	-40.26	0.00	-0.19	-40.62	-0.06	0.22	0.47
(5) $N_2O + H_2 \rightarrow N_2 + H_2O$	-85.87	-1.00	-1.26	-87.10	-1.03	-0.73	1.26
(6) $C_2H_2 + H_2 \rightarrow C_2H_4$	-50.06	0.72	-0.02	-50.25	0.70	0.44	0.31
(7) $CO + H_2O \rightarrow CO_2 + H_2$	-4.25	0.91	0.43	-3.78	0.83	0.47	-0.45
(8) $CO_2 + H_2O \rightarrow HCOOH$	-3.12	0.71	-0.18	-3.60	0.70	0.73	0.56
(9) $C_2H_2 + HF \rightarrow H_2C\text{–}CHF$	-27.06	1.53	0.25	-26.99	1.45	1.01	0.06
(10) $H_3C\text{–}CHO \rightarrow CO + CH_4$	-4.06	-1.38	0.04	-3.83	-1.31	-1.05	-0.32
(11) $C_2H_2 + C_2H_4 \rightarrow$ cyclobutene	-31.83	2.33	-0.10	-32.12	2.25	1.76	0.42
(12) $C_2H_4 + 4\ F_2 \rightarrow C_2F_4 + 4\ HF$	-446.71	-0.50	0.50	-446.21	-1.05	-0.46	0.08
(13) $SiO + 3\ H_2 \rightarrow SiH_4 + H_2O$	-40.60	0.85	-0.87	-42.03	1.00	0.65	1.62
(14) $SiCl_4 + CF_4 \rightarrow SiF_4 + CCl_4$	-21.87	0.38	0.61	-21.69	0.34	-0.14	0.26
(15) $BCl_3 + AlF_3 \rightarrow BF_3 + AlCl_3$	-29.97	-0.67	-0.78	-30.47	-0.51	-0.10	0.09
(16) $F_2 + Cl_2 \rightarrow 2\ ClF$	-28.54	0.25	0.81	-27.94	0.13	0.30	-0.40
(17) $CH_2O + H_2 \rightarrow CH_3OH$	-29.86	0.35	-0.40	-30.27	0.39	0.34	0.40
(18) $P_2 + 3\ F_2 \rightarrow 2\ PF_3$	-504	1.99	0.50	-502.84	1.32	0.55	-0.82
(19) $Li_2 + F_2 \rightarrow 2\ LiF$	-213.05	0.02	1.31	-212.49	-0.26	-0.09	0.37
(20) $SO_2 + 3\ H_2 \rightarrow H_2S + 2\ H_2O$	-69.83	-1.72	-1.68	-71.67	-1.52	-1.07	1.72
(21) $CO + 3\ H_2 \rightarrow H_2O + CH_4$	-65.30	0.12	-0.54	-66.04	0.15	0.18	0.80
MAD (kcal/mol)		0.97	0.66		0.94	0.64	0.61
MD (kcal/mol)		0.00	-0.24		-0.06	0.00	0.42
MAX (kcal/mol)		2.60	2.29		2.58	1.76	1.72

Table 3.10.: Statistical evaluation of the closed-shell CEPA/1 and LPNO-CEPA/1 method for the calculation of reaction energies for a test set composed from medium-sized molecules. All calculations were performed with the TZVP basis set (TZV/C fitting basis set) using the default values for the thresholds (MAD: mean absolute deviation; MD: mean deviation; MAX: maximum absolute deviation). The corresponding CCSD(T)/TZVP results serve as reference values (mean value: 21.03 kcal/mol).

Reaction	E_{reac} (kcal/mol)	Error (kcal/mol)	
	CCSD(T)	CEPA/1	LPNO-CEPA/1
(1) Heptahexaene → heptatriyne	-14.98	1.47	1.27
(2) 2 2,3-dimethylbut-2-ene → octamethylcyclobutane	-24.12	2.70	2.82
(3) 2-hydroxypyridine → 2-hydropyridone	1.24	-0.50	-0.33
(4) C_2H_4 + H_2CN_2 → 1-pyrazoline	-37.95	0.32	0.98
(5) 2 p-xylene → [2,2]paracyclophane + 2 H_2	52.80	4.93	3.81
(6) Octahedrane → cyclopentadienyletropenyle	18.22	-0.24	-1.43
(7) C_9O_3 (D_{3h} isomer 1) → C_9O_3 (D_{3h} isomer 2)	33.12	1.27	2.66
(8) n-octane → 2,2,3,3-tetramethylbutane	-4.45	1.69	1.69
(9) Propyne → allene	1.18	-0.50	-0.55
(10) Propyne → cyclopropene	23.40	0.06	0.18
(11) Propene → cyclopropane	7.90	0.04	0.21
(12) Buta-1,3-diene → cyclobutene	12.22	0.27	0.56
(13) Cyclopentene → vinylcyclopropane	22.73	0.20	-0.02
(14) neo-pentane → n-pentane	4.77	-0.53	-0.56
(15) Toluene → norbornadiene	42.79	0.04	0.60
(16) Styrene → cyclooctatetraene	33.54	-0.62	-0.70
(17) N-methylenemethanamin → aziridin	13.11	-0.02	0.21
(18) Acetic acid → methyl formate	15.37	-0.01	-0.05
(19) Ethanediol → dimethylperoxide	61.98	-0.06	-0.05
(20) Propan-2-one → oxetane	32.31	-0.17	0.10
(21) Dihydrofuran-2(3H)-one → vinyl acetate	15.03	0.01	-0.27
(22) Tetrahydropyran-2-one → pentan-2,4-dione	4.01	0.04	-0.23
(23) Hexanoic acid → methyl pivalate	6.37	0.42	0.46
	MAD (kcal/mol)	0.70	0.86
	MD (kcal/mol)	0.47	0.49
	MAX (kcal/mol)	4.93	3.81

pVDZ (S22 subset) or high quality W2 (H-bonded dimers, back-corrected for BSSE, thermal and relativistic corrections) reference values to within 0.3 – 0.6 kcal/mol and ~0.2 kcal/mol respectively. Thus, we anticipate a large potential of the LPNO-CEPA/1 method for such applications.

The test set which contains the van der Waals complexes was reinvestigated with the closed-shell LPNO-QCISD$_{1/2}$ and LPNO-CCSD$_{1/2}$ methods. The corresponding results are collected in Table 3.14. Quite surprisingly, the LPNO$_2$ methods are slightly more accurate than the LPNO$_1$ methods for this test set. Nonetheless, in both cases, the average deviation of ~0.3 kcal/mol from the corresponding canonical results is comparable to the that of LPNO-CEPA/1 for the same test set. It is encouraging that the approximations of the LPNO approach do not significantly reduce the accuracy of the parent methods, at least not for conservatively chosen threshold values. Further test calculations with the closed-shell

Table 3.11.: Comparison of LPNO based and canonical QCISD and CCSD methods for the prediction of reaction energies for a set of reactions involving larger molecules. The TZVP basis set (TZV/C auxiliary basis set) was used.

Reaction	E_{reac} (kcal/mol)	Error (kcal/mol)		E_{reac} (kcal/mol)	Error (kcal/mol)	
	QCISD	$LPNO_2$-QCISD	$LPNO_1$-QCISD	CCSD	$LPNO_2$-CCSD	$LPNO_1$-CCSD
(1) Heptahexaene → heptatriyne	-18.48	-1.14	-0.54	-18.55	-1.15	-0.74
(2) 2 2,3-dimethylbut-2-ene → octamethylcyclobutane	-21.55	2.54	-0.08	-21.56	2.31	-0.19
(3) 2-hydroxypyridine → 2-hydropyridone	0.67	0.07	0.11	1.34	-0.01	0.13
(4) C_2H_4 + H_2CN_2 →> 1-pyrazoline	-38.14	2.77	0.26	-38.72	2.59	0.11
(5) 2 p-xylene → [2,2]paracyclophane + 2 H_2	59.40	0.58	-0.98	59.40	0.44	-1.11
(6) Octahedrane → cyclopentadienyletropenyle	20.67	-3.47	-0.50	20.90	-3.16	-0.36
(7) C_9O_3 (D_{3h} isomer 1) → C_9O_3 (D_{3h} isomer 2)	33.55	2.60	1.07	34.28	1.70	0.47
(8) n-octane → 2,2,3,3-tetramethylbutane	-2.41	0.94	0.06	-2.35	0.88	0.06
(9) Propyne → allene	1.67	0.28	0.05	1.57	0.30	0.11
(10) Propyne → cyclopropene	24.11	0.73	0.08	23.87	0.70	0.08
(11) Propene → cyclopropane	7.74	0.12	-0.02	7.65	0.08	-0.03
(12) Buta-1,3-diene → cyclobutene	12.01	0.72	0.05	11.92	0.66	0.02
(13) Cyclopentene → vinylcyclopropane	22.77	-1.02	-0.03	22.78	-0.99	-0.03
(14) neo-pentane → n-pentane	4.15	-0.27	-0.03	4.13	-0.25	-0.03
(15) Toluene → norbornadiene	42.89	1.32	0.11	42.96	1.25	0.14
(16) Styrene → cyclooctatetraene	33.01	-0.30	-0.06	33.12	-0.29	0.01
(17) N-methylenemethanamin → aziridin	12.89	0.28	-0.02	12.75	0.26	-0.03
(18) Acetic acid → methyl formate	15.52	0.42	-0.01	15.68	0.40	0.01
(19) Ethanediol → dimethylperoxide	63.58	0.59	0.14	63.72	0.62	0.20
(20) Propan-2-one → oxetane	32.23	0.77	0.08	31.82	0.81	0.06
(21) Dihydrofuran-2(3H)-one → vinyl acetate	15.35	-0.96	-0.14	15.32	-0.82	-0.05
(22) Tetrahydropyran-2-one → pentan-2,4-dione	4.01	-1.14	-0.08	4.33	-1.17	-0.10
(23) Hexanoic acid → methyl pivalate	7.15	0.41	0.08	7.37	0.29	0.01
MAD (kcal/mol)		1.02	0.20		0.92	0.18
MD (kcal/mol)		0.30	-0.02		0.24	-0.05
MAX (kcal/mol)		3.47	1.07		3.16	1.11

Table 3.12.: Statistical evaluation of the closed-shell CEPA/1 and LPNO-CEPA/1 methods (default values for the thresholds) for the interaction energies of van der Waals bonded systems. The corresponding CCSD(T) results serve as reference values (MAD: mean absolute deviation; MD: mean deviation; MAX: maximum absolute deviation). All calculations were performed with the aug-cc-pVDZ basis set (and matching auxiliary basis set).

Dimer	E_{int} (kcal/mol)	Error (kcal/mol)	
	CCSD(T)	CEPA/1	LPNO-CEPA/1
$(CH_4)_2$ (D_{3d})	-0.97	0.09	0.11
$(C_2H_4)_2$ (D_{2d})	-1.94	0.26	0.27
Benzene $*$ H_2O (C_3)	-3.03	0.44	0.22
Benzene dimer (C_{2h})	-6.14	1.34	0.41
Pyrazine dimer (C_s)	-7.46	1.40	0.58
Ethene $*$ ethine (C_{2v})	-2.34	0.18	0.16
Benzene $*$ H_2O (C_s)	-4.52	0.37	0.36
Benzene $*$ NH_3 (C_s)	-3.74	0.42	0.29
Benzene $*$ HCN (C_s)	-6.45	0.57	0.41
Benzene dimer (C_{2d})	-5.67	0.80	0.39
	MAD (kcal/mol)	0.59	0.32
	MD (kcal/mol)	0.59	0.32
	MAX (kcal/mol)	1.40	0.58

LPNO methods involving weak intermolecular interactions of larger molecules confirm this observation.[199,235] However, it should be noted that compared to CCSD(T) or other high-quality reference values, the CEPA/1 method is clearly superior to QCISD and CCSD[24] for the calculation of non-covalent interactions and this transfers also to their LPNO counterparts. All test systems discussed so far are rather small molecules that can in principle be calculated with the parent CEPA or CC methods using basis sets of decent size. However, the scope of this work was to construct methods which are applicable to molecules with up to 100 atoms. Hence, in order to test the performance of the LPNO methods for larger molecular systems, the anthracene dimer (see Fig. 3.1 d)) previously discussed by Grimme *et al.*[236] was investigated. Using the same geometries as employed in this previous study the dimerization energy as a function of the basis set size was calculated. The closed-shell LPNO-NCPF/1 method was used together with three basis sets of increasing size (SV(P), TZVPP, and QZVP). With the largest basis set used, 2196 basis functions enter the calculation. The reference value is 9 $\pm$ 3 kcal/mol (Monte Carlo and extrapolated QCISD(T) calculations).[236] The MP2/QZVP results is 21.5 kcal/mol thus being far from the target value. Even worse, B3LYP/QZVP predicts a dimerization energy of -25.8 kcal/mol which amounts to an error of ~38 kcal/mol and a qualitatively erroneous results. The large MP2 error poses a difficult problem for local correlation approaches that use second order perturbation theory for estimating the local errors. The calculated LPNO-NCPF/1 dimerization energies are 17.5 kcal/mol (SV(P)), 14.3 kcal/mol (TZVPP), and 13.8 kcal/mol (QZVP). Thus, upon enlargement of the basis set size, the LPNO-NCPF/1 method converges smoothly towards the reference value.

Table 3.13.: Statistical evaluation of the closed-shell LPNO-CEPA/1 method for the calculation of dissociation energies of H-bonded dimers. The optimized CCSD(T)/aug-cc-pVQZ geometries and the (back-corrected to pure electronic energies) W2 reference values were taken from the work of Boese *et al.*[234] No BSSE correction was applied. All calculations were performed with the def2-QZVPP basis set (and matching fitting basis set) using the default values of the thresholds (MAD: mean absolute deviation; MD: mean deviation; MAX: maximum absolute deviation).

Reaction	E_{reac} (kcal/mol)	Error (kcal/mol)	
	W2	CEPA/1	LPNO-CEPA/1
$CO\cdots HF \rightarrow CO + HF$	1.72	-0.01	-0.07
$H_2O\cdots H_2O \rightarrow H_2O + H_2O$	4.97	0.01	-0.07
$HCl\cdots HCl \rightarrow HCl + HCl$	1.74	-0.12	-0.09
$HF\cdots H_2O \rightarrow HF + H_2O$	8.68	0.01	-0.13
$HF\cdots HF \rightarrow HF + HF$	4.57	0.00	-0.10
$HF\cdots HCN \rightarrow HF + HCN$	7.37	-0.14	-0.18
$OC\cdots HF \rightarrow CO + HF$	3.50	-0.13	-0.17
	MAD (kcal/mol)	0.06	0.12
	MD (kcal/mol)	-0.05	-0.12
	MAX (kcal/mol)	0.14	0.17
$H_3O^+\cdots H_2O \rightarrow H_3O^+ + H_2O$	33.68	0.05	-0.02
$NH_4^+\cdots H_2O \rightarrow NH_4^+ + H_2O$	20.45	0.01	-0.04
$HCC^-\cdots H_2O \rightarrow HCC^- + H_2O$	18.19	-0.17	-0.28
$CN^-\cdots H_2O \rightarrow CN^- + H_2O$	15.43	0.61	0.55
	MAD (kcal/mol)	0.21	0.22
	MD (kcal/mol)	0.13	0.05
	MAX (kcal/mol)	0.61	0.55

Table 3.14.: Statistical evaluation of the LPNO error for the interaction energies (E_{int}) of van der Waals bonded systems calculated with the closed-shell $LPNO_{1/2}$-QCISD and $LPNO_{1/2}$-CCSD methods (default values for the thresholds). All calculations were done with the aug-cc-pVDZ basis set and the matching fitting basis set (MAD: mean absolute deviation; MD: mean deviation; MAX: maximum absolute deviation).

Dimer	E_{int} (kcal/mol)	Error (kcal/mol)		E_{int} (kcal/mol)	Error (kcal/mol)	
	QCISD	$LPNO_2$-QCISD	$LPNO_1$-QCISD	CCSD	$LPNO_2$-CCSD	$LPNO_1$-CCSD
$(CH_4)_2$ (D_{3d})	-0.85	0.07	0.01	-0.84	0.06	0.00
$(C_2H_4)_2$ (D_{2d})	-1.58	0.19	-0.01	-1.59	0.18	-0.01
Benzene $*$ H_2O (C_3)	-2.52	-0.09	-0.21	-2.52	-0.10	-0.21
Benzene dimer (C_{2h})	-4.51	-0.85	-0.93	-4.51	-0.87	-0.95
Pyrazine dimer (C_s)	-5.77	-0.79	-0.80	-5.74	-0.85	-0.86
Ethene $*$ ethine (C_{2v})	-2.07	0.03	-0.06	-2.08	0.02	-0.07
Benzene $*$ H_2O (C_s)	-4.05	0.05	-0.03	-4.01	0.00	-0.08
Benzene $*$ NH_3 (C_s)	-3.25	0.00	-0.11	-3.23	-0.02	-0.14
Benzene $*$ HCN (C_s)	-5.79	0.03	-0.20	-6.18	0.38	0.16
Benzene dimer (C_{2d})	-4.74	-0.20	-0.43	-4.74	-0.22	-0.44
MAD (kcal/mol)		0.23	0.28		0.27	0.29
MD (kcal/mol)		-0.16	-0.28		-0.14	-0.26
MAX (kcal/mol)		0.85	0.93		0.87	0.95

Since many computational chemistry studies deal with open-shell systems it is of great importance that the LPNO approach also yields accurate relative energies in the open-shell case. To investigate the performance of the open-shell LPNO methods in this respect, two test sets including typical open-shell systems were used including radical stabilization energies (RSE43 test set taken from the GMNTK24 data base of Goerigk and Grimme[58] which consists of 43 radical stabilization energies of organic molecules) and reaction barriers (DBH24 test set of Truhlar *et al.*[237] composed of 12 forward and 12 backward barrier heights).

The error analysis for the RSE43 test set given in Table 3.15 shows that the relative energies obtained with the open-shell LPNO methods are in very good agreement with the predictions of the parent methods. The maximum absolute error never exceeds 1 kcal/mol and the mean absolute error is smaller than 0.3 kcal/mol. Thus, the effective error cancellation also works for relative energies of open-shell molecules. In most cases, the radical stabilization energy is slightly underestimated. Consistent with the observations made for absolute energies, the open-shell LPNO-CCSD method yields the most accurate results.

The same conclusions hold for the reaction barrier test set (Table 3.16). Compared to the results for RSE43 test set, slightly larger LPNO errors were observed for the DBH24 test set, but the absolute values of the barrier heights are itself larger compared to the radical stabilization energies. A few transition states included in the DBH24 test set show already some multireference character. In this cases, LPNO-CCSD is significantly more accurate and robust than LPNO-CEPA/1. For example, the LPNO error for the second barrier height is about 1 kcal/mol larger for LPNO-CEPA/1 while the convergence of the residual is significantly slower compared to LPNO-CCSD. This can be traced back to the exponential parameterization of the singles excitations in CC theory, which effectively introduces some orbital relaxation, and thus greatly improves the stability of single reference correlation methods.[83]

Table 3.15.: Analysis of radical stabilization energies ($R + CH_3^* \rightarrow R^* + CH_4$) from the RSE43 test set calculated with the open-shell LPNO based correlation methods using QROs and and the default values for the threshold. The reference values (E_{reac}) are obtained with the corresponding parent method and QROs. A CBS (cc-pVDZ/TZ) extrapolation was employed (cc-pVTZ fitting basis). All values are given in kcal/mol (MAD: mean absolute deviation; MD: mean deviation; MAX: maximum absolute deviation).

Radical	CEPA/1 (QROs)		QCISD (QROs)		CCSD (QROs)	
(kcal/mol)	E_{reac}	LPNO Error	E_{reac}	LPNO Error	E_{reac}	LPNO Error
$(C_6H_5)CH_2^*$	-14.32	0.02	-13.64	0.02	-14.12	0.36
CH_2CCN^*	3.15	0.48	4.25	0.43	3.84	0.72
CH_2CF^*	7.00	0.59	7.37	0.53	7.65	0.28
$CCl_3CH_2^*$	-0.95	0.99	-0.60	0.79	-0.46	0.67
$CH_3CF_2CH_2^*$	0.02	0.23	0.13	0.27	0.26	0.19
$CF_3CH_2^*$	1.32	0.23	1.39	0.22	1.51	0.16
$CH_2ClCH_2^*$	-3.13	0.15	-2.81	0.22	-2.74	0.18
$CH_2FCH_2^*$	-1.40	0.10	-1.31	0.14	-1.21	0.11
$HOCH_2CH_2^*$	-1.84	0.15	-1.77	0.20	-1.71	0.15
$CH_2CHCH_2^*$	-16.52	-0.34	-16.09	-0.33	-16.52	0.11
CH_2CHO^*	-9.21	0.15	-8.85	0.46	-9.29	0.86
CH_2CN^*	-7.69	0.03	-7.14	0.07	-7.49	0.38
$CH_2CONH_2^*$	-6.13	0.04	-5.90	0.12	-5.96	0.14
$CH_3NHCOCH_2^*$	-6.32	0.26	-5.96	0.26	-5.94	0.21
$CH_2COOCH_3^*$	-6.45	0.36	-6.13	0.34	-6.17	0.35
CH_2COOH^*	-6.17	0.36	-5.92	0.37	-6.04	0.43
$(CH_2CHCH_2)CH_2^*$	-3.06	0.17	-2.97	0.19	-2.89	0.12
CH_2F^*	-3.57	0.12	-3.44	0.09	-3.24	-0.01
$CH_2NH_2^*$	-11.66	0.10	-11.49	0.16	-11.35	0.05
$CH_2NH_3^{*+}$	4.75	0.08	4.78	0.13	4.81	0.10
$CH_3NHCH_2^*$	-12.43	0.39	-12.14	0.38	-11.94	0.22
CH_2NHCHO^*	-10.79	0.03	-10.31	0.13	-10.21	0.08
CH_2NHOH^*	-8.61	0.55	-7.96	0.44	-7.72	0.24
$(CH_3)_2NCH_2^*$	-12.77	0.67	-12.39	0.59	-12.14	0.39
$CH_2NO_2^*$	-3.08	-0.05	-2.70	0.04	-2.74	0.06
$CF_3OCH_2^*$	-3.71	0.32	-3.57	0.36	-3.41	0.24
$CH_3OCH_2^*$	-2.72	0.17	-2.61	0.19	-2.46	0.10
CH_2OCHO^*	-5.62	0.06	-5.46	0.20	-5.29	0.12
$CH_3COOCH_2^*$	-6.06	0.33	-5.72	0.41	-5.51	0.30
CH_2OH^*	-4.09	0.10	-4.04	0.11	-3.92	0.03
$PH_3CH_2^{*+}$	0.56	0.17	0.61	0.17	0.68	0.13
$CH_3SCH_2^*$	-10.65	0.35	-10.28	0.40	-10.03	0.21
CH_2SCHO^*	-8.50	0.58	-7.77	0.50	-7.52	0.30
$CH_2SH_2^{*+}$	2.73	0.15	2.79	0.19	2.86	0.13
CH_2SH^*	-9.16	0.11	-8.91	0.13	-8.72	-0.02
$CH_3SO_2CH_2^*$	-0.40	0.88	-0.02	0.71	0.41	0.44
$CH_3SOCH_2^*$	-3.45	0.92	-2.85	0.63	-2.52	0.32
H_2NCHCN^*	-21.77	0.46	-20.97	0.50	-20.98	0.60
$H_2NCHCONH_2^*$	-23.64	-0.06	-23.19	0.04	-23.09	0.00
$H_2NCHCOOH^*$	-24.78	0.07	-24.34	0.13	-24.29	0.11
H_2CCCH^*	-12.19	0.30	-11.58	0.17	-11.96	0.47
$(CH_3)_3C^*$	-6.54	0.00	-6.41	0.04	-6.27	-0.06
$(CH_3)_3CCH_2^*$	-2.50	0.21	-2.37	0.18	-2.28	0.09
MAD		0.28		0.28		0.24
MD		0.26		0.26		0.23
MAX		0.99		0.79		0.86

Table 3.16.: Error analysis of forward (fw) and backward (bw) barrier heights from the DBH24 test set calculated with open-shell LPNO based correlation methods using QROs and the def2-QZVPP basis set (def2-QZVPP/C fitting basis). The reference values (E_{reac}) are obtained with the corresponding parent method and QROs. All values are given in kcal/mol (MD: mean deviation; MAX: maximum deviation; TS: transition state).

Barrier	CEPA/1 (QROs)		QCISD (QROs)		CCSD (QROs)	
(kcal/mol)	E_{reac}	LPNO error	E_{reac}	LPNO error	E_{reac}	LPNO error
$H + N_2O \rightarrow$ TS (fw)	17.3	1.0	19.5	0.6	19.1	0.8
$OH + N_2 \rightarrow$ TS (bw)	86.6	1.8	91.4	1.0	92.3	0.8
$H + ClH \rightarrow$ TS (fw)	19.3	0.2	20.0	0.1	19.8	0.4
$HCl + H \rightarrow$ TS (bw)	19.3	0.2	20.0	0.1	19.8	0.4
$CH_3 + FCl \rightarrow$ TS (fw)	8.0	0.7	10.5	0.4	10.5	0.8
$CH_3F + Cl \rightarrow$ TS (bw)	61.7	1.1	65.6	0.7	65.7	0.9
$Cl^- \cdots CH_3Cl \rightarrow$ TS (fw)	13.7	0.6	14.6	0.6	15.1	0.2
$ClCH_3 \cdots Cl^- \rightarrow$ TS (bw)	13.7	0.6	14.6	0.6	15.1	0.2
$F^- \cdots CH_3Cl \rightarrow$ TS (fw)	2.5	0.4	3.1	0.4	3.7	0.1
$FCH_3 \cdots Cl^- \rightarrow$ TS (bw)	32.0	1.2	32.6	1.0	33.6	0.4
$OH^- + CH_3F \rightarrow$ TS (fw)	-5.1	1.3	-4.1	1.0	-3.1	0.5
$HOCH_3 + F^- \rightarrow$ TS (bw)	16.3	1.4	17.4	1.1	18.4	0.6
$H + N_2 \rightarrow$ TS (fw)	14.8	0.6	15.9	0.4	15.8	0.6
$HN_2 \rightarrow$ TS (bw)	12.2	0.1	12.3	0.1	12.0	0.6
$H + C_2H_4 \rightarrow$ TS (fw)	2.2	0.2	2.8	0.2	2.7	0.4
$CH_3CH_2 \rightarrow$ TS (bw)	43.5	0.5	44.7	0.3	44.7	0.6
$HCN \rightarrow$ TS (fw)	46.8	0.5	47.9	0.3	48.2	0.0
$HNC \rightarrow$ TS (bw)	32.5	0.6	33.5	0.4	33.7	0.2
$OH + CH_4 \rightarrow$ TS (fw)	8.4	0.5	9.5	0.3	9.6	0.2
$CH_3 + H_2O \rightarrow$ TS (bw)	20.1	0.6	21.5	0.4	21.6	0.3
$H + OH \rightarrow$ TS (fw)	10.8	0.3	11.4	0.3	11.3	0.5
$O + H_2 \rightarrow$ TS (bw)	15.5	0.4	16.2	0.3	16.2	0.4
$H + H_2S \rightarrow$ TS (fw)	4.4	0.2	4.9	0.2	4.8	0.3
$H_2 + HS \rightarrow$ TS (bw)	18.9	0.1	19.8	0.1	19.8	0.0
MD		0.6		0.5		0.4
MAX		1.8		1.1		0.9

Since the test sets consist of rather small open-shell molecules, for which also accurate reference data are available, it is instructive to test the open-shell LPNO methods for a more realistic scenario where the proposed methods might be useful. In a recent study, the oxygen activation mechanism of Fe(II) dioxygenases was studied which represents a challenging application for single reference correlation methods.[83,238] The involved transition metal model complexes are still small enough, such that canonical CCSD can be applied, at least in combination with relatively small basis sets. Hence, it is possible to evaluate the LPNO error for this example.

One step of the reaction mechanism on the septet surface (Fig. 3.18) was chosen in order to investigate whether LPNO-CCSD provides an accurate approximation to the CCSD barrier height. QROs obtained from an unrestricted B3LYP calculation were used as reference orbitals, since the UHF reference wavefunction is hopelessly poor for these transition metal compounds.[83,238]

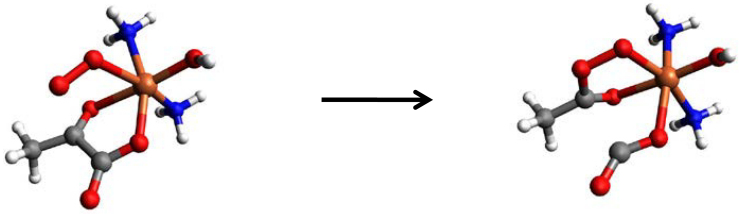

Figure 3.18.: Structure of the model complexes involved in one step of the oxygen activation mechanism of Fe(II) dioxygenases on the septet surface. The optimized geometries (details are documented in Ref. (238)) can be found in in the supplementary material of Ref. (198).

Table 3.17.: Calculated barrier heights for the reaction pictured in Fig. 3.18. The SV(P) basis set was only used for the hydrogen atoms (SV/C fitting basis; QZVPP/C for the large basis set calculations). QROs and the default threshold values were used.

Method	Basis set	$E_{barrier}$ (kcal/mol)
CCSD	SV(P)/TZVP	2.97
LPNO-CCSD	SV(P)/TZVP	2.74
LPNO-CCSD	QZVPP	2.69
UKS B3LYP	SV(P)/TZVP	6.49
UKS B3LYP	QZVPP	3.28

As shown in Table 3.17, the barrier height calculated with LPNO-CCSD and the small basis set (SVP for the hydrogen atoms, TZVP for all other atoms) is in very good agreement with the CCSD reference value while the corresponding B3LYP barrier is much higher. Unexpectedly, using the large QZVPP basis set for all atoms, the LPNO-CCSD value remains almost identical, while the B3LYP barrier height is decreasing by about 50 % and is then in good agreement with the CCSD value. It can be taken from this this example that it is possible to model highly complex bioinorganic reaction mechanisms with the LPNO methods in combination with sufficiently large basis sets provided that the respective reference determinant is of acceptable quality. Thus, LPNO-CCSD is a very promising method to tackle present day computational chemistry problems such as the calculation of barrier heights for cluster or QM/MM models of metal-enzyme active sites. Nonetheless, one will need to add perturbative triples to systematically approach chemical accuracy.

3.3.3. Performance of the LPNO-CCSD(T) method for relative energies

In order to evaluate the performance of the LPNO-CCSD(T) method with respect to the calculation of relative energies, the larger molecule reaction energy test set (see *e*.g. Table 3.18) was reinvestigated. First, the deviation from the corresponding canonical and semi-canonical CCSD(T)/TZVP values will be analyzed (data not shown). All LPNO-CCSD(T) calculations were performed with the TZVP basis set (and matching fitting basis set) using the default values for the local thresholds ($T_{\mathrm{CutPairs}} = 10^{-4}$ E_h, $T_{\mathrm{CutMKN}} = 10^{-3}$) and a single value for the TNO truncation threshold. Extrapolation was not used since it does not sig-

nificantly reduce the error (see Sec. 3.2.3) while introducing another source of uncertainty. Although the investigation of absolute LPNO-CCSD(T) energies showed that the errors due to the semi-local approximation can be quite large (see Sec. 3.2.3), these errors are much less pronounced in the calculated reaction energies. The semi-canonical CCSD(T) method reproduces the corresponding canonical CCSD(T) results to within 0.22 kcal/mol on average and the maximum absolute deviation is only ~1 kcal/mol for the isomerization reaction of heptahexaene to heptatriyne. The LPNO-CCSD(T) calculations with the preliminary default values for the truncation thresholds ($T_{\mathrm{CutPNO}} = 3.33 \times 10^{-7}$, $T_{\mathrm{CutTNO}} = 3.33 \times 10^{-7}$) yield a mean absolute deviation (MAD) of 0.68 kcal/mol from the canonical reference values and 0.56 kcal/mol with respect to semi-canonical CCSD(T). This indicates that the size of the LPNO error for relative energies calculated with the LPNO-CCSD(T) method is between that of the $LPNO_1$-CCSD and $LPNO_2$-CCSD methods which showed a MAD of 0.18 kcal/mol and 0.92 kcal/mol for the same test set respectively (see Table 3.11). However, the maximum absolute errors (MAX) observed for the isomerization reaction of the carbo[3]-oxocarbon (C_9O_3) molecule of 4.44 kcal/mol (canonical reference values) and 4.01 kcal/mol (semi-canonical reference values) are not negligible. Surprisingly, setting the TNO truncation threshold to zero does not improve on the results. The errors are even slightly larger (MAD of 0.71 kcal/mol and 0.55 kcal/mol with respect to the canonical and semi-canonical CCSD(T) values respectively), but the MAD for the isomerization of C_9O_3 is reduced by about half a kcal/mol. Looking at the perturbative triples contribution to the reaction energies separately, it becomes evident that almost the entire error is already present in this relatively small part (typically less than 5 % of E_{reac}) of the total reaction energy. This is probably due to the fact that the magnitude of the triples contribution from the individual molecules of the respective reaction usually differ much more than the corresponding doubles contribution to the total correlation energy. Thus, there is no effective error cancellation for relative energies calculated with the LPNO-CCSD(T) method, only the error due to the semi-local approximation decreases significantly compared to what was observed for absolute energies. This problem cannot be solved by tightening the TNO truncation threshold. As it was already observed for absolute energies, the LPNO-CCSD(T) reaction energies are quite insensitive with respect to T_{CutTNO}. Tighter values for this threshold merely add to the computation time but do not markedly improve on the accuracy of the calculated reaction energies. The only way to achieve higher accuracy for both, relative and absolute LPNO-CCSD(T) energies, is to tighten the PNO truncation threshold. For example, recalculating the same test set with $T_{\mathrm{CutPNO}} = 10^{-7}$ ($T_{\mathrm{CutTNO}} = 0$) reduces the MAD by ~20 % and the maximum error to 3.05 kcal/mol (3.48 kcal/mol with respect to canonical CCSD(T)) However, this does not represent a practical solution since upon significantly tightening the PNO truncation threshold, most of efficiency gains are taken way.

It is also interesting to evaluate the errors in the LPNO-CCSD(T) reaction energies relative to experimental reference values (back-corrected for thermal and zero-point energy contributions, estimated accuracy ±1 kcal/mol), which were taken from the GMTKN24 database.[58]

Table 3.18.: Comparison of canonical CCSD(T), semi-canonical CCSD(T) and LPNO-CCSD(T) reaction energies (TZVP basis set and matching fitting basis set) with back-corrected experimental values for 23 reactions composed from mediums-sized closed-shell molecules. The default values for the LPNO thresholds and two different values for the TNO truncation threshold ($T_{CutTNO} = 3.33 \times 10^{-7}$ and $T_{CutTNO} = 0$) were used. (MAD:mean absolute deviation; MD:mean deviation; MAX: maximum absolute deviation).

Reaction	E_{reac} (kcal/mol)	Error w.r.t. exp. reference values (kcal/mol)			
	Exp. reference	CCSD(T) canon.	CCSD(T) semi-canon.	LPNO-CCSD(T) $T_{CutTNO} = 0$	LPNO-CCSD(T) $T_{CutTNO} = 3.33^{-7}$
Reaction					
(1) Heptahexaene → heptatriyne	-14.3	-0.7	-1.7	-3.8	-3.8
(2) 2 2,3-dimethylbut-2-ene → octamethylcyclobutane	-19.2	-4.9	-5.0	-5.7	-5.2
(3) 2-hydropyridone → 2-hydroxypyridine	-1.0	-0.2	-0.2	-0.4	-0.4
(4) $C_2H_4 + H_2CN_2 \rightarrow$ 1-pyrazoline	-38.1	0.1	-0.2	0.0	0.3
(5) [2,2]paracyclophane + 2 $H_2 \rightarrow$ 2 p-xylene	-58.5	5.7	5.0	4.5	4.0
(6) Octahedrane → cyclopentadienyletropenyle	-19.5	1.3	0.5	-0.1	0.5
(7) C_9O_3 (D_{3h} isomer 1) → C_9O_3 (D_{3h} isomer 2)	-26.9	-6.2	-6.7	-10.7	-10.7
(8) 2,2,3,3-tetramethylbutane → n-octane	1.9	2.6	2.4	3.2	3.0
(9) Propyne → allene	1.6	-0.4	-0.3	0.0	0.1
(10) Propyne → cyclopropene	21.9	1.5	1.5	1.9	1.9
(11) Propene → cyclopropane	7.2	0.7	0.6	0.7	0.7
(12) Buta-1,3-diene → cyclobutene	11.1	1.1	1.0	1.0	1.1
(13) Cyclopentene → vinylcyclopropane	22.9	-0.2	-0.2	0.1	0.0
(14) neo-pentane → n-pentane	3.6	1.2	1.1	1.5	1.4
(15) Toluene → norbornadiene	46.9	-4.1	-4.3	-4.6	-4.5
(16) Styrene → cyclooctatetraene	36.0	-2.5	-2.6	-3.0	-3.0
(17) N-methylenemethanamin → aziridin	10.8	2.3	2.2	2.3	2.4
(18) Acetic acid → methyl formate	18.2	-2.8	-2.8	-2.7	-2.7
(19) Ethanediol → dimethylperoxide	64.2	-2.2	-2.1	-1.4	-1.4
(20) Propan-2-one →> oxetane	31.2	1.1	0.9	1.0	1.0
(21) Dihydrofuran-2(3H)-one → vinyl acetate	14.0	1.0	1.1	1.1	1.0
(22) Tetrahydropyran-2-one → pentan-2,4-dione	7.1	-3.1	-3.0	-3.3	-3.4
(23) Hexanoic acid → methyl pivalate	5.6	0.8	0.9	1.3	1.3
MAD (kcal/mol)		2.0	2.0	2.4	2.3
MD (kcal/mol)		-0.3	-0.5	-0.7	-0.7
MAX (kcal/mol)		6.2	6.7	10.7	10.7

Table 3.18 reports the corresponding analysis of the reaction energies calculated with the relatively small TZVP basis and $T_{CutPNO} = 3.33 \times 10^{-7}$. Both, canonical and semi-canonical CCSD(T), show a MAD of 2.0 kcal/mol and a maximum absolute error of 6.2 kcal/mol and 6.7 kcal/mol for reaction (7) respectively. This clearly indicates that the TZVP basis set is not sufficiently large enough for accurate computational thermochemistry. Nonetheless, it is still instructive to compare the error with respect to experimental values at the CCSD(T)/TZVP level since the basis set convergence for CCSD(T) and LPNO-CCSD(T) should be very similar. The MAD for LPNO-CCSD(T) with the preliminary threshold values for the truncation thresholds amounts to 2.3 kcal/mol which is in good agreement with the MAD observed for CCSD(T). Again, setting the TNO truncation threshold to zero does not lead to more accurate results. However, the maximum of 10.7 kcal/mol for reaction (5) is almost twice as large as for CCSD(T). It is obvious that large errors observed for the individual triples contributions of a molecule (as *e.g.* for heptahexaene) also show up in the corresponding reaction energies. The LPNO error of the triples contribution is less systematic and in some cases the individual error in absolute energies is even enhanced in the calculation of relative energies.

In order to evaluate whether it is possible to reach chemical accuracy with the present LPNO methods, the same test set was recalculated with the closed-shell LPNO-CEPA/1, LPNO$_1$-CCSD and LPNO-CCSD(T) methods using the large def2-QZVPP basis set and the default values for the thresholds ($T_{CutTNO} = 3.33 \times 10^{-7}$). The results documented in Table 3.19 show that except for reaction (5), the error of the LPNO-CCSD(T) method with respect to the experimental reference values (MAD of 1.7 kcal/mol) is significantly reduced with the more flexible and saturated basis set. This findings might also raise the question on the accuracy of the (back-corrected) experimental value for reaction (5). However, it is more astonishing that the deviation from the experimental reference values (MAD of 1.6 kcal/mol) observed for LPNO$_1$-CCSD are slightly smaller than for LPNO-CCSD(T) itself. The best performance with respect to this test set and the used computational settings is provided by the LPNO-CEPA/1 method which reproduces the experimental reference values to within 1.1 kcal/mol on average and also shows the smallest maximum absolute error (3.4 kcal/mol). Hence, among the LPNO methods tested so far, only LPNO-CEPA/1 in combination with large basis sets can approach real chemical accuracy.

3.3.4. Performance of LPNO-pCCSD methods for relative energies

The results of the previous section demonstrate that the closed-shell LPNO-CEPA/1 method is the most accurate (with respect to experimental reference values) among the present LPNO implementations described in this work. However, due to the missing orbital relaxation, LPNO-CEPA/1 is significantly less robust than the LPNO variants of the CCSD method. The coupled-pair iterations are sometimes prone to convergence problems, especially for electronically more complicated open-shell systems. A promising compromise between the

Table 3.19.: Comparison of the closed-shell LPNO-CEPA/1, $LPNO_1$-CCSD and LPNO-CCSD(T) reaction energies (def2-QZVPP basis set and matching fitting basis set) with back-corrected experimental values for 23 reactions composed from mediums-sized closed-shell molecules. The default values for the LPNO thresholds were applied ($T_{CutTNO} = 3.33 \times 10^{-7}$; MAD:mean absolute deviation; MD:mean deviation; MAX: maximum absolute deviation).

Reaction	E_{reac} (kcal/mol)	LPNO error (kcal/mol)		
(def2-QZVPP basis set)	Exp. reference	$LPNO_1$-CCSD	LPNO-CEPA/1	LPNO-CCSD(T)
(1) Heptahexaene → heptatriyne	-14.3	-4.5	0.4	-4.1
(2) 2 2,3-dimethylbut-2-ene → octamethylcyclobutane	-19.2	2.1	2.9	-0.5
(3) 2-hydropyridone → 2-hydroxypyridine	-1.0	-0.4	0.1	-0.3
(4) C_2H_4 + H_2CN_2 → 1-pyrazoline	-38.1	-1.5	0.1	-0.5
(5) [2,2]paracyclophane + 2 H_2 → 2 p-xylene	-58.5	-4.7	-3.4	-8.4
(6) Octahedrane → cyclopentadienyletropenyle	-19.5	-5.1	-1.3	-3.8
(7) C_9O_3 (D_{3h} isomer 1) → C_9O_3 (D_{3h} isomer 2)	-26.9	-0.4	-2.0	-3.9
(8) 2,2,3,3-tetramethylbutane → n-octane	1.9	-1.7	-1.8	0.5
(9) Propyne → allene	1.6	0.1	-0.8	0.2
(10) Propyne → cyclopropene	21.9	1.8	1.7	1.9
(11) Propene → cyclopropane	7.2	0.1	0.6	0.5
(12) Buta-1,3-diene → cyclobutene	11.1	-0.1	0.7	0.2
(13) Cyclopentene → vinylcyclopropane	22.9	-0.1	-0.2	0.1
(14) neo-pentane → n-pentane	3.6	-0.5	-0.4	0.6
(15) Toluene → norbornadiene	46.9	-1.6	-1.2	-2.7
(16) Styrene → cyclooctatetraene	36.0	-0.1	-0.3	-0.6
(17) N-methylenemethanamin → aziridin	10.8	-0.7	-0.1	-0.4
(18) Acetic acid → methyl formate	18.2	-1.1	-1.4	-1.0
(19) Ethanediol → dimethylperoxide	64.2	3.7	1.6	2.9
(20) Propan-2-one → oxetane	31.2	-0.4	0.1	0.0
(21) Dihydrofuran-2(3H)-one → vinyl acetate	14.0	1.7	1.2	1.4
(22) Tetrahydropyran-2-one → pentan-2,4-dione	7.1	-0.3	-0.8	-0.9
(23) Hexanoic acid → methyl pivalate	5.6	3.9	3.4	3.5
MAD (kcal/mol)		1.6	1.1	1.7
MD (kcal/mol)		-0.4	0.0	-0.7
MAX (kcal/mol)		5.1	3.4	8.4

the stability of CCSD and the higher accuracy of CEPA/1 is given by the recently developed parameterized CCSD (pCCSD) methods.[126,219] Huntington *et al.* have demonstrate via extensive benchmark calculations on small molecules that the canonical pCCSD(-1,1,1) (or pCCSD/1a), pCCSD(-1,1,-1) (or pCCSD/1b), pCCSD(-1.5,1,1) (or pCCSD/2a) and pCCSD(-1.5,1,-1) (or pCCSD/2b) methods are suitable methods for the calculation of reactions energies and barrier heights. Since the LPNO based correlation approach extends the range of applicability of CCSD and CEPA/1 to much larger molecular systems it is interesting to investigate if the LPNO variants of the pCCSD methods are also accurate models for computational thermochemistry and thermochemical kinetics.

At first, a the test set of 17 reactions given in Table 3.20 was considered which includes some larger and partly more electronically complex species. It represents a subset of the larger molecule test extensively used in the previous sections (reaction (1) is taken from the IDISP

test set of the GMTKN24 data base[58] and the remaining 16 reactions come from the ISO34 test set of isomerization reactions of the same data base). As already discussed in Sec. 3.3.2, the reference reaction energies provided therein are obtained from experimental values which have been back-corrected for thermal and zero-point energy contributions. The algorithm '1' of the closed-shell LPNO methods was used for all LPNO based CCSD and pCCSD calculations. One observes that LPNO-CEPA/1 with a MAD of 1.2 kcal/mol is only slightly more accurate (on average) than $LPNO_1$-CCSD with a MAD of 1.3 kcal/mol, but that the former method is more systematic (in terms of the standard deviation about the mean deviation) and has the smallest value of the maximum absolute deviation (3.4 kcal/mol) of all the methods considered. The LPNO-pCCSD/2a and LPNO-pCCSD/2b approaches are the most accurate methods of those considered, both yielding a MAD of 0.9 kcal/mol. The LPNO-pCCSD/1a and LPNO-pCCSD/1b methods have only slightly larger values of the statistical measures and each of these statistics are identical for both of these methods. The only disconcerting case is reaction (17), for which the deviation from the (back-corrected) experimental reference value is 3.7 kcal/mol for both of these methods (and for LPNO-pCCSD/2a as well) while LPNO-pCCSD/2b yields an error of 3.6 kcal/mol. Even so, the results of Table 3.20 clearly demonstrate that the LPNO-pCCSD/1a, LPNO-pCCSD/1b, LPNO-pCCSD/2a and LPNO-pCCSD/2b (as well as LPNO-CEPA/1) methods are sufficiently accurate computational models for large-scale applications in reaction thermochemistry.

The performance of the LPNO-pCCSD methods for the calculation of barrier heights for thermochemical kinetics, a considerably more difficult task than the calculation of reaction energies, was also evaluated. To this end, nine of the eleven pericyclic reactions previously investigated by Guner *et al.*[239] were considered, for which accurate experimental activation energies are available and the reactions of diazomethane with 1-phenylbutadiene and norbornene, since accurate experimental activation energies are also available for these reactions.[240] The molecular geometries and the thermal and zero-point vibrational energy (ZPVE) contributions were obtained at the B3LYP/cc-pVTZ level of theory and the reference values in Table 3.21 are the back-corrected (for thermal and ZPVE contributions) experimental activation energies. It is obvious from the data collected in Table 3.21, that LPNO-pCCSD/2a is the most accurate method and provides a significant improvement over LPNO-pCCSD/1a, LPNO-pCCSD/1b, LPNO-CEPA/1 and $LPNO_1$-CCSD for the calculation of the eleven barrier heights contained in this test set. The 'a' variants of the LPNO-pCCSD methods are slightly more accurate than the corresponding 'b' variants. The largest deviation for the LPNO-pCCSD methods occurs for the barrier of the sigmatropic shift of cyclopentadiene (reaction (5)), where a deviation larger than 3 kcal/mol was observed. The LPNO-pCCSD/1a results are actually comparable (on average) to (and even slightly better than) the CBS-QB3 results previously reported by Guner[239] and Ess,[240] while the LPNO-pCCSD/2a and LPNO-pCCSD/2b results are superior which indicates the potential of the LPNO-pCCSD methods as a suitable quantum chemical model for large scale applications in thermochemistry and thermochemical kinetics.

Table 3.20.: Comparison of the B3LYP, LPNO$_1$-CCSD, LPNO-pCCSD/1a, LPNO-pCCSD/1b, LPNO-pCCSD/2a, LPNO-pCCSD/2b and LPNO-CEPA/1 methods (in a def2-QZVPP basis and matching fitting basis set) with back-corrected experimental values for 17 reactions composed from mediums-sized closed-shell molecules. The default values for the LPNO thresholds were used (MAD: mean absolute deviation; SD: standard deviation; RMSD: root mean squared deviation; MAX: maximum absolute deviation).

	E_{reac} (kcal/mol)	Error (kcal/mol)						
Reaction	Reference	B3LYP	LPNO-CCSD	LPNO-pCCSD/1a	LPNO-pCCSD/1b	LPNO-pCCSD/2a	LPNO-pCCSD/2b	LPNO-CEPA/1
(1) 2 p-xylene → [2,2]paracyclophane + 2 H_2	58.5	18.2	4.7	2.0	2.0	1.0	0.9	3.4
(2) 2,2,3,3-tetramethylbutane → n-octane	1.9	-10.4	-1.7	-1.0	-1.0	-0.6	-0.6	-1.8
(3) Propyne → allene	1.6	-3.5	0.1	-0.3	-0.3	-0.4	-0.4	-0.8
(4) Propyne → cyclopropene	21.9	2.0	1.8	1.6	1.6	1.6	1.6	1.7
(5) Propene → cyclopropane	7.2	1.9	0.1	0.6	0.6	0.8	0.8	0.6
(6) Buta-1,3-diene → cyclobutene	11.1	4.4	-0.1	0.5	0.5	0.9	0.9	0.7
(7) Cyclopentene → vinylcyclopropane	22.9	-3.2	-0.1	-0.2	-0.1	-0.2	-0.2	-0.2
(8) neo-pentane → n-pentane	3.6	-2.9	-0.5	-0.1	-0.1	0.0	0.0	-0.4
(9) Toluene → norbornadiene	46.9	10.3	-1.6	-1.6	-1.7	-1.3	-1.4	-1.2
(10) Styrene → cyclooctatetraene	36.0	3.0	-0.1	0.1	0.0	0.3	0.3	-0.3
(11) N-methylenemethanamin → aziridin	10.8	1.6	-0.7	-0.3	-0.3	-0.1	-0.1	-0.1
(12) Acetic acid → methyl formate	18.2	-2.3	-1.1	-1.1	-1.1	-1.1	-1.2	-1.4
(13) Ethanediol → dimethylperoxide	64.2	-3.2	3.7	2.1	1.9	1.6	1.4	1.6
(14) Propan-2-one → oxetane	31.2	2.4	-0.4	-0.3	-0.2	-0.2	-0.2	0.1
(15) Dihydrofuran-2(3H)-one → vinyl acetate	14.0	-3.2	1.7	1.2	1.2	0.9	1.0	1.2
(16) Tetrahydropyran-2-one → pentan-2,4-dione	7.1	-4.0	-0.3	-1.0	-0.9	-1.3	-1.2	-0.8
(17) Hexanoic acid → methyl pivalate	5.6	4.7	3.9	3.7	3.7	3.7	3.6	3.4
MAD (kcal/mol)		4.8	1.3	1.0	1.0	0.9	0.9	1.2
SD (kcal/mol)		6.5	1.9	1.4	1.4	1.3	1.3	1.5
RMSD (kcal/mol)		6.3	2.0	1.4	1.4	1.3	1.2	1.5
MAX (kcal/mol)		18.2	4.7	3.7	3.7	3.7	3.6	3.4

Table 3.21.: Comparison of barrier heights computed with LPNO$_1$-CCSD, LPNO-pCCSD/1a, LPNO-pCCSD/1b, LPNO-pCCSD/2a, LPNO-pCCSD/2b, and LPNO-CEPA/1 with the back-corrected experimental barrier heights for various pericyclic reactions. The thermal and zero-point vibrational energy contributions of each molecule are calculated from unscaled B3LYP/cc-pVTZ harmonic frequencies at the optimized B3LYP/cc-pVTZ geometry. The default values for the LPNO thresholds were used (MAD: mean absolute deviation; SD: standard deviation; RMSD: root mean squared deviation; MAX: maximum absolute deviation)

.

	$E_{barrier}$ (kcal/mol)	Error (kcal/mol)						
Reaction	Reference	B3LYP	LPNO-CCSD	LPNO-pCCSD/1a	LPNO-pCCSD/1b	LPNO-pCCSD/2a	LPNO-pCCSD/2b	LPNO-CEPA/1
(1) Cyclobutene → 1,3-butadiene	33.6	-0.5	4.6	1.4	1.4	0.1	0.1	3.0
(2) 1,3,5-hexatriene → 1,3-cyclohexadiene	30.9	0.4	3.6	0.7	0.7	-0.6	-0.6	2.6
(3) ortho-xylylene → benzocylobutene	29.9	-1.5	1.8	-1.1	-1.3	-2.4	-2.6	0.9
(4) 1,3-pentadiene → 1,3-pentadiene	38.9	0.0	5.0	2.2	2.1	1.2	1.1	3.7
(5) Cyclopentadiene → cyclopentadiene	25.9	1.3	4.3	3.5	3.5	3.3	3.3	4.3
(6) 1,5-hexadiene → 1,5-hexadiene	35.2	0.6	6.7	2.4	2.4	0.7	0.7	4.8
(7) 1,3-butadiene + ethylene → cyclohexene	22.6	4.0	5.4	1.4	1.4	-0.2	-0.3	3.8
(8) Cyclopentadiene + ethylene → norbornene	21.4	3.2	1.9	-1.6	-1.6	-3.0	-3.0	0.8
(9) 2 cyclopentadiene → dicyclopentadiene	14.1	10.0	7.1	2.6	2.6	0.5	0.4	5.0
(10) 1-phenylbutadiene + diazomethane → TS	13.5	5.9	5.9	2.6	3.4	1.3	2.2	4.2
(11) Norbornene + diazomethane → TS	12.4	7.1	4.8	1.5	2.2	0.3	1.1	3.3
MAD (kcal/mol)		3.1	4.6	1.9	2.1	1.2	1.4	3.3
SD (kcal/mol)		3.6	1.7	1.6	1.7	1.7	1.9	1.4
RMSD (kcal/mol)		4.4	4.9	2.1	2.2	1.6	1.8	3.6
MAX (kcal/mol)		10.0	7.1	3.5	3.5	3.3	3.3	5.0

However, it should be noted that 'b' variants are less robust and convergence problems for the calculation of transition metal carbonyl complexes and some open-shell species used to evaluate the canonical pCCSD methods have occurred.[219] This issue will be further addressed in the Sec. 4.1.

3.3.5. Errors in hyperfine couplings

In order to investigate whether the LPNO methods may also represent an attractive route towards accurate and efficient molecular property calculations, the unrelaxed LPNO-VCEPA/1 density was used to calculate 42 hyperfine couplings of 15 small molecules out of a larger test set employed in a previous study.[241] The corresponding VCEPA/1 results serve as reference values. Table 3.22 shows that the mean absolute errors for diagonal elements of the total hyperfine coupling tensor (superscript (A); mean absolute values: 46 MHz, 74 MHz, 133 MHz) as well as the isotropic Fermi contact contribution (superscript $(A;c)$; mean absolute value: 69 MHz) and the anisotropic spin dipolar contributions (superscript $(A;d)$: mean absolute values: 55 MHz, 33 MHz, 64 MHz) are very small and the maximum absolute error is only 12 MHz (about 2 % relative error) for $A_{33}^{(A)}$of the ^{13}C hyperfine coupling constant of the HCO radical. The complete error analysis and the VCEPA/1 reference values can be found in Appendix C. The absolute values are not of great concern in the context of this work, but the excellent performance of LPNO-VCEPA/1 relative to the parent VCEPA/1 method for this test set indicates the LPNO approach might be successfully applied to molecular property calculations as well. The extension of the LPNO-CCSD method to the calculation of molecular properties is currently under development in our research group.

Table 3.22.: Error statistic for hyperfine coupling constants calculated with the (open-shell) LPNO-VCEPA/1 method using the default values for the thresholds and the special basis sets documented at the beginning of this chapter. The corresponding VCEPA/1 values serve as reference. All values are given in MHz (MAD: mean absolute deviation; MD: mean deviation; MAX: maximum absolute deviation).

(MHz)	MD	MAD	MAX
$A_{11}^{(A)}$	1	2	7
$A_{22}^{(A)}$	0	2	7
$A_{33}^{(A)}$	0	3	12
$A^{(A;c)}$	0	2	8
$A_{11}^{(A;d)}$	0	1	3
$A_{22}^{(A;d)}$	0	0	3
$A_{33}^{(A;d)}$	0	1	6

3.3.6. Errors in potential energy surfaces

The calculation of potential energy surfaces (PESs) is critical test for local correlation methods since the local approximations, especially cut-offs applied in real space, can introduce artificial jumps into the PESs. The C-C bond dissociation of ketene was suggested by Russ and Crawford[178] as a critical test for local correlation methods in this respect. The test calculations were carried out with the default values for the cut-offs and the SVP basis set. A rigid scan was performed along the C-C distance coordinate using the CCSD(T), CEPA/1 and closed-shell LPNO-CEPA/1 methods. The results shown in Fig. 3.19 demonstrate that: a) there are no recognizable discontinuities in the potential energy surface, b) CEPA/1 and LPNO-CEPA/1 are virtually indistinguishable and c) both CEPA variants trace the CCSD(T) reference curve extremely well and only differ by ~1 kcal/mol in the asymptote from it.

Furthermore, we conjectured that problems with the local approximation may arise if a system changes from a delocalized to a less delocalized electronic structure. To this end, the torsion coordinate of biphenyl was investigated with a variety of methods and the SV(P) basis set. In this system the coplanar configuration is fully conjugated while the tilted geometries are not. The results in Fig. 3.20 show that CEPA/1 is in excellent agreement with the CCSD(T) reference curve, even better than the CCSD curve. Furthermore, LPNO-CEPA/1 slightly underestimates the barrier by about 0.1-0.2 kcal/mol while MP2 slightly overestimates the barrier. In contrast, B3LYP shows large deviations from the CCSD(T) reference and also predicts the position of the minima shifted by almost 10 degrees.

As a second and slightly more challenging test, the torsion coordinate of ethane-1,2-diphenyl was studied, again using the SV(P) basis set. In this system the co-planar arrangement shows a significant ring-ring stacking interaction. The results in Fig. 3.21 demonstrate that CEPA/1 and LPNO-CEPA/1 both reproduce the CCSD(T) reference curve extremely well (deviations do not exceed 0.1 – 0.2 kcal/mol) while all other tested methods show significant problems. MP2 significantly overshoots the barrier between the minima at ~55 and ~180 degrees, while RHF and B3LYP both predict the wrong ordering of the minima, probably because neither of them takes the van der Waals interaction into account.

From these test calculations it is inferred that the potential energy surfaces calculated with closed-shell LPNO-CEPA/1 do not show any discernible discontinuities or artifacts. The agreement with the parent untruncated CEPA/1 method is excellent, and both methods are in very good agreement with the CCSD(T) reference values for all investigated cases.

In order to test the smoothness of potential energy curves calculated with the closed-shell $LPNO_{1/2}$-QCISD and $LPNO_{1/2}$-CCSD methods, the biphenyl and ethane-1,2-biphenyl systems were reinvestigated. The differences between the $LPNO_1$ and $LPNO_2$ variants as well as the differences of canonical QCISD and CCSD itself are extremely small for these molecules. Therefore, only the $LPNO_2$ results are compared to the curve calculated with canonical CCSD. As evident from Fig. 3.22, there is almost no discernible deviation between the curves calculated with the LPNO methods and their canonical counterparts respectively.

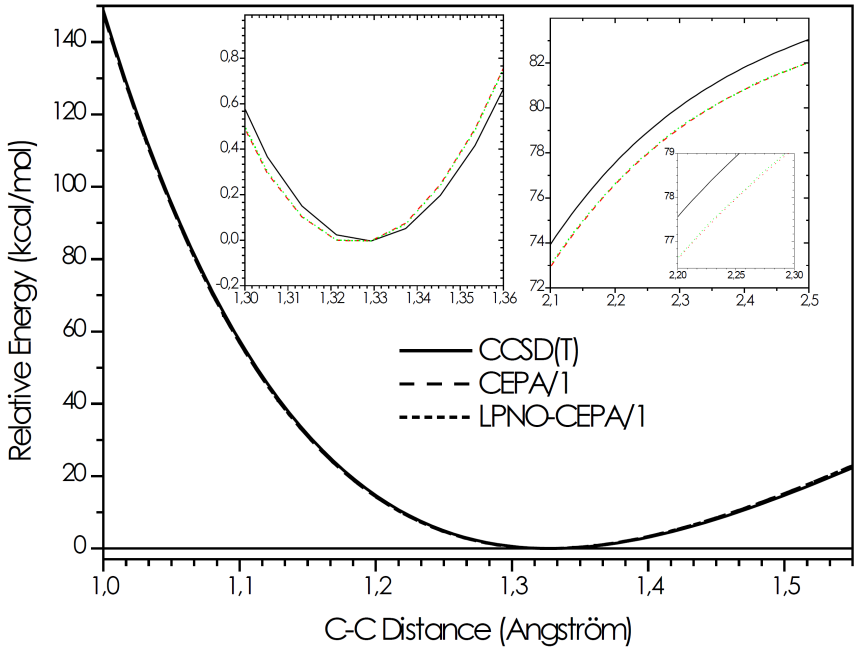

Figure 3.19.: Rigidly scanned PES for the dissociation of CO from ketene. All calculations were done with the SVP basis set (SV/C fitting basis) and the default values for the thresholds (solid line: CCSD(T); dashed line: CEPA/1; short dashed line: closed-shell LPNO-CEPA/1). The inset shows magnifications of the calculated curves. At the level of plotted resolution no difference is visible between CEPA/1 and LPNO-CEPA/1 (Fig. reproduced and modified from Ref. (196)).

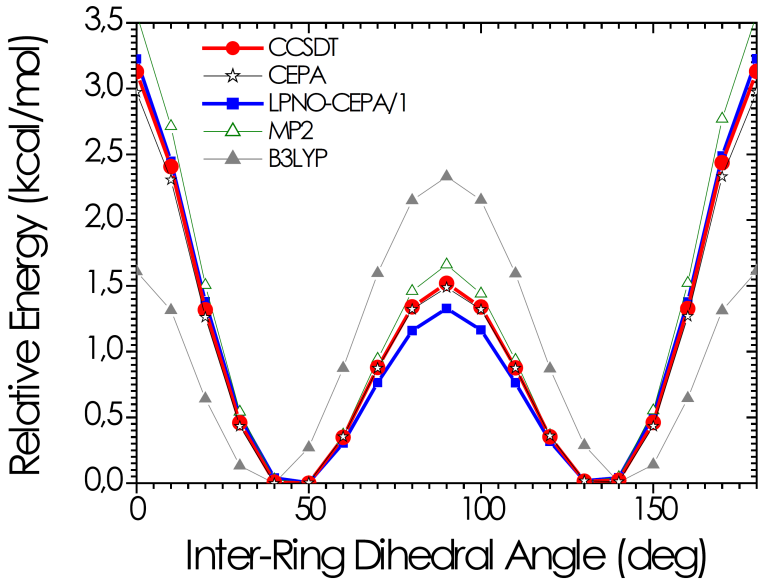

Figure 3.20.: Rotational barrier of biphenyl calculated with various methods (circles: CCSD(T); asterisks: CEPA/1; squares: closed-shell LPNO-CEPA/1; open triangles: MP2; filled triangles: B3LYP). The structures were obtained from a relaxed surface scan with the PBE functional using the TZVP basis set and van der Waals corrections. All calculations were done with the SV(P) basis set (SV/C fitting basis) and slightly less tight LPNO thresholds ($T_{CutPNO} = 10^{-6}$; $T_{CutPairs} = 10^{-4}$ E_h; $T_{CutMKN} = 10^{-2}$; Fig. reproduced and modified from Ref. (196)).

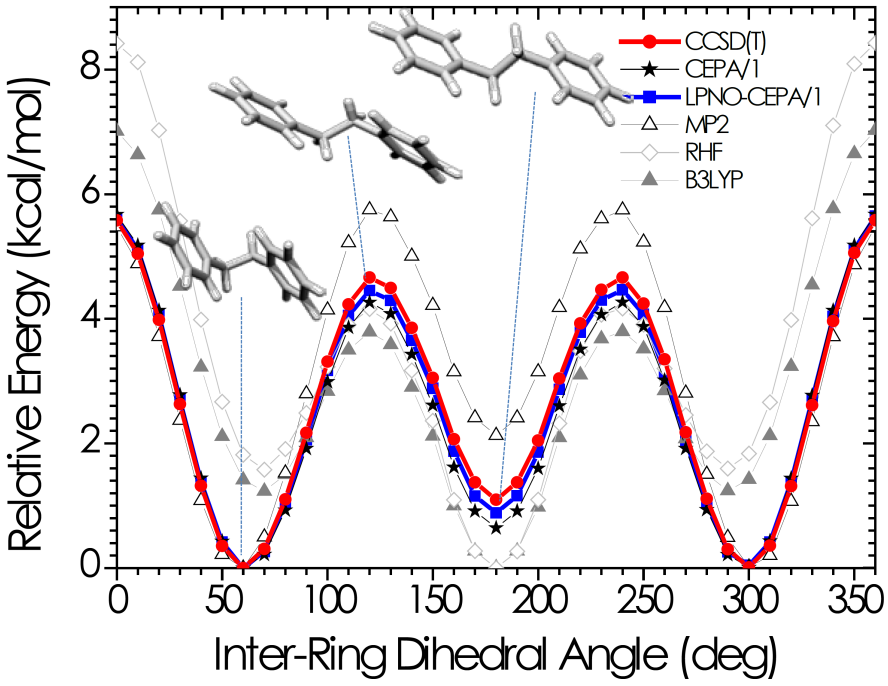

Figure 3.21.: Rotational barrier of ethane-1,2-biphenyl calculated with various methods (circles: CCSD(T); asterisks: CEPA/1; squares: closed-shell LPNO-CEPA/1; open triangles: MP2; filled triangles: B3LYP; open circles: RHF). The structures were obtained from a relaxed surface scan with the PBE functional using the TZVP basis set and Van der Waals corrections. All calculations were done with the SV(P) basis set (SV/C fitting basis) and slightly less tight LPNO thresholds ($T_{CutPNO} = 10^{-6}$; $T_{CutPairs} = 10^{-4}$ E_h; $T_{CutMKN} = 10^{-2}$; Fig. reproduced and modified from Ref. (196)).

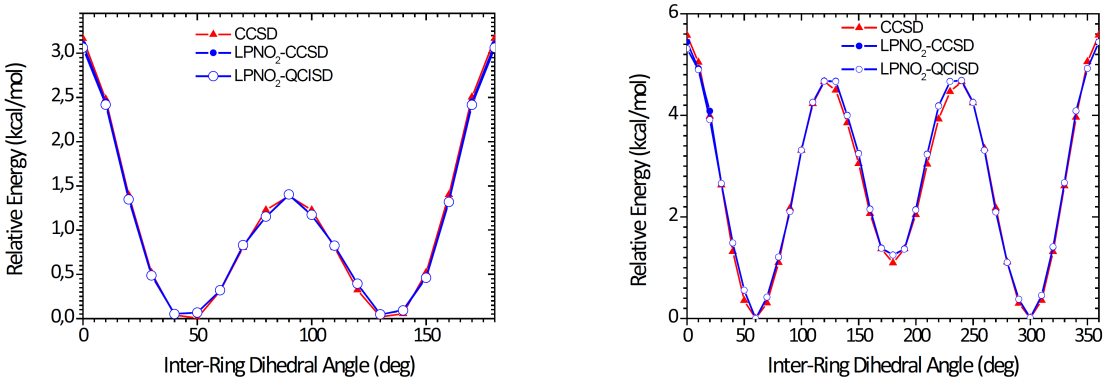

Figure 3.22.: Comparison of canonical CCSD (triangles) with closed-shell $LPNO_2$-CCSD (filled circles) and $LPNO_2$-QCISD (open circles) rotational barriers for biphenyl (left) and ethane-1,2-diphenyl (right) calculated with the SV(P) basis set and the matching fitting basis set. The default values for the LPNO thresholds were applied. The structures were obtained from relaxed surface scans using the PBE functional and the TZVP basis set (Fig. reproduced and modified from Ref. (197)).

The results are consistent with the observations made for LPNO-CEPA and clearly demonstrate that the closed-shell LPNO methods yield essentially smooth potential energy curves

which reproduce the PESs calculated with their canonical counterparts to within about 0.1 kcal/mol.

In order to investigate the performance of the open-shell LPNO methods for the calculation of potential energy surfaces, the O–O bond dissociation of hydrogen peroxide was chosen as test example since it can be regarded as minimal model for O-O bond breaking steps in reaction mechanisms of biologically important processes.[242] Fig. 3.23 shows a rigid scan along the O–O distance coordinate calculated with the open-shell LPNO-CCSD and CCSD methods using QROs and the SVP basis set.

The LPNO-CCSD curve is smooth and only slightly deviates in the asymptote from the spin-unrestricted CCSD reference curve. This may be traced back to the further approximations made to the dressed quantities including non-linear singles terms which increase significantly for larger O–O distances. However, the accurate description of this part of the PES is not in the usual scope of single reference methods. Around the equilibrium distance, the LPNO-CCSD curve is in excellent agreement with the canonical CCSD curve with a deviation smaller than 1 kcal/mol (Fig. 3.24).

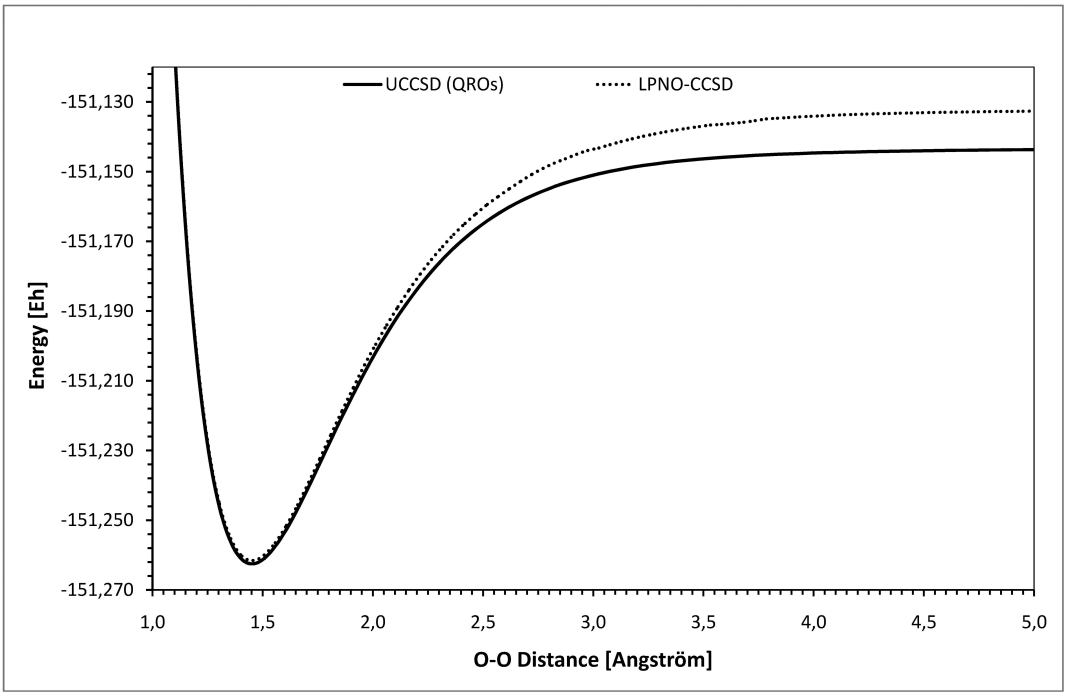

Figure 3.23.: Rigidly scanned potential energy surface of the O–O bond cleavage of hydrogen peroxide. The SVP basis set (SV/C fitting basis set) was employed. QROs and the default values for the LPNO thresholds were used (solid line: spin-unrestricted CCSD using QROs; dashed line: open-shell LPNO-CCSD; Fig. reproduced and modified from Ref. (198)).

Furthermore, the minimum (1.4504 Å and 1.4507 Å for LPNO-CCSD and CCSD respectively) is not shifted and up to about 2.0 Å, the curvature closely resembles that of the reference curve, which is important for biochemical applications.[242] The LPNO-QCISD curve mainly lies on top of the LPNO-CCSD curve, except for large O-O distances where the

error (compared to spin-unrestricted QCISD with QROs) for is significantly smaller compared to LPNO-CCSD. In contrast, the open-shell LPNO-CEPA/1 curve shows artificial kinks and jumps. However, this is not surprising since the spin-unrestricted CEPA/1 curve is also rough. This again indicates that the CEPA methods are less robust than QCISD and CCSD once the wavefunction possesses a slight multireference character. The potential energy surfaces calculated with open-shell LPNO-QCISD and LPNO-CEPA/1 can be found in Appendix C.

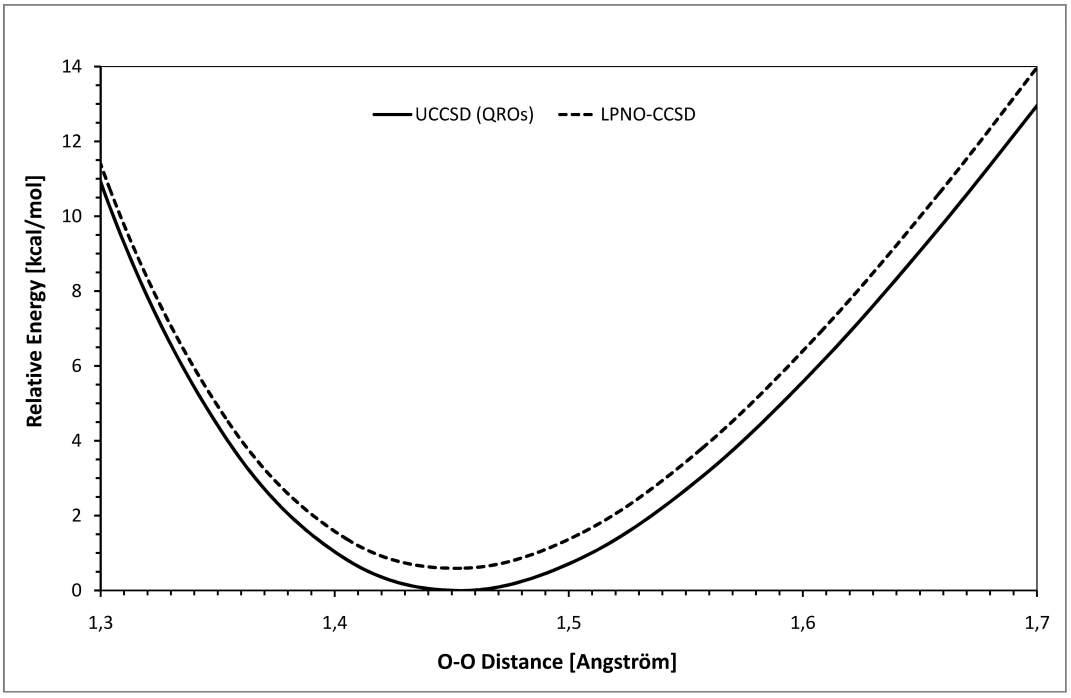

Figure 3.24.: Zoom into the minimum region of the PES shown in Fig 3.23. The energy difference relative to the spin-unrestricted CCSD (UCCSD) minimum is plotted (Fig. reproduced and modified from Ref. (198)).

3.4. Efficiency of the LPNO methods

The results of the comprehensive numerical tests presented in the previous Sections consistently show that the LPNO approach represents indeed an accurate approximation to single reference correlation methods. However, in order to really benefit from this finding, it is crucial that the LPNO methods also be efficient. This subject will be addressed in the present Section.

3.4.1. Effective scaling behavior

First, the effective scaling behavior with respect to the system size N was investigated. The measured scaling behavior of the closed-shell LPNO-CEPA/1 method in comparison to CEPA/1, CCSD and CCSD(T) calculations is shown in Fig. 3.25 for the simple case of linear

hydrocarbon chains.

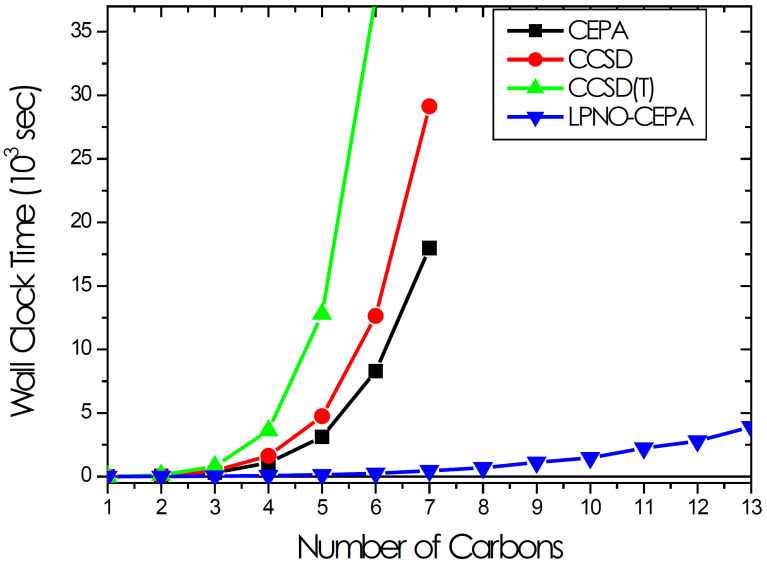

Figure 3.25.: Measured scaling behavior of the closed-shell CCSD(T), CCSD, CEPA/1 and LPNO-CEPA/1 methods. The calculations were carried out on linear hydrocarbon chains in standardized geometries ($H_3C–(CH_2)_{n-2}–CH_3$; all angles 109.4712°; R_{CH} = 109 pm and R_{CC} = 155 pm). The following values for the LPNO thresholds were applied: $T_{\mathrm{CutPNO}} = 10^{-6}$; $T_{\mathrm{CutPairs}} = 10^{-4}$ E_h; $T_{\mathrm{CutMKN}} = 10^{-2}$ (Fig. reproduced and modified from Ref. (196)).

The CCSD(T) method shows a measured scaling of $\mathcal{O}(N^{6.5})$ which is close to the expected $\mathcal{O}(N^7)$ scaling and very quickly becomes unfeasible. CCSD and CEPA/1 both behave similarly and come close to the expected $\mathcal{O}(N^6)$ scaling (measured scaling of $\mathcal{O}(N^{5.7})$ and $\mathcal{O}(N^{5.4})$ respectively). The LPNO-CEPA/1 method is obviously much cheaper than the untruncated methods. However, its measured scaling of $\mathcal{O}(N^{3.5})$ is still far from linearity (even if it looks close to linear in Fig. 3.25). Even this scaling is too optimistic since already the initial integral transformation that produces the MO basis $\mathbf{J}^{ij}$ and $\mathbf{K}^{ij}$ integrals scales as $\mathcal{O}(N^5)$. The AO to PNO integral transformation has a formal scaling of only $\mathcal{O}(N^3)$ but with a large prefactor, while the PNO construction itself scales as $\mathcal{O}(N^4)$. In the calculation of the residual vector the four-internal contribution presently scales as $\mathcal{O}(N^4)$, while the doubles contribution to the singles residual involving one-external integrals has an even worse scaling of $\mathcal{O}(N^5)$ but a rather small prefactor. As it will be discussed in the next Section, these are all of the computationally significant steps, whereas all other contributions add negligible parts to the overall computation time of the closed-shell LPNO-CEPA/1 method. It would be desirable to arrive at a scheme with a somewhat lower formal scaling. Presently, the LPNO-CEPA/1 method, likewise to RI-MP2, obviously benefits from its small prefactor. Analogously to closed-shell LPNO-CEPA/1, the formal scaling of the closed-shell LPNO variants of QCISD and CCSD is still $\mathcal{O}(N^5)$. However, due to the various nonlinear terms that enter the formalism, the calculation of the residual is more involved for the latter and it is of interest to investigate whether the effective scaling behavior is still comparable to that

of LPNO-CEPA/1. To this end, the test calculations on the linear hydrocarbon chains were repeated with the closed-shell LPNO$_{1/2}$-QCISD and LPNO$_{1/2}$-CCSD methods. Obviously, these linear molecules represent the best case scenario for local correlation approaches. Quite surprisingly, an effective scaling around cubic is observed (Fig. 3.26) which is even smaller compared to the measure scaling for LPNO-CEPA/1. This can be reduced to the point that slightly different algorithms (Algorithm '1' and '2' respectively) which treat the four-internal contribution more efficiently are used for the LPNO variants of QCISD and CCSD, while the Algorithm '0' was employed for closed-shell LPNO-CEPA/1 (see Sec. 2.3.2). The measured scaling is still far from linearity, but the savings relative to the canonical QCISD and CCSD methods are dramatic.

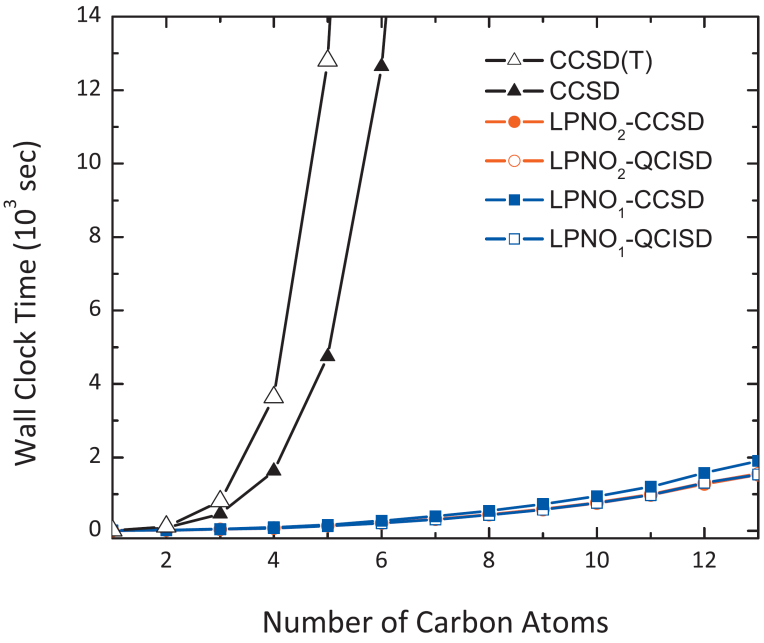

Figure 3.26.: Measured scaling of the LPNO methods relative to their canonical counterparts. The calculations were carried out on linear hydrocarbon chains $H_3C–(CH_2)_{n-2}–CH_3$ in standardized geometries (see caption of Fig. 3.25) using the default values for the LPNO thresholds (Fig. reproduced and modified from Ref. (197)).

The effective scaling behavior with respect to the system size N was also reinvestigated for the open-shell variants. Although the present open-shell LPNO-CCSD implementation contains additional contributions with an asymptotic $\mathcal{O}(N^5)$ scaling, the prefactor of these fifth order steps are relatively small. However, the measured effective scaling is expected to be slightly steeper compared to the closed-shell implementations. In order to the make a similar analysis for the open-shell LPNO-CCSD variant, a series of linear alkyl radicals with increasing number of carbon atoms was calculated with the open-shell LPNO-CCSD method using the SVP (SV/C) basis set. The effective scaling of the open-shell LPNO-CEPA/1 method using the '$PNOSigmaOpt$ 2' algorithm (see Sec. 2.3.4) and open-shell LPNO-QCISD (data not shown) is very similar to that of open-shell LPNO-CCSD, although no

additional contributions with fifth order scaling enter the procedures. Applying a nonlinear regression analysis to the curve given in Fig. 3.27, again an effective scaling proportional to the third power of the system size is found. At first, this might be surprising since the additional overhead due to the separate spin-cases increases the prefactor of various contributions. However, using the same default values for the truncation threshold as in the closed-shell case, the average number of PNOs per electron pair is smaller for the open-shell variants, such that the additional overhead is compensated to some extent.

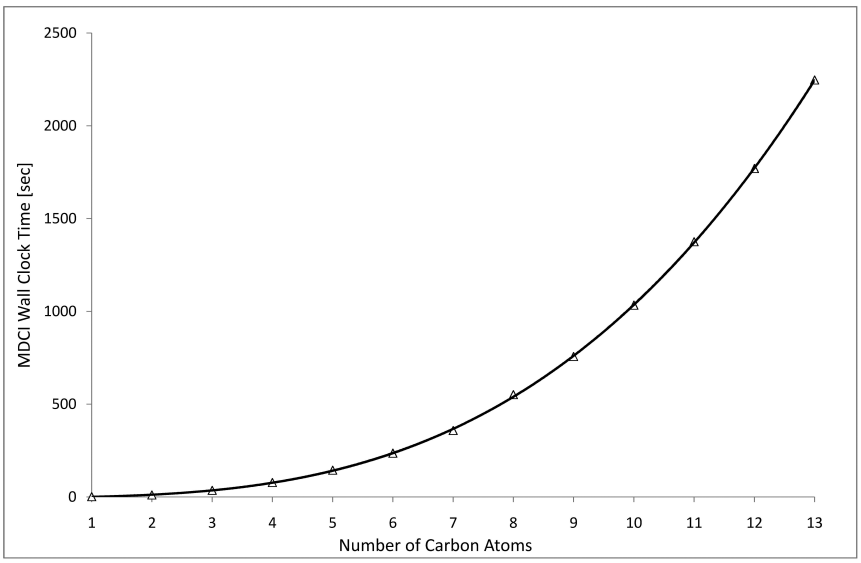

Figure 3.27.: Measured scaling of the open-shell LPNO-CCSD method (default values for the LPNO thresholds, SVP basis set and matching fitting basis set) for linear $H_3C–(CH_2)_{n-2}–CH_2$ radical chains (optimized BP86/SVP geometries; Fig. reproduced and modified from Ref. (198).

3.4.2. Detailed timing analysis

At fist, the closed-shell LPNO-CEPA/1 method was investigated in terms of the dependence of the timings on the three thresholds. To this end, we have carried out additional calculations on the $(Gly)_3$ system using the TZV(2d,p) basis set. It is evident from Table 3.23 that the threshold T_{CutPairs} leads to a speed-up of almost a factor of two while introducing and error of only ~0.1 mE_h. The difference between the calculations with $T_{\mathrm{CutMKN}} = 10^{-2}$ and $T_{\mathrm{CutMKN}} = 10^{-3}$ of 27 μE_h is even smaller, while the total gain in the computation time is ~15 % (the speed-up in the PNO integral transformation is roughly a factor of two). However, the calculation with $T_{\mathrm{CutMKN}} = 0$ is about 60 % more expensive than the one with $T_{\mathrm{CutMKN}} = 10^{-2}$. Thus, the introduction of this additional threshold appears to be well justified and has negligible impacts on the accuracy. Compared to the chosen default values ($T_{\mathrm{CutPNO}} = 3.33 \times 10^{-7}$, $T_{\mathrm{CutPairs}} = 10^{-4}$ E_h, $T_{\mathrm{CutMKN}} = 10^{-3}$) almost 70 % of the computation time could be saved by going to more aggressive threshold values ($T_{\mathrm{CutPNO}} = 10^{-6}$, $T_{\mathrm{CutPairs}} = 10^{-4}$ E_h, $T_{\mathrm{CutMKN}} = 10^{-2}$). While this might be appropriate

for some applications, the error introduced by the less tight T_{CutPNO} value (~0.2 mE_h for this example) is not entirely negligible.

Table 3.23.: Analysis of timings for closed-shell LPNO-CEPA/1 calculations of the $(Gly)_3$ molecule as a function of the LPNO truncation thresholds using the TZV(2d,p) basis set (TZV/C fitting basis set). All timings are given in seconds and have been obtained with a 2.4 GHz Intel® Core 2 Duo® CPU allowing for 4 GB main memory.

T_{CutPNO}	3.33×10^{-7}	3.33×10^{-7}	3.33×10^{-7}	3.33×10^{-7}	10^{-6}	10^{-6}
T_{CutPairs} (E_h)	0	10^{-4}	10^{-4}	10^{-4}	10^{-4}	10^{-4}
T_{CutMKN}	10^{-3}	10^{-2}	10^{-3}	0	10^{-3}	10^{-2}
F, J^{ij}, K^{ij}	582	582	582	582	582	582
PNO generation	223	110	123	109	111	108
PNO transformation	1121	438	788	1664	619	362
(3 + 4 ext. PNO integrals)	595	116	355	1151	180	47
Pair-pair setup	462	153	155	155	131	127
Residual (15 iterations):						
4-external	140	166	163	133	49	46
3-external	12	24	26	6	5	6
2-external	692	339	346	338	201	202
1-external	380	219	213	194	174	175
0-external	1819	1037	1040	1040	585	585
Singles-singles	61	61	60	62	58	57
Wall-clock time	6491	3554	4143	5677	2889	2488
Ecorr (E_h)	-2.383819	-2.383934	-2.383961	-2.383941	-2.382336	-2.382301

As an example for a somewhat larger calculation, the timings for the Diclophenac molecule (30 atoms, see Fig. 3.1 b)) calculated with the closed-shell LPNO-CEPA/1 method using the '$PNOSigmaOpt$ 0' algorithm and the accurate TZVPP basis set (749 basis functions) are documented in Table 3.24. The entire calculation finishes in less than one day using a moderately fast 2.4 GHz Intel® Core 2 Duo® CPU and takes only about 13 h with the less tight thresholds. However, the more aggressive threshold values introduce an error of ~4 mE_h which, depending on the desired application, might be too large. It is observed that the initial integral transformation, the PNO integral transformation, and the coupled-pair type iterations take about the same amount of time. Furthermore, it is evident from Table 3.24 that the computationally most expensive terms involve the two-electron integrals without external labels and with one external label while the computation of the contributions involving three-external and four-external integrals takes negligible time. Especially the latter, which represents the computationally bottleneck for the canonical method, is sped up a lot since it can be calculated entirely in the truncated PNO pair basis.

Recently, Subotnik *et al.* published timings for their latest local correlation methods that were considered to provide a "tremendous increase in speed and accuracy" over previous approaches.[156] This method is based on real-space cut-offs that take the distance and spatial extent of localized internal orbitals into account. Their test cases were the phenalenyl cation

Table 3.24.: Analysis of timings for closed-shell LPNO-CEPA/1 calculations on the Diclophenac molecule (Fig. 3.1 b)) using the TZVPP basis set (TZVPP/C auxiliary basis set) and two different settings for the LPNO thresholds. All timings are given in seconds. The calculations were performed on a 2.4 GHz Intel® Core 2 Duo® CPU allowing for 4 GB main memory.

T_{CutPNO}	3.33×10^{-7}	10^{-6}
T_{CutPairs} (E_h)	10^{-4}	10^{-4}
T_{CutMKN}	10^{-3}	10^{-2}
F, J^{ij}, K^{ij}	18551	18551
PNO generation	3609	3397
PNO transformation	11870	3573
(3 + 4 ext. PNO integrals)	4995	289
Pair-pair setup	2576	2079
Residual (17 iterations):		
4-external	2475	672
3-external	187	63
2-external	3214	1760
1-external	4041	3361
0-external	11227	5812
Singles-singles	7007	6075
Wall-clock time	72719	48458
Ecorr (E_h)	-3.364928	-3.360599

and anion calculated with the the cc-pVDZ basis set (22 atoms, 227 basis functions).[156] The hardware used by Subotnik *et al.* was a 2.2 GHz Apple® XServe® G5 while we used a single core of a QuadCore AMD® Opteron® processor with 2.0 GHz and 16 GB of main memory which is admittedly the faster processor, but the difference in floating point performance should be well below a factor of two. Subotnik *et al.* reported that each canonical CCSD iteration took 10193 s (with the use of D_{3h} symmetry). Surprisingly, we found that our canonical CCSD program, which does not take advantage of molecular symmetry, is a factor of seven faster and only 1457 s per iteration were needed. The fastest calculation reported by Subotnik *et al.* (their version '3b') took 382 s per iteration but led to a deviation of 8.1 kcal/mol from the canonical CCSD result. Their most accurate result (version '6') had a deviation of 1.6 kcal/mol but took 1392 s per iteration. Our canonical CEPA/1 program took 520 s per iteration while the LPNO-CEPA/1 calculation requires just 85 s per iteration and the deviation from the CEPA/1 result is only 1.2 kcal/mol. Furthermore, the energy difference between the cation and anion (159.6 kcal/mol with canonical CCSD(T)) is also reproduced to within 0.6 kcal/mol by CEPA/1 (160.2 kcal/mol) and LPNO-CEPA/1 (159.0 kcal/mol). These results once more demonstrate the high efficiency of the LPNO approach and the accuracy of the CEPA/1 and LPNO-CEPA/1 for typical applications in computational chemistry.

In order to test the performance of the closed-shell LPNO based QCISD and CCSD methods, calculations were carried out on some larger molecules in the range of 42 – 86 atoms. Sys-

tematic studies on the Penicillin molecule (42 atoms, 128 correlated electrons, see Fig. 3.28 a)) with up to 1000 basis functions are collected in Table 3.25 and Table 3.26. The timings documented in these tables sometimes differ by up to ~10% for identical tasks. This is an indication of how the varying system load may affect such timing comparisons also in actual applications on standard PC cluster architectures.

Table 3.25.: Summary of timings for closed-shell $LPNO_{1/2}$-QCISD and $LPNO_{1/2}$-CCSD calculations on the Penicillin molecule with four different basis sets of increasing size. All timings are given in seconds. The SCF times refer to a total of 14 SCF iterations (converged to seven digits in the energy) and the MDCI times refer to an average of 13 iterations to converge the maximum element of the residual to 10^{-5} (convergence in the correlation energy is then ~10^{-6} E_h). All calculations were carried out on a single core of MACPRO® 3.1 (two quad-core Intel® XEON® 3.0 GHz CPUs). N_{BF} denotes the number of basis functions.

		$LPNO_2$-QCISD	$LPNO_1$-QCISD	$LPNO_2$-CCSD	$LPNO_1$-CCSD
SV(P)	t_{SCF}	986	896	985	991
$N_{BF} = 367$	$t_{MDCI-total}$	3660	3671	3827	4632
	$t_{MDCI-iter}$	2353	2173	2552	3047
TZVP	t_{SCF}	4752	4926	4656	4991
$N_{BF} = 567$	$t_{MDCI-total}$	10930	10007	11320	12784
	$t_{MDCI-iter}$	6107	4043	6587	6691
TZV(2d,p)	t_{SCF}	9713	9532	9377	9604
$N_{BF} = 687$	$t_{MDCI-total}$	20909	19097	21757	25128
	$t_{MDCI-iter}$	11991	7714	13120	14069
TZV(2df,2pd)	t_{SCF}	32468	32956	33534	33699
$N_{BF} = 999$	$t_{MDCI-total}$	56734	51494	60260	70180
	$t_{MDCI-iter}$	35814	21601	38896	39260

Inspection of Table 3.25 reveals the striking feature that the wall-clock time needed to complete the entire LPNO based calculation is only 2 – 4 times larger than the time required to converge the RHF calculations. The ratio even drops for larger basis sets. For significantly larger molecules the scaling of the LPNO methods is worse than that of the RHF iterations and therefore the ratio will become more unfavorable. However, at least in the range up to 50 atoms and about 1000 basis functions the LPNO calculations are not much more costly than a SCF calculation. Hence, they hold great promise to be highly useful for computational chemistry applications. Closer inspection of Table 3.25 reveals some interesting features: for the QCISD method, the less accurate $LPNO_2$ variant is not much more efficient than the more accurate $LPNO_1$ variant. From the Table 3.26 it is obvious that the extra time required for the initial generation of the Coulomb and Exchange operators is saved in the coupled cluster iterations since the generation of the singles Fock matrix ($\mathbf{G}(\mathbf{t}_1)$, Eq. (A.9)) is avoided. This particularly pays off for large and more accurate basis sets. Hence, avoiding the construction of the singles Fock matrix may lead to significant savings of computation time in local correlation calculations. Similar observations were made by Schütz and Werner

in the context of their PAO based local CCSD method.[167] However, both the PAO and the PNO based methods will profit from efficient approximations made in the algorithm for the singles Fock matrix construction.[214,243] This subject will be discussed in detail in the next Section. Comparison of $LPNO_2$-QCISD and $LPNO_2$-CCSD reveals that the extra terms required for CCSD are computationally insignificant and there is no computational reason to prefer QCISD over CCSD. This is, however, slightly different for the more accurate $LPNO_1$-CCSD variant. Here the generation of $\mathbf{G}(\mathbf{t}_1)$ and the MO basis Coulomb and Exchange operators are both required. Therefore, the $LPNO_1$-CCSD method is slightly more expensive than the other three methods.

Table 3.26.: Detailed analysis of the timings collected in Table 3.25 (closed-shell LPNO based QCISD and CCSD calculations on Penicillin with the TZV(2df,2pd) basis set).

	$LPNO_2$-QCISD	$LPNO_1$-QCISD	$LPNO_2$-CCSD	$LPNO_1$-CCSD
Fock matrix construction	2252	2322	2332	2409
$(ij\|K)$, $(ai\|K)$	444	470	448	559
$(ik\|ja)$, $(ij\|ka)$	946	845	889	873
$(ia\|jb)$	-	1048	-	1016
$(ij\|ab)$	-	4030	-	4145
PNO generation	1807	2006	1713	2147
PNO integral transformation	14813	17939	14826	18398
Residual (13 iterations)	37815	19939	38896	39139
$(ik\|jl)$ term	1774	1658	2133	2226
External Fock term	93	87	93	93
$(ac\|bd)$ term	1325	1470	1627	2026
Doubles $(ia\|jb)$, $(ij\|ab)$	757	1916	777	2041
Singles $(ia\|jb)$, $(ij\|ab)$	7	4947	7	7
Doubles and singles $(ik\|ja)$	7192	6024	6724	6083
Singles $(ib\|ac)$	431	438	320	345
$\mathbf{G}(\mathbf{t}_1)$	22943	-	21787	22021
Fock matrix dressing	994	1149	1357	1076
$(ik\|jl)$ dressing	2117	2057	3346	2555
$(ia\|jb), (ij\|ab)$ dressing	164	176	485	403

A detailed inspection of the timings in Table 3.26 shows that there are three computationally significant steps in closed-shell LPNO based QCISD and CCSD calculations: (a) the initial integral transformation that generates the three-index RI integrals over canonical orbitals and the generation of the two external Coulomb and Exchange operators (if applicable), (b) the integral transformation that generates the necessary two-electron integrals over PNOs and (c) the iterative residual calculation. Within the iterations, the computationally most demanding step is the calculation of the singles Fock matrix followed by various terms in the singles residual that are computed essentially in the untruncated MO basis.

Finally, we also document calculations on two larger 'real-life' chemical systems, namely a model for Vitamine B_{12} poised by CN^- and an iron porphyrin with axially bound imidazole and CO groups (Fig. 3.28 b) and c)). These systems consist of 62 and 86 atoms respectively.

With the SV(P) basis set, 554 and 782 basis enter the calculations. For Vitamin B_{12}-CN^-, the SCF iterations converged after 29 cycles and the LPNO$_1$-QCISD iterations after 16 cycles. They took about 10000 seconds and 21400 seconds respectively. For CO–Heme, the SCF iterations converged after 23 cycles and the LPNO$_1$-QCISD iterations after 18 cycles with total computation times of 16600 and 114500 seconds respectively. The calculated correlation energies of -4.9226 E_h (Vitamin B_{12}-CN^-) and -7.13078 E_h (CO-Heme) are probably not of great interest in this context, but these examples clearly illustrate that larger and more chemically interesting systems can be successfully treated in very reasonable overall turnaround times using the LPNO methodology. The memory and disk space requirements are not overly large. The calculations were allowed to use 6 GB of main memory during the integral transformation, but it would be certainly possible to run the calculations also on machines with only 4 GB of main memory. The temporary data amounted to ~15 GB for Vitamin-B_{12}-CN^- and ~50 GB for CO-Heme. The majority of the used disk space is occupied by the two external integrals in the MO basis and hence, about 5 and 15 GB of disk space respectively would be sufficient for the LPNO$_2$ variants. Both test calculations can be carried out as well with the more realistic TZV(2d,p) basis set that amounts to ~1000 basis functions for Vitamin B_{12}-CN^- and ~1500 basis functions for CO-Heme. The former calculation is completed within ~2 days with roughly equal amounts of computation time spent in the SCF and correlation part. The latter calculation takes about twice as long but detailed timings were not attempted.

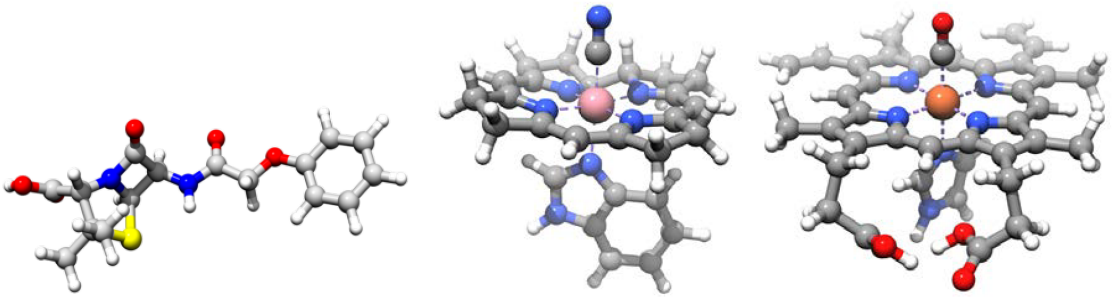

Figure 3.28.: Structures of the test systems used to demonstrate the efficiency of the LPNO based QCISD and CCSD methods (a) Penicillin; b) cyanide complex of Vitamin B_{12}; c) CO bound Heme). The optimized geometries (obtained with the MM3[244] force field) can be found in the supplementary material of Ref. (214) (Fig. reproduced and modified from Ref. (197)).

Finally, it will be demonstrated that the high efficiency of the closed-shell variants also holds for the open-shell variants. The test calculations were carried out on a single core of a 2.4 GHz Intel® Xeon® E5620 CPU allowing for 16 GB of main memory. The first test system is the quinone radical anion weakly bounded to 20 H_2O molecules (Fig. 3.29).

The molecule possesses a doublet ground state and consists of 72 atoms. Using the frozen core approximation, 201 correlated electrons have to be treated which corresponds to 20100

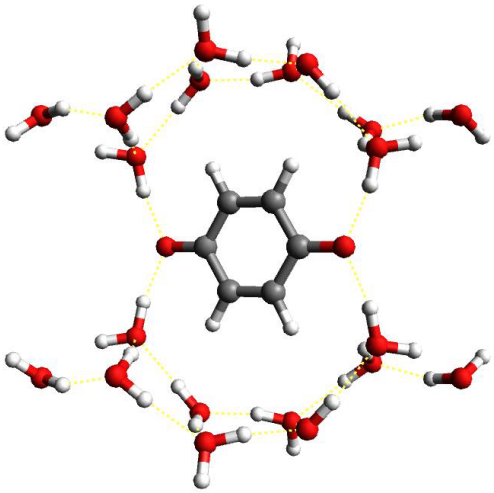

Figure 3.29.: Structure of the benzoquinone radical anion surrounded by 20 H_2O molecules. The optimized geometry was taken from a previous study by Sinneker *et al.*[245] (Fig. reproduced and modified from Ref. (198)).

electron pairs in the spin-unrestricted formalism. Using the TZVP basis set (TZVP/C fitting basis set), 796 basis functions enter the calculation. Table 3.27 shows a detailed analysis of the timings observed for the correlation part of open-shell LPNO-CCSD, LPNO-QCISD and LPNO-CEPA/1 calculations. For the two latter, the preceding steps are more expensive than the entire iterations and the computationally most demanding steps are the initial RI integral transformation and the PNO integral transformation. Due to the extra work needed for the dressings and non-linear two-external terms, the iterations are slightly more expensive for LPNO-QCISD, but an additional iteration was needed for LPNO-CEPA/1 to converge the residuals. The total wall-clock times for the correlation part of LPNO-CEPA/1 and LPNO-QCISD were 8 h 8 min and 8 h 36 min respectively while the LPNO-CCSD calculation took 11 h 19 min. For the latter the iterations are significantly more expensive due to the additional fifth order scaling contribution in the doubles residuals and the singles Fock matrix construction. The timings for identical tasks do not differ much since they were taken subsequently on a separate machine in order to minimize the influence of varying system loads.

Further timings were only taken for open-shell LPNO-CCSD since it is the most advanced method according to the accuracy and efficiency tests performed so far. Now the larger TZVPP basis set (TZVPP/C fitting basis) was employed leading to 1484 basis functions for the benzoquinone complex shown in Fig. 3.29. Furthermore, a multi-threaded version of the BLAS routines was employed and eight threads were used allowing for 32 GB of main memory which leads to significant speed-ups for the integral transformation routines. The entire LPNO-CCSD calculation took 5 d 23 h 38 min. The SCF part (22 iterations) of the calculation amounts to 18.5 % of the total wall clock time while the time needed to finish the correlation part ('MDCI') took only about four times longer. For the latter,

Table 3.27.: Detailed timing analysis for the correlation part of open-shell LPNO calculations using QROs and the TZVP basis set (TZVP/C fitting basis set). The test system is the benzoquinone radical anion surrounded by 20 H_2O molecules shown in Fig. 3.29. All values are given in seconds (unless noted explicitly) and have been rounded to integers. The timings shown in the second half of the table refer to the average time needed per iteration.

	LPNO-CEPA/1	LPNO-QCISD	LPNO-CCSD
Localization of occupied MOs	6	6	6
Fock matrix formation	678	676	678
First half transformation	634	619	625
Second half transformation	6087	6078	6073
PNO integral transformation	8495	8639	8632
Initial guess and PNO construction	1290	1266	1272
PNO recanonicalization	23	23	23
LMO analysis	1	1	1
$\mathbf{K}^{ii}$-PNOs	...	10	11
PNO overlap matrices	186	180	181
Precomputing pair-pair interactions	550	549	548
Recalculate guess amplitudes	0	0	0
Iterations	11346	12922	22667
(number of iterations)	(13)	(12)	(12)
Average time per iteration	873	1077	1889
DIIS solver	18	19	18
State vector update	0	0	0
<D|H|0>	0	0	0
<S|H|0>	0	0	0
<D|H|D> (4-internal + int. Fock term)	37	37	40
<D|H|D> (external Fock term)	9	9	9
<D|H|D> (2-external)	26	103	111
<D|H|D> (4-external)	2	2	2
Additional 2-external contribution	...	...	494
<S|H|S> (2-external)	264	267	0
<D|H|S> (1-external)	6	7	7
<S|H|D> (1-external)	510	513	518
<S|H|D>, <D|H|S> (3-external)	0	0	0
Singles Fock matrix	...	...	550
Fock matrix dressing	...	28	28
$(ik\|jl)$ dressing	...	29	39
$(ij\|ab)$, $(ia\|jb)$ dressing	...	63	72
Pair energies	0	0	0
Shift	0	...	...
Total MDCI time	8h 8min	8h 36min	11h 19min

the computationally demanding steps are the initial RI integral transformation (3.9 % of t_{MDCI}), the initial guess and PNO construction (2.1 % of t_{MDCI}), the local RI PNO integral transformation (15.6 % of t_{MDCI}) and the LPNO-CCSD iterations (76.2 % of t_{MDCI}, 13 iterations). Three parts of the residual account for almost the entire computation time needed for the iterations: a) the nonlinear singles contribution the two-external pair-pair interactions (34.8 % of t_{Iter}, fourth and fifth sum of Eq. (B.3) and Eq. (B.4) respectively and seventh and

eighth sum of Eq. (B.5)), b) the singles-doubles interaction with one external label (28.0 % of t_{Iter}, fourth and fifth line of Eq. (B.1) and Eq. (B.2) respectively) and c) the calculation of the singles Fock matrix (31.6 % of t_{Iter}, Eq. (B.12) – (B.13)). The first two contributions correspond to the fifth order scaling terms in the doubles and singles residuals respectively, while the latter becomes expensive if large basis sets are used but might be sped up by using more efficient algorithms for construction of the singles Fock matrix such as the RIJCOSX approximation[214] (see Sec. 3.4.3). The integral transformations are memory intensive and hence, they can be performed most efficient on machines with large main memory. During the PNO construction and the iterations not more than about 6.5 GB of main memory were needed, but especially for the latter the CPU requirements are large since many BLAS level 3 operations have to be carried out. Although the fifth order scaling steps become dominant, the effective scaling of the correlation part, compared to the timings observed with the smaller TZVP basis, is still below fourth order.

A somewhat limiting factor in the present implementation is the disk storage of the two-external MO basis Coulomb and Exchange operators. It amounts to about 100 GB which is a factor of ten more than the disk space needed to store the PNO integrals, overlap matrices and pre-calculated pair-pair operators altogether. However, as it was shown for the closed-shell case, they are crucial for the accuracy of the LPNO approach. Nevertheless, if the LPNO approach is to be routinely applied to systems with more than 2000 basis functions both the disk storage requirements and the formal scaling must be significantly reduced. This will be the subject of future investigations.

Due to the three separate spin-cases and the resulting larger number of correlated electron pairs, canonical spin-unrestricted CCSD calculations on closed-shell molecules usually take a factor of 3 – 4 longer than the corresponding spin-restricted CCSD calculations. In order to compare the closed- and open-shell LPNO-CCSD implementations, the Penicillin molecule (Fig. 3.28 a)) was reinvestigated using the TZVP (TZV/C) basis set (567 basis functions). The calculations were performed on a faster PC (2.4 GHz Intel® Xeon® E5620 CPU allowing for 16 GB of main memory) and thus, the timings differ from those documented in Table 3.25. The total wall-clock time for closed-shell LPNO-CCSD was 3 h 37 min while the calculation with the open-shell variant took only about a factor of two longer (6 h 45 min). This can be traced back to the smaller number of PNOs per pair and the larger percentage of weak pairs that can be neglected for the latter. The closed-shell $LPNO_1$-CCSD method recovers about 0.2 % more of the target correlation energy and the difference between the total energies obtained with closed-shell and open-shell LPNO-CCSD is about -4.7 kcal/mol. For chemically interesting relative energies, this difference is expected to be much smaller. It is nevertheless advisable not to mix the results of the closed-shell and open-shell variants for the calculations of relative energies if both closed-shell and open-shell molecules are involved in the respective chemical application.

As a final example, a large model complex for the Ni-Fe hydrogenase active site (Fig. 3.30)

in the triplet state was investigated. The complex consists of 165 atoms and within the frozen core approximation, 439 correlated electrons enter the calculation. The def2-SVP (def2-SV/C) basis set was used for the hydrogen and carbon atoms and the def2-TZVP(-f) basis set was employed for the nickel, iron and sulfur atoms, which in total gives 1669 basis functions.

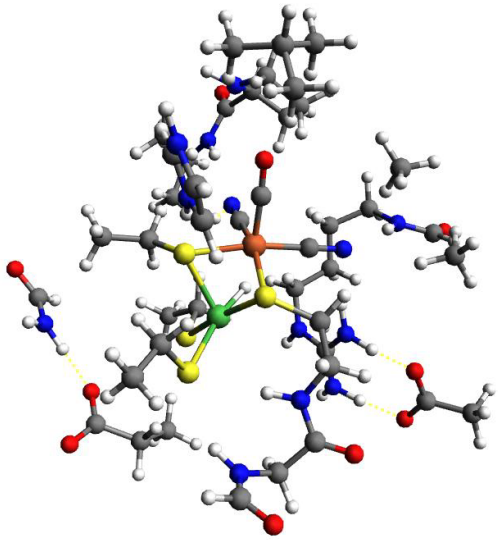

Figure 3.30.: Structure of a large model complex for the Ni-Fe hydrogenase active site in the triples state. The optimized geometry can be found in in the supplementary material of Ref. (198) (Fig. reproduced and modified from Ref. (198)).

Using large main memory (48 GB) and a multithreaded version of the BLAS routines (eight threads were used) the initial steps are completed in less than two days, but each iteration takes roughly the same amount of computation time while using only about 13.5 GB of memory. However, the bottleneck is the 'I/O' needed for the two-external Coulomb and Exchange integrals in the MO basis, which give rise to about 500 GB of disk space in this case. Thus, this is a calculation that is certainly doable with appropriate high performance hardware but is presently outside the range of routine applications.

3.4.3. Speed-ups obtained from the RIJCOSX approximation and parallelization

As it is obvious from the detailed timings presented in the previous Section, the three most time consuming steps of a LPNO-CCSD calculation are: a) the SCF procedure to obtain the reference function, b) the RI-PNO integral transformation, and c) the iterative calculation of the residual whose computation time is dominated (at least for the closed-shell version) by forming the singles Fock matrix, particularly if large basis sets are used. Due to the similarity of this term to the Fock matrix in SCF theory, the efficient calculation of the former may be realized through approximations developed for the latter. In particular, the RIJCOSX

approximation[214,215] seems to be well suited for that purpose. The associated formalism is outlined in Sec. 2.3.5.

Since the correlation energy is typically not more than ~1% of the total energy, and the singles Fock matrix contribution is a only small fraction of that, one may expect that approximating the construction of the singles Fock matrix only would yield at least up to three orders of magnitude better agreement with the analytic case compared to the RIJCOSX error in the SCF iterations. In order to evaluate this assumption, the Penicillin molecule was again used as test system. The calculations were carried out with the closed-shell LPNO$_1$-CCSD method using the large def2-QZVPP basis set (1921 contracted basis functions) together with the def2-QZVPP/C fitting basis set (4418 auxiliary basis functions), where the specific aspects of the singles Fock matrix term are especially pronounced. The corresponding results are documented in Table 3.28. They were obtained with serial runs on a single core of an Intel® Xeon® E7-8837 (2.67 GHZ) processor and large main memory (32 GB) was used to speed up the integral transformations. Model 1 corresponds to the case where the RIJCOSX approximation is exclusively used for the singles Fock matrix construction, while in Model 2 the SCF Fock matrix and their recalculation in the correlation part was also carried out via the RIJCOSX algorithm. The COSX SCF grid, if used, corresponds to G_D^+ of the previous study,[215] and for the singles Fock matrix construction, the medium grid of this setup explained in the same reference was used. Furthermore, overlap fitting was employed throughout. For density fitting, the corresponding Coulomb (def2-QZVPP/J) and correlation (def2-QZVPP/C) auxiliary basis sets were used.

Table 3.28.: Analysis of LPNO$_1$-CCSD/def2-QZVPP calculations on the Penicillin molecule using the RIJCOSX approximation. The reference refers to the fully analytic calculation (Model 1 and Model 2 are described in the text above). Energies (E), the absolute energetic errors (ΔE) and timings (t) are shown for different parts of calculation (SCF, correlation (subscript 'MDCI') and total (subscript 'tot' resp. 'wall')). Further notations: t_F: time spent to recalculate the Fock matrix in the correlation part; t_G: elapsed time to calculate the singles Fock matrix in all iterations; N_e: number of correlated electrons within the frozen core approximation; t_{residual}: total time needed for LPNO-CCSD iterations.

	Reference	Model 1	Model 2
E_{SCF} (E_h)	-1497.563694	-1497.563694	-1497.564662
ΔE_{SCF} (μE_h)	0.0	0.0	-968.16
t_{SCF} (s)	198209	198261	22337
E_{corr} (E_h)	-4.633543581	-4.633544235	-4.633597609
ΔE_{corr} (μE_h)	0.0	-0.654	-54.028
$\Delta E_{\mathrm{corr}}/N_e$ (μE_h)	0.0	-0.005	-0.422
t_F (s)	19307	19241	2280
t_G (s)	172960	17880	19470
t_{residual} (s)	199750	44545	46075
t_{MDCI} (s)	392193	236134	208165
t_{wall}	6 d 20 h 2 min	5 d 0 h 40 min	2 d 16 h 3 min
E_{tot} (E_h)	-1502.197238	-1502.197238	-1502.198255
ΔE_{tot} (μE_h)	0.0	0.0	1017.0

Looking at the SCF part first, the introduction of the RIJCOSX approximation results in a ninefold acceleration of the computation time and error of about 0.001 E_h in the converged SCF energy. The same observations can be made if the Fock matrix is recalculated in the correlation part ('MDCI') of the calculation (Model 2). The error in the correlation energy is well below the one kcal/mol limit for Model 1, whereas for Model 2, it amounts to 54 μE_h. The speed-up for the singles Fock part is about 9 – 10 for both models. Furthermore, while in the analytic case, the evaluation of the singles Fock term strongly dominates the total time spent in the iterations (~90 %), this ratio is reduced to ~40 % of the total time needed for the residual calculation if the singles Fock matrix is constructed via the RIJCOSX approximation. The entire correlation part of the calculation is also about two times faster in the latter case. The total wall-clock time for the analytic case amounts to about 6 d 20 h, 5 d for Model 1, and 2 d 16 h for Model 2. This corresponds to a total acceleration factor of 1.4 for Model 1 and 2.6 for Model 2 respectively. The error in the total energy for Model 1 is again below the one kcal/mol region while for Model 2, it amounts to ~0.001 E_h. However, as it has been shown for the larger molecules reaction energy test documented *e.g.* in Table 3.19, the usage of the RIJCOSX approximation for both, the SCF and correlation part of the LPNO-CCSD calculation, still yields accurate results while large savings in computation times can be achieved.[246] Thus, one can conclude that the RIJCOSX algorithm is particularly efficient and accurate in approximating the singles Fock term present in CCSD theory, and combined with its usage in the SCF part, significant speed-ups for LPNO-CCSD calculations can be obtained with negligible loss in accuracy. Thus, eliminating one of the computational bottlenecks of the LPNO-CCSD method means further increasing the size limit for accurate determination of energetic properties.

Further improvements in the applicability of the methods trivially result from parallelization of the code. A comprehensive study on the performance of the parallel implementations will not be given here but has been published elsewhere.[199] However, in order to confirm that the parallel implementations significantly increase the efficiency of the LPNO methods, two examples calculated with the closed-shell and open-shell LPNO-CCSD methods will be documented below. It has been checked that the results of the serial calculations are exactly reproduced by the corresponding parallel calculations.

The first example is a parallel calculation on the Penicillin molecule which was carried out on a total number of eight cores of a Intel® Xeon® E7- 8837 (2.67 GHZ) processor using common disk space for all processes and allowing for 32 GB main memory in total. The closed-shell $LPNO_1$-CCSD method using the RIJCOSX approximation both, the SCF part and the construction of the singles Fock matrix (Model 2 from above) was employed. The total wall-clock time needed for a single point energy calculation is reduced to 14 h thus leading to a 4.5 fold speed-up compared to the serial calculation. This is due to the fact that during the PNO integral transformation step, which is now the remaining bottleneck, all processes perform the gathering of the local data at the same time which slows down the 'I/O' tremendously and leads to bad scaling with respect to the number of processes

(only about a factor of 3 on 8 cores). However, as already mentioned above, the RIJCOSX algorithm performs well in parallel calculations for both, the SCF and singles Fock terms. The SCF procedure took 6 h 10 min on a single and only 54 min on 8 cores (scaling factor: 6.9). For the singles Fock term the speed-up with respect to the serial calculation is almost eightfold which decreases its computation from 5 h 24 min to 41 min. Compared to the fully analytic serial calculation which lasted about 6 d 20 h, it is impressive to observe that by applying the RIJCOSX approximation and parallelization together, the wall-clock times of a closed-shell LPNO-CCSD calculation using a large and flexible basis set with almost 2000 basis functions were successfully reduced to a time scale of routine calculations for molecules with similar size as Penicillin.

As a second example, the open-shell LPNO-CCSD/TZVPP calculation on the benzoquinone molecule weakly bounded to 20 H_2O molecules (Fig. 3.29) was repeated with identical parallel setup (eight processes using common disk space) and using the same PC. Since the 2.67 GHZ Intel® Xeon® E7-8837 processor is significantly faster than the one used for the open-shell LPNO-CCSD timings documented in the previous Section (2.4 GHz Intel® Xeon® E5620 CPU) and twice as much main memory was allocated in total for the parallel calculation, the serial calculation was also repeated leading to a wall-clock time of 2 d 19 h and 22 min. The SCF part finished in 11 h 41 min while the correlation part took 2 d 7 h and 41 min. For the latter, the most time consuming steps are the PNO integral transformation and the iterative calculation of the residuals which amount to ~30 % and ~54 % of the total wall-clock time respectively. The parallel calculation finishes in 18 h 27 min and thus only a 3.6 fold speed-up compared to the serial calculation could be gained. The SCF part of the calculations scales very good with the number of processes (speed-up factor > 7) but the correlation part is only accelerated by a factor of 3.3 on 8 cores. This is due to the bad scaling of the PNO integral transformation with the number of processes (speed-up factor of only 2.2) which now strongly dominates the total computation time (~45 % of the total wall-clock time). The residual calculation itself shows a speed-up factor slightly larger than five on eight processors. For the computationally expensive steps of the latter only the doubles singles interaction with one-external label shows a scaling factor smaller than four while the computation time needed for singles Fock matrix term scales almost linear with the number of processors. Obviously the PNO integral transformation represents the bottleneck of the current parallel LPNO implementation. Hence it needs to be further optimized and work in this direction is under way in our research group. To this end, the local data should be split into small portions which are directly written to the global files.

Nonetheless, the timings observed for the current LPNO implementations consistently demonstrate the high efficiency of this approach, particularly for larger molecules (up to ~100 atoms) in combination with large and flexible basis sets. Using the parallel implementation together with the RIJCOSX approximation for the construction of the singles Fock matrix and the SCF part, even correlated calculations with 2000 basis functions (depending on the number of correlated electrons) become routine applications, at least on modern computer hardware.

4. Discussion

In this work, we have developed an accurate and efficient approximation to single reference correlation methods which constitute a new family of local correlation methods denoted 'local pair natural orbital' (LPNO) methods.[196–198] The production level implementations can be applied to larger molecules of both closed-shell and open-shell types. The LPNO method achieves efficiency through localization of the internal space and truncation of the electron pair list together with compression of the external space using a truncated pair natural orbitals expansion. Of course, neither idea is unprecedented, but their combination and efficient implementation was carried out for the first time. The relationship of the proposed methodology to earlier treatments and other local correlation approaches, as well as possible improvements and perspectives for future developments and applications, will be discussed in this Chapter.

4.1. Assessment of the LPNO approach

The following attractive features of the LPNO methods make them particularly suitable for large scale computational chemistry applications:

a) accurate approximation of the canonical correlation energy and relative energies like e.g. barrier heights and reaction energies;
b) high efficiency relative to their canonical counterparts;
c) smooth and controllable remaining error;
d) excellent behavior with respect to basis set extension;
e) very compact form of the LPNO wavefunction;
f) 'black-box' character of the methods;
g) absence of any real-space cut-offs or fragmentation schemes.

Using the LPNO approach, we have developed production level implementations for various coupled pair methods (LPNO-(N)CEPA/0,1,2,3; LPNO-(N)CPF/1,2,3), quadratic configuration interaction and coupled cluster with single and double excitations (LPNO-QCISD, LPNO-CCSD) including perturbative connected triple excitations as well (LPNO-QCISD(T), LPNO-CCSD(T); only closed-shell implementation).[196–198] Furthermore, LPNO versions of variational CEPA[113] (LPNO-VCEPA; only open-shell version) and parametrized coupled cluster with single and double excitations (LPNO-pCCSD) were implemented.[219] The LPNO methods are available in two different versions: a spin-restricted form, suitable for efficient

and accurate calculations of closed-shell systems, and a spin-unrestricted open-shell version, which by default utilizes quasi-restricted orbitals, but is also general enough to be run with spin-unrestricted HF or KS reference determinants of broken-symmetry type. Two different algorithms are available for the closed-shell version denoted as LPNO_1 and LPNO_2. The latter entirely avoids the construction of the $\mathbf{J}^{ij}$ and $\mathbf{K}^{ij}$ integrals in the MO basis which give rise to storage problems for large systems with more than 2000 basis functions. However, the LPNO_2 algorithm is also less accurate than the LPNO_1 variant.

For all LPNO methods except LPNO-QCISD(T) and LPNO-CCSD(T), only three cut-off parameter enter the procedure that have been given conservative default values. They do not need to be changed or reinvestigated in detail prior to any application study. Hence, the LPNO methods can be used analogously to their canonical counterparts. If perturbative triple excitations should be included as well, a fourth cut-off parameter is needed. These four cut-off parameters are:

1. a threshold $\mathrm{T}_{\mathrm{CutPairs}}$ for the MP2 pair correlation energies (default value: 10^{-4} $\mathrm{E_h}$);
2. a threshold ($\mathrm{T}_{\mathrm{CutPNO}}$) for the pair natural orbital (PNO) occupation numbers (default value: 3.33×10^{-7});
3. a threshold ($\mathrm{T}_{\mathrm{CutMKN}}$) that controls the size of the auxiliary basis set for each electron pair (default value: 10^{-3});
4. a threshold ($\mathrm{T}_{\mathrm{CutTNO}}$) for the triple natural orbital (TNO) occupation numbers (default value: 3.33×10^{-7}, only needed for LPNO-QCISD/CCSD(T)).

For achieving both efficiency and high accuracy, the second parameter ($\mathrm{T}_{\mathrm{CutPNO}}$) is most crucial since it controls the size of the external correlation space per electron pair. The three other parameters merely enhance the efficiency of the procedure, but without significantly affecting its numerical behavior. However, for the present open-shell implementation the value of the pair cut-off ($\mathrm{T}_{\mathrm{CutPairs}}$) needs to be rather tight to ensure that the truncation error is small enough, at least if QROs are used. Using the default value, one merely benefits from error cancellation. The laborious integral transformation associated with the large number of PNOs becomes feasible through the extensive use of local density fitting (RI) techniques. The chosen default values for the thresholds ensure robustness and the results of the parent (canonical) methods are reproduced to within high accuracy.

Extended test calculations have consistently shown that the closed-shell LPNO variants together with the chosen default values for the cut-off parameters recover around 99.7 – 99.9 % of the basis set correlation energy. This is about one order of magnitude more accurate than the old PNO-CEPA implementations that had been developed and extensively used in the 1970s.[107] The less accurate algorithm (LPNO_2-QCISD, LPNO_2-CCSD) still recovers 98.7 – 99.3 % of the target correlation energy in the given basis and has modest disk space requirements. Comprehensive numerical tests on absolute and relative energies as well as timings consistently show that the outstanding performance of the LPNO methods carries over to the open-shell case with minor modifications. The open-shell version is slightly less

accurate, but still more than 99.5% of the canonical correlation energy is recovered on average. The LPNO-CCSD method is the most promising in terms of accuracy and robustness if open-shell molecules are involved in the respective computational study. For closed-shell systems LPNO-CEPA/1 is the method of choice, at least in terms of relative energy calculations. Finally, hyperfine couplings calculated with the variational LPNO-VCEPA/1 method, for which a well defined expectation value type density exists, indicate the great potential of the LPNO approach for the efficient calculation of molecular properties.

As already mentioned above, the PNOs have a number of attractive features. Only a small number of significant PNOs span the correlation space of an electron pair and the number of PNOs associated with the weak pairs is almost vanishing (0 – 5 PNOs/pair). This leads to a very compact representation of the wavefunction, and the number of doubles amplitudes that need to be optimized iteratively can be reduced by more than three orders of magnitude. The PNOs associated with an electron pair are located in the same region of space as the internal pair but stay as delocalized as physically necessary and thus, they span an optimal correlation subspace. Furthermore, the number of PNOs per pair increases only slowly with the size of the basis set. For a number of examples, it was observed that for a given system the average number of PNOs per electron pair roughly increases with the square root of the number of basis functions. Asymptotically, the number of PNOs spanning the external correlations space for each pair is constant. Hence, the LPNO methods perform best in conjunction with large and flexible basis sets, which are indispensable in order to obtain accurate results with wavefunction based correlation methods. Another attractive feature is the numerical stability of the LPNO approach. It shows rapid convergence with respect to the truncation thresholds and a well localized internal space is not of crucial importance. The truncation errors are very smooth and can be easily controlled since no real-space cut-off parameter or hierarchical classifications of electron pairs are applied. In this way, kinks and jumps in potential energy surfaces, to which local correlation methods are prone to, can be avoided. Furthermore, the convergence of the iterative residual calculation is as rapid as for the canonical methods. Although the effective scaling of the computation time with respect to the system size N is still $\sim\mathcal{O}(N^3)$, the LPNO methods are efficient enough for studies on molecules with up to 100 atoms and 2000 basis functions in reasonable wall-clock times, *e.g.* not more than a few days for a single point energy calculation depending on the number of correlated electrons. They are up to three orders of magnitude faster than their canonical counterparts. For larger molecules, the total wall clock time required to complete correlation part of the calculations is only 2 – 5 times larger compared to the preceding SCF procedure. Parallelization and the use of the RIJCOSX approximation (for LPNO-CCSD) further enhance the range of applicability. Although it was not pursued in this work, LPNO calculations can be also run in conventional mode (*i.e.* all integrals are stored on disk or kept in memory) which is of particular advantage if ANO basis sets[247] are used. The robustness of the LPNO approach combined with its efficiency and simple 'black-box' use make the LPNO methods highly suitable for large-scale applications in computational chemistry.

Unfortunately, the first attempt to extend the LPNO approach to the perturbative treatment of connected triple excitations was not very successful since the errors are to large and chemical accuracy could not reached. However, the results of the preliminary LPNO-CCSD(T) implementation indicate that this may be accomplished after a better treatment of the two-external pair-pair operators is available.

Although the coupled pair methods typically yield better results for relative energies than the QCISD or CCSD method,[24] they are less stable due to the missing orbital relaxation. A compromise, taking the best of both worlds, is the recently developed parametrized CCSD (pCCSD) method of Huntington *et al.*,[126] which was also implemented in the framework of the LPNO approach.[219] Specifically, the LPNO-pCCSD/1a and LPNO-pCCSD/2a methods (i.e. $\gamma = 1$) might be useful for applications in computational thermochemistry and chemical kinetics since they are almost as robust as CCSD and consistently provide results of intermediate accuracy between canonical CCSD and CCSD(T). In contrast, the 'b' variants (i.e. $\gamma = -1$) showed convergence problems for certain open-shell transition state structures and transition metal carbonyl complexes,[219] while no issues were observed for LPNO-pCCSD/1a, LPNO-pCCSD/2a and LPNO-CCSD. This seems to indicate that the modification of the $\widehat{T}_1\widehat{T}_2$ terms (see Eq. (2.110)) in the singles residual with $\gamma = -1$ can lead to some instability in the solution of the equations. This may be connected to the fact that the Thouless theorem[248] is not strictly valid for these methods, as a result of the scaling of the $\widehat{T}_1\widehat{T}_2$ terms in the singles residual equation (*i.e.* $e^{\widehat{T}_1}$ can no longer be factored from the modified residual equation and the relation $e^{\widehat{T}_1}|\Phi_0\rangle = |\Phi_0'\rangle$, where $|\Phi_0'\rangle$ is another single determinant wavefunction, cannot be utilized to show invariance of the ($\gamma \neq 1$) equations with respect to orbital rotations). Since one of the stated objectives of this work was to develop methods which are about as robust as the canonical counterparts, we do not advocate the use of the LPNO-pCCSD/1b and LPNO-pCCSD/2b methods, as these latter two approaches do not adhere to this criterium. But this also indicates that the LPNO-pCCSD approaches may have their limitation, in particular as the $\widehat{T}$-amplitudes grow in magnitude, these methods lose reliability and convergence problems occur. This is often the case for open-shell molecules with more complicated electronic structures which may already possess some multireference character indicated by large $\widehat{T}_1$-diagnostic values and a large magnitude of the $\widehat{T}_2$-amplitudes.[83,249] However, it should be noted that the coupled pair methods are usually much more prone to such convergence problems.

In addition, the general LPNO-pCCSD(α,β) family of methods (i.e. $\gamma = 1$) might be useful for certain niche applications by employing an optimization scheme such as that suggested in the work of Huntington *et al.*[219] For example, with the use of such a procedure, one might be able to find suitable sets of parameters for the treatment of weak interactions, for the calculation of anharmonic corrections to vibrational frequencies for a particular molecule, for conformational studies and in general, for the treatment of potential energy surfaces near the equilibrium geometry. Although the results obtained with the LPNO-pCCSD methods look promising, and they remain still exact for two-electron systems, it is always dangerous

to introduce parameters that affect the theory itself since this might lead to unpredictable errors similar to what is observed for DFT methods. Hence, a proper implementation of LPNO-CCSD(T) will be clearly superior to the LPNO-pCCSD methods.

4.2. Comparison of the LPNO approach with the old PNO-CEPA methods

Comparison of our implementation with the PNO-CEPA methods from the pioneer days of electron correlation methods (see Refs. given in the Introduction) reveals some important differences. First, we do not differentiate between singlet and triplet coupled external pairs, but use the generator state formalism[186] instead, in which this differentiation becomes obsolete and the formalism becomes simpler. Second, we do not pursue a diagonal PNO expansion. While such a form is suggested by the theory of natural orbitals, we feel uneasy with it since the PNOs used are only approximate. The additional off-diagonal terms are not expensive to keep, and hence it may be advantageously to include them in the treatment as well. Third, and perhaps most importantly, we do not transform the amplitudes back to the AO basis for the formation of the external exchange operator. This would negate almost all of the computational advantages. Instead, it is much more efficient to generate the sets of four external integrals in a pre-processing step via the RI approximation and reuse them later in the construction of the external exchange operators. This renders the four-external (and also the three-external) contribution to the residual computationally trivial. A very similar suggestion was previously worked out by Schütz and Manby in their local coupled-cluster approach.[211,212] Of course, the several hundred megabyte storage that are required in this step were not available at the time the first PNO-CEPA programs were implemented. Furthermore, the RI approximation was not yet recognized as a powerful tool in quantum chemistry. The LPNO approach also deviates from the previous procedures in not truncating the single excitations. Previously the PNOs of the diagonal pairs have been used to this end. First of all, we feel that although the singles do not bring in much correlation energy, they do provide the important electronic relaxation and should be kept as accurately as possible. The necessary computational effort is small compared to the fairly laborious AO to PNO integral transformation. Secondly, it is difficult to see how the singles should be consistently treated in a spin-unrestricted formalism if the PNOs of the diagonal pairs are used as an expansion basis. The combination of all these differences, and a fairly tight PNO cut-off, ensures that the loss of correlation energy is only of the order of 0.1 – 0.5 % for the LPNO methods. Hence, it is about one order of magnitude smaller compared to the early treatments. Moreover, in this work the PNO approach has been successfully applied to QCI and CC methods for the first time.

4.3. Comparison with PAO based local correlation approaches

In the last two decades many attempts have been made to develop efficient and accurate approximations to wavefunction based correlation methods based on a variety of different ideas, such as the domain concept based on projected atomic orbitals (PAOs) which was first introduced by Pulay about 30 years ago.[139] This approach has been extended and implemented with high efficiency by Werner, Schütz and their co-workers for an impressive array of correlation methods (see Refs. in the Introduction). Moreover, applications to large molecules have been demonstrated as well.[164] Although over local correlation approaches such as the recently developed CIM methods of Li and Piecuch[149,150] also show a large potential, the domain concept probably had the largest impact on the development of efficient correlation methods. Compared to the PAO based approaches, the LPNO methodology is simpler since it essentially only involves two thresholds that control the number of electron pairs to be kept and the size and accuracy of the PNO expansion. The third cut-off (T_{CutMKN}) is of rather technical nature and has essentially no impact on the numerical behavior of the method while the fourth cut-off parameter is only needed in case of perturbative inclusion of connected triple excitations. Since the default values for the two critical cut-offs were chosen rather conservatively, the LPNO methods are of 'black-box' character and can be applied in the same way as their canonical counterparts. The PNOs adapt themselves automatically to the requirements of the dynamic correlation field, and hence they are as localized or delocalized as the physics demand it. In PAO-based treatments, the size of the correlation domains is a critical factor that may either require some experimentation or insight from the user in order to ensure that no essential physics is lost.[176] The error of the LPNO methods is very smooth and virtually smooth potential energy surfaces are obtained. This requires extra precaution and experimentation in the PAO based approaches, while the subject of choosing appropriate correlation domains that may change from one structure to the other over a potential energy surface does not arise for the LPNO methods. Hence, the LPNO methods have more 'black-box' character than the local coupled cluster method based on PAOs.

However, Werner and co-workers have shown that the largest part of the domain error can be removed in explicitly correlated local calculations.[96,174] In this way, the error of the PAO methods is reduced to a level similar to what was observed for the LPNO methods. Another advantage of the PAO based procedures appears to be the removal of the basis set superposition error that remains in the LPNO approach in a very similar form as for the canonical methods. Moreover, Werner and co-workers have also succeeded at implementing perturbative triple excitations more accurately.[165] However, it appears that the LPNO based methods recover more correlation energy than the PAO methods, at least if default domains are used for the latter and no explicit correlation is added. The use of extended domains reduces the error of the PAO based local correlation methods but the calculations become also significantly more expensive. Furthermore, the LPNO approach behaves better with respect to basis set extension. The number of significant PNOs per pair tends towards a

constant as the quality of the basis set is increased, while the number of PAOs to be kept increases linearly with basis set extension. However, it is also clear that the linear scaling PAO based approaches must be faster than the LPNO based calculations, at least if the molecules become large enough. We expect that the LPNO methods will probably be competitive in their timings for calculations on medium sized molecules with large basis sets but will likely be slower than the PAO methods for calculations on large molecules, especially if relatively small basis sets are employed. However, this is not the typical scenario in computational studies, since for very large molecules such as enzyme active sites, the geometry optimization and the interpretation of the results is often difficult. Moreover, large and flexible basis sets are essential for obtaining accurate results with wavefunction based correlation methods. Thus, it is often more favorable to use hybrid methods like the QM/MM approach[250] for which only a subsystem (typically smaller than 150 atoms) is treated quantum chemically. Hence, based on the results and timings obtained in this work we consider this drawback to be acceptable and improvements of the LPNO approach are already envisioned and ongoing work in our laboratory.

4.4. Improvements and Perspectives

A number of improvements and further developments of the present LPNO approach are envisioned or already in progress in our laboratory. These can be divided into two parts:

a) improve the scaling behavior of the algorithms and remove computational bottlenecks;
b) extend and improve the LPNO formalism.

The first point a) is related to rather technical problems that are currently being investigated in our laboratory. The attractive features of the LPNO methods presently come at the prize that they are not linear scaling and that, in fact, even $\mathcal{O}(N^5)$ terms such as the initial integral transformation remain even though they have a rather small prefactor. Although the MO basis Coulomb and Exchange operators with up to two-external labels can be calculated with acceptable efficiency via the RI-approximation (particularly if large main memory is available) and the parallel speed-up of the initial integral transformation is almost linear, their storage requirements can become rather large (up to several hundreds of GB) for big molecules. Thus, the applicability of the present LPNO_1 and open-shell implementations for which these integrals are mandatory, is currently limited to about 1500 – 2500 basis functions (depending on how many electrons are correlated) due to the $\mathcal{O}(N^4)$ disk space requirements for the storage of MO basis two-external Coulomb and Exchange integrals. Unfortunately, the errors of the LPNO_2 variant for which the construction of these integrals is only done during the PNO integral transformation are too large. Apparently, the accurate treatment of the two-external pair-pair interactions is crucial for obtaining accurate results. The same observations was made for the present LPNO-CCSD(T) implementation. Obviously, the approximation of the truncated PNO pair subspace of pair (k, j), for example through that

of pair (i,j) is not very accurate, particularly in cases where the number PNOs associated to the pairs in question significantly differs from each other. It seems to be necessary and it should be possible to retain the accuracy of the $LPNO_1$ approaches while not having to store the canonical Coulomb and Exchange operators. Furthermore, if systems with more than 150 atoms should be treated, even the storage of the one-external integrals over canonical orbitals should be avoided. This is certainly feasible, but has not been necessary for the molecular systems treated so far. However, routes to achieve this goal should be also investigated. Moreover, the formal scaling of the expensive initial integral transformations should be further reduced as well.

While linear scaling has neither been attempted nor achieved in the present work, there are many computational chemistry applications for which the efficiency of the present LPNO implementations is sufficient. However, for calculations on very large molecules, the LPNO methods will be significantly slower or even impossible to perform compared to true linear scaling approaches. Thus, further developments should concentrate on reducing the scaling of the LPNO methods. Due to the inherent locality in the PNOs, we are confident that such reductions can be realized without diminishing the accuracy of the method significantly. To this end, it seems to be attractive to combine the concepts of the LPNO approach with local MP2 approaches.[60] Thus, one could generate the initial guess along similar lines as pursued in linear scaling local RI-MP2 theory[168] with conservative domain choices. This would open up the possibility to generate the PNOs with linear scaling time and disk space requirements. The computationally expensive AO to PNO integral transformation could then be approached along the same lines since an asymptotically constant number of atoms will contribute their basis functions to each PNO set associated with a given electron pair.

In this context, it is interesting to investigate the spatial extent of the PNOs of a given pair. If these regions would not be excessively large, one might consider to combine domain based methods with PNO approaches to further enhance the efficiency of the local approaches. To this end, calculations were carried out on the glycine trimer using the TZV(2d,p) basis (24 atoms, 378 basis functions). A Mulliken population analysis was applied to the PNOs of each pair and the number of significant atoms was counted on the basis of the Mulliken cut-offs 10^{-1}, 10^{-2}, 10^{-3}, and 10^{-4}. The average number of significant atoms per PNO was found to be 2, 7, 13, and 18 respectively. Maintaining the chosen default value of $T_{\mathrm{CutMKN}} = 10^{-3}$, the average number of atoms per PNO would be 13 while the average number of significant atoms for each localized internal electron pair is about 10. However, what really matters is not the average number of significant atoms per PNO but rather the average number of atoms for each electron pair. This number is determined by the most diffuse PNO in the truncated PNO expansion of the pair in question. These are usually the PNOs with the lowest occupation numbers since, following the logics of natural orbitals, they have the largest number of nodes. Performing the analysis in a way that selects the largest number of atoms found for any PNO of a given pair, the average number of significant atoms per electron pair for $(Gly)_3$ was found to be 5, 11, 17 and 21 respectively with the same Mulliken cut-offs

as before. Thus, PNO domains would be fairly large but it seems worthwhile to exploit this locality, at least for large systems. Possibly, the systematic behavior of the PNOs would offer new possibilities to increase the efficiency of such an approach. The correlation energy recovered by each PNO is proportional to its occupation number.[108,109,115] Hence, one could consider cutting off the weakly occupied PNOs more aggressively without compromising the accuracy of the method. These issues are presently being investigated in our research group.
The fact that the single excitations have been left untruncated in the present LPNO implementations significantly adds to the computational cost of the procedure, particularly with regard to the singles-doubles interaction with one-external label and the singles Fock matrix construction. For the latter, the scaling and efficiency was already greatly enhanced through the use of the COSX algorithm, while the former still scales as $\mathcal{O}(O^3V^2)$ (O: size of the internal orbital space; V: size of the external orbital space) and remains as computational bottleneck in the calculation of the singles residual. A way to solve this problem would be to truncate also the virtual correlation subspace spanned by the single excitations. However, this can be also dangerous and tight cut-off values might be necessary. This subject will be further addressed below.
It is certainly possible to achieve near linear scaling in LPNO based single reference correlation methods. However, any further approximation must not reduce the accuracy significantly for the sake of a formally more favorable scaling of the computation time with the system size. In addition, the parallelization should be further improved, since the speed-up for computationally significant contributions like the PNO integral transformation is not optimal yet. To this end, the gathering processes should be performed in smaller steps and not only at the end of the loops for all processes at the same time. In this way, the large amount of data that needs to be written to the disk can be directly written into the global files and no barriers would be necessary. A more efficient parallelization additionally increases the number of applications which can be carried out using the LPNO methods.

The second point (b) focuses on the improvement of the LPNO formalism and its perspectives for extensions and further developments.
The first issue in this respect is the treatment of the single excitations. Although they do not contribute much to the correlation energy, they are important for the robustness of the method in electronically difficult situations. The presence of the $e^{\widehat{T}_1}$ operator is, in fact, one of the largest advantages of the CC methods since it provides almost the entire orbital relaxation which may well be of long range.[83] This will become probably only fully evident in the treatment of response properties. Thus, we have decide to leave the single excitation manifold untruncated, at least in the first development stage. However, besides the computational bottlenecks which have arisen thereby, the back-projection of doubles amplitudes from the truncated PNO pair basis to the full virtual MO basis needed in the singles-doubles coupling term introduces an additional error source. Hence, a good compromise between accuracy and computational costs has to be found for treatment of the single excitations. One might

think about an separate set of "$\mathbf{K}^{ii}$-PNOs" (Eg. (2.87)) for the entire single excitations. Another possibility would be the use of orbital-specific virtual subspaces similar to the work of Yang *et al.*[134,135] or Rolik *et al.*[161]

The problem with the singles treatment could be also circumvented if Brückner-type orbitals[251] would be used since such a procedure ensures that all singles amplitudes are exactly zero. However, one has to find a smart way to implement it efficiently in the spirit of the LPNO approach since repeating the computationally expensive PNO integral transformation before each iteration step would most likely take away most of the efficiency gains.

Another point addresses two desirable properties for approximate quantum chemical methods: the invariance with respect to rotations of internal orbitals (i.e. unitary invariance) and the satisfaction of a variational principle. The former is largely a non-issue for local correlation methods since the internal orbitals are always required to be localized in such approach. The LPNO methods are not unitary invariant due to the projections on truncated subspaces. However, as it was convincingly demonstrated in the previous chapter, this does not spoil their accuracy. Nevertheless, it is a unattractive feature of the theory, and it would be more satisfying to have a formalism that is both invariant and stationary, at least with respect to the variations of the excitation amplitudes. Variational CEPA (VCEPA)[113] was successfully implemented using the LPNO approach and it would be of great interest to do the same for strictly size-extensive orbital invariant (SEOI) functional recently proposed Kollmar.[207] The availability of such a functional opens the door for completely stationary solutions in which both the orbitals and the wavefunction amplitudes are fully relaxed.

Another important issue is the inclusion of the perturbative correction for connected triple excitations denoted as (T) since this is known to be crucial for obtaining accurate results with coupled cluster methods. The CCSD(T) method it is the 'gold standard' of computationally chemistry since it is very robust and consistently yields results with chemical accuracy, at least if sufficiently large basis sets are used. In the present work, a first attempt to extend the PNO based local correlation approach to perturbative triple excitations, thus yielding the LPNO-QCISD(T) and LPNO-CCSD(T) models, was carried out. The key concept involves the construction of triples-natural orbitals (TNOs) that span the joint pair space of the three electron pairs that are involved in a given contribution to the triples correlation energy. Such an approach necessitates a number of rather laborious integral transformations. However, it was not their computational cost that was the determining factor to reject the present LPNO-QCISD(T) and LPNO-CCSD(T) implementation, but the rather large errors which were observed in test calculations. Although the truncation errors seem to be very smooth, extrapolation techniques also failed to change this situation significantly. Moreover, a corresponding open-shell implementation would only be possible with further approximations for the projection of the three-external integrals to the truncated TNO basis. The main reason for the relatively large errors is most likely the approximate treatment of the two-external Exchange integrals which are constructed in the PNO integral transformation. The sensibility

of the two-external pair-pair operators with respect to the truncation of the PNO expansion was also observed for the $LPNO_2$-CCSD method. Therefore, it seems necessary to improve the treatment of this integrals first. Nonetheless, it should be possible to find a suitable implementation of the perturbative triples correction in the spirit of the LPNO framework which is both efficient and accurate.

Another important point concerns the present open-shell implementation. It would be attractive to treat the electrons from the DOMO space as efficiently as in the corresponding closed-shell implementation and without neglecting any additional terms. In this way it would be possible to exactly match the results obtained with open- and closed-shell variants for closed-shell molecules. For example, this would greatly improve the practical use of the LPNO methods for computational studies of reaction cycles, in which both closed- and open-shell molecules are involved. Therefore, it would be necessary to use a different initial guess (similar to NEVPT2[252] for a single electron pair) ensuring that the following truncation can be done in a fully consistent manner. Nonetheless, the current implementation, which is based on spin-unrestricted equations and has the benefit of generality allowing also for reference determinants of broken-symmetry type, is only slightly less accurate than the corresponding closed-shell variants and only about twice as expensive. In addition, improved PNOs are expected to further reduce the PNO truncation error. One should try to find a similar definition for Meyer-style PNOs for the open-shell case, but other PNO construction schemes should also be investigated in detail.

The convergence to complete basis set (CBS) limit represents an important issues as well. Due to the Coulomb cusp, inherent to any N-electron wavefunction, fairly large basis sets are needed for accurate result with single reference correlation methods which make use of smooth gaussian-type functions to describe the shape of the AOs. The convergence to the CBS limit can be greatly enhanced through inclusion of explicit correlation into the wavefunction. Werner *et al.* have shown that explicit correlation can be combined with local correlation in an efficient way.[174] Although the LPNO methods perform best with large and flexible basis sets and extrapolation to the CBS limit works fairly well in practice,[235] it is still interesting to investigate if the additional overhead due to the explicit correlated terms pays off compared to the use of larger basis sets. Tew *et al.* have already shown for the F12-MP2 method that the PNO concept can be successfully incorporated into explicit correlated schemes.[136]

One could easily envision other extensions that would increase the domain of applicability of the LPNO methods. It will be straightforward to pursue a fragment correlation approach in which only user defined fragments are being correlated while less interesting parts of the molecule (such as bulky substituents) are treated at the SCF or MP2 levels.[151] Such an approach has already been realized by Mata *et al.* in the framework of PAO based correlation methods[253] and by Fedorov and Kitura.[148] Secondly, it would be a promising route for further developments to combine the LPNO methods with incremental correlation schemes[144,145] or

the cyclic cluster model[254] in order to make the attractive features of the LPNO approach also accessible for solid state calculations.

The truncation of the virtual space based on PNOs is similar to higher-order singular value decomposition[138] or a tensor factorization[134] of the doubles amplitudes. Orbital specific virtual subspaces[134,173] and the approach by Rolik *et al.*[161] which combines the cluster in molecule (CIM) concept[149] with the OSV approach and are also closely related. Furthermore, general tensor decomposition techniques are presently investigated by Auer *et al.*[137] The connection between these alternative approaches certainly holds promise for future extensions (*e.g.* for general order local CC methods) and technical improvements like compressed auxiliary basis sets.

Another issue is the treatment of excited states. Recently, it has been shown by Hellmich *et al.*[255] that excited states can be calculated efficiently via a PNO-CIS(D) program. It would be interesting to see whether it is also possible to combine the LPNO approach with the EOM-CCSD method in an efficient and accurate way.

A very important direction for future developments is the efficient and accurate calculation of molecular properties since they are often better to compare with experimental results than energies itself.[26] Thus, it is of great interest to investigate whether the LPNO approach can be also successfully applied for the calculation of response properties. A preliminary test on the calculation of hyperfine couplings with the open-shell LPNO-VCEPA/1 method showed that this might be indeed possible, but more experience has to be gained and it is still a long way until one can finally judge on this point. However, if this can be realized through efficient implementations, it would greatly enhance the usefulness of the LPNO methods for computational chemistry applications.

Furthermore, the extension of the methodology to the multireference case is a promising direction for further developments. Multireference PNO-CI and PNO-CEPA programs had been developed and used with great success in the past by Taylor,[114] Fink and Staemmler[115] However, for new developments in this direction applicable to reference spaces of significant sizes, an efficient internally contracted multireference CI/CC program is needed fist. It may be considered an advantage that within the CEPA style correlation methods it is relatively easy to maintain stationarity of the wavefunction amplitudes via the coupled-pair functional recipe. This will ultimately render the calculation of response properties more efficient than in a coupled cluster framework. Furthermore, the multireference treatment will be much simpler and better defined compared to the coupled cluster approach. However, to which extent such savings can be actually realized within the LPNO framework remains to be proven through efficient implementations.

However, regardless of the type of extensions or formal improvements, the LPNO methods should stay as robust and accurate as they are while their simple usage should be retained as well.

4.5. Conclusions

The PNO methods first developed and successfully applied in the 1970s (see Refs. in the Introduction) were revived and modified. Production level implementations of closed- and open-shell local pair natural orbital (LPNO) coupled pair, QCISD and CCSD methods including perturbative triple excitations as well have been developed and comprehensively tested. It was shown that the introduced approximations essentially retain the accuracy of the parent methods while enormous speed-ups in the computation times are obtained. Extensive numerical tests on absolute and relative energies as well as the observed timings consistently demonstrate the outstanding performance and the attractive features of the LPNO methods. They can be confidentially used in a 'black box' fashion in the same way as their canonical counterparts since there are only very few cut-off thresholds involved that have been given conservative default values. The closed-shell versions were released with the ORCA 2.8 release and the open-shell versions are available to the ORCA users since the 2.9 release. The preliminary LPNO-QCISD(T) and LPNO-CCSD(T) methods are implemented in a development version of the ORCA program package.[206]

The most promising methods so far are open-shell LPNO-CCSD and closed-shell LPNO-CEPA/1. The latter is particularly suited for the accurate calculation of non-covalent interactions and closed-shell main group compounds. Furthermore, with the LPNO-pCCSD/1a and LPNO-pCCSD/2a methods which are in general more robust than the LPNO based CEPA methods, it may be possible to treat more electronically complicated molecular systems at the same level of accuracy, *i.e.* intermediate accuracy between canonical CCSD and CCSD(T). However, the ultimate goal of finding an efficient and accurate approximation to the 'gold-standard' of computational chemistry provide by the CCSD(T) method has not been fully achieved yet and further developments in this direction are currently pursued in our research group. The large impact of this new developments can be seen on the fact that many research groups started to get interested in local correlation methods which make use of approximate pair natural orbitals and related schemes to compress the virtual correlation space.[134–136,161,163,255]

However, the final criterion for the usefulness of a given method is its behavior in practical computational chemistry applications. This can ultimately only be judged by extensive confrontation of the theoretical methodology with 'real life' chemical problems. First successful computational chemistry applications which make use of the LPNO methods, involving Rhodium catalyzed asymmetric olefin hydrogenation,[256] protein ligand interaction energies,[257] van der Waals interactions,[199,235] relative energies of transition metal complexes with $(Cu_2O_2)^{2+}$ core,[258] proline-based chiral stationary phases,[259] and acene dimerization[260] have been already reported in the literature and it is seems likely that many more will follow soon. Hence, we are most confident that the LPNO methods provide a very useful 'model chemistry' applicable to many problems in contemporary chemical research.

They LPNO methods might be also very useful for obtaining benchmark results of large

molecule test sets such as *e.g.* contained in the GMTKN30 database of Goerigk and Grimme.[50]) However, it should be kept in mind that all the methods discussed in this work are based on the single reference formalism, and thus they are not suitable for certain classes of molecules.

Although the current implementation leaves room for improvements and further developments are necessary to fully explore the potential of the LPNO approach, the present LPNO methods are already highly suitable and useful for large-scale computational chemistry applications. Thus, due to the high efficiency and accuracy combined with the robustness of the LPNO approximation, the LPNO methods have a good chance at becoming a standard tool capable of tackling many interesting problems in contemporary chemical research while reducing the dominance of the DFT methods in computational chemistry to some extent.

Appendices

A. The working equations for closed-shell LPNO$_1$-CCSD

The complete closed-shell LPNO$_1$-CCSD working equations, as they are implemented in the ORCA[206] quantum chemistry program package, are given below. The terms highlighted in blue (Eq. (A.13)) are neglected in the actual implementation.

The singles residual reads:

$$\begin{aligned} R_a^i = \quad & F_{ia} + \sum_b \tilde{F}_{ba} t_b^i - \sum_j \tilde{F}_{ij} t_a^j + \mathbf{G}(\mathbf{t}_1)_{ia} + \sum_{j,b} \Big(\mathbf{d}^{ji} \Big(2\,\overline{\mathbf{t}}^{ji} - \overline{\mathbf{t}}^{ji\dagger} \Big) \mathbf{d}^{ji\dagger} \Big)_{ab} \tilde{F}_{jb} \\ & - \sum_{j,k,b} \Big(2\,(ik|jb) - (ij|kb) \Big) \Big(\mathbf{d}^{kj} \bar{\boldsymbol{\tau}}^{kj} \mathbf{d}^{kj\dagger} \Big)_{ab} \\ & + \sum_{j,\bar{a}} d_{a\bar{a}}^{ij} \left(\sum_{\bar{b},\bar{c}} \left(\Big(2\,(i\bar{b}|\bar{a}\bar{c}) - (i\bar{c}|\bar{a}\bar{b}) \Big) \bar{\tau}_{\bar{b}\bar{c}}^{ij} + \Big(2\,(j\bar{b}|\bar{a}\bar{c}) - (j\bar{c}|\bar{a}\bar{b}) \Big) \bar{\tau}_{\bar{c}\bar{b}}^{ij} \right) \right) \\ & + \sum_{j,b} \Big(\tilde{F}_{jb} - 2\,F_{jb} \Big)\, t_b^i t_a^j \\ \stackrel{!}{=} \quad & 0 \quad . \end{aligned} \tag{A.1}$$

The doubles residual has the following form:

$$\begin{aligned} \bar{R}_{\bar{a}\bar{b}}^{ij} = \quad & \Big(\bar{\mathbf{K}}^{ij} \Big)_{\bar{a}\bar{b}} + \Big(\mathbf{d}^{ij\dagger} \bar{\tilde{\mathbf{F}}}^{v\dagger} \mathbf{d}^{ij} \bar{\mathbf{t}}^{ij} + \bar{\mathbf{t}}^{ij} \mathbf{d}^{ij\dagger} \bar{\tilde{\mathbf{F}}}^{v} \mathbf{d}^{ij} \Big)_{\bar{a}\bar{b}} + \bar{\tilde{\mathbf{K}}} \Big(\bar{\boldsymbol{\tau}}^{ij} \Big)_{\bar{a}\bar{b}} \\ & - \sum_k \left(\bar{\tilde{F}}_{jk} \Big(\mathbf{S}^{ij,ik} \bar{\mathbf{t}}^{ik} \mathbf{S}^{ij,ik\dagger} \Big)_{\bar{a}\bar{b}} + \bar{\tilde{F}}_{ik} \Big(\mathbf{S}^{ij,kj} \bar{\mathbf{t}}^{kj} \mathbf{S}^{ij,kj\dagger} \Big)_{\bar{a}\bar{b}} \right) \\ & + \sum_{k,l} \widetilde{(ik|jl)} \Big(\mathbf{S}^{ij,kl} \bar{\boldsymbol{\tau}}^{kl} \mathbf{S}^{ij,kl\dagger} \Big)_{\bar{a}\bar{b}} \\ & + \sum_k \Big(\mathbf{S}^{ij,ki} (2\bar{\mathbf{t}}^{ki\dagger} - \bar{\mathbf{t}}^{ki}) \mathbf{S}^{ki,jk} (\Delta\bar{\tilde{\mathbf{K}}}^{jk\dagger} - \tfrac{1}{2} \Delta\bar{\tilde{\mathbf{J}}}^{jk}) \mathbf{S}^{jk,ij} \\ & \quad - \tfrac{1}{2} \mathbf{S}^{ij,ki} \bar{\mathbf{t}}^{ki} \mathbf{S}^{ki,jk} \Delta\bar{\tilde{\mathbf{J}}}^{jk} \mathbf{S}^{jk,ij} - \mathbf{S}^{ij,jk} \Delta\bar{\tilde{\mathbf{J}}}^{jk\dagger} \mathbf{S}^{jk,ki} \bar{\mathbf{t}}^{ki\dagger} \mathbf{S}^{ki,ij} \Big)_{\bar{a}\bar{b}} \\ & + \sum_k \Big(\mathbf{S}^{ij,ik} (\Delta\bar{\tilde{\mathbf{K}}}^{ik} - \tfrac{1}{2} \Delta\bar{\tilde{\mathbf{J}}}^{ik\dagger}) \mathbf{S}^{ik,kj} (2\bar{\mathbf{t}}^{kj} - \bar{\mathbf{t}}^{kj\dagger}) \mathbf{S}^{kj,ij} \end{aligned}$$

$$
\begin{aligned}
&\left. -\tfrac{1}{2}\mathbf{S}^{ij,ik}\Delta\bar{\tilde{\mathbf{J}}}^{ik\dagger}\mathbf{S}^{ik,kj}\bar{\mathbf{t}}^{kj\dagger}\mathbf{S}^{kj,ij} - \mathbf{S}^{ij,kj}\bar{\mathbf{t}}^{kj}\mathbf{S}^{kj,ik}\Delta\bar{\tilde{\mathbf{J}}}^{ik}\mathbf{S}^{ik,ij}\right)_{\bar{a}\bar{b}} \\
&+\sum_k \left(\mathbf{S}^{ij,ik}(2\bar{\mathbf{t}}^{ik} - \bar{\mathbf{t}}^{ik\dagger})\mathbf{d}^{ki\dagger}(\mathbf{K}^{kj} - \tfrac{1}{2}\mathbf{J}^{kj})\mathbf{d}^{ij} \right. \\
&\left. +\mathbf{d}^{ij\dagger}(\mathbf{K}^{ik} - \tfrac{1}{2}\mathbf{J}^{ik})\mathbf{d}^{ik}(2\bar{\mathbf{t}}^{kj} - \bar{\mathbf{t}}^{kj\dagger})\mathbf{S}^{ij,kj\dagger}\right)_{\bar{a}\bar{b}} \\
&-\sum_k \left(\tfrac{1}{2}\mathbf{S}^{ij,ik}\bar{\mathbf{t}}^{ik\dagger}\mathbf{d}^{ki\dagger}\mathbf{J}^{jk\dagger}\mathbf{d}^{ij} + \tfrac{1}{2}\mathbf{d}^{ij\dagger}\mathbf{J}^{ik}\mathbf{d}^{kj}\bar{\mathbf{t}}^{kj\dagger}\mathbf{S}^{kj,ij} \right. \\
&\left. +\mathbf{d}^{ij\dagger}\mathbf{J}^{jk}\mathbf{d}^{ki}\bar{\mathbf{t}}^{ik}\mathbf{S}^{ik,ij} + \mathbf{S}^{ij,kj}\bar{\mathbf{t}}^{kj}\mathbf{d}^{kj\dagger}\mathbf{J}^{ik\dagger}\mathbf{d}^{ij}\right)_{\bar{a}\bar{b}} \\
&-\sum_k \left(\Big(\sum_a (jk|ia)d^{ij}_{a\bar{a}}\Big)\bar{t}^k_{\bar{b}} + \Big(\sum_b (ik|jb)d^{ij}_{b\bar{b}}\Big)\bar{t}^k_{\bar{a}} \right) \\
&+\sum_{\bar{c}} \left((i\bar{a}|\bar{c}\bar{b})\bar{t}^j_{\bar{c}} + (j\bar{b}|\bar{a}\bar{c})\bar{t}^i_{\bar{c}} \right) \\
&-\sum_k \left(\Big(\mathbf{S}^{ij,ik}(\bar{\mathbf{K}}^{ik}\bar{\mathbf{t}}^j)\Big)\bar{t}^k_{\bar{b}} + \Big(\mathbf{S}^{ij,jk}(\bar{\mathbf{K}}^{jk}\bar{\mathbf{t}}^i)\Big)\bar{t}^k_{\bar{a}} + \Big(\mathbf{S}^{ij,ik}(\bar{\mathbf{J}}^{ik}\bar{\mathbf{t}}^j)\Big)\bar{t}^k_{\bar{a}} + \Big(\mathbf{S}^{ij,jk}(\bar{\mathbf{J}}^{jk}\bar{\mathbf{t}}^i)\Big)\bar{t}^k_{\bar{b}} \right) \\
&\stackrel{!}{=} \quad 0 \quad , \qquad \text{(A.2)}
\end{aligned}
$$

where

$$\Delta\bar{\tilde{J}}^{ij}_{\bar{a}\bar{b}} = \bar{\tilde{J}}^{ij}_{\bar{a}\bar{b}} - \bar{J}^{ij}_{\bar{a}\bar{b}} \quad , \qquad \text{(A.3)}$$

and

$$\Delta\bar{\tilde{K}}^{ij}_{\bar{a}\bar{b}} = \bar{\tilde{K}}^{ij}_{\bar{a}\bar{b}} - \bar{K}^{ij}_{\bar{a}\bar{b}} \quad . \qquad \text{(A.4)}$$

The 'dressed' quantities are given by

$$\bar{\tau}^{ij}_{\bar{a}\bar{b}} = \bar{t}^{ij}_{\bar{a}\bar{b}} + \bar{t}^i_{\bar{a}}\bar{t}^j_{\bar{b}} \quad , \qquad \text{(A.5)}$$

$$\tilde{F}_{ai} = \quad F_{ai} + \sum_k \mathbf{d}^{ik}\left(2\,\bar{\mathbf{K}}^{ik} - \bar{\mathbf{K}}^{ik\dagger}\right)\mathbf{d}^{ik\dagger}\mathbf{t}^k \quad , \qquad \text{(A.6)}$$

$$\tilde{F}_{ab} = \quad F_{ab} - \sum_{k,l}\left(\mathbf{d}^{kl}\left(\bar{\boldsymbol{\tau}}^{kl}\left(2\,\bar{\mathbf{K}}^{lk} - \bar{\mathbf{K}}^{lk\dagger}\right)^\dagger\right)\mathbf{d}^{kl\dagger}\right)_{ab} \quad , \qquad \text{(A.7)}$$

$$\tilde{F}_{ij} = \quad F_{ij} + \sum_k \left\langle \left(\mathbf{S}^{ik,jk}\left(2\,\bar{\mathbf{K}}^{jk} - \bar{\mathbf{K}}^{jk\dagger}\right)\mathbf{S}^{ik,jk\dagger}\right)\bar{\boldsymbol{\tau}}^{ik\dagger}\right\rangle \quad , \qquad \text{(A.8)}$$

$$\mathbf{G}(\mathbf{t}_1)_{pq} = \sum_{jb} t_b^j (2\,(pq|jb) - (pj|qb)) \quad , \tag{A.9}$$

$$\tilde{\tilde{F}}_{ab} = \tilde{F}_{ab} + \mathbf{G}(\mathbf{t}_1)_{ab} - \sum_i F_{ib}\, t_a^i \quad , \tag{A.10}$$

$$\tilde{\tilde{F}}_{ij} = \tilde{F}_{ij} + \mathbf{G}(\mathbf{t}_1)_{ij} + \sum_a F_{ia}\, t_a^j \quad , \tag{A.11}$$

$$(\widetilde{ik|jl}) = \quad (ik|jl) + \left\langle \left(\mathbf{S}^{ij,kl} \bar{\mathbf{K}}^{kl} \mathbf{S}^{ij,kl\dagger} \right) \bar{\boldsymbol{\tau}}^{ij\dagger} \right\rangle + \sum_a \left((lj|ka) t_a^i + (ki|la) t_a^j \right) \quad , \tag{A.12}$$

$$\bar{\tilde{\mathbf{K}}}(\bar{\boldsymbol{\tau}}^{ij})_{\bar{a}\bar{b}} = \sum_{\bar{c},\bar{d}} \left((\bar{a}\bar{c}|\bar{b}\bar{d}) - \sum_k \left((k\bar{d}|\bar{a}\bar{c})\bar{t}_{\bar{b}}^k - (k\bar{c}|\bar{b}\bar{d})\bar{t}_{\bar{a}}^k \right) \right) \tau_{\bar{c}\bar{d}}^{ij} \quad , \tag{A.13}$$

$$\begin{aligned} \bar{\tilde{K}}_{\bar{a}\bar{b}}^{ij} = \quad & \bar{K}_{\bar{a}\bar{b}}^{ij} + \sum_k \Bigg(\left(\mathbf{S}^{ij,ik} \bar{\mathbf{t}}^{ik} \mathbf{S}^{ik,kj} (\bar{\mathbf{K}}^{kj} - \tfrac{1}{2} \bar{\mathbf{K}}^{kj\dagger}) \mathbf{S}^{kj,ij} \right)_{\bar{a}\bar{b}} - \tfrac{1}{2} \left(\mathbf{S}^{ij,ik} \boldsymbol{\tau}^{ki} \mathbf{S}^{ki,kj} \bar{\mathbf{K}}^{kj} \mathbf{S}^{kj,ij} \right)_{\bar{a}\bar{b}} \\ & - \Big(\sum_b (ik|jb) d_{b\bar{b}}^{ij} \Big) \bar{t}_{\bar{a}}^k \Bigg) + \sum_{\bar{c}} (j\bar{c}|\bar{a}\bar{b}) \bar{t}_{\bar{c}}^i \quad , \end{aligned} \tag{A.14}$$

$$\bar{\tilde{J}}_{\bar{a}\bar{b}}^{ij} = \quad \bar{J}_{\bar{a}\bar{b}}^{ij} - \sum_k \left(\tfrac{1}{2} \left(\mathbf{S}^{ij,kj} \bar{\mathbf{K}}^{kj} \mathbf{S}^{kj,ik} \bar{\boldsymbol{\tau}}^{ki\dagger} \mathbf{S}^{ik,ij} \right)_{\bar{a}\bar{b}} + \Big(\sum_a (ij|ka) d_{a\bar{a}}^{ik} \Big) \bar{t}_{\bar{b}}^k \right) + \sum_{\bar{c}} (j\bar{b}|\bar{a}\bar{c})\, \bar{t}_{\bar{c}}^i \quad . \tag{A.15}$$

B. The working equations for open-shell LPNO-CCSD

The complete open-shell LPNO-CCSD working equations, as they are implemented in the ORCA[206] quantum chemistry program package, are given below. The terms highlighted in blue (Eq. (B.21) – (B.25); Eq. (B.28) – (B.29)) are neglected in the actual implementation.

The α-spin singles residual reads

$$\begin{aligned} R_{a_\alpha}^{i_\alpha} = \; & F_{a_\alpha i_\alpha} + \sum_{b_\alpha} \tilde{F}_{a_\alpha b_\alpha} t_{b_\alpha}^{i_\alpha} - \sum_{j_\alpha} t_{a_\alpha}^{j_\alpha} \tilde{F}_{j_\alpha i_\alpha} + \mathbf{G}_\alpha(\mathbf{t}_1)_{i_\alpha a_\alpha} \\ & + \sum_{j_\alpha, b_\alpha} \left(\tilde{F}_{j_\alpha b_\alpha} \left(\mathbf{d}^{i_\alpha j_\alpha} \overline{\mathbf{t}}^{i_\alpha j_\alpha} \mathbf{d}^{i_\alpha j_\alpha \dagger} \right)_{a_\alpha b_\alpha} + t_{a_\alpha}^{j_\alpha} \left(\tilde{F}_{j_\alpha b_\alpha} - 2\, F_{j_\alpha b_\alpha} \right) t_{b_\alpha}^{i_\alpha} \right) \\ & + \sum_{j_\beta, b_\beta} \tilde{F}_{j_\beta b_\beta} \left(\mathbf{d}^{i_\alpha j_\beta(\alpha)} \overline{\mathbf{t}}^{i_\alpha j_\beta} \mathbf{d}^{i_\alpha j_\beta(\beta)\dagger} \right)_{a_\alpha b_\beta} \\ & - \sum_{j_\alpha, k_\alpha, b_\alpha} \left(\mathbf{d}^{j_\alpha k_\alpha} \overline{\boldsymbol{\tau}}^{j_\alpha k_\alpha} \mathbf{d}^{j_\alpha k_\alpha \dagger} \right)_{a_\alpha b_\alpha} (i_\alpha j_\alpha | k_\alpha b_\alpha) \\ & - \sum_{j_\alpha, k_\beta, b_\beta} \left(\mathbf{d}^{j_\alpha k_\beta(\alpha)} \overline{\boldsymbol{\tau}}^{j_\alpha k_\beta} \mathbf{d}^{j_\alpha k_\beta(\beta)\dagger} \right)_{a_\alpha b_\beta} (i_\alpha j_\alpha | k_\beta b_\beta) \\ & + \sum_{j_\alpha, \bar{a}_\alpha} d_{a_\alpha \bar{a}_\alpha}^{i_\alpha j_\alpha} \left(\sum_{\bar{b}_\alpha, \bar{c}_\alpha} (j_\alpha \bar{b}_\alpha | \bar{a}_\alpha \bar{c}_\alpha) \overline{\tau}_{\bar{c}_\alpha \bar{b}_\alpha}^{i_\alpha j_\alpha} \right) \\ & + \sum_{j_\beta, \bar{a}_\alpha} d_{a_\alpha \bar{a}_\alpha}^{i_\alpha j_\beta(\alpha)} \left(\sum_{\bar{b}_\beta, \bar{c}_\alpha} (j_\beta \bar{b}_\beta | \bar{a}_\alpha \bar{c}_\alpha)\, \overline{\tau}_{\bar{c}_\alpha \bar{b}_\beta}^{i_\alpha j_\beta} \right) \\ \stackrel{!}{=} \; & 0 \quad , \end{aligned} \tag{B.1}$$

and the β-spin singles residual becomes

$$\begin{aligned} R_{a_\beta}^{i_\beta} = \; & F_{a_\beta i_\beta} + \sum_{b_\beta} \tilde{F}_{a_\beta b_\beta} t_{b_\beta}^{i_\beta} - \sum_{j_\beta} t_{a_\beta}^{j_\beta} \tilde{F}_{j_\beta i_\beta} + \mathbf{G}_\beta(\mathbf{t}_1)_{i_\beta a_\beta} \\ & + \sum_{j_\beta, b_\beta} \left(\tilde{F}_{j_\beta b_\beta} \left(\mathbf{d}^{i_\beta j_\beta} \overline{\mathbf{t}}^{i_\beta j_\beta} \mathbf{d}^{i_\beta j_\beta \dagger} \right)_{a_\beta b_\beta} + t_{a_\beta}^{j_\beta} \left(\tilde{F}_{j_\beta b_\beta} - 2\, F_{j_\beta b_\beta} \right) t_{b_\beta}^{i_\beta} \right) \\ & + \sum_{j_\alpha, b_\alpha} \tilde{F}_{j_\alpha b_\alpha} \left(\mathbf{d}^{j_\alpha i_\beta(\alpha)} \overline{\mathbf{t}}^{j_\alpha i_\beta} \mathbf{d}^{j_\alpha i_\beta(\beta)\dagger} \right)_{b_\alpha a_\beta} \end{aligned}$$

$$
\begin{aligned}
&- \sum_{j_\beta,k_\beta,b_\beta} \left(\mathbf{d}^{j_\beta k_\beta} \bar{\boldsymbol{\tau}}^{j_\beta k_\beta} \mathbf{d}^{j_\beta k_\beta\dagger}\right)_{a_\beta b_\beta} (i_\beta j_\beta | k_\beta b_\beta) \\
&- \sum_{j_\beta,k_\alpha,b_\alpha} \left(\mathbf{d}^{k_\alpha j_\beta(\alpha)} \bar{\boldsymbol{\tau}}^{k_\alpha j_\beta} \mathbf{d}^{k_\alpha j_\beta(\beta)\dagger}\right)_{b_\alpha a_\beta} (i_\beta j_\beta | k_\alpha b_\alpha) \\
&+ \sum_{j_\beta,\bar{a}_\beta} d^{i_\beta j_\beta}_{a_\beta \bar{a}_\beta} \left(\sum_{\bar{b}_\beta,\bar{c}_\beta} (j_\beta \bar{b}_\beta | \bar{a}_\beta \bar{c}_\beta) \bar{\tau}^{i_\beta j_\beta}_{\bar{c}_\beta \bar{b}_\beta} \right) \\
&+ \sum_{j_\alpha,\bar{a}_\beta} d^{j_\alpha i_\beta(\beta)}_{a_\beta \bar{a}_\beta} \left(\sum_{\bar{b}_\alpha,\bar{c}_\beta} (j_\alpha \bar{b}_\alpha | \bar{a}_\beta \bar{c}_\beta) \bar{\tau}^{j_\alpha i_\beta}_{\bar{b}_\alpha \bar{c}_\beta} \right) \\
\overset{!}{=}\ & 0 \quad . \qquad \text{(B.2)}
\end{aligned}
$$

The $\alpha\alpha$-spin doubles residual reads

$$
\begin{aligned}
\bar{R}^{i_\alpha j_\alpha}_{\bar{a}_\alpha \bar{b}_\alpha} = \ & \left(\bar{\mathbf{K}}^{i_\alpha j_\alpha} - \bar{\mathbf{K}}^{i_\alpha j_\alpha\dagger}\right)_{\bar{a}_\alpha \bar{b}_\alpha} \\
&+ \left(\bar{\mathbf{t}}^{i_\alpha j_\alpha} \mathbf{d}^{i_\alpha j_\alpha\dagger} \tilde{\bar{\mathbf{F}}}^{v\dagger}_{\alpha\alpha} \mathbf{d}^{i_\alpha j_\alpha} - \mathbf{d}^{i_\alpha j_\alpha\dagger} \tilde{\bar{\mathbf{F}}}^{v}_{\alpha\alpha} \mathbf{d}^{i_\alpha j_\alpha} \bar{\mathbf{t}}^{i_\alpha j_\alpha\dagger} \right)_{\bar{a}_\alpha \bar{b}_\alpha} + \bar{\tilde{\mathbf{K}}}\left(\bar{\boldsymbol{\tau}}^{i_\alpha j_\alpha}\right)_{\bar{a}_\alpha \bar{b}_\alpha} \\
&+ \sum_{k_\alpha} \Bigg(\left(-\tilde{\bar{F}}_{k_\alpha j_\alpha} \mathbf{S}^{i_\alpha j_\alpha, k_\alpha i_\alpha} \bar{\mathbf{t}}^{k_\alpha i_\alpha\dagger} \mathbf{S}^{i_\alpha j_\alpha, k_\alpha i_\alpha\dagger} - \tilde{\bar{F}}_{k_\alpha i_\alpha} \mathbf{S}^{i_\alpha j_\alpha, k_\alpha j_\alpha} \bar{\mathbf{t}}^{k_\alpha j_\alpha} \mathbf{S}^{i_\alpha j_\alpha, k_\alpha j_\alpha\dagger} \right)_{\bar{a}_\alpha \bar{b}_\alpha} \\
&\qquad + \sum_{l_\alpha} \left((i_\alpha \widetilde{k_\alpha | j_\alpha} l_\alpha) \mathbf{S}^{i_\alpha j_\alpha, k_\alpha l_\alpha} \bar{\boldsymbol{\tau}}^{k_\alpha l_\alpha} \mathbf{S}^{i_\alpha j_\alpha, k_\alpha l_\alpha\dagger} \right)_{\bar{a}_\alpha \bar{b}_\alpha} \Bigg) \\
&+ \sum_{k_\alpha} \Bigg(-\mathbf{S}^{i_\alpha j_\alpha, i_\alpha k_\alpha} \bar{\mathbf{t}}^{i_\alpha k_\alpha\dagger} \left(\mathbf{d}^{i_\alpha j_\alpha\dagger} \mathbf{K}^{j_\alpha k_\alpha} \mathbf{d}^{i_\alpha k_\alpha} - \mathbf{d}^{i_\alpha j_\alpha\dagger} \mathbf{J}^{j_\alpha k_\alpha}_{\alpha\alpha} \mathbf{d}^{i_\alpha k_\alpha} \right)^\dagger \\
&\qquad + \left(\mathbf{d}^{i_\alpha j_\alpha\dagger} \mathbf{K}^{j_\alpha k_\alpha} \mathbf{d}^{i_\alpha k_\alpha} - \mathbf{d}^{i_\alpha j_\alpha\dagger} \mathbf{J}^{j_\alpha k_\alpha}_{\alpha\alpha} \mathbf{d}^{i_\alpha k_\alpha} \right) \bar{\mathbf{t}}^{i_\alpha k_\alpha} \mathbf{S}^{i_\alpha j_\alpha, i_\alpha k_\alpha\dagger} \\
&\qquad - \mathbf{S}^{i_\alpha j_\alpha, k_\alpha j_\alpha} \bar{\mathbf{t}}^{k_\alpha j_\alpha\dagger} \left(\mathbf{d}^{i_\alpha j_\alpha\dagger} \mathbf{K}^{i_\alpha k_\alpha} \mathbf{d}^{k_\alpha j_\alpha} - \mathbf{d}^{i_\alpha j_\alpha\dagger} \mathbf{J}^{i_\alpha k_\alpha}_{\alpha\alpha} \mathbf{d}^{k_\alpha j_\alpha} \right)^\dagger \\
&\qquad + \left(\mathbf{d}^{i_\alpha j_\alpha\dagger} \mathbf{K}^{i_\alpha k_\alpha} \mathbf{d}^{k_\alpha j_\alpha} - \mathbf{d}^{i_\alpha j_\alpha\dagger} \mathbf{J}^{i_\alpha k_\alpha}_{\alpha\alpha} \mathbf{d}^{k_\alpha j_\alpha} \right) \bar{\mathbf{t}}^{k_\alpha j_\alpha} \mathbf{S}^{i_\alpha j_\alpha, k_\alpha j_\alpha\dagger} \Bigg)_{\bar{a}_\alpha \bar{b}_\alpha} \\
&+ \sum_{k_\alpha} \Bigg(+\mathbf{S}^{i_\alpha j_\alpha, i_\alpha k_\alpha} \bar{\mathbf{t}}^{i_\alpha k_\alpha} \mathbf{S}^{i_\alpha k_\alpha, j_\alpha k_\alpha} \bar{\tilde{\mathbf{K}}}^{j_\alpha k_\alpha\dagger} \mathbf{S}^{j_\alpha k_\alpha, i_\alpha j_\alpha} \\
&\qquad - \mathbf{S}^{j_\alpha k_\alpha, i_\alpha j_\alpha\dagger} \left(\mathbf{S}^{i_\alpha j_\alpha, i_\alpha k_\alpha} \bar{\mathbf{t}}^{i_\alpha k_\alpha} \mathbf{S}^{i_\alpha k_\alpha, j_\alpha k_\alpha} \bar{\tilde{\mathbf{K}}}^{j_\alpha k_\alpha\dagger} \right)^\dagger \\
&\qquad - \mathbf{S}^{i_\alpha j_\alpha, j_\alpha k_\alpha} \bar{\mathbf{t}}^{j_\alpha k_\alpha} \mathbf{S}^{j_\alpha k_\alpha, i_\alpha k_\alpha} \bar{\tilde{\mathbf{K}}}^{i_\alpha k_\alpha\dagger} \mathbf{S}^{i_\alpha k_\alpha, i_\alpha j_\alpha} \\
&\qquad + \mathbf{S}^{i_\alpha k_\alpha, i_\alpha j_\alpha\dagger} \left(\mathbf{S}^{i_\alpha j_\alpha, j_\alpha k_\alpha} \bar{\mathbf{t}}^{j_\alpha k_\alpha} \mathbf{S}^{j_\alpha k_\alpha, i_\alpha k_\alpha} \bar{\tilde{\mathbf{K}}}^{i_\alpha k_\alpha\dagger} \right)^\dagger \Bigg)_{\bar{a}_\alpha \bar{b}_\alpha}
\end{aligned}
$$

$$
\begin{aligned}
&+\sum_{k_\alpha}\Bigg(-\bar{t}^{k_\alpha}_{\bar{a}_\alpha}\Big(\Big(\mathbf{S}^{i_\alpha j_\alpha,j_\alpha k_\alpha}\big(\bar{\mathbf{K}}^{j_\alpha k_\alpha}\bar{\mathbf{t}}^{i_\alpha}\big)\Big)_{\bar{b}_\alpha}-\Big(\mathbf{S}^{i_\alpha j_\alpha,j_\alpha k_\alpha}\big(\bar{\mathbf{J}}^{j_\alpha k_\alpha}_{\alpha\alpha}\bar{\mathbf{t}}^{i_\alpha}\big)\Big)_{\bar{b}_\alpha}\\
&\qquad-\Big(\mathbf{S}^{i_\alpha j_\alpha,i_\alpha k_\alpha}\big(\bar{\mathbf{K}}^{i_\alpha k_\alpha}\bar{\mathbf{t}}^{j_\alpha}\big)\Big)_{\bar{b}_\alpha}+\Big(\mathbf{S}^{i_\alpha j_\alpha,i_\alpha k_\alpha}\big(\bar{\mathbf{J}}^{i_\alpha k_\alpha}_{\alpha\alpha}\bar{\mathbf{t}}^{j_\alpha}\big)\Big)_{\bar{b}_\alpha}\Big)\\
&\quad+\Big(\Big(\mathbf{S}^{i_\alpha j_\alpha,j_\alpha k_\alpha}\big(\bar{\mathbf{K}}^{j_\alpha k_\alpha}\bar{\mathbf{t}}^{i_\alpha}\big)\Big)_{\bar{a}_\alpha}-\Big(\mathbf{S}^{i_\alpha j_\alpha,j_\alpha k_\alpha}\big(\bar{\mathbf{J}}^{j_\alpha k_\alpha}_{\alpha\alpha}\bar{\mathbf{t}}^{i_\alpha}\big)\Big)_{\bar{a}_\alpha}\\
&\qquad-\Big(\mathbf{S}^{i_\alpha j_\alpha,i_\alpha k_\alpha}\big(\bar{\mathbf{K}}^{i_\alpha k_\alpha}\bar{\mathbf{t}}^{j_\alpha}\big)\Big)_{\bar{a}_\alpha}+\Big(\mathbf{S}^{i_\alpha j_\alpha,i_\alpha k_\alpha}\big(\bar{\mathbf{J}}^{i_\alpha k_\alpha}_{\alpha\alpha}\bar{\mathbf{t}}^{j_\alpha}\big)\Big)_{\bar{a}_\alpha}\Big)\bar{t}^{k_\alpha}_{\bar{b}_\alpha}\Bigg)_{\bar{a}_\alpha\bar{b}_\alpha}\\
&+\sum_{k_\beta}\Bigg(+\mathbf{S}^{i_\alpha j_\alpha,i_\alpha k_\beta(\alpha)}\bar{\mathbf{t}}^{i_\alpha k_\beta}\Big(\mathbf{d}^{i_\alpha j_\alpha\dagger}\mathbf{K}^{j_\alpha k_\beta}\mathbf{d}^{i_\alpha k_\beta(\beta)}\Big)^\dagger\\
&\qquad-\mathbf{d}^{i_\alpha j_\alpha\dagger}\mathbf{K}^{j_\alpha k_\beta}\mathbf{d}^{i_\alpha k_\beta(\beta)}\bar{\mathbf{t}}^{i_\alpha k_\beta\dagger}\mathbf{S}^{i_\alpha j_\alpha,i_\alpha k_\beta(\alpha)\dagger}\\
&\qquad-\mathbf{S}^{i_\alpha j_\alpha,j_\alpha k_\beta(\alpha)}\bar{\mathbf{t}}^{j_\alpha k_\beta}\Big(\mathbf{d}^{i_\alpha j_\alpha\dagger}\mathbf{K}^{i_\alpha k_\beta}\mathbf{d}^{j_\alpha k_\beta(\beta)}\Big)^\dagger\\
&\qquad+\mathbf{d}^{i_\alpha j_\alpha\dagger}\mathbf{K}^{i_\alpha k_\beta}\mathbf{d}^{j_\alpha k_\beta(\beta)}\bar{\mathbf{t}}^{j_\alpha k_\beta\dagger}\mathbf{S}^{i_\alpha j_\alpha,j_\alpha k_\beta(\alpha)\dagger}\Bigg)_{\bar{a}_\alpha\bar{b}_\alpha}\\
&+\sum_{k_\beta}\Bigg(+\mathbf{S}^{i_\alpha j_\alpha,i_\alpha k_\beta(\alpha)}\bar{\mathbf{t}}^{i_\alpha k_\beta}\mathbf{S}^{i_\alpha k_\beta(\beta),j_\alpha k_\beta(\beta)}\bar{\bar{\mathbf{K}}}^{j_\alpha k_\beta\dagger}\mathbf{S}^{i_\alpha j_\alpha,j_\alpha k_\beta(\alpha)\dagger}\\
&\qquad-\mathbf{S}^{i_\alpha j_\alpha,j_\alpha k_\beta(\alpha)}\Big(\mathbf{S}^{i_\alpha j_\alpha,i_\alpha k_\beta(\alpha)}\bar{\mathbf{t}}^{i_\alpha k_\beta}\mathbf{S}^{i_\alpha k_\beta(\beta),j_\alpha k_\beta(\beta)}\bar{\bar{\mathbf{K}}}^{j_\alpha k_\beta\dagger}\Big)^\dagger\\
&\qquad-\mathbf{S}^{i_\alpha j_\alpha,j_\alpha k_\beta(\alpha)}\bar{\mathbf{t}}^{j_\alpha k_\beta}\mathbf{S}^{j_\alpha k_\beta(\beta),i_\alpha k_\beta(\beta)}\bar{\bar{\mathbf{K}}}^{i_\alpha k_\beta\dagger}\mathbf{S}^{i_\alpha j_\alpha,i_\alpha k_\beta(\alpha)\dagger}\\
&\qquad+\mathbf{S}^{i_\alpha j_\alpha,i_\alpha k_\beta(\alpha)}\Big(\mathbf{S}^{i_\alpha j_\alpha,j_\alpha k_\beta(\alpha)}\bar{\mathbf{t}}^{j_\alpha k_\beta}\mathbf{S}^{j_\alpha k_\beta(\beta),i_\alpha k_\beta(\beta)}\bar{\bar{\mathbf{K}}}^{i_\alpha k_\beta\dagger}\Big)^\dagger\Bigg)_{\bar{a}_\alpha\bar{b}_\alpha}\\
&+\sum_{k_\alpha}\Bigg(\sum_{a_\alpha}\Big(\Big((i_\alpha k_\alpha|j_\alpha a_\alpha)-(j_\alpha k_\alpha|i_\alpha a_\alpha)\Big)d^{i_\alpha j_\alpha}_{a_\alpha\bar{a}_\alpha}\Big)\bar{t}^{k_\alpha}_{\bar{b}_\alpha}\\
&\qquad-\bar{t}^{k_\alpha}_{\bar{a}_\alpha}\sum_{b_\alpha}\Big(\Big((i_\alpha k_\alpha|j_\alpha b_\alpha)-(j_\alpha k_\alpha|i_\alpha b_\alpha)\Big)d^{i_\alpha j_\alpha}_{b_\alpha\bar{b}_\alpha}\Big)\Bigg)\\
&+\sum_{\bar{c}_\alpha}\Bigg(\Big((i_\alpha\bar{a}_\alpha|\bar{c}_\alpha\bar{b}_\alpha)-(i_\alpha\bar{b}_\alpha|\bar{a}_\alpha\bar{c}_\alpha)\Big)\bar{t}^{j_\alpha}_{\bar{c}_\alpha}-\Big((j_\alpha\bar{a}_\alpha|\bar{c}_\alpha\bar{b}_\alpha)-(j_\alpha\bar{b}_\alpha|\bar{a}_\alpha\bar{c}_\alpha)\Big)\bar{t}^{i_\alpha}_{\bar{c}_\alpha}\Bigg)\\
&\overset{!}{=}\quad 0\quad,
\end{aligned}
\tag{B.3}
$$

and the $\beta\beta$-spin doubles residual becomes

$$
\begin{aligned}
\bar{R}^{i_\beta j_\beta}_{\bar{a}_\beta \bar{b}_\beta} = \quad & \left(\bar{\mathbf{K}}^{i_\beta j_\beta} - \bar{\mathbf{K}}^{i_\beta j_\beta \dagger}\right)_{\bar{a}_\beta \bar{b}_\beta} \\
& + \left(\bar{\mathbf{t}}^{i_\beta j_\beta} \mathbf{d}^{i_\beta j_\beta \dagger} \bar{\tilde{\mathbf{F}}}^{v\dagger}_{\beta\beta} \mathbf{d}^{i_\beta j_\beta} - \mathbf{d}^{i_\beta j_\beta \dagger} \bar{\tilde{\mathbf{F}}}^{v}_{\beta\beta} \mathbf{d}^{i_\beta j_\beta} \bar{\mathbf{t}}^{i_\beta j_\beta \dagger}\right)_{\bar{a}_\beta \bar{b}_\beta} + \bar{\tilde{\mathbf{K}}}\left(\bar{\boldsymbol{\tau}}^{i_\beta j_\beta}\right)_{\bar{a}_\beta \bar{b}_\beta} \\
& + \sum_{k_\beta} \Bigg(\left(-\bar{\tilde{F}}_{k_\beta j_\beta} \mathbf{S}^{i_\beta j_\beta, k_\beta i_\beta} \bar{\mathbf{t}}^{k_\beta i_\beta \dagger} \mathbf{S}^{i_\beta j_\beta, k_\beta i_\beta \dagger} - \bar{\tilde{F}}_{k_\beta i_\beta} \mathbf{S}^{i_\beta j_\beta, k_\beta j_\beta} \bar{\mathbf{t}}^{k_\beta j_\beta} \mathbf{S}^{i_\beta j_\beta, k_\beta j_\beta \dagger} \right)_{\bar{a}_\beta \bar{b}_\beta} \\
& \qquad + \sum_{l_\beta} \left((i_\beta \widetilde{k_\beta | j_\beta} l_\beta) \mathbf{S}^{i_\beta j_\beta, k_\beta l_\beta} \bar{\boldsymbol{\tau}}^{k_\beta l_\beta} \mathbf{S}^{i_\beta j_\beta, k_\beta l_\beta \dagger} \right)_{\bar{a}_\beta \bar{b}_\beta} \Bigg) \\
& + \sum_{k_\beta} \Bigg(-\mathbf{S}^{i_\beta j_\beta, i_\beta k_\beta} \bar{\mathbf{t}}^{i_\beta k_\beta \dagger} \left(\mathbf{d}^{i_\beta j_\beta \dagger} \mathbf{K}^{j_\beta k_\beta} \mathbf{d}^{i_\beta k_\beta} - \mathbf{d}^{i_\beta j_\beta \dagger} \mathbf{J}^{j_\beta k_\beta}_{\beta\beta} \mathbf{d}^{i_\beta k_\beta} \right)^\dagger \\
& \qquad + \left(\mathbf{d}^{i_\beta j_\beta \dagger} \mathbf{K}^{j_\beta k_\beta} \mathbf{d}^{i_\beta k_\beta} - \mathbf{d}^{i_\beta j_\beta \dagger} \mathbf{J}^{j_\beta k_\beta}_{\beta\beta} \mathbf{d}^{i_\beta k_\beta} \right) \bar{\mathbf{t}}^{i_\beta k_\beta} \mathbf{S}^{i_\beta j_\beta, i_\beta k_\beta \dagger} \\
& \qquad - \mathbf{S}^{i_\beta j_\beta, k_\beta j_\beta} \bar{\mathbf{t}}^{k_\beta j_\beta \dagger} \left(\mathbf{d}^{i_\beta j_\beta \dagger} \mathbf{K}^{i_\beta k_\beta} \mathbf{d}^{k_\beta j_\beta} - \mathbf{d}^{i_\beta j_\beta \dagger} \mathbf{J}^{i_\beta k_\beta}_{\beta\beta} \mathbf{d}^{k_\beta j_\beta} \right)^\dagger \\
& \qquad + \left(\mathbf{d}^{i_\beta j_\beta \dagger} \mathbf{K}^{i_\beta k_\beta} \mathbf{d}^{k_\beta j_\beta} - \mathbf{d}^{i_\beta j_\beta \dagger} \mathbf{J}^{i_\beta k_\beta}_{\beta\beta} \mathbf{d}^{k_\beta j_\beta} \right) \bar{\mathbf{t}}^{k_\beta j_\beta} \mathbf{S}^{i_\beta j_\beta, k_\beta j_\beta \dagger} \Bigg)_{\bar{a}_\beta \bar{b}_\beta} \\
& + \sum_{k_\beta} \Bigg(+\mathbf{S}^{i_\beta j_\beta, i_\beta k_\beta} \bar{\mathbf{t}}^{i_\beta k_\beta} \mathbf{S}^{i_\beta k_\beta, j_\beta k_\beta} \bar{\tilde{\mathbf{K}}}^{j_\beta k_\beta \dagger} \mathbf{S}^{j_\beta k_\beta, i_\beta j_\beta} \\
& \qquad - \mathbf{S}^{j_\beta k_\beta, i_\beta j_\beta \dagger} \left(\mathbf{S}^{i_\beta j_\beta, i_\beta k_\beta} \bar{\mathbf{t}}^{i_\beta k_\beta} \mathbf{S}^{i_\beta k_\beta, j_\beta k_\beta} \bar{\tilde{\mathbf{K}}}^{j_\beta k_\beta \dagger} \right)^\dagger \\
& \qquad - \mathbf{S}^{i_\beta j_\beta, j_\beta k_\beta} \bar{\mathbf{t}}^{j_\beta k_\beta} \mathbf{S}^{j_\beta k_\beta, i_\beta k_\beta} \bar{\tilde{\mathbf{K}}}^{i_\beta k_\beta \dagger} \mathbf{S}^{i_\beta k_\beta, i_\beta j_\beta} \\
& \qquad + \mathbf{S}^{i_\beta k_\beta, i_\beta j_\beta \dagger} \left(\mathbf{S}^{i_\beta j_\beta, j_\beta k_\beta} \bar{\mathbf{t}}^{j_\beta k_\beta} \mathbf{S}^{j_\beta k_\beta, i_\beta k_\beta} \bar{\tilde{\mathbf{K}}}^{i_\beta k_\beta \dagger} \right)^\dagger \Bigg)_{\bar{a}_\beta \bar{b}_\beta} \\
& + \sum_{k_\beta} \Bigg(-\bar{t}^{k_\beta}_{\bar{a}_\beta} \Bigg(\left(\mathbf{S}^{i_\beta j_\beta, j_\beta k_\beta} \left(\bar{\mathbf{K}}^{j_\beta k_\beta} \bar{\mathbf{t}}^{i_\beta} \right) \right)_{\bar{b}_\beta} - \left(\mathbf{S}^{i_\beta j_\beta, j_\beta k_\beta} \left(\bar{\mathbf{J}}^{j_\beta k_\beta}_{\beta\beta} \bar{\mathbf{t}}^{i_\beta} \right) \right)_{\bar{b}_\beta} \\
& \qquad - \left(\mathbf{S}^{i_\beta j_\beta, i_\beta k_\beta} \left(\bar{\mathbf{K}}^{i_\beta k_\beta} \bar{\mathbf{t}}^{j_\beta} \right) \right)_{\bar{b}_\beta} + \left(\mathbf{S}^{i_\beta j_\beta, i_\beta k_\beta} \left(\bar{\mathbf{J}}^{i_\beta k_\beta}_{\beta\beta} \bar{\mathbf{t}}^{j_\beta} \right) \right)_{\bar{b}_\beta} \Bigg) \\
& \qquad + \Bigg(\left(\mathbf{S}^{i_\beta j_\beta, j_\beta k_\beta} \left(\bar{\mathbf{K}}^{j_\beta k_\beta} \bar{\mathbf{t}}^{i_\beta} \right) \right)_{\bar{a}_\beta} - \left(\mathbf{S}^{i_\beta j_\beta, j_\beta k_\beta} \left(\bar{\mathbf{J}}^{j_\beta k_\beta}_{\beta\beta} \bar{\mathbf{t}}^{i_\beta} \right) \right)_{\bar{a}_\beta} \\
& \qquad - \left(\mathbf{S}^{i_\beta j_\beta, i_\beta k_\beta} \left(\bar{\mathbf{K}}^{i_\beta k_\beta} \bar{\mathbf{t}}^{j_\beta} \right) \right)_{\bar{a}_\beta} + \left(\mathbf{S}^{i_\beta j_\beta, i_\beta k_\beta} \left(\bar{\mathbf{J}}^{i_\beta k_\beta}_{\beta\beta} \bar{\mathbf{t}}^{j_\beta} \right) \right)_{\bar{a}_\beta} \Bigg) \bar{t}^{k_\beta}_{\bar{b}_\beta} \Bigg)_{\bar{a}_\beta \bar{b}_\beta}
\end{aligned}
$$

$$
\begin{aligned}
&+\sum_{k_\alpha}\Bigg(\mathbf{S}^{i_\beta j_\beta,k_\alpha i_\beta(\beta)}\overline{\mathbf{t}}^{k_\alpha i_\beta\dagger}\mathbf{d}^{k_\alpha i_\beta(\alpha)\dagger}\mathbf{K}^{k_\alpha j_\beta}\mathbf{d}^{i_\beta j_\beta}\\
&\quad-\Big(\mathbf{d}^{k_\alpha i_\beta(\alpha)\dagger}\mathbf{K}^{k_\alpha j_\beta}\mathbf{d}^{i_\beta j_\beta}\Big)^\dagger\overline{\mathbf{t}}^{k_\alpha i_\beta}\mathbf{S}^{i_\beta j_\beta,k_\alpha i_\beta(\beta)\dagger}\\
&\quad-\mathbf{S}^{i_\beta j_\beta,k_\alpha j_\beta(\beta)}\overline{\mathbf{t}}^{k_\alpha j_\beta\dagger}\mathbf{d}^{k_\alpha j_\beta(\alpha)\dagger}\mathbf{K}^{k_\alpha i_\beta}\mathbf{d}^{i_\beta j_\beta}\\
&\quad+\Big(\mathbf{d}^{k_\alpha j_\beta(\alpha)\dagger}\mathbf{K}^{k_\alpha i_\beta}\mathbf{d}^{i_\beta j_\beta}\Big)^\dagger\overline{\mathbf{t}}^{k_\alpha j_\beta}\mathbf{S}^{i_\beta j_\beta,k_\alpha j_\beta(\beta)\dagger}\Bigg)_{\bar a_\beta\bar b_\beta}\\
&+\sum_{k_\alpha}\Bigg(+\mathbf{S}^{i_\beta j_\beta,k_\alpha i_\beta(\beta)}\overline{\mathbf{t}}^{k_\alpha i_\beta\dagger}\mathbf{S}^{k_\alpha i_\beta(\alpha),k_\alpha j_\beta(\alpha)}\bar{\bar{\mathbf{K}}}^{j_\beta k_\alpha\dagger}\mathbf{S}^{k_\alpha j_\beta(\beta),i_\beta j_\beta}\\
&\quad-\mathbf{S}^{k_\alpha j_\beta(\beta),i_\beta j_\beta\dagger}\Big(\mathbf{S}^{i_\beta j_\beta,k_\alpha i_\beta(\beta)}\overline{\mathbf{t}}^{k_\alpha i_\beta\dagger}\mathbf{S}^{k_\alpha i_\beta(\alpha),k_\alpha j_\beta(\alpha)}\bar{\bar{\mathbf{K}}}^{j_\beta k_\alpha\dagger}\Big)^\dagger\\
&\quad-\mathbf{S}^{i_\beta j_\beta,k_\alpha j_\beta(\beta)}\overline{\mathbf{t}}^{k_\alpha j_\beta\dagger}\mathbf{S}^{k_\alpha j_\beta(\alpha),k_\alpha i_\beta(\alpha)}\bar{\bar{\mathbf{K}}}^{i_\beta k_\alpha\dagger}\mathbf{S}^{k_\alpha i_\beta(\beta),i_\beta j_\beta}\\
&\quad+\mathbf{S}^{k_\alpha i_\beta(\beta),i_\beta j_\beta\dagger}\Big(\mathbf{S}^{i_\beta j_\beta,k_\alpha j_\beta(\beta)}\overline{\mathbf{t}}^{k_\alpha j_\beta\dagger}\mathbf{S}^{k_\alpha j_\beta(\alpha),k_\alpha i_\beta(\alpha)}\bar{\bar{\mathbf{K}}}^{i_\beta k_\alpha\dagger}\Big)^\dagger\Bigg)_{\bar a_\beta\bar b_\beta}\\
&+\sum_{k_\beta}\Bigg(\sum_{a_\beta}\Bigg(\Big((i_\beta k_\beta|j_\beta a_\beta)-(j_\beta k_\beta|i_\beta a_\beta)\Big)d^{i_\beta j_\beta}_{a_\beta\bar a_\beta}\Bigg)\overline{t}^{k_\beta}_{\bar b_\beta}\\
&\quad-\overline{t}^{k_\beta}_{\bar a_\beta}\sum_{b_\beta}\Bigg(\Big((i_\beta k_\beta|j_\beta b_\beta)-(j_\beta k_\beta|i_\beta b_\beta)\Big)d^{i_\beta j_\beta}_{b_\beta\bar b_\beta}\Bigg)\Bigg)\\
&+\sum_{\bar c_\beta}\Bigg(\Big((i_\beta\bar a_\beta|\bar c_\beta\bar b_\beta)-(i_\beta\bar b_\beta|\bar a_\beta\bar c_\beta)\Big)\overline{t}^{j_\beta}_{\bar c_\beta}-\Big((j_\beta\bar a_\beta|\bar c_\beta\bar b_\beta)-(j_\beta\bar b_\beta|\bar a_\beta\bar c_\beta)\Big)\overline{t}^{i_\beta}_{\bar c_\beta}\Bigg)\\
&\overset{!}{=}\ 0\quad,
\end{aligned}
\tag{B.4}
$$

while the $\alpha\beta$-spin doubles residual is given by

$$
\begin{aligned}
\bar R^{i_\alpha j_\beta}_{\bar a_\alpha\bar b_\beta}=\ &\Big(\bar{\mathbf{K}}^{i_\alpha j_\beta}\Big)_{\bar a_\alpha\bar b_\beta}+\Big(\overline{\mathbf{t}}^{i_\alpha j_\beta}\mathbf{d}^{i_\alpha j_\beta(\beta)\dagger}\tilde{\bar{\mathbf{F}}}^{v\dagger}_{\beta\beta}\mathbf{d}^{i_\alpha j_\beta(\beta)}+\mathbf{d}^{i_\alpha j_\beta(\alpha)\dagger}\tilde{\bar{\mathbf{F}}}^{v}_{\alpha\alpha}\mathbf{d}^{i_\alpha j_\beta(\alpha)}\overline{\mathbf{t}}^{i_\alpha j_\beta}\Big)_{\bar a_\alpha\bar b_\beta}+\bar{\bar{\mathbf{K}}}\Big(\bar{\boldsymbol{\tau}}^{i_\alpha j_\beta}\Big)_{\bar a_\alpha\bar b_\beta}\\
&+\sum_{k_\alpha}\Bigg(-\Big(\tilde{\bar F}_{k_\alpha i_\alpha}\mathbf{S}^{i_\alpha j_\beta(\alpha),k_\alpha j_\beta(\alpha)}\overline{\mathbf{t}}^{k_\alpha j_\beta}\mathbf{S}^{i_\alpha j_\beta(\beta),k_\alpha j_\beta(\beta)\dagger}\Big)_{\bar a_\alpha\bar b_\beta}\\
&\quad+\sum_{l_\beta}\Big((i_\alpha\widetilde{k_\alpha|j_\beta}l_\beta)\mathbf{S}^{i_\alpha j_\beta(\alpha),k_\alpha l_\beta(\alpha)}\bar{\boldsymbol{\tau}}^{k_\alpha l_\beta}\mathbf{S}^{i_\alpha j_\beta(\beta),k_\alpha l_\beta(\beta)\dagger}\Big)_{\bar a_\alpha\bar b_\beta}\Bigg)\\
&-\sum_{k_\beta}\Big(\tilde{\bar F}_{k_\beta j_\beta}\mathbf{S}^{i_\alpha j_\beta(\alpha),i_\alpha k_\beta(\alpha)}\overline{\mathbf{t}}^{i_\alpha k_\beta}\mathbf{S}^{i_\alpha j_\beta(\beta),i_\alpha k_\beta(\beta)\dagger}\Big)_{\bar a_\alpha\bar b_\beta}
\end{aligned}
$$

$$
\begin{aligned}
&+\sum_{k_\alpha}\Bigg(+\Big(\mathbf{d}^{i_\alpha j_\beta(\alpha)\dagger}\mathbf{K}^{i_\alpha k_\alpha}\mathbf{d}^{k_\alpha j_\beta(\alpha)}-\mathbf{d}^{i_\alpha j_\beta(\alpha)\dagger}\mathbf{J}^{i_\alpha k_\alpha}_{\alpha\alpha}\mathbf{d}^{k_\alpha j_\beta(\alpha)}\Big)\bar{\mathbf{t}}^{k_\alpha j_\beta}\mathbf{S}^{k_\alpha j_\beta(\beta),i_\alpha j_\beta(\beta)}\\
&\quad-\mathbf{S}^{i_\alpha j_\beta(\alpha),k_\alpha j_\beta(\alpha)}\bar{\mathbf{t}}^{k_\alpha j_\beta}\Big(\mathbf{d}^{i_\alpha j_\beta(\beta)\dagger}\mathbf{J}^{i_\alpha k_\alpha}_{\alpha\beta}\mathbf{d}^{k_\alpha j_\beta(\beta)}\Big)^\dagger\\
&\quad+\mathbf{S}^{i_\alpha k_\alpha,i_\alpha j_\beta(\alpha)\dagger}\bar{\mathbf{t}}^{i_\alpha k_\alpha\dagger}\mathbf{d}^{i_\alpha k_\alpha\dagger}\mathbf{K}^{k_\alpha j_\beta}\mathbf{d}^{i_\alpha j_\beta(\beta)}\Bigg)_{\bar{a}_\alpha\bar{b}_\beta}\\
&+\sum_{k_\beta}\Bigg(+\mathbf{S}^{i_\alpha j_\beta(\alpha),i_\alpha k_\beta(\alpha)}\bar{\mathbf{t}}^{i_\alpha k_\beta}\Big(\mathbf{d}^{i_\alpha j_\beta(\beta)\dagger}\mathbf{K}^{j_\beta k_\beta}\mathbf{d}^{i_\alpha k_\beta(\beta)}-\mathbf{d}^{i_\alpha j_\beta(\beta)\dagger}\mathbf{J}^{j_\beta k_\beta}_{\beta\beta}\mathbf{d}^{i_\alpha k_\beta(\beta)}\Big)^\dagger\\
&\quad-\mathbf{d}^{i_\alpha j_\beta(\alpha)\dagger}\mathbf{J}^{j_\beta k_\beta}_{\beta\alpha}\mathbf{d}^{i_\alpha k_\beta(\alpha)}\bar{\mathbf{t}}^{i_\alpha k_\beta}\mathbf{S}^{i_\alpha k_\beta(\beta),i_\alpha j_\beta(\beta)}\\
&\quad-\mathbf{d}^{i_\alpha j_\beta(\alpha)\dagger}\mathbf{K}^{i_\alpha k_\beta}\mathbf{d}^{i_\alpha k_\beta(\beta)}\bar{\mathbf{t}}^{j_\beta k_\beta}\mathbf{S}^{j_\beta k_\beta,i_\alpha j_\beta(\beta)}\Bigg)_{\bar{a}_\alpha\bar{b}_\beta}\\
&+\sum_{k_\alpha}\Bigg(+\mathbf{S}^{i_\alpha k_\alpha,i_\alpha j_\beta(\alpha)\dagger}\bar{\bar{\mathbf{K}}}^{i_\alpha k_\alpha}\mathbf{S}^{i_\alpha k_\alpha,k_\alpha j_\beta(\alpha)}\bar{\mathbf{t}}^{k_\alpha j_\beta}\mathbf{S}^{k_\alpha j_\beta(\beta),i_\alpha j_\beta(\beta)}\\
&\quad-\mathbf{S}^{i_\alpha j_\beta(\alpha),k_\alpha j_\beta(\alpha)}\bar{\mathbf{t}}^{k_\alpha j_\beta}\mathbf{d}^{k_\alpha j_\beta(\beta)\dagger}\tilde{\mathbf{J}}^{k_\alpha i_\alpha}_{\alpha\beta}\mathbf{d}^{i_\alpha j_\beta(\beta)}\\
&\quad+\mathbf{S}^{i_\alpha k_\alpha,i_\alpha j_\beta(\alpha)\dagger}\bar{\mathbf{t}}^{i_\alpha k_\alpha}\mathbf{S}^{i_\alpha k_\alpha,k_\alpha j_\beta(\alpha)}\bar{\bar{\mathbf{K}}}^{j_\beta k_\alpha\dagger}\mathbf{S}^{k_\alpha j_\beta(\beta),i_\alpha j_\beta(\beta)}\Bigg)_{\bar{a}_\alpha\bar{b}_\beta}\\
&+\sum_{k_\beta}\Bigg(+\mathbf{S}^{i_\alpha j_\beta(\alpha),i_\alpha k_\beta(\alpha)}\bar{\mathbf{t}}^{i_\alpha k_\beta}\mathbf{S}^{j_\beta k_\beta,i_\alpha k_\beta(\beta)\dagger}\bar{\bar{\mathbf{K}}}^{j_\beta k_\beta\dagger}\mathbf{S}^{j_\beta k_\beta,i_\alpha j_\beta(\beta)}\\
&\quad-\mathbf{d}^{i_\alpha j_\beta(\alpha)\dagger}\tilde{\mathbf{J}}^{j_\beta k_\beta}_{\beta\alpha}\mathbf{d}^{i_\alpha k_\beta(\alpha)}\bar{\mathbf{t}}^{i_\alpha k_\beta}\mathbf{S}^{i_\alpha k_\beta(\beta),i_\alpha j_\beta(\beta)}\\
&\quad+\mathbf{S}^{i_\alpha j_\beta(\alpha),i_\alpha k_\beta(\alpha)}\bar{\bar{\mathbf{K}}}^{i_\alpha k_\beta}\mathbf{S}^{k_\beta j_\beta,i_\alpha k_\beta(\beta)\dagger}\bar{\mathbf{t}}^{k_\beta j_\beta}\mathbf{S}^{k_\beta j_\beta,i_\alpha j_\beta(\beta)}\Bigg)_{\bar{a}_\alpha\bar{b}_\beta}\\
&+\sum_{k_\alpha}\Bigg(-\bar{t}^{k_\alpha}_{\bar{a}_\alpha}\Big(\Big(\mathbf{S}^{i_\alpha j_\beta(\beta),k_\alpha j_\beta(\beta)}\big(\bar{\mathbf{K}}^{k_\alpha j_\beta\dagger}\bar{\mathbf{t}}^{i_\alpha}\big)\Big)_{\bar{b}_\beta}+\Big(\mathbf{d}^{i_\alpha j_\beta(\beta)\dagger}\big(\mathbf{J}^{k_\alpha i_\alpha\dagger}_{\alpha\beta}\mathbf{t}^{j_\beta}\big)\Big)_{\bar{b}_\beta}\Big)\Bigg)_{\bar{a}_\alpha\bar{b}_\beta}\\
&+\sum_{k_\beta}\Bigg(-\Big(\Big(\mathbf{S}^{i_\alpha j_\beta(\alpha),i_\alpha k_\beta(\alpha)}\big(\bar{\mathbf{K}}^{i_\alpha k_\beta}\bar{\mathbf{t}}^{j_\beta}\big)\Big)_{\bar{a}_\alpha}+\Big(\mathbf{d}^{i_\alpha j_\beta(\alpha)\dagger}\big(\mathbf{J}^{j_\beta k_\beta}_{\beta\alpha}\mathbf{t}^{i_\alpha}\big)\Big)_{\bar{a}_\alpha}\Big)\bar{t}^{k_\beta}_{\bar{b}_\beta}\Bigg)_{\bar{a}_\alpha\bar{b}_\beta}\\
&-\sum_{k_\alpha}\bar{t}^{k_\alpha}_{\bar{a}_\alpha}\Bigg(\sum_{b_\beta}\Big((i_\alpha k_\alpha|j_\beta b_\beta)d^{i_\alpha j_\beta(\beta)}_{b_\beta\bar{b}_\beta}\Big)\Bigg)-\sum_{k_\beta}\Bigg(\sum_{a_\alpha}\Big((j_\beta k_\beta|i_\alpha a_\alpha)d^{i_\alpha j_\beta(\alpha)}_{a_\alpha\bar{a}_\alpha}\Big)\Bigg)\bar{t}^{k_\beta}_{\bar{b}_\beta}\\
&+\sum_{\bar{c}_\alpha}(j_\beta\bar{b}_\beta|\bar{a}_\alpha\bar{c}_\alpha)\bar{t}^{i_\alpha}_{\bar{c}_\alpha}+\sum_{\bar{c}_\beta}(i_\alpha\bar{a}_\alpha|\bar{c}_\beta\bar{b}_\beta)\bar{t}^{j_\beta}_{\bar{c}_\beta}\\
&\stackrel{!}{=}\ 0\quad.
\end{aligned}
\tag{B.5}
$$

The 'dressed' quantities are given by:

$$\begin{aligned}\tilde{F}_{k_\alpha c_\alpha} = \quad & F_{k_\alpha c_\alpha} + \sum_{l_\alpha} \left(\mathbf{d}^{k_\alpha l_\alpha} \left(\bar{\mathbf{K}}^{k_\alpha l_\alpha} - \bar{\mathbf{K}}^{k_\alpha l_\alpha \dagger} \right) \mathbf{d}^{k_\alpha l_\alpha \dagger} \mathbf{t}^{l_\alpha} \right)_{c_\alpha} \\ & + \sum_{l_\beta} \left(\mathbf{d}^{k_\alpha l_\beta(\alpha)} \bar{\mathbf{K}}^{k_\alpha l_\beta} \mathbf{d}^{k_\alpha l_\beta(\beta)\dagger} \mathbf{t}^{l_\beta} \right)_{c_\alpha}\end{aligned} \tag{B.6}$$

$$\begin{aligned}\tilde{F}_{k_\beta c_\beta} = \quad & F_{k_\beta c_\beta} + \sum_{l_\beta} \left(\mathbf{d}^{k_\beta l_\beta} \left(\bar{\mathbf{K}}^{k_\beta l_\beta} - \bar{\mathbf{K}}^{k_\beta l_\beta \dagger} \right) \mathbf{d}^{k_\beta l_\beta \dagger} \mathbf{t}^{l_\beta} \right)_{c_\beta} \\ & + \sum_{l_\alpha} \left(\left(\mathbf{d}^{l_\alpha k_\beta(\alpha)} \bar{\mathbf{K}}^{l_\alpha k_\beta} \mathbf{d}^{l_\alpha k_\beta(\beta)\dagger} \right)^\dagger \mathbf{t}^{l_\alpha} \right)_{c_\beta}\end{aligned} \tag{B.7}$$

$$\begin{aligned}\tilde{F}_{a_\alpha c_\alpha} = \quad & F_{a_\alpha c_\alpha} - \tfrac{1}{2} \sum_{k_\alpha, l_\alpha} \left(\mathbf{d}^{k_\alpha l_\alpha} \left(\bar{\boldsymbol{\tau}}^{k_\alpha l_\alpha} \left(\bar{\mathbf{K}}^{k_\alpha l_\alpha} - \bar{\mathbf{K}}^{k_\alpha l_\alpha \dagger} \right)^\dagger \right) \mathbf{d}^{k_\alpha l_\alpha \dagger} \right)_{a_\alpha c_\alpha} \\ & - \sum_{k_\beta, l_\alpha} \left(\mathbf{d}^{l_\alpha k_\beta(\alpha)} \left(\bar{\boldsymbol{\tau}}^{l_\alpha k_\beta} \bar{\mathbf{K}}^{l_\alpha k_\beta \dagger} \right) \mathbf{d}^{l_\alpha k_\beta(\alpha)\dagger} \right)_{a_\alpha c_\alpha}\end{aligned} \tag{B.8}$$

$$\begin{aligned}\tilde{F}_{a_\beta c_\beta} = \quad & F_{a_\beta c_\beta} - \tfrac{1}{2} \sum_{k_\beta, l_\beta} \left(\mathbf{d}^{k_\beta l_\beta} \left(\bar{\boldsymbol{\tau}}^{k_\beta l_\beta} \left(\bar{\mathbf{K}}^{k_\beta l_\beta} - \bar{\mathbf{K}}^{k_\beta l_\beta \dagger} \right)^\dagger \right) \mathbf{d}^{k_\beta l_\beta \dagger} \right)_{a_\beta c_\beta} \\ & - \sum_{k_\alpha, l_\beta} \left(\mathbf{d}^{k_\alpha l_\beta(\beta)} \left(\bar{\boldsymbol{\tau}}^{k_\alpha l_\beta \dagger} \bar{\mathbf{K}}^{k_\alpha l_\beta} \right) \mathbf{d}^{k_\alpha l_\beta(\beta)\dagger} \right)_{a_\beta c_\beta}\end{aligned} \tag{B.9}$$

$$\begin{aligned}\tilde{F}_{k_\alpha i_\alpha} = \quad & F_{k_\alpha i_\alpha} + \tfrac{1}{2} \sum_{l_\alpha} \left\langle \left(\mathbf{S}^{i_\alpha l_\alpha, k_\alpha l_\alpha} \left(\bar{\mathbf{K}}^{k_\alpha l_\alpha} - \bar{\mathbf{K}}^{k_\alpha l_\alpha \dagger} \right) \mathbf{S}^{i_\alpha l_\alpha, k_\alpha l_\alpha \dagger} \right) \bar{\boldsymbol{\tau}}^{i_\alpha l_\alpha \dagger} \right\rangle \\ & + \sum_{l_\beta} \left\langle \left(\mathbf{S}^{i_\alpha l_\beta(\alpha), k_\alpha l_\beta(\alpha)} \bar{\mathbf{K}}^{k_\alpha l_\beta} \mathbf{S}^{i_\alpha l_\beta(\beta), k_\alpha l_\beta(\beta)\dagger} \right) \bar{\boldsymbol{\tau}}^{i_\alpha l_\beta \dagger} \right\rangle\end{aligned} \tag{B.10}$$

$$\begin{aligned}\tilde{F}_{k_\beta i_\beta} = \quad & F_{k_\beta i_\beta} + \tfrac{1}{2} \sum_{l_\beta} \left\langle \left(\mathbf{S}^{i_\beta l_\beta, k_\beta l_\beta} \left(\bar{\mathbf{K}}^{k_\beta l_\beta} - \bar{\mathbf{K}}^{k_\beta l_\beta \dagger} \right) \mathbf{S}^{i_\beta l_\beta, k_\beta l_\beta \dagger} \right) \bar{\boldsymbol{\tau}}^{i_\beta l_\beta \dagger} \right\rangle \\ & + \sum_{l_\alpha} \left\langle \left(\mathbf{S}^{l_\alpha i_\beta(\alpha), l_\alpha k_\beta(\alpha)} \bar{\mathbf{K}}^{l_\alpha k_\beta} \mathbf{S}^{l_\alpha i_\beta(\beta), l_\alpha k_\beta(\beta)\dagger} \right) \bar{\boldsymbol{\tau}}^{l_\alpha i_\beta \dagger} \right\rangle\end{aligned} \tag{B.11}$$

$$\mathbf{G}_\alpha(\mathbf{t}_1)_{p_\alpha q_\alpha} = \sum_{j_\alpha, b_\alpha} \left((p_\alpha q_\alpha | j_\alpha b_\alpha) - (p_\alpha j_\alpha | q_\alpha b_\alpha) \right) t_{b_\alpha}^{j_\alpha} + \sum_{j_\beta, b_\beta} (p_\alpha q_\alpha | j_\beta b_\beta)\, t_{b_\beta}^{j_\beta} \tag{B.12}$$

$$\mathbf{G}_\beta(\mathbf{t}_1)_{p_\beta q_\beta} = \sum_{j_\beta, b_\beta} \left((p_\beta q_\beta | j_\beta b_\beta) - (p_\beta j_\beta | q_\beta b_\beta) \right) t_{b_\beta}^{j_\beta} + \sum_{j_\alpha, b_\alpha} (p_\beta q_\beta | j_\alpha b_\alpha)\, t_{b_\alpha}^{j_\alpha} \tag{B.13}$$

$$\tilde{\tilde{F}}_{a_\alpha c_\alpha} = \tilde{F}_{a_\alpha c_\alpha} + \mathbf{G}_\alpha(\mathbf{t}^1)_{c_\alpha a_\alpha} - \sum_{i_\alpha} t^{i_\alpha}_{a_\alpha} F_{i_\alpha c_\alpha} \tag{B.14}$$

$$\tilde{\tilde{F}}_{a_\beta c_\beta} = \tilde{F}_{a_\beta c_\beta} + \mathbf{G}_\beta(\mathbf{t}^1)_{c_\beta a_\beta} - \sum_{i_\beta} t^{i_\beta}_{a_\beta} F_{i_\beta c_\beta} \tag{B.15}$$

$$\tilde{\tilde{F}}_{k_\alpha i_\alpha} = \tilde{F}_{k_\alpha i_\alpha} + \mathbf{G}_\alpha(\mathbf{t}^1)_{i_\alpha k_\alpha} + \sum_{a_\alpha} t^{i_\alpha}_{a_\alpha} F_{k_\alpha a_\alpha} \tag{B.16}$$

$$\tilde{\tilde{F}}_{k_\beta i_\beta} = \tilde{F}_{k_\beta i_\beta} + \mathbf{G}_\beta(\mathbf{t}^1)_{i_\beta k_\beta} + \sum_{a_\beta} t^{i_\beta}_{a_\beta} F_{k_\beta a_\beta} \tag{B.17}$$

$$\begin{aligned}(i_\alpha \widetilde{k_\alpha | j_\alpha} l_\alpha) = \;& (i_\alpha k_\alpha | j_\alpha l_\alpha) + \tfrac{1}{2}\left\langle \left(\mathbf{S}^{i_\alpha j_\alpha, k_\alpha l_\alpha} \bar{\mathbf{K}}^{k_\alpha l_\alpha} \mathbf{S}^{i_\alpha j_\alpha, k_\alpha l_\alpha \dagger}\right) \bar{\boldsymbol{\tau}}^{i_\alpha j_\alpha \dagger} \right\rangle \\ & + \sum_{a_\alpha} \left((l_\alpha j_\alpha | k_\alpha a_\alpha) t^{i_\alpha}_{a_\alpha} + (k_\alpha i_\alpha | l_\alpha a_\alpha) t^{j_\alpha}_{a_\alpha} \right)\end{aligned} \tag{B.18}$$

$$\begin{aligned}(i_\beta \widetilde{k_\beta | j_\beta} l_\beta) = \;& (i_\beta k_\beta | j_\beta l_\beta) + \tfrac{1}{2}\left\langle \left(\mathbf{S}^{i_\beta j_\beta, k_\beta l_\beta} \bar{\mathbf{K}}^{k_\beta l_\beta} \mathbf{S}^{i_\beta j_\beta, k_\beta l_\beta \dagger}\right) \bar{\boldsymbol{\tau}}^{i_\beta j_\beta \dagger} \right\rangle \\ & + \sum_{a_\beta} \left((l_\beta j_\beta | k_\beta a_\beta) t^{i_\beta}_{a_\beta} + (k_\beta i_\beta | l_\beta a_\beta) t^{j_\beta}_{a_\beta} \right)\end{aligned} \tag{B.19}$$

$$\begin{aligned}(i_\alpha \widetilde{k_\alpha | j_\beta} l_\beta) = \;& (i_\alpha k_\alpha | j_\beta l_\beta) + \left\langle \left(\mathbf{S}^{i_\alpha j_\beta(\alpha), k_\alpha l_\beta(\alpha)} \bar{\mathbf{K}}^{k_\alpha l_\beta} \mathbf{S}^{i_\alpha j_\beta(\beta), k_\alpha l_\beta(\beta)\dagger}\right) \bar{\boldsymbol{\tau}}^{i_\alpha j_\beta \dagger} \right\rangle \\ & + \sum_{a_\alpha} (l_\beta j_\beta | k_\alpha a_\alpha) t^{i_\alpha}_{a_\alpha} + \sum_{a_\beta} (k_\alpha i_\alpha | l_\beta a_\beta) t^{j_\beta}_{a_\beta}\end{aligned} \tag{B.20}$$

$$\bar{\tilde{\mathbf{K}}}(\bar{\boldsymbol{\tau}}^{i_\alpha j_\alpha})_{\bar{a}_\alpha \bar{b}_\alpha} = \sum_{\bar{c}_\alpha, \bar{d}_\alpha} \left((\bar{a}_\alpha \bar{c}_\alpha | \bar{b}_\alpha \bar{d}_\alpha) - \sum_{k_\alpha} \left((k_\alpha \bar{d}_\alpha | \bar{a}_\alpha \bar{c}_\alpha) \bar{t}^{k_\alpha}_{\bar{b}_\alpha} + \bar{t}^{k_\alpha}_{\bar{a}_\alpha} (k_\alpha \bar{c}_\alpha | \bar{b}_\alpha \bar{d}_\alpha) \right) \right) \bar{\tau}^{i_\alpha j_\alpha}_{\bar{c}_\alpha \bar{d}_\alpha} \tag{B.21}$$

$$\bar{\tilde{\mathbf{K}}}(\bar{\boldsymbol{\tau}}^{i_\beta j_\beta})_{\bar{a}_\beta \bar{b}_\beta} = \sum_{\bar{c}_\beta, \bar{d}_\beta} \left((\bar{a}_\beta \bar{c}_\beta | \bar{b}_\beta \bar{d}_\beta) - \sum_{k_\beta} \left((k_\beta \bar{d}_\beta | \bar{a}_\beta \bar{c}_\beta) \bar{t}^{k_\beta}_{\bar{b}_\beta} + \bar{t}^{k_\beta}_{\bar{a}_\beta} (k_\beta \bar{c}_\beta | \bar{b}_\beta \bar{d}_\beta) \right) \right) \bar{\tau}^{i_\beta j_\beta}_{\bar{c}_\beta \bar{d}_\beta} \tag{B.22}$$

$$\bar{\tilde{\mathbf{K}}}(\bar{\boldsymbol{\tau}}^{i_\alpha j_\beta})_{\bar{a}_\alpha \bar{b}_\beta} = \sum_{\bar{c}_\alpha, \bar{d}_\beta} \left((\bar{a}_\alpha \bar{c}_\alpha | \bar{b}_\beta \bar{d}_\beta) - \sum_{k_\beta} (k_\beta \bar{d}_\beta | \bar{a}_\alpha \bar{c}_\alpha) \bar{t}^{k_\beta}_{\bar{b}_\beta} - \sum_{k_\alpha} \bar{t}^{k_\alpha}_{\bar{a}_\alpha} (k_\alpha \bar{c}_\alpha | \bar{b}_\beta \bar{d}_\beta) \right) \tau^{i_\alpha j_\beta}_{\bar{c}_\alpha \bar{d}_\beta} \tag{B.23}$$

$$
\begin{aligned}
\bar{\tilde{K}}^{i_\alpha k_\alpha}_{\bar{a}_\alpha \bar{c}_\alpha} = \quad & \sum_{l_\alpha} \Bigg(\Big(\tfrac{1}{2} \mathbf{S}^{i_\alpha k_\alpha, i_\alpha l_\alpha} \bar{\mathbf{t}}^{i_\alpha l_\alpha} \mathbf{S}^{i_\alpha l_\alpha, k_\alpha l_\alpha} \left(\bar{\mathbf{K}}^{k_\alpha l_\alpha} - \bar{\mathbf{K}}^{k_\alpha l_\alpha \dagger} \right)^\dagger \mathbf{S}^{k_\alpha l_\alpha, i_\alpha k_\alpha} \Big)_{\bar{a}_\alpha \bar{c}_\alpha} \\
& \quad - \bar{t}^{l_\alpha}_{\bar{a}_\alpha} \Big(\mathbf{S}^{k_\alpha l_\alpha, i_\alpha k_\alpha \dagger} \left(\bar{\mathbf{K}}^{k_\alpha l_\alpha} \bar{\mathbf{t}}^{i_\alpha} - \bar{\mathbf{K}}^{k_\alpha l_\alpha \dagger} \bar{\mathbf{t}}^{i_\alpha} \right) \Big)_{\bar{c}_\alpha} \\
& \quad + \bar{t}^{l_\alpha}_{\bar{a}_\alpha} \Big(\sum_{c_\alpha} \left((i_\alpha k_\alpha | l_\alpha c_\alpha) - (i_\alpha l_\alpha | k_\alpha c_\alpha) \right) d^{i_\alpha k_\alpha}_{c_\alpha \bar{c}_\alpha} \Big) \Bigg) \\
& + \tfrac{1}{2} \sum_{l_\beta} \Big(\mathbf{S}^{i_\alpha k_\alpha, i_\alpha l_\beta(\alpha)} \bar{\mathbf{t}}^{i_\alpha l_\beta} \mathbf{S}^{i_\alpha l_\beta(\beta), k_\alpha l_\beta(\beta)} \bar{\mathbf{K}}^{k_\alpha l_\beta \dagger} \mathbf{S}^{k_\alpha l_\beta(\alpha), i_\alpha k_\alpha} \Big)_{\bar{a}_\alpha \bar{c}_\alpha} \\
& + \sum_{\bar{d}_\alpha} \Big((k_\alpha \bar{c}_\alpha | \bar{a}_\alpha \bar{d}_\alpha) - (k_\alpha \bar{d}_\alpha | \bar{a}_\alpha \bar{c}_\alpha) \Big) \bar{t}^{i_\alpha}_{\bar{d}_\alpha}
\end{aligned}
\tag{B.24}
$$

$$
\begin{aligned}
\bar{\tilde{K}}^{j_\beta k_\beta}_{\bar{b}_\beta \bar{c}_\beta} = \quad & \sum_{l_\beta} \Bigg(\Big(\tfrac{1}{2} \mathbf{S}^{j_\beta k_\beta, j_\beta l_\beta} \bar{\mathbf{t}}^{j_\beta l_\beta} \mathbf{S}^{j_\beta l_\beta, k_\beta l_\beta} \left(\bar{\mathbf{K}}^{k_\beta l_\beta} - \bar{\mathbf{K}}^{k_\beta l_\beta \dagger} \right)^\dagger \mathbf{S}^{k_\beta l_\beta, j_\beta k_\beta} \Big)_{\bar{b}_\beta \bar{c}_\beta} \\
& \quad - \bar{t}^{l_\beta}_{\bar{b}_\beta} \Big(\mathbf{S}^{k_\beta l_\beta, j_\beta k_\beta \dagger} \left(\bar{\mathbf{K}}^{k_\beta l_\beta} \bar{\mathbf{t}}^{j_\beta} - \bar{\mathbf{K}}^{k_\beta l_\beta \dagger} \bar{\mathbf{t}}^{j_\beta} \right) \Big)_{\bar{c}_\beta} \\
& \quad + \bar{t}^{l_\beta}_{\bar{b}_\beta} \Big(\sum_{c_\beta} \left((j_\beta k_\beta | l_\beta c_\beta) - (j_\beta l_\beta | k_\beta c_\beta) \right) d^{j_\beta k_\beta}_{c_\beta \bar{c}_\beta} \Big) \Bigg) \\
& + \tfrac{1}{2} \sum_{l_\alpha} \Big(\mathbf{S}^{j_\beta k_\beta, l_\alpha j_\beta(\beta)} \bar{\mathbf{t}}^{l_\alpha j_\beta \dagger} \mathbf{S}^{l_\alpha j_\beta(\alpha), l_\alpha k_\beta(\alpha)} \bar{\mathbf{K}}^{l_\alpha k_\beta} \mathbf{S}^{l_\alpha k_\beta(\beta), j_\beta k_\beta} \Big)_{\bar{b}_\beta \bar{c}_\beta} \\
& + \sum_{\bar{d}_\beta} \Big((k_\beta \bar{c}_\beta | \bar{b}_\beta \bar{d}_\beta) - (k_\beta \bar{d}_\beta | \bar{b}_\beta \bar{c}_\beta) \Big) \bar{t}^{j_\beta}_{\bar{d}_\beta}
\end{aligned}
\tag{B.25}
$$

$$
\begin{aligned}
\bar{\tilde{K}}^{j_\beta k_\alpha}_{\bar{b}_\beta \bar{c}_\alpha} = \quad & \sum_{l_\beta} \Bigg(\tfrac{1}{2} \Big(\mathbf{S}^{k_\alpha j_\beta(\beta), j_\beta l_\beta} \bar{\mathbf{t}}^{j_\beta l_\beta} \mathbf{S}^{j_\beta l_\beta, k_\alpha l_\beta(\beta)} \bar{\mathbf{K}}^{k_\alpha l_\beta \dagger} \mathbf{S}^{k_\alpha l_\beta(\alpha), k_\alpha j_\beta(\alpha)} \Big)_{\bar{b}_\beta \bar{c}_\alpha} \\
& \quad - \bar{t}^{l_\beta}_{\bar{b}_\beta} \Big(\mathbf{S}^{k_\alpha l_\beta(\alpha), k_\alpha j_\beta(\alpha) \dagger} (\bar{\mathbf{K}}^{k_\alpha l_\beta} \bar{\mathbf{t}}^{j_\beta}) \Big)_{\bar{c}_\alpha} - \bar{t}^{l_\beta}_{\bar{b}_\beta} \Big(\sum_{c_\alpha} (j_\beta l_\beta | k_\alpha c_\alpha) d^{k_\alpha j_\beta(\alpha)}_{c_\alpha \bar{c}_\alpha} \Big) \Bigg) \\
& + \tfrac{1}{2} \sum_{k_\alpha} \Big(\mathbf{S}^{k_\alpha j_\beta(\beta), l_\alpha j_\beta(\beta)} \bar{\mathbf{t}}^{l_\alpha j_\beta \dagger} \mathbf{S}^{l_\alpha j_\beta(\alpha), k_\alpha l_\alpha} \left(\bar{\mathbf{K}}^{k_\alpha l_\alpha} - \bar{\mathbf{K}}^{k_\alpha l_\alpha \dagger} \right)^\dagger \mathbf{S}^{k_\alpha l_\alpha, k_\alpha j_\beta(\alpha)} \Big)_{\bar{b}_\beta \bar{c}_\alpha} \\
& + \sum_{\bar{d}_\beta} (k_\alpha \bar{c}_\alpha | \bar{b}_\beta \bar{d}_\beta) \bar{t}^{j_\beta}_{\bar{d}_\beta}
\end{aligned}
\tag{B.26}
$$

$$
\begin{aligned}
\bar{\tilde{K}}^{i_\alpha k_\beta}_{\bar{a}_\alpha \bar{c}_\beta} = \quad & \sum_{l_\alpha} \Bigg(\tfrac{1}{2} \Big(\mathbf{S}^{i_\alpha k_\beta(\alpha), i_\alpha l_\alpha} \bar{\mathbf{t}}^{i_\alpha l_\alpha} \mathbf{S}^{i_\alpha l_\alpha, l_\alpha k_\beta(\alpha)} \bar{\mathbf{K}}^{l_\alpha k_\beta} \mathbf{S}^{l_\alpha k_\beta(\beta), i_\alpha k_\beta(\beta)} \Big)_{\bar{a}_\alpha \bar{c}_\beta} \\
& \quad - \bar{t}^{l_\alpha}_{\bar{a}_\alpha} \Big(\mathbf{S}^{l_\alpha k_\beta(\beta), i_\alpha k_\beta(\beta) \dagger} (\bar{\mathbf{K}}^{l_\alpha k_\beta \dagger} \bar{\mathbf{t}}^{i_\alpha}) \Big)_{\bar{c}_\beta} - \bar{t}^{l_\alpha}_{\bar{a}_\alpha} \Big(\sum_{c_\beta} (i_\alpha l_\alpha | k_\beta c_\beta) d^{i_\alpha k_\beta(\beta)}_{c_\beta \bar{c}_\beta} \Big) \Bigg)
\end{aligned}
$$

$$+\tfrac{1}{2}\sum_{l_\beta}\left(\mathbf{S}^{i_\alpha k_\beta(\alpha),i_\alpha l_\beta(\alpha)}\bar{\mathbf{t}}^{i_\alpha l_\beta}\mathbf{S}^{i_\alpha l_\beta(\beta),k_\beta l_\beta}\left(\bar{\mathbf{K}}^{k_\beta l_\beta}-\bar{\mathbf{K}}^{k_\beta l_\beta\dagger}\right)^{\dagger}\mathbf{S}^{k_\beta l_\beta,i_\alpha k_\beta(\beta)}\right)_{\bar{a}_\alpha\bar{c}_\beta}$$
$$+\sum_{\bar{d}_\alpha}(k_\beta\bar{c}_\beta|\bar{a}_\alpha\bar{d}_\alpha)\bar{t}^{i_\alpha}_{\bar{d}_\alpha} \tag{B.27}$$

$$\tilde{J}^{k_\alpha i_\alpha}_{c_\beta b_\beta} = \sum_{l_\beta}\left(-\tfrac{1}{2}\left(\mathbf{d}^{k_\alpha l_\beta(\beta)}\bar{\mathbf{K}}^{k_\alpha l_\beta\dagger}\mathbf{S}^{k_\alpha l_\beta(\alpha),i_\alpha l_\beta(\alpha)}\bar{\mathbf{t}}^{i_\alpha l_\beta}\mathbf{d}^{i_\alpha l_\beta(\beta)\dagger}\right)_{c_\beta b_\beta}\right.$$
$$\left.-\left((\mathbf{d}^{k_\alpha l_\beta(\alpha)}\bar{\mathbf{K}}^{k_\alpha l_\beta\dagger}\mathbf{d}^{k_\alpha l_\beta(\beta)\dagger})\mathbf{t}^{i_\alpha}\right)_{c_\beta}t^{l_\beta}_{b_\beta}-(i_\alpha k_\alpha|l_\beta c_\beta)\,t^{l_\beta}_{b_\beta}\right)$$
$$+\sum_{d_\alpha}t^{i_\alpha}_{d_\alpha}\,(k_\alpha d_\alpha|b_\beta c_\beta) \tag{B.28}$$

$$\tilde{J}^{j_\beta k_\beta}_{a_\alpha c_\alpha} = \sum_{l_\alpha}\left(-\tfrac{1}{2}\left(\mathbf{d}^{l_\alpha j_\beta(\alpha)}\bar{\mathbf{t}}^{l_\alpha j_\beta}\mathbf{S}^{l_\alpha j_\beta(\beta),l_\alpha k_\beta(\beta)}\bar{\mathbf{K}}^{l_\alpha k_\beta\dagger}\mathbf{d}^{l_\alpha k_\beta(\alpha)\dagger}\right)_{a_\alpha c_\alpha}\right.$$
$$\left.-t^{l_\alpha}_{a_\alpha}\left((\mathbf{d}^{l_\alpha k_\beta(\alpha)}\bar{\mathbf{K}}^{l_\alpha k_\beta}\mathbf{d}^{l_\alpha k_\beta(\beta)\dagger})\mathbf{t}^{j_\beta}\right)_{c_\alpha}-t^{l_\alpha}_{a_\alpha}\,(j_\beta k_\beta|l_\alpha c_\alpha)\right)$$
$$+\sum_{d_\beta}t^{j_\beta}_{d_\beta}\,(k_\beta d_\beta|a_\alpha c_\alpha) \tag{B.29}$$

C. More detailed documentation of selected results

Table C.1.: Error analysis of open-shell LPNO-CEPA/1 calculations for a series of medium sized high-spin open-shell molecules using QROs and default cut-off values together with the TZVPP basis set (TZVPP/C auxiliary basis). The geometries were either taken from the GMTKN24 data base[58] or can be found in the supplementary material of Ref. (198) (N_{BF}: number of basis functions; N_{Aux}: number of auxiliary functions; N_{PNO} (av): average number of significant PNOs for each electron pair; $\%E_{corr}$: percentage of the recovered correlation energy; Δ_{abs}: absolute deviation from the canonical reference values; TS: transition state; hs: high-spin).

				With MP2 correction		Only strong pairs	
Molecule	N_{BF}	N_{Aux}	N_{PNO} (av)	$\%E_{corr}$	Δ_{abs} (kcal/mol)	$\%E_{corr}$	Δ_{abs} (kcal/mol)
Quinone	304	728	27	99.58	3.80	98.53	13.38
Benzyl radical	315	742	31	99.62	2.78	98.82	8.56
Octyl radical	486	1118	26	99.74	2.45	98.80	11.17
$[Mn(H_2O)_6]^{2+}$ (hs)	394	973	24	99.77	2.45	98.54	15.50
$H_2NCHCONH_2$	225	530	26	99.60	2.49	98.83	7.28
$(CH_3)_3CCH_2$	309	710	26	99.79	1.21	98.66	7.85
$CH_3SO_2CH_2$	228	554	23	99.51	3.13	98.53	9.50
$NH_2 + C_2H_5$ (TS)	191	438	29	99.68	1.23	99.12	3.35

Table C.2.: Error analysis of open-shell LPNO-QCISD calculations for a series of medium sized high-spin open-shell molecules using QROs and default cut-off values together with the TZVPP basis set (TZVPP/C auxiliary basis). The geometries were either taken from the GMTKN24 data base[58] or can be found in the supplementary material of Ref. (198) (N_{BF}: number of basis functions; N_{Aux}: number of auxiliary functions; N_{PNO} (av): average number of significant PNOs for each electron pair; $\%E_{corr}$: percentage of the recovered correlation energy; Δ_{abs}: absolute deviation from the canonical reference values; TS: transition state; hs: high-spin).

				With MP2 correction		Only strong pairs	
Molecule	N_{BF}	N_{Aux}	N_{PNO} (av)	$\%E_{corr}$	Δ_{abs} (kcal/mol)	$\%E_{corr}$	Δ_{abs} (kcal/mol)
Quinone	304	728	27	99.67	2.95	98.60	12.53
Benzyl radical	315	742	31	99.70	2.17	98.89	7.95
Octyl radical	486	1118	26	99.78	2.05	98.84	10.77
$[Mn(H_2O)_6]^{2+}$ (hs)	394	973	24	99.80	2.15	98.56	15.21
$H_2NCHCONH_2$	225	530	26	99.67	2.06	98.89	6.85
$(CH_3)_3CCH_2$	309	710	26	99.80	1.14	98.66	7.78
$CH_3SO_2CH_2$	228	554	23	99.61	2.51	98.61	8.88
$NH_2 + C_2H_5$ (TS)	191	438	29	99.72	1.04	99.16	3.15

Table C.3.: Hyperfine coupling constants calculated with the (open-shell) VCEPA/1 method using the the basis sets documented in Sec. 3.1. All values are given in MHz (diagonal elements of the total hyperfine coupling tensor (superscript (A)) as well as the isotropic Fermi contact contribution (superscript $(A;c)$) and the anisotropic spin dipolar contributions (superscript $(A;d)$) are shown).

Molecule	Nucleus	$A_{11}^{(A)}$	$A_{22}^{(A)}$	$A_{33}^{(A)}$	$A^{(A;c)}$	$A_{11}^{(A;d)}$	$A_{22}^{(A;d)}$	$A_{33}^{(A;d)}$
$^2H_2O^+$	^{17}O	73	78	-370	-73	146	151	-297
$^2H_2O^+$	^1H	-4	-102	-131	-79	75	-23	-52
$^2H_2O^+$	^1H	-4	-102	-131	-79	75	-23	-52
^2HCO	^{17}O	-1	4	-160	-53	51	56	-108
^2HCO	^{13}C	311	317	440	356	-45	-39	84
^2HCO	^1H	352	360	390	367	-15	-7	23
$^2ClO_2$	^{35}Cl	-18	-21	190	50	-68	-71	139
$^2ClO_2$	^{17}O	35	37	-132	-20	55	57	-112
$^2ClO_2$	^{17}O	35	37	-132	-20	55	57	-112
$^2CH_3$	^{13}C	-3	-3	225	73	-76	-76	152
$^2CH_3$	^1H	-34	-71	-113	-73	38	2	-40
$^2CH_3$	^1H	-34	-71	-113	-73	38	2	-40
$^2CH_3$	^1H	-34	-71	-113	-73	38	2	-40
$^2SiH_3$	^{29}Si	-144	-144	-413	-234	90	90	-180
$^2SiH_3$	^1H	-60	-64	-83	-69	9	5	-14
$^2SiH_3$	^1H	-60	-64	-83	-69	9	5	-14
$^2SiH_3$	^1H	-60	-64	-83	-69	9	5	-14
$^2C_3H_5$	^{13}C	-19	-30	-51	-33	15	3	-18
$^2C_3H_5$	^{13}C	-13	-14	125	33	-45	-47	92
$^2C_3H_5$	^{13}C	-13	-14	125	33	-45	-47	92
$^2C_3H_5$	^1H	9	16	19	15	-6	2	5
$^2C_3H_5$	^1H	-24	-48	-73	-48	24	1	-25
$^2C_3H_5$	^1H	-21	-45	-64	-43	23	-1	-21
$^2C_3H_5$	^1H	-24	-48	-73	-48	24	1	-25
$^2C_3H_5$	^1H	-21	-45	-64	-43	23	-1	-21
^3NH	^{14}N	-26	39	39	17	-43	22	22
^3NH	^1H	-4	-97	-97	-66	62	-31	-31
$^3OH^+$	^{17}O	109	-125	-125	-47	156	-78	-78
$^3OH^+$	^1H	12	-119	-119	-75	87	-43	-43
$^3O_2$	^{17}O	44	-91	-91	-46	90	-45	-45
$^3O_2$	^{17}O	44	-91	-91	-46	90	-45	-45
$^3SH_+$	^{33}S	-31	108	108	62	-93	47	47
$^3SH_+$	^1H	-39	-76	-76	-63	24	-12	-12
$^3S_2$	^{33}S	-20	55	55	30	-50	25	25
$^3S_2$	^{33}S	-20	55	55	30	-50	25	25
^3SO	^{33}S	-34	56	56	26	-60	30	30
^3SO	^{17}O	32	-61	-61	-30	62	-31	-31
^2OH	^{17}O	93	94	-323	-45	138	140	-278
^2OH	^1H	17	-90	-145	-73	90	-18	-72
$^2NH_2$	^{14}N	-16	-17	110	26	-42	-42	84
$^2NH_2$	^1H	-6	-75	-124	-68	62	-7	-56
$^2NH_2$	^1H	-6	-75	-124	-68	62	-7	-56
^4N	^{14}N	9	9	9	9	0	0	0

Table C.4.: Errors in hyperfine coupling constants calculated with the (open-shell) LPNO-VCEPA/1 method using the default values for the thresholds and the basis sets documented in Sec. 3.1. The corresponding VCEPA/1 values (Table C.3) serve as reference. All values are given in MHz (MAD: mean absolute deviation; MD: mean deviation; MAX: maximum absolute deviation) Diagonal elements of the total hyperfine coupling tensor (superscript (A)) as well as the isotropic Fermi contact contribution (superscript $(A;c)$) and the anisotropic spin dipolar contributions (superscript $(A;d)$) are shown.

Molecule	Nucleus	$A_{11}^{(A)}$	$A_{22}^{(A)}$	$A_{33}^{(A)}$	$A^{(A;c)}$	$A_{11}^{(A;d)}$	$A_{22}^{(A;d)}$	$A_{33}^{(A;d)}$
$^2H_2O^+$	^{17}O	-7	-7	-9	-8	1	1	-1
$^2H_2O^+$	^1H	-2	-2	-2	-2	0	0	0
$^2H_2O^+$	^1H	-2	-2	-2	-2	0	0	0
^2HCO	^{17}O	3	5	6	5	-2	1	1
^2HCO	^{13}C	6	7	12	8	-2	-1	3
^2HCO	^1H	-2	-2	-1	-2	0	0	0
$^2ClO_2$	^{35}Cl	-3	-4	5	0	-3	-3	6
$^2ClO_2$	^{17}O	6	6	3	5	1	1	-2
$^2ClO_2$	^{17}O	6	6	3	5	1	1	-2
$^2CH_3$	^{13}C	5	5	6	5	0	0	0
$^2CH_3$	^1H	0	0	0	0	0	0	0
$^2CH_3$	^1H	0	0	0	0	0	0	0
$^2CH_3$	^1H	0	0	0	0	0	0	0
$^2SiH_3$	^{29}Si	2	2	2	2	0	0	0
$^2SiH_3$	^1H	1	1	1	1	0	0	0
$^2SiH_3$	^1H	1	1	1	1	0	0	0
$^2SiH_3$	^1H	1	1	1	1	0	0	0
$^2C_3H_5$	^{13}C	0	0	-8	-3	3	2	-5
$^2C_3H_5$	^{13}C	1	1	4	2	-1	-1	2
$^2C_3H_5$	^{13}C	1	1	4	2	-1	-1	2
$^2C_3H_5$	^1H	0	-1	2	0	0	-1	1
$^2C_3H_5$	^1H	-1	-1	-2	-1	0	0	-1
$^2C_3H_5$	^1H	0	0	-1	-1	0	0	-1
$^2C_3H_5$	^1H	-1	-1	-2	-1	0	0	-1
$^2C_3H_5$	^1H	0	0	-1	-1	0	0	-1
^3NH	^{14}N	-1	-1	-1	-1	0	0	0
^3NH	^1H	-1	-2	-2	-2	0	0	0
$^3OH^+$	^{17}O	-2	-2	-2	-2	0	0	0
$^3OH^+$	^1H	-3	-3	-3	-3	0	0	0
$^3O_2$	^{17}O	4	2	2	2	1	-1	-1
$^3O_2$	^{17}O	6	3	3	4	2	-1	-1
$^3SH_+$	^{33}S	-1	-1	-1	-1	0	0	0
$^3SH_+$	^1H	1	0	0	0	0	0	0
$^3S_2$	^{33}S	-1	0	0	0	0	0	0
$^3S_2$	^{33}S	-1	-1	-1	-1	0	0	0
^3SO	^{33}S	1	2	2	1	-1	0	0
^3SO	^{17}O	2	2	2	2	0	0	0
^2OH	^{17}O	-6	-5	-7	-6	0	1	-1
^2OH	^1H	0	0	-1	0	0	0	0
$^2NH_2$	^{14}N	2	2	3	3	0	0	0
$^2NH_2$	^1H	1	1	1	1	0	0	0
$^2NH_2$	^1H	1	1	1	1	0	0	0
^4N	^{14}N	1	1	1	1	0	0	0

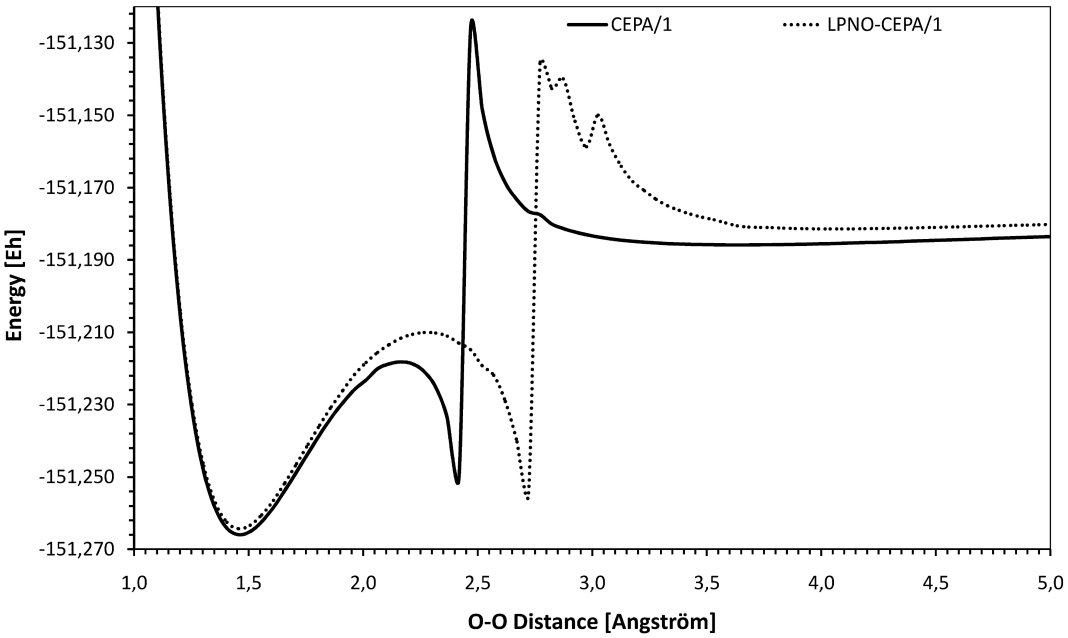

Figure C.1.: Rigidly scanned potential energy surface of the O–O bond cleavage of hydrogen peroxide. The SVP basis set (SV/C fitting basis set) was employed. QROs and the default values for the LPNO thresholds were used (solid line: spin-unrestricted CEPA/1 using QROs; dashed line: open-shell LPNO-CEPA/1).

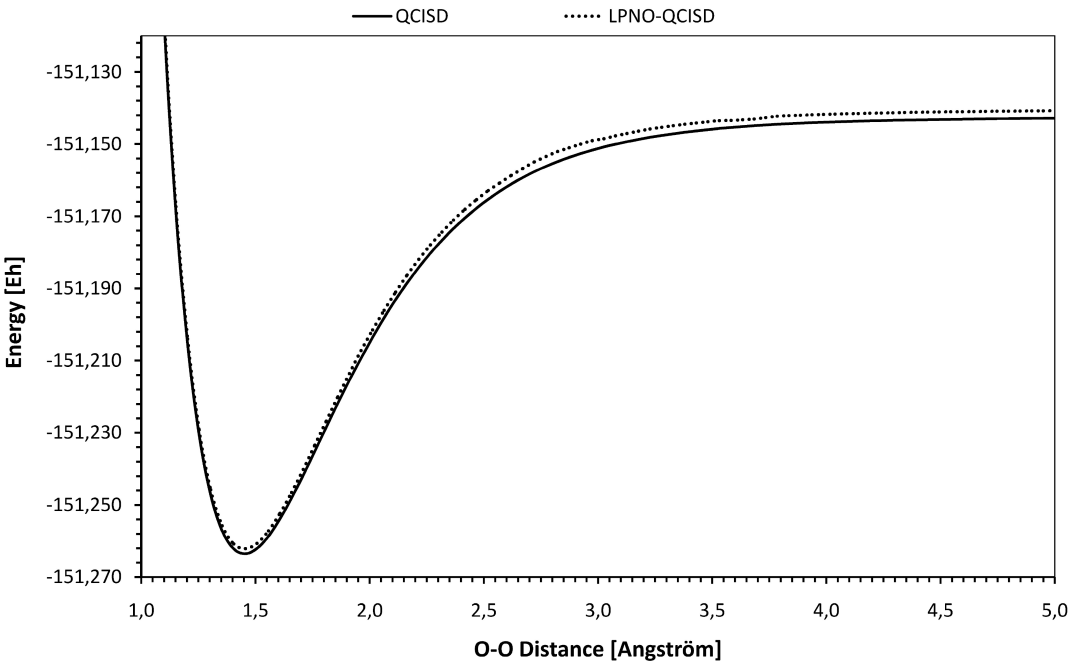

Figure C.2.: Rigidly scanned potential energy surface of the O–O bond cleavage of hydrogen peroxide. The SVP basis set (SV/C fitting basis set) was employed. QROs and the default values for the LPNO thresholds were used (solid line: spin-unrestricted QCISD using QROs; dashed line: open-shell LPNO-QCISD).

Bibliography

[1] I. M. A. F. X. Comte. *Cours der Philosophie positive*. Schleicher, Paris, 1838.

[2] P. A. M. Dirac. Quantum Mechanics of Many-Electron Systems. *Proc. R. Soc. Lond. A*, 123:714, 1929.

[3] T. Helgaker, W. Klopper, and D. Tew. Quantitative quantum chemistry. *Mol. Phys.*, 106:2107, 2008.

[4] K. Raghavachari and J. B. Anderson. Electron Correlation Effects in Molecules. *J. Phys. Chem.*, 100:12960, 1996.

[5] C. D. Sherrill. Fontiers in electronic structure theory. *J. Chem. Phys.*, 132:110902, 2010.

[6] M. Hofmann and H. F. Schaefer III. *Computational Chemistry*, volume 3, page 487. Academic Press, 2002.

[7] A. Born and R. Oppenheimer. Zur Quantentheorie der Molekeln. *Annalen der Physik*, 389:457, 1927.

[8] E. Schrödinger. An Undulatory Theory of the Mechanics of Atoms and Molecules. *Phys. Rev.*, 28:1049, 1926.

[9] J. K. MacDonald. Successive Approximations by the Rayleigh-Ritz Variation Method. *Phys. Rev.*, 43:830, 1933.

[10] M. Griebel and J. Hamaekers. Tensor product multiscale many-particle spaces with finite-order weights for the electronic Schrödinger equation. *Zeitschrift für Physikalische Chemie*, 224:527, 2010.

[11] T. Kato. On the eigenfunctions of many-particle systems in quantum mechanics. *Comm. Pure Appl. Math.*, 10:151, 1957.

[12] W. Pauli. Über den Zusammenhang des Abschlusses der Elektronengruppen im Atom mit der Komplexstruktur der Spektren. *Zeitschrift für Physik A: Hadrons and Nuclei*, 31:765, 1925.

[13] S.F. Boys. Electronic Wave Functions. I. A General Method of Calculation for the Stationary States of Any Molecular System. *Proc. R. Soc. London Ser. A*, 200:542, 1950.

[14] J. Slater and H. C. Verma. The Theory of Complex Spectra. *Phys. Rev.*, 34:1293, 1929.

[15] W. Klopper, F. R. Manby, S. Ten-No, and E. F. Valeev. R12 methods in explicitly correlated molecular electronic structure theory. *Int. Rev. Phys. Chem.*, 25:427, 2006.

[16] D. R. Hartree. The calculation of atomic structures. *Repts. Progr. Phys.*, 11:113, 1948.

[17] C. Sherrill and H. F. Schaefer III. *The Configuration Interaction Method: Advances in Highly Correlated Approaches*, volume 34, page 143. Academic Press, San Diego, 1999.

[18] A. C. Hurley. *Electron Correlation in Small Molecules*. Academic Press, London, 1976.

[19] J. Čížek. On the Correlation Problem in Atomic and Molecular Systems. Calculation of Wavefunction Components in Ursell-Type Expansion Using Quantum-Field Theoretical Methods. *J. Chem. Phys.*, 45:4256, 1966.

[20] P. G. Szalay, M. Nooijen, and J. Bartlett. Alternative ansätze in single reference coupled-cluster

theory. III. A critical analysis of different methods. *J. Chem. Phys.*, 103:281, 1995.

[21] M. Kállay and P. Surjan. Higher excitations in coupled-cluster theory. *J. Chem. Phys.*, 115:2945, 2001.

[22] R. J. Bartlett. To Multireference or not to Multireference: That is the Question? *Int. J. Mol. Sci.*, 3:579, 2002.

[23] R. J. Bartlett. Many-body perturbation theory and coupled cluster theory for electron correlation in molecules. *Ann. Rev. Phys. Chem.*, 32:359, 1981.

[24] F. Neese, A. Hansen, F. Wennmohs, and S. Grimme. Accurate Theoretical Chemistry with Coupled Pair Models. *Acc. Chem. Res.*, 42:641, 2009.

[25] F. Neese. Prediction of molecular properties and molecular spectroscopy with density functional theory: From fundamental theory to exchange-coupling. *Coord. Chem. Rev.*, 253:526, 2009.

[26] F. Neese, W. Ames, G. Christian, M. Kampa, D. G. Liakos, D. A. Pantazis, M. Roemelt, P. Surawatanawong, and S. F. Ye. Dealing with Complexity in Open-Shell Transition Metal Chemistry from a Theoretical Perspective: Reaction Pathways, Bonding, Spectroscopy, and Magnetic Properties. *Advances in Inorganic Chemistry: Theoretical and Computational Inorganic Chemistry*, 62:301, 2010.

[27] W. Koch and M. C. Holthausen. *A Chemist's guide to Density Functional Theory*. Wiley-VCH, Weinheim, 2000.

[28] F. Neese. A Critical Evaluation of DFT, including Time-Dependent DFT, Applied to Bioinorganic Chemistry. *J. Biol. Inorg. Chem.*, 11:702, 2006.

[29] J. P. Perdew. Density-functional approximation for the correlation-energy of the inhomogeneous electron-gas. *Phys. Rev. B*, 33:8822, 1986.

[30] A.D. Becke. Density-functional exchange-energy approximation with correct asymptotic behavior. *Phys. Rev. A.*, 38:3098, 1988.

[31] C. Lee, W. Yang, and R. G. Parr. Development of the Colle-Salvetti correlation-energy formula into a functional of the electron density. *Phys. Rev. B.*, 37:785, 1988.

[32] A. D. Becke. A new mixing of hartree-fock and local density-functional theories. *J. Chem. Phys.*, 98:1372–1377, 1993.

[33] F. Neese. Analytic Derivative Calculation of Zero-Field Splittings. *J. Chem. Phys.*, 127:164112, 2007.

[34] F. Neese. Prediction of electron paramagnetic resonance g values using coupled perturbed Hartree-Fock and Kohn-Sham theory. *J. Chem. Phys.*, 115:11080, 2001.

[35] F. Neese. Metal and Ligand Hyperfine Couplings in Transition Metal Complexes. The Effect of Spin-Orbit Coupling as Studied by Coupled Perturbed Kohn-Sham Theory. *J. Chem. Phys.*, 118:3939, 2003.

[36] S. Grimme and M. Parac. Substantial Errors from Time-Dependent Density Functional Theory for the Calculation of Excited States of Large π Systems. *ChemPhysChem*, 4:292, 2003.

[37] S. Grimme. Calculation of the Electronic Spectra of Large Molecules. volume 20 of *Rev. Comp. Chem.*, page 153. Wiley, Hoboken, NJ, USA, 2004.

[38] D. J. Tozer, R. A. Amos, N. C. Handy, B. O. Roos, and L. Serrano-Andres. Does density functional theory contribute to the understanding of excited states of unsaturated organic compounds? *Mol. Phys.*, 97:859, 1999.

[39] P. C. Redfern, P. Zapol, L. A. Curtiss, and Raghavachari K. Assessment of Gaussian-3 and

Density Functional Theories for Enthalpies of Formation of C_1 – C_{16} Alkanes. *J. Phys. Chem. A*, 104:5850, 2000.

[40] L. A. Curtiss, K. Raghavachari, P. C. Redfern, and J. A. Pople. Assessment of Gaussian-3 and density functional theories for a larger experimental test set. *J. Chem. Phys.*, 112:7374, 2000.

[41] M. D. Wodrich, C. Corminboeuf, and P. v. R. Schleyer. Systematic Errors in Computed Alkane Energies Using B3LYP and Other Popular DFT Functionals. *Org. Lett.*, 8:3631, 2006.

[42] S. Grimme. Seemingly Simple Stereoelectronic Effects in Alkane Isomers and the Implications for Kohn-Sham Density Functional Theory. *Angew. Chem. Int. Ed.*, 45:4460, 2006.

[43] S. Grimme, M. Steinmetz, and M. Korth. How to compute isomerization energies of organic molecules with quantum chemical methods. *J. Org. Chem.*, 72:2118, 2007.

[44] R. Schreiner. Relative Energy Computations with Approximate Density Functional Theory – A Caveat! *Angew. Chem. Int. Ed.*, 46:4217, 2007.

[45] S. Grimme, M. Steinmetz, and M. Korth. Stereoelectronic Substituent Effects in Saturated Main Group Molecules: Severe Problems of Current Kohn-Sham Density Functional Theory. *J. Chem. Theo. Comp*, 3:42, 2007.

[46] M. Piacenza and S. Grimme. Van der Waals Interactions in Aromatic Systems: Structure and Energetics of Dimers and Trimers of Pyridine. *ChemPhysChem*, 6:1554, 2005.

[47] S. Grimme. Semiempirical GGA-type density functional constructed with a long-range dispersion correction. *J. Comp. Chem.*, 27:1787, 2006.

[48] S. Grimme, J. Antony, T. Schwabe, and C. Mück-Lichtenfeld. Density functional theory with dispersion corrections for supramolecular structures, aggregates, and complexes of (bio)organic molecules. *Org. Biomol. Chem.*, 5:741, 2007.

[49] D. G. Truhlar and Y. Zhao. Density Functionals with Broad Applicability in Chemistry. *Acc. Chem. Res.*, 41:157, 2008.

[50] L. Goerigk and S. Grimme. Efficient and Accurate Double-Hybrid-Meta-GGA Density Functionals – Evaluation with the Extended GMTKN30 Database for General Main Group Thermochemistry, Kinetics, and Noncovalent Interactions. *J. Chem. Theory Comput.*, 7:291, 2011.

[51] S. Grimme and L. Goerigk. A thorough benchmark of density functional methods for general main group thermochemistry, kinetics, and noncovalent interactions. *Phys. Chem. Chem. Phys*, 13:6670, 2011.

[52] S. Grimme, C. Mück-Lichtenfeld, E.-U. Würthwein, A.W. Ehler, T.P.M. Goumans, and K. Lammertsma. Consistent Theoretical Description of 1,3-Dipolar Cycloaddition Reactions. *J. Phys. Chem. A*, 110:2583, 2006.

[53] T. Schwabe and S. Grimme. Towards chemical accuracy for the thermodynamics of large molecules: new hybrid density functionals including non-local correlation effects. *Phys. Chem. Chem. Phys.*, 8:4398, 2006.

[54] S. Grimme. Semiempirical hybrid density functional with perturbative second-order correlation. *J. Chem. Phys.*, 124:034108, 2006.

[55] F. Neese, T. Schwabe, and S. Grimme. Analytic derivatives for perturbatively corrected "double hybrid" density functionals: Theory, implementation, and applications. *J. Chem. Phys.*, 126:124115, 2007.

[56] S. Grimme and F. Neese. Double-hybrid density functional theory for excited electronic states of molecules. *J. Chem. Phys.*, 127:154116, 2007.

[57] A. Tarnopolsky, A. Karton, R. Sertchook, D. Vuzman, and J.M.L. Martin. Double-Hybrid Functionals for Thermochemical Kinetics. *J. Phys. Chem. A*, 112:3, 2008.

[58] L. Goerigk and S. Grimme. A General Database for Main Group Thermochemistry, Kinetics, and Noncovalent Interactions – Assessment of Common and Reparameterized (meta-)GGA Density Functionals. *J. Chem. Theory Comput.*, 6:107, 2010.

[59] C. Møller and M. S. Plesset. Note on an Approximation Treatment for Many-Electron Systems. *Phys. Rev.*, 46:618, 1934.

[60] M. Schütz, G. Hetzer, and H. J. Werner. Low-order scaling local electron correlation methods. I. Linear scaling local MP2. *J. Chem. Phys.*, 111:5691, 1999.

[61] P. E. Maslen and M. Head-Gordon. Noniterative local second order Møller-Plesset theory: Convergence with local correlation space. *J. Chem. Phys.*, 109:7093, 1998.

[62] A. K. Wilson and J. Almlöf. Møller-Plesset correlation energies in a localized orbital basis using a Laplace transform technique. *Theor. Chim. Acta*, 95:49, 1997.

[63] E. J. Baerends, D. E. Ellis, and P. Ros. Self-consistent molecular Hartree-Fock-Slater calculations I. The computational procedure. *Chem. Phys.*, 2:41, 1973.

[64] J. L. Whitten. Coulombic potential energy integrals and approximations. *J. Chem. Phys.*, 58:4496, 1973.

[65] B. I. Dunlap, J. W. D. Connolly, and J. R. Sabin. On some approximations in applications of X_α theory. *J. Chem. Phys*, 71:3396, 1979.

[66] O. Vahtras, J. Almlöf, and M. W. Feyereisen. Integral approximations for LCAO-SCF calculations. *Chem. Phys. Lett.*, 213:514, 1993.

[67] M. Feyereisen, G. Fitzgerald, and A. Komornicki. Use of approximate integrals in ab initio theory. An application in MP2 energy calculations. *Chem. Phys. Lett.*, 208:359, 1993.

[68] F. Weigend and Häser; M. RI-MP2: first derivatives and global consistency. *Theo. Chem. Acc.*, 97:331, 1997.

[69] F. Weigend, M. Häser, H. Patzelt, and R. Ahlrichs. RI-MP2: optimized auxiliary basis sets and demonstration of efficiency. *Chem. Phys. Lett.*, 294:143, 1998.

[70] S. Grimme. Improved second-order møller-plesset perturbation theory by separate scaling of parallel- and antiparallel-spin pair correlation energies. *J. Chem. Phys.*, 118:9095, 2003.

[71] S. Grimme. Accurate Calculation of the Heats of Formation for Large Main Group Compounds with Spin-Component Scaled MP2 Methods. *J. Phys. Chem. A*, 109:3067, 2005.

[72] B. Brandow. Linked-Cluster Expansions for the Nuclear Many-Body Problem. *Rev. Mod. Phys.*, 39:771, 1967.

[73] S. R. Langhoff and E. R. Davidson. Configuration interaction calculations on the nitrogen molecule. *Int. J. Quantum Chem.*, 8:61, 1974.

[74] F. Coester. Bound states of a many-particle system. *Nucl. Phys.*, 7:421, 1958.

[75] F. Coester and H. Kümmel. Short-range correlations in nuclear wave functions. *Nucl. Phys.*, 17:477, 1960.

[76] J. Gauss. Coupled-Cluster Theory. In *Encyclopedia of Computational Chemistry*, page 615. Wiley, Chichester, 1998.

[77] R. J. Bartlett and M. Musial. Coupled-cluster theory in quantum chemistry. *Rev. Mod. Phys.*, 79:291, 2007.

[78] T. D. Crawford and H. F. Schaefer III. An Introduction to Coupled Cluster Theory for Com-

putational Chemists. volume 14 of *Rev. Comp. Chem.*, page 33. Wiley, Hoboken, NJ, USA, 2000.

[79] A. Karton, E. Rabinovich, J. M. L. Martin, and B. Ruscic. W4 theory for computational thermochemistry: In pursuit of confident sub-kJ/mol predictions. *J. Chem. Phys.*, 125:144108, 2006.

[80] A. Tajti, P. G. Szalay, A. G. Császár, M. Kállay, J. Gauss, E. F. Valeev, B. A. Flowers, J. Vázquez, and J. F. Stanton. HEAT: High accuracy extrapolated *ab* initio thermochemistry. *J. Chem. Phys.*, 121:11599, 2004.

[81] S. Hirata. Symbolic algebra in quantum chemistry. *Theo. Chem. Acc.*, 116:2, 2006.

[82] G. D. Purvis and R. J. Bartlett. A full coupled-cluster singles and doubles model: The inclusion of disconnected triples. *J. Chem. Phys.*, 76:1910, 1982.

[83] F. Neese, D. G. Liakos, and S. F. Ye. Correlated wavefunction methods in bioinorganic chemistry. *Journal of Biological Inorganic Chemistry*, 16:821, 2011.

[84] J. Gauss. Molecular Properties. In *Modern Methods and Algorithms in Quantum Chemistry*, page 1. John von Neumann Institute for Computing (NIC Series Vol. 3), Jülich, 2000.

[85] T. J. Lee and G. E. Scuseria. Achieving Chemical Accuracy with Coupled-Cluster Theory. In *Quantum Mechanical Electronic Structure Calculations with Chemical Accuracy (Understanding Chemical Reactivity)*, page 47. Kluwer, Dordrecht, 1995.

[86] J. A. Pople, M. Head-Gordon, and K. Raghavachari. Quadratic configuration interaction. A general technique for determining electron correlation energies. *J. Chem. Phys.*, 87:5968, 1987.

[87] K. Raghavachari, G. W. Trucks, J. A. Pople, and M. Head-Gordon. A fifth-order perturbation comparison of electron correlation theories. *Chem. Phys. Lett.*, 157:479, 1989.

[88] S. Wilson. A critical analysis of the "CCSD(T)" model for the study of electron correlation effects in atoms and molecules. Technical Report RAL-TR-2003-035, 2003.

[89] T. Janowski and P. Pulay. Efficient Parallel Implementation of the CCSD External Exchange Operator and the Perturbative Triples (T) Energy Calculation. *J. Chem. Theory Comp.*, 4:1585, 2008.

[90] A. Halkier, T. Helgaker, P. Jørgensen, W. Klopper, H. Koch, J. Olson, and A. K. Wilson. Basis-set convergence in correlated calculations on Ne, N_2, and H_2O. *Chem. Phys. Lett.*, 286:243, 1998.

[91] D. G. Truhlar. Basis-set extrapolation. *Chem. Phys. Lett.*, 294:45, 1998.

[92] A. Schäfer, C. Huber, and R. Ahlrichs. Fully optimized contracted Gaussian basis sets of triple zeta valence quality for atoms Li to Kr. *J. Chem. Phys.*, 100:5829, 1994.

[93] T. H. Dunning. Gaussian basis sets for use in correlated molecular calculations. I. The atoms boron through neon and hydrogen. *J. Chem. Phys*, 90:1007, 1989.

[94] E. F. Valeev and T. D. Crawford. Simple coupled-cluster singles and doubles method with perturbative inclusion of triples and explicitly correlated geminals: The CCSD(T)$_{\overline{\mathrm{R12}}}$ model. *J. Chem. Phys.*, 128:244113, 2008.

[95] T. B. Adler, G. Knizia, and H.-J. Werner. A simple and efficient CCSD(T)-F12 approximation. *J. Chem. Phys.*, 127:221106, 2007.

[96] G. Knizia, T. B. Adler, and H.-J. Werner. Simplified CCSD(T)-F12 methods: Theory and benchmarks. *J. Chem. Phys.*, 130:054104, 2009.

[97] H. P. Kelly and A. M. Sessler. Correlation Effects in Many Fermion Systems: Multiple-Particle

Excitation Expansion. *Phys. Rev.*, 132:2091, 1963.

[98] H. P. Kelly. Correlation Effects in Many Fermion Systems. II. Linked Clusters. *Phys. Rev.*, 134:1450, 1964.

[99] W. Meyer. Ionization energies of water from pno-ci calculations. *Int. J. Quant. Chem.*, 5 (S5):341, 1971.

[100] W. Meyer. PNO-CI Studies of Electron Correlation Effects. 1. Configuration Expansion by Means of Nonorthogonal Orbitals, and Application to Ground-State and Ionized States of Methane. *J. Chem. Phys.*, 58:1017, 1973.

[101] W. Meyer. PNO-CI and CEPA Studies of Electron Correlation Effects. 2. Potential Curves and Dipole-Moment Functions of OH Radical. *Theo. Chim. Acta*, 35:277, 1974.

[102] H. J. Werner and W. Meyer. PNO-CI and PNO-CEPA Studies of Electron Correlation Effects. 5. Static Dipole Polarizabilities of Small Molecules. *Mol. Phys.*, 31:855, 1976.

[103] P. Rosmus and W. Meyer. PNO-CI and CEPA studies of electron correlation effects. 6. Electron affinities of the first-row and second-row diatomic hydrides and the spectroscopic constants of their negative ions. 69:2745, 1978.

[104] R. Ahlrichs, P. Scharf, and C. Ehrhardt. The coupled pair functional (CPF). A size consistent modification of the CI(SD) based on an energy functional . *J. Chem. Phys.*, 82:890, 1985.

[105] P. R. Taylor, G. B. Bacskay, N. S. Hush, and A. C. Hurley. The coupled-pair approximation in a basis of independent-pair natural orbitals. *Chem. Phys. Lett.*, 41:444, 1976.

[106] P. Pulay and S. Saebø. Variational CEPA: Comparison with different many-body methods. *Chem. Phys. Lett.*, 117:37, 1985.

[107] W. Meyer. Configuration Expansion by Means of Pseudonatural Orbitals. In *Methods of Electronic Structure Theory*, page 413. Plenum Press, New York, 1977.

[108] R. Ahlrichs, F. Driessler, H. Lischka, V. Staemmler, and W. Kutzelnigg. PNO-CI (pair natural orbital configuration interaction) and CEPA-PNO (coupled electron pair approximation with pair natural orbitals) calculations of molecular systems. II. The molecules BeH_2, BH, BH_3, CH_4, CH_3^-, NH_3 (planar and pyramidal), H_2O, OH_3^+, HF and the Ne atom. *J. Chem. Phys.*, 62:1235, 1975.

[109] V. Staemmler and R. Jaquet. CEPA calculations on open-shell molecules. I. Outline of the method. *Theoret. Chim. Acta*, 59:487, 1981.

[110] V. Staemmler and R. Jaquet. CEPA calculations on open-shell molecules. II. Singlet-triplet energy splitting in π^2 configurations of diatomic molecules. *Theoret. Chim. Acta*, 59:501, 1981.

[111] W. Kutzelnigg. Pair correlation theories. In *Methods of Electronic Structure Theory*, page 1. Plenum Press, New York, 1977.

[112] R. Ahlrichs and P. Scharf. The Coupled Pair Approximation. In *Advances in Chemical Physics: Ab Initio Methods in Quantum Chemistry Part I*, page 501. Wiley, Hoboken, NJ, USA, 1987.

[113] C. Kollmar and F. Neese. The coupled electron pair approximation: variational formulation and spin adaptation. *Molecular Physics*, 108:2449, 2010.

[114] P. R. Taylor. A rapidly convergent CI expansion based on several reference configurations, using optimized correlating orbitals. *J. Chem. Phys*, 74:1256, 1981.

[115] R. Fink and V. Staemmler. A multi-configuration reference CEPA method based on pair natural orbitals. *Theor. Chim. Acta*, 87:129, 1993.

[116] P. Fulde and H. Stoll. On the coupled-electron-pair approximation based on a multireference state. *J. Chem. Phys.*, 97:4185, 1992.

[117] J.-P. Malrieu, J.-P. Daudey, and R. Caballol. Multireference self-consistent size-consistent singles and doubles configuration interaction for ground and excited states. *J. Chem. Phys.*, 101:8908, 1994.

[118] J.-P. Daudey, J.-L. Heully, and J.-P. Malrieu. Size-consistent self-consistent truncated or selected configuration interaction. *J. Chem. Phys.*, 99:1240, 1993.

[119] M. Nooijen and R. J. Le Roy. Orbital invariant single-reference coupled electron pair approximation with extensive renormalized triples correction. *J. Mol. Struct. (Theochem)*, 768:25, 2006.

[120] S. Koch and W. Kutzelnigg. Comparison of CEPA and CP-MET methods. *Theo. Chim. Acta*, 59:387, 1981.

[121] F. Neese and F. Wennmohs. A comparative study of single reference correlation methods of the coupled-pair type. *Chem. Phys.*, 343:217, 2008.

[122] C. Hampel, K. A. Peterson, and H. J. Werner. A comparison of the efficiency and accuracy of the quadratic configuration interaction (QCISD), coupled cluster (CCSD), and Brueckner coupled cluster (BCCD) methods. *Chem. Phys. Lett.*, 190:1, 1992.

[123] W. Meyer and P. Rosmus. PNO-CI and CEPA studies of electron correlation effects. 3. Spectroscopic constants and dipole moment functions for the ground states of the first-row and second-row diatomic hydrides. *J. Chem. Phys.*, 63:2356, 1975.

[124] P. Botschwina and W. Meyer. A PNO-CEPA calculation of the barrier height for the collinear atom exchange reaction Cl' + HCl $\rightarrow$ Cl'H + Cl. *Chem. Phys. Lett.*, 44:449, 1976.

[125] P. Botschwina, P. Rosmus, and E.-A. Reinsch. Spectroscopic properties of the hydroxonium ion calculated from SCEP CEPA wavefunctions. *Chem. Phys. Lett.*, 102:299, 1983.

[126] L. M. J. Huntington and M. Nooijen. pCCSD: Parameterized coupled-cluster theory with single and double excitations. *J. Chem. Phys.*, 133:184109, 2010.

[127] H. M. McConnell and B. G. McFarland. Physics and chemistry of spin labels. *Quarterly Reviews of Biophysics*, 3:91, 1970.

[128] N. Cox, L. Rapatskiy, J. H. Su, D. A. Pantazis, M. Sugiura, L. Kulik, P. Dorlet, A. W. Rutherford, F. Neese, A. Boussac, W. Lubitz, and J. Messinger. Effect of Ca^{2+}/Sr^{2+} Substitution on the Electronic Structure of the Oxygen-Evolving Complex of Photosystem II: A Combined Multifrequency EPR, ^{55}Mn-ENDOR, and DFT Study of the S_2 State. *J. Am. Chem. Soc.*, 133:3635, 2011.

[129] W. D. Edwards and M. C. Zerner. A generalized restricted open-shell Fock operator. *Theor. Chim. Acta*, 72:347, 1987.

[130] L. Noodleman. Valence bond description of antiferromagnetic coupling in transition metal dimers. *J. Chem. Phys.*, 74:5737, 1981.

[131] L. Noodleman and E. R. Davidson. Ligand spin polarization and antiferromagnetic coupling in transition metal dimers. *Chem. Phys.*, 109:131, 1986.

[132] M. Nooijen and R. J. Bartlett. General spin adaptation of open-shell coupled cluster theory. *J. Chem. Phys*, 104:2652, 1996.

[133] P. J. Knowles, M. Schütz, and H.-J. Werner. Ab Initio Methods for Electron Correlation in Molecules. In *Modern Methods and Algorithms in Quantum Chemistry*. John von Neumann Institute for Computing (NIC Series Vol. 3), Jülich, 2000.

[134] J. Yang, Y. Kurashige, F. R. Manby, and G. K.-L. Chan. Tensor factorizations of local second-order Møller-Plesset theory. *J. Chem. Phys.*, 134:044123, 2011.

[135] J. Yang, G. K.-L. Chan, F. R. Manby, M. Schütz, and H.-J. Werner. The orbital-specific-virtual local coupled cluster singles and doubles method. *J. Chem. Phys.*, 136:144105, 2012.

[136] D. P. Tew, B. Hellmich, and C. Hättig. Local explicitly correlated second-order Møller-Plesset perturbation theory with pair natural orbitals. *J. Chem. Phys*, 135:074107, 2011.

[137] Udo Benedikt, A. A. Auer, M. Espig, and W. Hackbusch. Tensor decompositions on post-Hartree-Fock methods. I. Two-electron integrals and MP2. *J. Chem. Phys.*, 134:054118, 2011.

[138] M. Head-Gordon, F. Bell, and D. S. Lambrecht. Higher order singular value decomposition in quantum chemistry. *Molecular Physics*, 108:2759, 2010.

[139] P. Pulay. Localizability of dynamic electron correlation. *Chem. Phys. Lett.*, 100:151, 1983.

[140] S. Saebø and P. Pulay. Local configuration interaction: An efficient approach for larger molecules. *Chem. Phys. Lett.*, 113:138, 1985.

[141] S. Saebø and P. Pulay. Local treatment of electron correlation. *Ann. Rev. Phys. Chem.*, 44:213, 1993.

[142] S. Saebø and P. Pulay. The local correlation treatment. II. Implementation and tests. *J. Chem. Phys.*, 88:1884, 1988.

[143] S. Saebø and P. Pulay. Fourth-order Møller-Plessett perturbation theory in the local correlation treatment. I. Method. *J. Chem. Phys.*, 86:914, 1987.

[144] H. Stoll. On the correlation energy of graphite. *J. Chem. Phys.*, 97:8449, 1992.

[145] J. Friedrich, M. Hanrath, and M. Dolg. Fully automated implementation of the incremental scheme: Application to CCSD energies for hydrocarbons and transition metal compounds. *J. Chem. Phys.*, 126:154110, 2007.

[146] N. Flocke and R. J. Bartlett. Localized correlation treatment using natural bond orbitals. *Chem. Phys. Lett.*, 367:80, 2003.

[147] N. Flocke and R. J. Bartlett. A natural linear scaling coupled-cluster method. *J. Chem. Phys.*, 121:10935, 2004.

[148] D. G. Fedorov and K. Kitaura. Coupled-cluster theory based upon the fragment molecular-orbital method. *J. Chem. Phys.*, 123:134103, 2005.

[149] W. Li, J. R. Gour, P. Piecuch, and S. Li. Local correlation calculations using standard and renormalized coupled-cluster approaches. *J. Chem. Phys.*, 131:114109, 2009.

[150] W. Li and P. Piecuch. Improved Design of Orbital Domains within the Cluster-in-Molecule Local Correlation Framework: Single-Environment Cluster-in-Molecule Ansatz and Its Application to Local Coupled-Cluster Approach with Singles and Doubles. *J. Phys. Chem. A*, 114:8644, 2010.

[151] M. S. Gordon, D. G. Fedorov, S. R. Pruitt, and L. V. Slipchenko. Fragmentation Methods: A Route to Accurate Calculations on Large Systems. *Chemical Reviews*, 112:632, 2012.

[152] P. Arora, W. Li, P. Piecuch, J. W. Evans, M. Albao, and M. S. Gordon. Diffusion of Atomic Oxygen on the Si(100) Surface. *J. Phys. Chem. C*, 114:12649, 2010.

[153] W. D. Laidig, G. D. Purvis III, and R. J. Bartlett. Localized orbitals in the coupled cluster singles and doubles model. *Int. J. Quant. Chem.*, 22 (S16):561, 1982.

[154] W. D. Laidig, G. D. Purvis III, and R. J. Bartlett. Can simple localized bond orbitals and coupled cluster methods predict reliable molecular energies? *J. Phys. Chem.*, 89(11):2161, 1985.

[155] R. A. Friesner. New methods for electronic-structure calculations on large molecules. *Annu. Rev. Phys. Chem.*, 42:341, 1991.

[156] J. E. Subotnik, A. Sodt, and M. Head-Gordon. The limits of local correlation theory: Electronic delocalization and chemically smooth potential energy surfaces. *J. Chem. Phys.*, 128:034103, 2008.

[157] P. E. Maslen, A. D. Dutoi, M. S. Lee, Y. H. Shao, and M. Head-Gordon. Accurate local approximations to the triples correlation energy: formulation, implementation and tests of 5th-order scaling models. *Mol. Phys.*, 103:425, 2005.

[158] W. Klopper, J. Noga, H. Koch, and T. Helgaker. Multiple basis sets in calculations of triples corrections in coupled-cluster theory. *Theor. Chem. Acc.*, 97:164, 1997.

[159] P. Neogrády, M. Pitoňák, and M. Urban. Optimized virtual orbitals for correlated calculations: an alternative approach. *Mol. Phys.*, 103:2141, 2005.

[160] L. Adamowicz and R. J. Bartlett. Optimized virtual orbital space for high-level correlated calculations. *J. Chem. Phys.*, 86:6314, 1987.

[161] Z. Rolik and M. Kállay. Cost reduction of high-order coupled-cluster methods via active-space and orbital transformation techniques. *J. Chem. Phys.*, 134:124111, 2011.

[162] Z. Rolik and M. Kállay. A general-order local coupled-cluster method based on the cluster-in-molecule approach. *J. Chem. Phys.*, 135:104111, 2011.

[163] E. G. Hohenstein and C. D. Sherrill. Efficient evaluation of triple excitations in symmetry-adapted perturbation theory via second-order Møller-Plesset perturbation theory natural orbitals. *J. Chem. Phys.*, 133:104107, 2010.

[164] J. M. Dieterich, H. J. Werner, R. A. Mata, S. Metz, and W. Thiel. Reductive half-reaction of aldehyde oxidoreductase toward acetaldehyde: Ab initio and free energy quantum mechanical/molecular mechanical calculations. *J. Chem. Phys*, 132:035101, 2010.

[165] H.-J. Werner and M. Schütz. An efficient local coupled cluster method for accurate thermochemistry of large systems. *J. Chem. Phys.*, 135:144116, 2011.

[166] C. Hampel and H.-J. Werner. Local treatment of electron correlation in coupled cluster theory. *J. Chem. Phys.*, 104:6286, 1996.

[167] M. Schütz and H.-J. Werner. Low-order scaling local electron correlation methods. IV. Linear scaling local coupled-cluster (LCCSD). *J. Chem. Phys.*, 114:661, 2001.

[168] H.-J. Werner, F. R. Manby, and P. J. Knowles. Fast linear scaling second-order Møller-Plesset perturbation theory (MP2) using local and density fitting approximations. *J. Chem. Phys.*, 118:8149, 2003.

[169] M. Schütz and H.-J. Werner. Local perturbative triples correction (T) with linear cost scaling. *Chem. Phys. Lett.*, 318:370, 2000.

[170] M. Schütz. Low-order scaling local electron correlation methods. V. Connected triples beyond (T): Linear scaling local CCSDT-1b. *J. Chem. Phys.*, 116:8772, 2002.

[171] T. Korona and H.-J. Werner. Local treatment of electron excitations in the EOM-CCSD method. *J. Chem. Phys.*, 118:3006, 2003.

[172] D. Kats, T. Korona, and M. Schütz. Local CC2 electronic excitation energies for large molecules with density fitting. *J. Chem. Phys.*, 125:104106, 2006.

[173] Y. Kurashige, J. Yang, G. K.-L. Chan, and F. R. Manby. Optimization of orbital-specific virtuals in local Møller-Plesset perturbation theory. *J. Chem. Phys.*, 136:124106, 2012.

[174] T. B. Adler, H.-J. Werner, and F. R. Manby. Local explicitly correlated second-order perturbation theory for the accurate treatment of large molecules. *J. Chem. Phys.*, 130:054106, 2009.

[175] Y. Liu. *Linear scaling high-spin open-shell local correlation methods*. PhD dissertation, University Stuttgart, Germany, 2011.

[176] H.-J. Werner and K. Pflüger. On the selection of domains and orbital pairs in local correlation treatments. *Annual Reports in Computational Chemistry*, 2:53–80, 2006.

[177] J. W. Boughton and P. Pulay. Comparison of the Boys and Pipek-Mezey localizations in the local correlation approach and automatic virtual basis selection. *J. Comp. Chem.*, 14:736, 1993.

[178] N. J. Russ and T. D. Crawford. Potential energy surface discontinuities in local correlation methods. *J. Chem. Phys.*, 121:691, 2004.

[179] C. Edmiston. Pseudonatural Orbitals as a Basis for the Superposition of Configurations. I. He_2^+. *J. Chem. Phys.*, 45:1833, 1966.

[180] C. Edmiston and M. Krauss. Configuration-Interaction Calculation of H_3 and H_2. *J. Chem. Phys.*, 42:1119, 1965.

[181] W. Kutzelnigg. Direct Determination of Natural Orbitals and Natural Expansion Coefficients of Many-Electron Wavefunctions. I. Natural Orbitals in the Geminal Product Approximation. *J. Chem. Phys.*, 40:3640, 1964.

[182] R. Ahlrichs and W. Kutzelnigg. Direct Calculation of Approximate Natural Orbitals and Natural Expansion Coefficients of Atomic and Molecular Electronic Wavefunctions. II. Decoupling of the Pair Equations and Calculation of the Pair Correlation Energies for the Be and LiH Ground States. *J. Chem. Phys.*, 48:1819, 1968.

[183] W. Meyer. Theory of self-consistent electron pairs - iterative method for correlated many-electron wavefunctions. *J. Chem. Phys.*, 64(7):2901–2907, 1976.

[184] W. Meyer, R. Ahlrichs, and C. E. Dykstra. The Method of Self Consistent Electron Pairs. A Matrix Oriented Direct CI. In *Advanced Theories and Computational Approaches to the Electronic Structure of Molecules*, page 19. Kluwer Academic, Dordrecht, 1984.

[185] G. E. Scuseria, C. L. Janssen, and H. F. Schaefer. An efficient reformulation of the closed-shell coupled cluster single and double excitation (CCSD) equations. *J. Chem. Phys.*, 89:7382, 1988.

[186] P. Pulay, S. Saebø, and W. Meyer. An efficient reformulation of the closed-shell self-consistent electron pair theory. *J. Chem. Phys.*, 81:1901, 1984.

[187] P. A. M. Dirac. Note on Exchange Phenomena in the Thomas Atom. *Mathematical Proceedings of the Cambridge Philosophical Society*, 26:376, 1930.

[188] P.-O. Löwdin. Natural Orbitals in the Quantum Theory of Two-Electron Systems. *Phys. Rev.*, 97:1474, 1955.

[189] P.-O. Löwdin. Quantum theory of cohesive properties of solids. *Adv. Phys.*, 5:1, 1956.

[190] E. R. Davidson. Properties and Uses of Natural Orbitals. *Rev. Mod. Phys.*, 44:451, 1972.

[191] P.-O. Löwdin and H. Shull. Natural Orbitals in the Quantum Theory of Two-Electron Systems. *Phys. Rev.*, 101(6):1730–1739, 1956.

[192] I. Shavitt, B. J. Rosenberg, and S. Palakit. Comparison of configuration interaction expansions based on different orbital transformations. *Int. J. Quantum Chem.*, 10 (S10):33, 1976.

[193] L. Bytantas, J. Ivanic, and K. Ruedenberg. Split-localized orbitals can yield stronger configuration interaction convergence than natural orbitals. *J. Chem. Phys.*, 119:8217, 2003.

[194] P. J. Hay. On the calculation of natural orbitals by perturbation theory. *J. Chem. Phys.*, 59:2468, 1973.

[195] R. Ahlrichs and F. Driessler. Direct Determination of Pair Natural Orbitals - A New Method to Solve Multi-Configuration Hartree-Fock Problem for Two-Electron Wave Functions. *Theo. Chim. Acta*, 36:275, 1975.

[196] F. Neese, F. Wennmohs, and A. Hansen. Efficient and accurate local approximations to coupled-electron pair approaches: An attempt to revive the pair natural orbital method. *J. Chem. Phys.*, 130:114108, 2009.

[197] F. Neese, A. Hansen, and D. G. Liakos. Efficient and accurate approximations to the local coupled cluster singles doubles method using a truncated pair natural orbital basis. *J. Chem. Phys.*, 131:064103, 2009.

[198] A. Hansen, D. G. Liakos, and F. Neese. Efficient and accurate local single reference correlation methods for high-spin open-shell molecules using pair natural orbitals. *J. Chem. Phys.*, 135:214102, 2011.

[199] D. G. Liakos, A. Hansen, and F. Neese. Weak Molecular Interactions Studied with Parallel Implementations of the Local Pair Natural Orbital Coupled Pair and Coupled Cluster Methods. *J. Chem. Theory Comp.*, 7:76, 2011.

[200] C. Kollmar. Convergence optimization of restricted open-shell self-consistent field calculations. *Int. J. Quantum Chem.*, 62:617, 1997.

[201] F. Neese. Importance of Direct Spin-Spin Coupling and Spin-Flip Excitations for the Zero-Field Splittings of Transition Metal Complexes: A Case Study. *J. Am. Chem. Soc.*, 128:10213, 2006.

[202] S. Sinnecker and F. Neese. Spin-Spin Contributions to the Zero-Field Splitting Tensor in Organic Triplets, Carbenes and Biradicals – A Density Functional and Ab Initio Study. *J. Phys. Chem. A*, 110:12267, 2006.

[203] S. F. Boys. Construction of Some Molecular Orbitals to Be Approximately Invariant for Changes from One Molecule to Another. *Rev. Mod. Phys.*, 32:296, 1963.

[204] G. Knizia. *Explicitly correlated quantum chemistry for high-spin open-shell molecules*. PhD dissertation, University Stuttgart, Germany, 2010.

[205] Brillouin, L. Les problèmes de perturbations et les champs self-consistents. *J. Phys. Radium*, 3:373, 1932.

[206] F. Neese. The ORCA program system. *Wiley Interdisciplinary Reviews: Computational Molecular Science*, 2:73, 2012.

[207] C. Kollmar and F. Neese. An orbital-invariant and strictly size extensive post-Hartree-Fock correlation functional. *J. Chem. Phys.*, 135:084102, 2011.

[208] H.-J. Werner. Matrix formulated MCSCF and MCSCF-CI methods. In *Advances in Chemical Physics: Ab Initio Methods in Quantum Chemistry Part II*. Wiley, Hoboken, NJ, USA, 1987.

[209] R. Ahlrichs. Many body perturbation calculations and coupled electron pair models. *Comput. Phys. Commun.*, 17:31, 1979.

[210] J. Pipek and P. G. Mezey. A fast intrinsic localization procedure applicable for *a*b initio and semiempirical linear combination of atomic orbital wave functions. *J. Chem. Phys.*, 90:4916, 1989.

[211] M. Schütz and F. R. Manby. Linear scaling local coupled cluster theory with density fitting. Part I: 4-external integrals. *Phys. Chem. Chem. Phys.*, 5:3349, 2003.

[212] M. Schütz. A new, fast, semi-direct implementation of linear scaling local coupled cluster theory. *Phys. Chem. Chem. Phys.*, 4:3941, 2002.

[213] I. Nebot-Gil, J. Sanchez-Marin, J. L. Heully, J. P. Malrieu, and D. Maynau. Eigenvalue Problem Formulation of Coupled-Cluster Expansions through Intermediate Hamiltonians. *Chem. Phys. Lett.*, 234:45, 1995.

[214] F. Neese, F. Wennmohs, A. Hansen, and U. Becker. Efficient, approximate and parallel hartree-fock and hybrid dft calculations. a chain-of-spheres algorithm for the hartree-fock exchange. *Chem. Phys.*, 356:98–109.

[215] R. Izsák and F. Neese. An overlap fitted chain of spheres exchange method. *J. Chem. Phys.*, 135:144105, 2011.

[216] A. D. Yau. *A parallel direct open-shell coupled-cluster singles and doubles algorithm*. Phd disseration, University of Florida, USA, 2004.

[217] M. Jungen and R. Ahlrichs. *A*b initio calculations on small hydrides including electron correlation. *Theoret. Chim. Acta*, 17:339, 1970.

[218] F. Neese. An improvement of the resolution of the identity approximation for the formation of the Coulomb matrix. *J. Comput. Chem.*, 24:1740, 2003.

[219] L. M. J. Huntington, A. Hansen, F. Neese, and M. Nooijen. Accurate thermochemistry from a parameterized coupled-cluster singles and doubles model and a local pair natural orbital based implementation for applications to larger systems. *Journal of Chemical Physics*, 136:064101, 2012.

[220] P. Pulay. Convergence acceleration of iterative sequences. The case of SCF iterations. *Chem. Phys. Lett.*, 73:393, 1980.

[221] F. Weigend and R. Ahlrichs. Balanced basis sets of split valence, triple zeta valence and quadruple zeta valence quality for H to Rn: Design and assessment of accuracy. *Phys. Chem. Chem. Phys.*, 7:3297, 2005.

[222] R. Ahlrichs *et al.* TURBOMOLE Basis Set Library, http://bases.turbo-forum.com/TBL/tbl.html.

[223] D. E. Bernholdt and R. J. Harrison. Fitting basis sets for the RI-MP2 approximate second-order many-body perturbation theory method. *J. Chem. Phys.*, 109:1593, 1998.

[224] V. Barone. Structure, Magnetic Properties and Reactivities of Open-Shell Species from Density Functional and Self-Consistent Hybrid Methods. In *Recent Advances in Density Functional Theory, Part I*, page 287. World Scientific, Singapore, 1995.

[225] W. Kutzelnigg, U. Fleischer, and M. Schindler. The IGLO-Method: Ab-initio Calculation and Interpretation of NMR Chemical Shifts and Magnetic Susceptibilities. In *NMR-Basic Principles and Progress, Vol. 213* , page 165. Springer Verlag, Heidelberg, 1991.

[226] F. Weigend. A fully direct RI-HF algorithm: Implementation, optimised auxiliary basis sets, demonstration of accuracy and efficiency. *Phys. Chem. Chem. Phys.*, 4:4285, 2002.

[227] J. Gauss and D. Cremer. Analytical Energy Gradients in Møller-Plesset Perturbation and Quadratic Configuration Interaction Methods: Theory and Application. *Adv. Quant. Chem.*, 23:205, 1992.

[228] C. Denekamp and M. Yaniv. Benzene loss from trityl cations – A mechanistic study. *J. Am. Soc. Mass Spectrom.*, 17:730, 2006.

[229] S. F. Boys and F. Bernardi. The calculation of small molecular interactions by the differences of separate total energies. Some procedures with reduced errors. *Mol. Phys.*, 19:553, 1970.

[230] W. Kutzelnigg and P. v. Herigonte. Electron Correlation at the Dawn of the 21st Century. *Adv. Quantum. Chem.*, 36:185, 2000.

[231] L. A. Curtiss, K. Raghavachari, P. C. Redfern, and J. A. Pople. Assessment of Gaussian-2 and density functional theories for the computation of enthalpies of formation. *J. Chem. Phys.*, 106:1063, 1997.

[232] R. McWeeny. *Methods of Molecular Quantum Mechanics*. Academic Press, London, 1992.

[233] P. Jurečka, J. Šponer, J. Černý, and P. Hobza. Benchmark database of accurate (MP2 and CCSD(T) complete basis set limit) interaction energies of small model complexes, DNA base pairs, and amino acid pairs. *Phys. Chem. Chem. Phys.*, 8:1985, 2006.

[234] A. D. Boese, J. M. L. Martin, and W Klopper. Basis Set Limit Coupled Cluster Study of H-Bonded Systems and Assessment of More Approximate Methods. *J. Phys. Chem. A*, 111:11122, 2007.

[235] D. G. Liakos and F. Neese. Improved Correlation Energy Extrapolation Schemes Based on Local Pair Natural Orbital Methods. *J. Phys. Chem. A*, 2012. DOI: 10.1021/jp302096v.

[236] S. Grimme, C. Diedrich, and M. Korth. The Importance of Inter- and Intramolecular van der Waals Interactions in Organic Reactions: the Dimerization of Anthracene Revisited. *Angew. Chem. Int. Ed.*, 45:625, 2006.

[237] D. G. Truhlar, J. J. Zheng, and Y. Zhao. Representative Benchmark Suites for Barrier Heights of Diverse Reaction Types and Assessment of Electronic Structure Methods for Thermochemical Kinetics. *J. Chem. Theory Comput.*, 3:569, 2007.

[238] S. Ye, C. Riplinger, A. Hansen, C. Krebs, J. M. Bollinger, Jr., and F. Neese. Electronic structure analysis of the oxygen activation mechanism by the Fe^{II}- and α-ketoglutarate-dependent dioxygenases. *Chem. Eur. J.*, 18:6555, 2012.

[239] V. Guner, K. S. Khuong, A. G. Leach, P. S. Lee, M. D. Bartberger, and K. N. Houk. A Standard Set of Pericyclic Reactions of Hydrocarbons for the Benchmarking of Computational Methods: The Performance of ab Initio, Density Functional, CASSCF, CASPT2, and CBS-QB3 Methods for the Prediction of Activation Barriers, Reaction Energetics, and Transition State Geometries. *J. Phys. Chem. A*, 107(51):11445, 2003.

[240] D. H. Ess and K. N. Houk. Activation Energies of Pericyclic Reactions: Performance of DFT, MP2, and CBS-QB3 Methods for the Prediction of Activation Barriers and Reaction Energetics of 1,3-Dipolar Cycloadditions, and Revised Activation Enthalpies for a Standard Set of Hydrocarbon Pericyclic Reactions. *J. Phys. Chem. A*, 109(42):9542, 2005.

[241] S. Koßmann and F. Neese. Correlated ab Initio Spin Densities for Larger Molecules: Orbital-Optimized Spin-Component-Scaled MP2 Method. *J. Phys. Chem. A*, 114:11768, 2010.

[242] P. E. M. Siegbahn and M. R. A. Blomberg. Bond-Dissociation Using Hybrid DFT. *Int. J. Quantum Chem.*, 110:317, 2010.

[243] R. Polly, H. J. Werner, F. R. Manby, and P. J. Knowles. Fast Hartree-Fock theory using local density fitting approximations. *Mol. Phys.*, 102:2311, 2004.

[244] J.-H. Lii and N. L. Allinger. The MM3 force field for amides, polypeptides and proteins. *J. Comput. Chem*, 12:186, 1991.

[245] S. Sinnecker, E. Reijerse, F. Neese, and W. Lubitz. Hydrogen bond geometries from electron paramagnetic resonance and electron-nuclear double resonance parameters: Density functional study of quinone radical anion-solvent interactions. *J. Am. Chem. Soc.*, 126:3280, 2004.

[246] R. Izsák, A. Hansen, and F. Neese. The resolution of identity and chain of spheres approxima-

tions for the LPNO-CCSD singles Fock term. *Mol. Phys.*, 2012 (accecpted for publication).

[247] F. Neese and E. F. Valeev. Revisiting the Atomic Natural Orbital Approach for Basis Sets: Robust Systematic Basis Sets for Explicitly Correlated and Conventional Correlated *ab initio* Methods? *J. Chem. Theory Comput.*, 7:33, 2011.

[248] D. J. Thouless. *The Quantum Mechanics of Many-Body Systems*. Academic Press, New York, 1961.

[249] J. N. Harvey. The coupled-cluster description of electronic structure: perspectives for bioinorganic chemistry. *J. Biol. Inorg. Chem.*, 16:831, 2011.

[250] H. Senn and W. Thiel. QM/MM Methods for Biological Systems. *Top. Curr. Chem.*, 268:137, 2007.

[251] R. K. Nesbet. Brueckner's Theory and the Method of Superposition of Configurations. *Phys. Rev.*, 109:1632, 1958.

[252] C. Angeli, R. Cimiraglia, and J. P. Malrieu. *N*-electron valence state perturbation theory: A spinless formulation and an efficient implementation of the strongly contracted and of the partially contracted variants. *J. Chem. Phys.*, 117:9138, 2002.

[253] R. A. Mata, H.-J. Werner, and M. Schütz. Correlation regions within a localized molecular orbital approach. *J. Chem. Phys.*, 128:144106, 2008.

[254] T. Bredow, G. Geudtner, and K. Jug. Development of the cyclic cluster method for ionic systems. *J. Comput. Chem.*, 22:89, 2001.

[255] B. Hellmich and C. Hättig. Local pair natural orbitals for excited states. *J. Chem. Phys.*, 135:214106, 2011.

[256] A. Anoop, W. Thiel, and F. Neese. A Local Pair Natural Orbital Coupled Cluster Study of Rh Catalyzed Asymmetric Olefin Hydrogenation. *J. Chem. Theory Comp.*, 6:3137, 2010.

[257] J. Antony, S. Grimme, D. G. Liakos, and F. Neese. Protein-Ligand Interaction Energies with Dispersion Corrected Density Functional Theory and High-Level Wave Function Based Methods. *J. Phys Chem. A*, 115:11210, 2011.

[258] D. G. Liakos and F. Neese. Interplay of Correlation and Relativistic Effects in Correlated Calculations on Transition-Metal Complexes: The $(\mathrm{Cu_2O_2})^{2+}$ Core Revisited. *J. Chem. Theory Comp.*, 7:1511, 2011.

[259] M. Ashtari and N. M. Cann. Proline-based chiral stationary phases: A molecular dynamics study of the interfacial structure. *J. Chromatogr. A*, 1218:6331, 2011.

[260] S. S. Zade, N. Zamoshchik, A. R. Reddy, G. Fridman-Marueli, D. Sheberla, and M. Bendikov. Products and Mechanism of Acene Dimerization. A Computational Study. *J. Am. Chem. Soc.*, 133:10803, 2011.